The role of cellular chloride channels in human respiratory syncytial virus infection

Hayley Marie Pearson

Submitted in accordance with the requirements for the degree of
Doctor of Philosophy

The University of Leeds
Faculty of Biological Sciences
School of Molecular and Cellular Biology

January 2022

The candidate confirms that the work submitted is her own, except where work which has formed part of jointly authored publications has been included. The contribution of the candidate and the other authors to this work has been explicitly indicated below. The candidate confirms that appropriate credit has been given within the thesis where reference has been made to the work of others.

Chapters 3 and 4 form work published in Thorax: *Pearson H, Todd EJAA, Ahrends M, Hover S, Whitehouse A, Stacey M, Lippiat JD, Wilkens L, Fieguth H, Danov O, Hesse C, Barr JN, and Mankouri J.* "TMEM16A/ANO1 calcium-activated chloride channel as a novel target for the treatment of human respiratory syncytial virus infection" 2021. All work from this publication was directly attributable to the candidate except for Figure 4 G-I (western blots produced by co-author Miss Eleanor JAA Todd, University of Leeds), Figure 8 A-D and S1 (PCLS data generated by collaborators and co-authors - Dr Christina Hesse and team at Fraunhofer Institute for Toxicology and Medicine, Hanover, Germany). These data contribute to Chapter 3, Figure 3-7 G-J, Figure 3-11 A-D and F-G of this thesis, respectively.

Acknowledgements

Firstly, I would like to say a massive thank you to my former primary supervisor Dr Jamel Mankouri for being a fantastic mentor for the past 4.5 years. Your positive attitude and confidence in me have helped me through the lowest points of the PhD process. Thanks for always having your door open for advice, or a chat! You are truly missed at Leeds, but I wish you all the best with your new career and with fatherhood!

I would also like to thank my current primary supervisor Dr JN Barr for taking me (and the rest of team Mankouri) under your wing. Your help and feedback whist writing up have been invaluable, and I very much appreciate all the time you've taken to provide comments and give advice. But more than that, you have been my 'unofficial co-supervisor' since my first year, when you once again took Team Mankouri under your wing for those 6 months, so thank you for all your help and kind words of wisdom over the years.

To my co-supervisor Dr Martin Stacey, I would like to say thank you for all your input into this project and for helping me to navigate the tricky world of immunology. To the rest of my supervisory team: co-supervisor Dr Jon Lippiat and former co-supervisor Prof Adrian Whitehouse, I extend my appreciation for your input into this project.

To the former Team Mankouri, I owe a huge debt of thanks. Especially to Dr Sammy Hover, without whom I would definitely not be at the stage I am today. When I first joined the lab, you were an amazing teacher and I have learnt so much from you. You inspire me to become a better scientist (cheesy but true!). Thank you for all your help, advice, and friendship over the years, and for your valuable comments on my thesis. Thank you to Frankie Charlton, for making me laugh and keeping me sane through long hours in tissue culture. A huge thank you to Ellie Todd, who began this project in her masters year, and has been kind enough to share protocols and offer help and advice ever since. To the other members of the Mankouri lab group over the years, thank you all for keeping everyday interesting and for helping me improve: Aseel Alyahyawi, Ibrahim Al-Masoud, and the students I taught along the way, Robert Peverley and Samah Zurqi.

To Barr group, my adopted lab group, thank you for welcoming me in, being so friendly, and letting me share your space and equipment. A special thank you to Dr Amelia Shaw for many years of friendship (since our undergrad days) and for all your troubleshooting help and advice. I appreciate the hours we've spent complaining about science, usually over wine! Additionally, I would like to thank you for all your help with my post-doc application, and now we get to spend three more years working together!

I would like to extend my thanks to the rest of Virology and Garstang Level 9 for the fun lab drinks over the years. A special mention to Dani Pierce, my conference buddy and friend who has made the last 4.5 years infinitely better. Thanks for always letting me practice my talks with you.

On a personal note, a very important thank you goes to my amazing mum, Catherine Bibby. Words can't begin to describe the level of gratitude I have for everything you have done for me over the years and continue to do. You have always believed in me and have helped me to achieve my career aspirations. Thank you for your unconditional love and support that has helped me get to this point in my life. To the rest of my family, thank you for always asking about how my project is going, and pretending you understand it! Our family get togethers are always a lovely chance to relax and have fun (and not think about science!), and I am grateful to each one of you for everything you have done for me.

My last thank you goes to my fiancé, Sam Bradley, for being my rock. Your support during my dramatic first year, your patience through the write up process, and your advice throughout the whole project is truly appreciated. Thank you for always making me laugh, helping me see the bright side of any situation, and keeping me (moderately) sane during lockdowns. I can't wait to be your wife.

Abstract

Human respiratory syncytial virus (HRSV) is a common cause of respiratory tract infections (RTIs) globally. Of those infected, 25%–40% aged ≤1 year develop severe lower RTIs leading to pneumonia and bronchiolitis, with ~10% requiring hospitalisation. There is currently no HRSV vaccine and clinically approved treatments are only moderately effective. New and more effective anti-HRSV strategies are urgently required.

It is established that viruses require cellular ion channels to infect cells. Ion channels are a diverse class of transmembrane proteins that selectively allow ions across membranes, influencing a multitude of cellular processes. Modulation of these channels by viruses is an important host-pathogen interaction that regulates critical stages of the virus multiplication cycle including entry, replication, and egress.

Cellular chloride (Cl^-) channels are large family of ion channels which were historically overlooked, however the importance of these proteins, especially within the respiratory tract, is now being revealed. This thesis examined the role of Cl^- channels during HRSV infection. Utilising GFP-expressing HRSV in combination with an extensive panel of channel-specific pharmacological inhibitors, a critical requirement for calcium (Ca^{2+})-activated chloride channels (CaCCs) during HRSV infection was highlighted. For the first time, a role for TMEM16A as a host-factor was revealed and the channel was implicated as a post-exposure antiviral target.

An investigation into the mechanisms underpinning the relationship between HRSV and TMEM16A revealed that the channel was involved at the genome

replication and/or transcription stage of infection, and evidence suggested that this interaction may occur at or near the Golgi, in HRSV replication factories.

Lastly, a role for TMEM16A was described within the HRSV-mediated production of antiviral protein interferon γ-induced protein 10 (IP-10), which supported a hypothesis wherein HRSV sequestered TMEM16A for replication, and simultaneously prevented the cellular antiviral response. Therefore, these findings have revealed TMEM16A as an exciting target for future host-directed antiviral therapeutics.

Table of contents

List of Figures

List of Tables

Abbreviations

Abbreviation	Description
4-CN	4-chloro-1-naphthol
6HB	six-helix bundle
ABC	ATP-binding cassette
AGS	Aicardi-Goutières syndrome
ANO1-10	anoctamin 1-10 (also known as TMEM16A-K, excluding I)
ASL	airway surface liquid
ATP	adenosine triphosphate
BCA	bicinchoninic acid
Best1-4	bestrophin 1-4
BKPyV	BK polyoma virus
BUNV	Bunyamwera virus
Ca^{2+}	calcium ion
Ca_v	Voltage-gated calcium channel
CaCC	calcium-activated chloride channel
cAMP	cyclic adenosine monophosphate
CBS	cystathionine-β-synthase
CCHFV	Crimean-Congo haemorrhagic fever virus
CDC	Centre for Disease Control and Prevention
CF	cystic fibrosis
CFTR	cystic fibrosis transmembrane conductance regulator
CHIKV	Chikungunya virus
Cl^-	chloride ion
ClC	voltage-gated chloride channel
CLCA	chloride channel accessories
CLIC	chloride intracellular channel
CNS	central nervous system
COPD	chronic obstructive pulmonary disease
COVID-19	coronavirus disease 2019
CPE	cytopathic effect
cRNA	complementary RNA
CTD	C-terminal domain
CTP	cytosine triphosphate
CX3CR1	CX3 chemokine receptor 1
DENV	Dengue virus
DIDS	4,4’-diisothiocyanostilbene-2,2’-disulfonic acid
DMEM	Dulbecco Modified Eagle Medium
DRG	dorsal root ganglion
dsRNA	double stranded RNA
EBOV	Ebola virus
ECL	enhanced chemiluminescence

EDTA	ethylenediaminetetraacetic acid
ELISA	enzyme-linked immunosorbent assay
ENaC	epithelial sodium channel
ER	endosomal reticulum
ERD	enhanced RSV disease
ESCRT	endosomal sorting complex required for transport
F	fusion protein
FBS	foetal bovine serum
FDA	Food and Drug Administration
FFA	focus forming assay
G	glycoprotein
GABA	γ-aminobutyric acid
GAPDH	glyceraldehyde 3-phosphate dehydrogenase
GCU	green calibrated unit
GFP	green fluorescent protein
GI	gastrointestinal
Glu_{gate}	glutamate gate
GP	glycoprotein
GPCR	G-protein coupled receptor
GS/GE	gene start/gene end
GTP	guanosine triphosphate
H^+	hydrogen ion (proton)
HA	hemagglutinin
HAZV	Hazara virus
HCO_3^-	bicarbonate ion
HCV	hepatitis C virus
HGBA	histo-blood group antigen
HIV	human immunodeficiency virus
hpi	hours post-infection
hpt	hours post-transfection
HPV	Human papillomavirus
HRP	horseradish peroxidase
HRSV	human respiratory syncytial virus
IAV	influenza A virus
IB	inclusion body
IBAG	inclusion body-associated granule
IBDV	infectious bursal disease virus
IC_{50}	half-maximal inhibitory concentration
ICAM-1	intercellular adhesion molecule 1
ICC	interstitial cells of the Cajal
IFN	interferon
IFNR	interferon receptor

IGF1R	insulin-like growth factor-1 receptor
IKKε	IκB kinase epsilon
IL	interleukin
IMPDH	inosine monophosphate dehydrogenase
IP3/IP3R	inositol trisphosphate/ receptor
IP-10	interferon gamma-induced protein 10
IRF (3/7/9)	interferon regulatory factor (3/7/9)
ISG	interferon stimulated gene
ISRE	interferon-stimulated response element
JAK	Janus kinase
JEV	Japanese encephalitis virus
K^+	potassium ion
K_v	Voltage-gated potassium channel
L	large protein
LDH	lactate dehydrogenase
le	leader region
LMIC	low- and middle-income countries
LRTI	lower respiratory tract infection
M	matrix protein
MAPK	mitogen-activated protein kinase
MAVS	mitochondrial antiviral-signalling protein
MDA5	melanoma differentiation-associated protein 5
MERS-CoV	Middle Eastern respiratory syndrome coronavirus
MK2	MAPK-activated protein kinase 2
MOI	multiplicity of infection
mRNA	messenger RNA
N	nucleocapsid protein
NA	neuraminidase
Na^+	sodium ion
Na_V	Voltage-gated sodium channel
NBD	nucleotide binding domain
NCPV	National Collection of Pathogenic Viruses
NFκB	nuclear factor kappa-light-chain-enhancer of activated B cells
NoV	norovirus
NPC1	Niemann-Pick C1
NPPB	5-nitro-2-(3-phenylpropylamino) benzoic acid
NS1/NS2	non-structural protein 1/2
NSV	negative-strand RNA virus
NTD	N-terminal domain
NTP	nucleoside triphosphate
ORF	open reading frame
P	phosphoprotein
P/S	penicillin/streptomycin

PA	polymerase acidic protein
PBS	phosphate buffered saline
PCLS	precision cut lung slices
PEG	polyethylene glycol
PFA	paraformaldehyde
PFU	plaque forming units
PHE	Public Health England
PIV5	parainfluenza virus 5 (canine)
PKCζ	protein kinase C zeta
PSV	positive-sense RNA virus
PVDF	polyvinylidene difluoride
R+IAA-94	R(+)-[(6,7-Dichloro-2-cyclopentyl-2,3-dihydro-2-methyl-1-oxo-1H-inden-5-yl)-oxyacetic acid
RIG-I	retinoic acid-inducible gene I
RNP	ribonucleoprotein
RPE	retinal pigment epithelium
RPM	revolutions per minute
RTI	respiratory tract infection
RV	rhinovirus
RVD	regulatory volume decrease
SARS-CoV-1/2	sever acute respiratory syndrome coronavirus 1 and 2
S_{cen}	central site
SDS-PAGE	sodium dodecyl sulphate-polyacrylamide gel electrophoresis
S_{ext}	external site
SFTSV	severe fever with thrombocytopenia syndrome virus
SG	stress granules
SH	small hydrophobic protein
S_{int}	internal site
SR	sarcoplasmic reticulum
STAT	signal transducer and activator of transcription
TANK	TRAF-associated NFκB activator
TBS	tris-buffered saline
$TCID_{50}$	median tissue culture infectious dose
TEA	tetraethylammonium
TGN	trans-Golgi network
TLR-4	toll-like receptor 4
TMD	transmembrane domain
TMPRSS2	transmembrane protease serine 2
TNF-α	tumour necrosis factor alpha
TPC	two-pore calcium channel
tr	trailer region
TRAF3	TNF-receptor-associated factor 3

TRIS	tris(hydroxymethyl)aminomethane
UV	ultraviolet
VDAC	voltage dependent anion channel
VDCC	voltage dependent calcium channel
VGCC	voltage gated calcium channel
VP1/3	viral protein 1 or 3
VRAC	volume-regulated anion channel
vRdRp	viral RNA-dependent RNA polymerase
vRNA	viral ribonucleic acid
WNV	West Nile virus
WT	wild type
YFV	yellow fever virus
ZIKV	Zika virus

Chapter 1 Introduction

1.1 Human respiratory syncytial virus

Human respiratory syncytial virus (HRSV), also known as human orthopneumovirus, is a negative-strand RNA virus (NSV) belonging to the *Pneumoviridae* family of the order *Mononegavirales* [1]. The virus was described in 1956, initially isolated from laboratory chimpanzees which had acquired a respiratory illness from human workers. [2]. Soon after, HRSV was identified as the causative agent of seasonal outbreaks of upper and lower respiratory tract infections (RTIs) in children [3,4]. Now, 65 years after its discovery, there are still no vaccines available for the prevention of HRSV infection, and only very limited therapeutic options.

HRSV is so-called because of its distinguishing ability to form syncytia in infected epithelial cells [5], wherein neighbouring cells become fused forming large, multi-nucleated cells between which the virus can spread rapidly throughout the respiratory tract and avoid detection by the immune system [6].

1.2 HRSV epidemiology, symptoms, and transmission

HRSV is a global pathogen. As with many other respiratory viruses, HRSV infection occurs in a seasonal pattern throughout the year with different peaks of incidence depending on the hemisphere; peak months in the Northern Hemisphere being October-April and in the Southern Hemisphere being March-September [7]. The virus is spread either through inhalation of infected respiratory droplets, such as those generated from coughing or sneezing, or from direct contact with HRSV-contaminated surfaces and objects (called fomites) such as

door handles [8] and this direct route is considered to be the major source of infection [8,9]. HRSV enters the body through exposed mucosal surfaces of the eyes or nose [10], after which it migrates to the respiratory tract. In temperate climates, the winter months offer the perfect conditions for HRSV transmission including cold temperatures which stabilise the virus within droplets, humidity which allows for virus-containing droplets to form on surfaces, and rain which drives people indoors where virus transmission is more efficient [11]. In contrast, HRSV seasonality is less well-defined in tropical regions of the world (areas which have wet and dry seasons rather than the four seasons) [12]. Surveillance suggests that HRSV infection in these countries operates in very different cycles with many tropical regions displaying year-round infections. Peaks in HRSV cases occur at different times of year and often correlate with the temperature, humidity, and rainfall cycles within that region. Other socio-economic factors can affect HRSV seasonality in tropical regions, for example in the Philippines, seasonal malnutrition correlates with the rainy season, and the peak in cases of both HRSV infection and pneumonia occurs approximately 10 weeks after this [12].

Almost all children become infected with HRSV by the age of 2 years, and re-infection occurs throughout life [13]. For most, this manifests as generic cold-like symptoms including a runny nose, sore throat, coughing, sneezing and headaches. However, in 0.5 - 2% of all children, the infection can progress to the lower respiratory tract causing inflammation of the respiratory airways or lungs (bronchiolitis or pneumonia), the symptoms of which include difficulty breathing, fever and severe cough. The primary risk factor for severe HRSV-related illness is age, and this primarily occurs in children under 6 months due to the small size

of their airways. Particularly at risk are premature babies, or babies born with underlying health conditions such as heart or lung disease, as well as those who are immunocompromised [13,14]. Most healthy adults can clear the infection without any major problems, however those over 65 represent another high-risk category for severe complications following HRSV infection. Settings such as nurseries, hospitals and care homes are hot spots of infection wherein high-risk individuals all inhabit the same small spaces and touch the same surfaces, increasing transmission [8,15].

HRSV infection is the leading cause of hospitalisation of children under 5 in the UK and US. For children in the UK, between 1995-2009, an average of 450,000 GP visits were attributed to HRSV infection per year, along with 29,000 hospitalisations and 83 deaths [16]. In the US, the Centre for Disease Control and Prevention (CDC) estimates that HRSV infection is responsible for an average of 58,000 hospitalisations of children under 5 per year, with 100-500 deaths [13]. However, the vast majority of HRSV cases occur in low- and middle-income countries (LMIC). Globally, in 2015 it was estimated that 33.1 million cases of HRSV in children under 5 occurred, resulting in 3.2 million hospitalisations and 59,600 deaths – 30 million (90%) of these cases occurred in LMICs, resulting in many deaths and accounting for a large economic burden [17].

Furthermore, HRSV infection is also a significant burden on the elderly, responsible for an average of 175,000 GP visits, 14,000 hospitalisations and 7,915 deaths of adults over 65 annually in the UK between 1995-2009 [18]. In the US, 177,000 hospitalisations of adults aged 65 years or older with HRSV also occur per year, with 14,000 deaths [19].

As a result of the current severe acute respiratory syndrome-associated coronavirus 2 (SARS-CoV-2) pandemic, the rate of HRSV infection in the winter of 2020/2021 was comparatively low to previous years, likely due to lockdowns, mask wearing, social distancing and other restrictions put in place to prevent SARS-CoV-2 transmission [20,21]. Consequently, the summer of 2021 saw an unseasonable surge in HRSV cases in children, with many reporting more severe symptoms than previous years. The risk of older infants and toddlers developing severe HRSV infections was much higher due to limited past exposure during the pandemic [22]. This highlights the ever-present need for research into HRSV and for the discovery of novel antiviral targets with the potential for therapeutic applications.

1.3 HRSV therapeutics

1.3.1 Palivizumab

HRSV is a major health concern due to the absence of a vaccine. Palivizumab (or Synagis®) is currently the only prophylactic antiviral licenced for use in high-risk children (FDA approval, 1998) [23]. Palivizumab is a monoclonal antibody which targets the HRSV fusion (F) protein expressed on the surface of the virion. F plays a key role in the entry of the virus into cells, therefore, by targeting F, Palivizumab neutralises the virus and prevents infection. Treatment via an intramuscular injection once a month for five months during winter provides passive immunisation against HRSV. However, due to its high cost and moderate effectiveness, there is doubt over the value of use. Whilst prophylaxis with Palivizumab did reduce the incidence of hospitalisation of high-risk infants by ~55% [23], there is no evidence to suggest that the overall burden of HRSV has

been impacted since the introduction of Palivizumab [24]. Surveillance of HRSV revealed that most children in developed countries who become infected are otherwise healthy [13] and so the cost-effective strategy of targeting high-risk infants may not be effective in relieving HRSV-related disease burden. Identifying children likely to suffer severe symptoms is difficult, and the guidelines for use of Palivizumab are debated [24], highlighting the need for HRSV vaccines and post-exposure antivirals.

1.3.2 Ribavirin

Currently, the broad-spectrum antiviral ribavirin is the only FDA approved drug used to treat severe bronchiolitis caused by HRSV infection in infants (FDA approval, 1985). However, there are concerns over its many side effects, the aerosolised route of administration and cost; therefore, ribavirin is not currently recommended for routine clinical use (American Academy of Pediatrics). Other than HRSV, ribavirin is also used to treat other viral infections including hepatitis C (HCV), hepatitis E, and viral haemorrhagic fevers caused by Crimean-Congo haemorrhagic fever virus (CCHFV), Lassa virus and various Hantaviruses.

Once inside the cell, ribavirin is sequentially phosphorylated by cellular kinases to form ribavirin 5′-monophosophate (RMP), -diphosphate (RDP) and -triphosphate (RTP) (Figure 1-1) [25]. The antiviral effects of ribavirin are mediated by both direct and indirect mechanisms (reviewed in [26]). RMP acts as a direct competitive inhibitor of inosine monophosphate dehydrogenase (IMPDH), a crucial enzyme in the synthesis of guanosine [27], therefore causing a decrease in the pool of available guanosine nucleosides for viral RNA synthesis. Furthermore, RTP is a guanosine analogue, which means it can be incorporated into newly synthesised viral RNA in the place of the guanosine

nucleoside. As RTP can base pair with either cytosine (the natural base pair for guanosine) or uracil with equal affinity, mutations often arise within the viral RNAs [26,28,29]. These mutations accumulate in the presence of ribavirin, leading to ‘error catastrophe’, where the new viral progeny are no longer viable. For HRSV and HCV, G-A and C-U transitions are significantly increased in the presence of ribavirin, leading to a reduction in progeny virus [28,29]. Additionally, RTP is a competitive inhibitor for the enzymes involved in 5-methylguanosine cap formation, resulting in viral messenger RNA (mRNA) which cannot be translated due to abnormal cap structures [30]. Ribavirin is also thought to have immunomodulatory effects and can aid viral clearance by switching the host T-cell response from Th2 to Th1, therefore inducing antiviral factors.

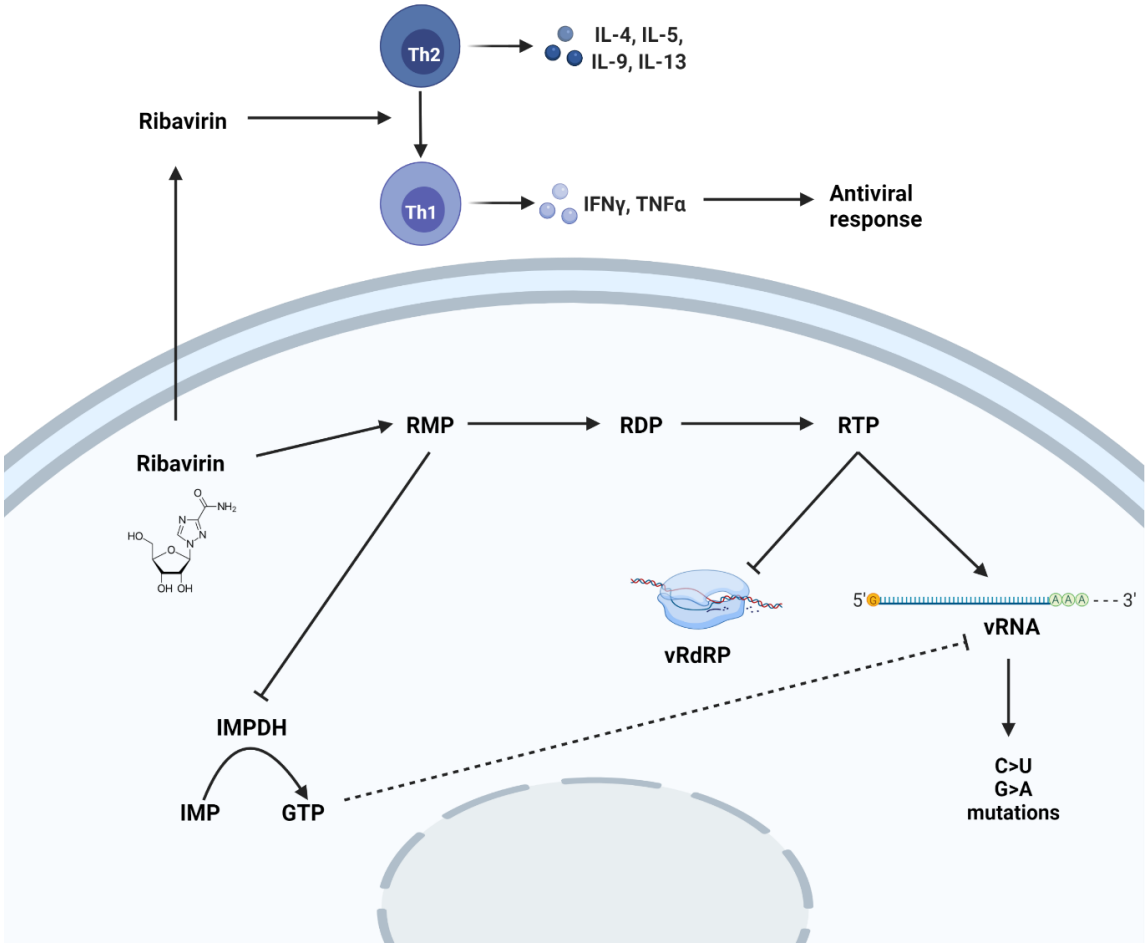

Figure 1-1 Ribavirin mechanism of action. Ribavirin is converted to 5′-monophosophate (RMP), -diphosphate (RDP) and -triphosphate (RTP) via cellular kinases. RMP competitively inhibits guanosine triphosphate (GTP) synthesis via inosine monophosphate dehydrogenase (IMPDH), resulting in a smaller pool of guanosine nucleosides (GTP) for viral RNA synthesis and a disruption to the mRNA capping mechanism. RTP both inhibits the vRdRp, and gets incorporated into the newly synthesised viral RNA, increasing the mutation rate, and resulting in 'error catastrophe' [26]. Created with BioRender.com

1.3.3 Challenges facing HRSV vaccine development

Historically, the search for a HRSV vaccine has been problematic. In 1966, trials of a formalin-inactivated vaccine ended in tragedy as two immunised infants later died following subsequent natural HRSV infection [31]. Many more infants

suffered severe LRTI symptoms which led to frequent hospitalisations. It is now known that this was due to enhanced HRSV disease (ERD), and this has since improved our understanding of how we might produce a successful HRSV vaccine in the future [32]. ERD occurs when a vaccine elicits non-neutralising antibodies in seronegative trial participants who are then left vulnerable to subsequent HRSV infection with a higher risk of severe disease. Therefore, guidelines for new HRSV vaccines going to clinical trial are particularly stringent [32,33].

As well as its chequered past, HRSV vaccine development faces other unique challenges (reviewed in [34]). For example, the young age of infants at peak disease poses its own challenges due to the underdeveloped immune system. Furthermore, it is known that HRSV infection dampens the immune response, which is another hurdle the vaccine must overcome. Additionally, it is difficult to assess levels of protection; we know that natural infection does not induce complete protection as HRSV infection reoccurs throughout a person's lifetime. Re-infection with the same strain of virus also commonly occurs, with the subsequent infections usually being less severe. Therefore, it may be necessary to tailor HRSV vaccines to different populations (e.g., infants and older adults) based on their propensity to develop ERD, differences in their immune responses, and correlates of protection. As with all NSVs, HRSV encodes its own viral RNA-dependent RNA polymerase (vRdRp) so that it can produce mRNAs that can be translated by the cellular translation machinery, and replication products that allow amplification of the negative-sense genome, for packaging into new virions. vRdRps are inherently error-prone due to the lack of a proof-reading mechanism [35], therefore single nucleotide polymorphisms are common

in NSVs, increasing genetic diversity and adding yet another challenge to vaccine development.

1.3.4 Current HRSV vaccine candidates

Vaccine candidates for HRSV consist of five main strategies: live-attenuated, subunit-based, vector-based, particle-based, and immuno-prophylaxis (monoclonal antibodies; mAbs) [34]. As of April 2021, there are 67 vaccines and mAbs which are active candidates or in development [36]. Four candidates have reached phase 3 clinical trials and three of these are subunit-based vaccines targeting the pre-fusion conformation of the F protein. These are GlaxoSmithKline's HRSV vaccines for maternal immunisation ('GSK3888550A') and for older adults ('GSK3844766A'), and Pfizer's 'RSV preF' designed for maternal use. Maternal vaccines are an ideal way to protect very young infants from severe disease and it is known that the pre-fusion conformation of the F protein induces a strong, neutralising antibody response, hence these candidates hold great promise. The fourth vaccine candidate currently in phase 3 trials, 'MEDI8897' (or Nirsevimab) by Astra Zeneca, is a monoclonal antibody with an extended half-life and also targets the pre-fusion conformation of F. MEDI8897 is indicated for paediatric patients and has so far shown promising results in healthy pre-term babies who were 70.1% protected against medically attended LRTI and 78.4% protected against hospitalisation when compared to the placebo group [37]. Unlike Palivizumab which requires multiple injections throughout the HRSV season, MEDI8897 is a single shot given once per HRSV season. It is hoped that, once FDA approved, MEDI8897 will be suitable for use in all infants and that its higher potency and longer half-life will resolve the issues seen with Palivizumab.

Recent advancements in nucleic acid-based vaccines, spurred on by the race to produce vaccines for coronavirus disease 2019 (COVID-19, caused by SARS-CoV-2 infection), has resulted in the development of a promising mRNA-based HRSV vaccine (mRNA-1345, Moderna) which has recently been fast-tracked into phase 1 trials for use in paediatrics and elderly patients. The vaccine encodes the pre-fusion F protein to elicit protective immunity. This new technology could bring an end to the 65 year long wait for a HRSV vaccine.

1.4 HRSV genome and virion structure

The HRSV RNA genome is 15,222 nucleotides in length, encoding 11 proteins through 10 genes which are separated by intergenic regions and flanked by gene start (GS) and gene end (GE) sequences [38]. The genes encoding the non-structural proteins (NS1 and NS2) reside at the 3' end of the genome and genes encoding the 9 structural proteins follow: nucleocapsid protein (N), phosphoproteins (P), matrix protein (M), small hydrophobic protein (SH), glycoprotein (G), F, M2 and large (L) protein (Figure 1-2) [1]. The M2 gene encodes two proteins (M2-1 and M2-2) through overlapping open reading frames (ORFs) on the M2 mRNA. Genomic RNA is encapsidated in N protein to form a helical ribonucleoprotein (RNP) complex [39,40], a feature common to all NSVs. The RNP is thought to offer protection from nucleases, facilitate protein-RNA interactions and shield the viral RNA from detection by the innate immune response.

The virion itself comprises an outer lipid envelope derived from the host cell plasma membrane by budding (Figure 1-2). The three surface glycoproteins (F, G and SH), form homo-oligomers and are embedded in the lipid envelope,

spaced 8-11 nm apart [1]. SH spans the membrane whereas F and G extend outwards to form spike-like projections around 10-14 nm in length. A layer of M coats the inside of the lipid envelope around 5 nm away from the lipid envelope, and a second layer of M2-1 lies underneath this, 13 nm from the envelope [41]. Within the virion resides the RNP associated with the replication complex proteins L, P and M2.

HRSV is pleomorphic, meaning that the size and shape of the virions differ greatly, falling into three particle morphologies: filamentous, spherical, and asymmetrical [41,42]. Filamentous HRSV particles occur most often during infection and are roughly 70-190 nm in diameter and up to 2 µm in length, whereas spherical virions range between 80-140 nm in diameter but can be as large as 600 nm [1]. Asymmetric particles most closely resemble the spherical morphology, however the membrane proteins are absent at regions of the virion close to neighbouring particles [42]. The filamentous morphology is suggested to be the most infectious form, however exactly why this occurs is not well understood. In 2018, it was shown that the surface of filamentous HRSV particles contained the stable pre-fusion form of the F protein whereas the spherical particles held the post-fusion form [43]. This will be expanded upon in 1.5.1 but essentially meant that the filamentous virions were infectious, but the spherical virions were not. Furthermore, in the spherical virions the M layer was disassociated from the viral envelope, and the RNP was not linked to M via M2-1, indicating they were probably a result of virion disruption or damage [43]. However, studies prior to this had observed that a combination of pre- and post-fusion F proteins were present on both types of virions and that all morphologies had similarly structured regions containing M underneath the lipid envelope

[41,42]. The role of each of these morphologies in the context of active infection is therefore still debated and requires further investigation.

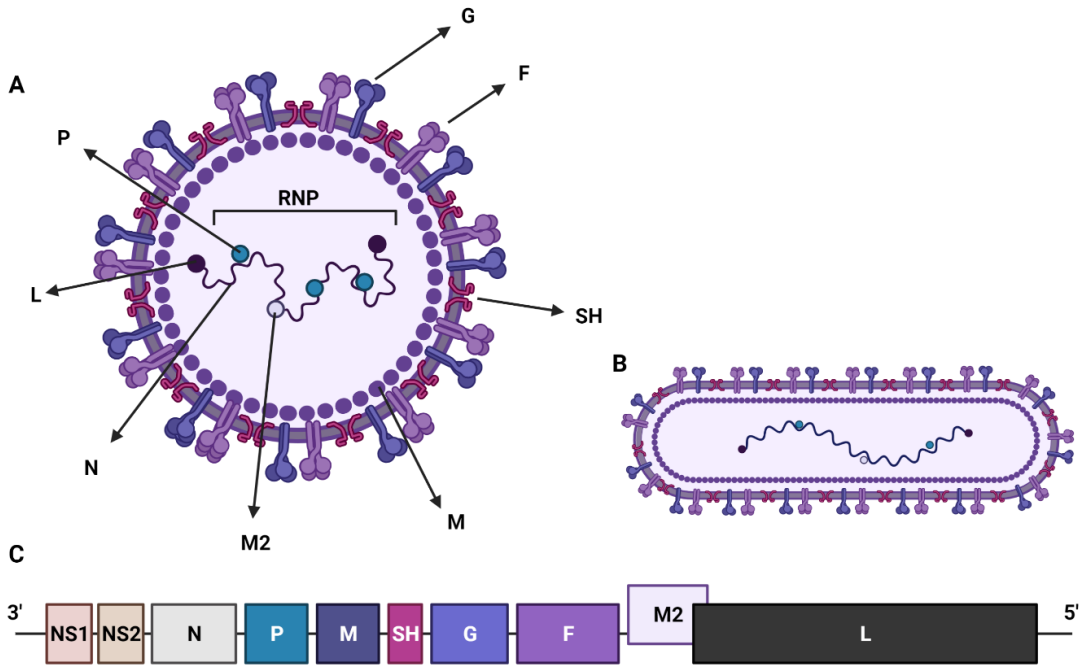

Figure 1-2 HRSV virion and genome structure. A-B) The virion comprises a single strand of negative-sense RNA coated in N protein and in association with the polymerase components (P, L and M2) to form the RNP complex. M coats the inner layer of a lipid bilayer, which encapsulates the RNP. SH spans the membrane, with G and F embedded on the outer surface of the virion. The virion can be spherical (A) or filamentous (B). **C)** The HRSV genome comprises 10 genes that encode 11 viral proteins. *NS1/2, non-structural protein 1/2. N, nucleocapsid protein. P, phosphoprotein. M, matrix protein. SH, small hydrophobic protein. G, glycoprotein. F, fusion protein. L, large protein*. Created with BioRender.com.

1.5 The role of viral proteins during the HRSV life cycle

An overview of the HRSV life cycle is shown schematically in Figure 1-3 and is summarised here. The sections that follow provide a description of the viral proteins involved and delve into the molecular detail of each life cycle stage.

The HRSV life cycle broadly follows that of other NSVs. The virions enter cells by attaching to cell surface receptors and initiating cellular uptake. Once in the cytoplasm, the virus uses the virion-associated vRdRp to perform primary transcription, generating a single mRNA from each of the ten HRSV genes, which are subsequently translated on host cell ribosomes. At a poorly defined time point following the onset of transcription, the activity of the vRdRp switches from transcription to replication, which is a two-stage process that ultimately leads to a rapid amplification of the negative-sense genome. In the first stage, the genome acts as a template for the vRdRp-mediated synthesis of a complementary copy known as the anti-genome. In the second stage, this anti-genome is again copied by the vRdRp to form further genomes, destined for further rounds of transcription (known as secondary transcription) or for incorporation into assembled viruses. Once assembled, the progeny can go on to infect naive cells either through release and re-infection or by the formation of syncytia which allows cell-to-cell spread.

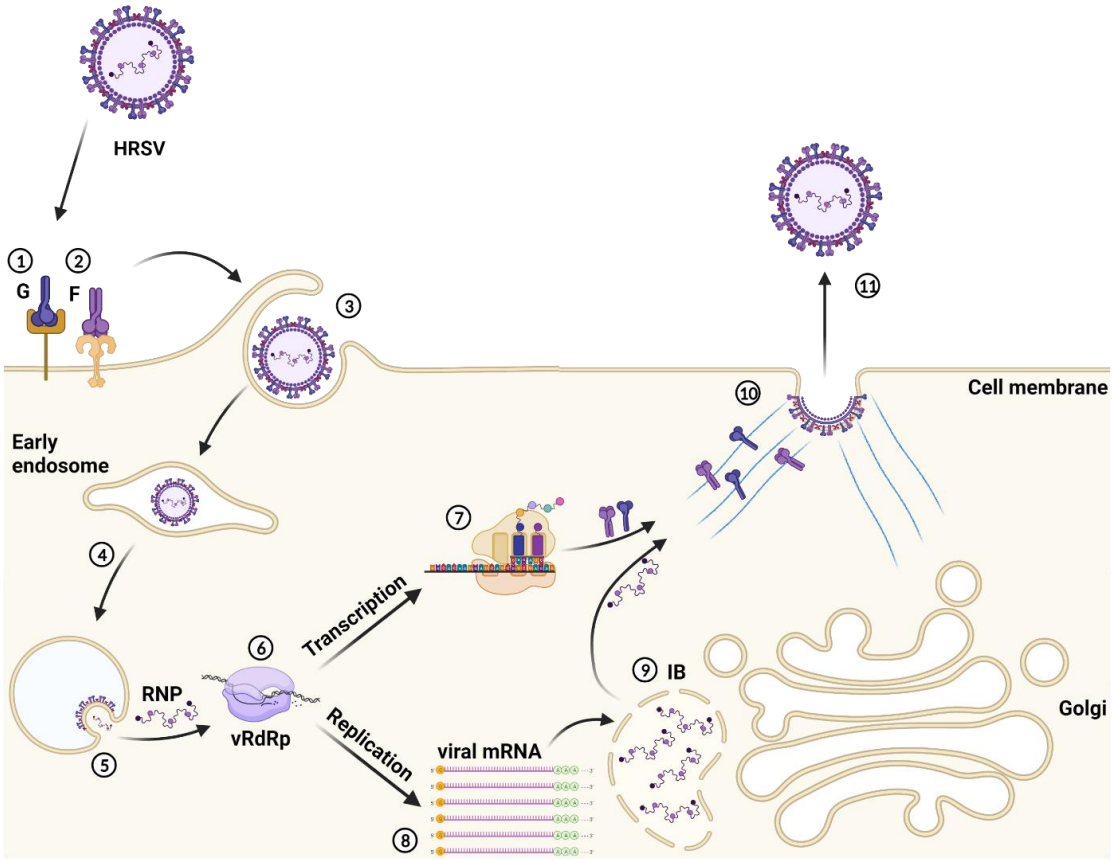

Figure 1-3 HRSV life cycle. 1. HRSV G protein attaches to cell surface receptors. **2.** The F protein binds to high-affinity cellular receptors and **3.** triggers cellular uptake of the virion via macropinocytosis. **4.** HRSV escapes the endosomal network when the F protein mediates fusion of the virus and endosomal membranes. **5.** The RNP complex is released into the cytoplasm. **6.** The vRdRp controls transcription of negative-sense HRSV genomes into positive-sense mRNAs with a 5'-cap and poly(A) tail, enabling **7.** the mRNA to be translated by cellular machinery, producing viral proteins. **8.** The vRdRp switches from transcription to replication of the viral genomes. **9.** Synthesis of new RNPs takes place in viral replication factories called inclusion bodies (IB). **10.** G, F and the RNPs travel along actin filaments and gather at the cell membrane where the M protein drives self-assembly of the virions. **11.** Infectious viral progeny are released from the cell. Schematic created in BioRender.com.

1.5.1 The role of HRSV glycoproteins in virus entry and fusion

1.5.1.1 The glycoproteins involved in entry: G and F

The glycoproteins, G and F, which are found on the virion envelope, are the mediators of HRSV entry into cells. The full-length G protein is a 298 aa, single-pass type II membrane protein, however it can also be expressed as a soluble protein resulting from translation initiation from an alternative start codon. The soluble form of G is thought to play a role in immune evasion by acting as an antigen decoy for antibodies targeting G [44]. The inherent variability of the G protein sequence gives rise to the different HRSV subtypes (A and B) and is one of the main reasons that HRSV circulates annually and causes re-infections. On the other hand, F is a type I membrane protein that is highly conserved between HRSV subtypes, and is considerably bigger than G, at 574 aa in length. Initially synthesised as an inactive monomer (F_0), F must be cleaved by host proteases to become 'fusion-ready'. F_0 contains two polybasic furin cleavage sites [45,46]. The first cleavage event occurs within the *trans*-Golgi network (TGN) [47] shortly after synthesis and generates the 'pre-fusogenic' conformation of F, consisting of two subunits (F_1 and F_2) which are covalently linked through a di-sulphide bridge. This conformation of F is displayed upon the surface of virions as a trimer of the cleaved F_1-F_2 heterodimer (and is also the conformation targeted by the vaccine candidates currently in phase 3 trials, discussed previously in 1.3.4). The second cleavage event takes place within the endosomes of newly infected cells; a 27 amino acid peptide ('pep27') between the two furin cleavage sites is removed, resulting in the generation of the 'pre-fusion' conformation of the F protein [45,48].

1.5.1.2 Attachment

Infection begins with initial attachment of G to receptors on the cell surface of host ciliated epithelial cells. The G protein contains a CX3C motif which allows attachment to the CX3 chemokine receptor 1 (CX3CR1) [49,50] expressed on epithelial cells at the apical surface of the lungs (Figure 1-3, 1) [51]. In cell culture, G also attaches to heparan sulphate [52], although this is not thought to represent a physiological interaction as there is little evidence of heparin expression on ciliated epithelial cells.

With the virion attached to the cell via G, F can encounter high-affinity cellular receptors (Figure 1-3, 2); candidates include toll-like receptor 4 (TLR-4) [53], intercellular adhesion molecule 1 (ICAM-1) [54] and nucleolin [55,56]. It was recently suggested that the interaction between G and CX3CR1 caused the upregulation of pro-viral factors including nucleolin [57] which would help explain this two-step binding process. Another study found that the binding of HRSV F to another entry receptor, insulin-like growth factor-1 receptor (IGF1R), triggered the protein kinase C zeta (PKCζ) signalling pathway resulting in the recruitment of nucleolin from the nucleus to the plasma membrane [58].

1.5.1.3 Entry

The process by which HRSV enters the cell is still debated. It was originally thought that direct fusion of the virion and cell membranes occurred, since HRSV fusion was pH-independent and was insensitive to lysosome acidification, indicating at the time that entry did not involve the endocytic pathway. However, as knowledge surrounding these processes has increased, so too has evidence that HRSV enters through a more complex process [59]. Observations using

fluorescence microscopy have reported that rather than fusing at the cell membrane, HRSV utilises macropinocytosis, the non-specific uptake of large amounts of extracellular material, to enter cells [48] (Figure 1-3, 3). The second cleavage event of F, which is crucial for activation, is then suggested to take place within the endosomal network [48,56] (Figure 1-3, 4). Once pep27 is cleaved, F mediates the fusion of the endosomal and virus membranes to release the RNP into the cytoplasm of the cell. A dramatic conformational change results in the insertion of the exposed fusion peptide located at the new F_1 N-terminus into the endosomal membrane. This triggers a subsequent conformational change in F_2 mediated by the formation of a highly stable six-helix bundle (6HB), derived from all three F_1 monomers within the trimeric spike. The 6HB pulls the two membranes into close contact forming a stable fusion pore and allowing the RNP to escape from the endosome [60,61] (Figure 1-3, 5).

1.5.1.4 The third glycoprotein: SH

The third glycoprotein expressed on the surface of HRSV is SH, a small (64 aa), type II transmembrane protein that forms pentameric ring structures which demonstrate cation channel activity [62,63]. Ion channels encoded by viruses are termed viroporins, and little is known about the roles of such proteins during HRSV infection. SH has no known role in attachment or entry of the virus into cells [64,65]. A mutant HRSV lacking the SH gene was indistinguishable to wildtype in terms of its growth when infecting cultured cells *in vitro*, however the mutant appeared attenuated in mouse models of human disease, implying some role in pathogenesis [65]. A study which drew on comparisons between parainfluenza virus 5 (PIV5) SH and HRSV SH revealed that HRSV SH may be involved in preventing apoptosis in infected cells by inhibiting the activation of

nuclear factor κ-light-chain-enhancer of activated B cells (NFκB) by tumour necrosis factor-α (TNF-α) in a similar manner to PIV5 SH [66]. However, the presence of HRSV SH was also able to protect infected A549 cells against apoptosis; as A549 cells are not sensitive to TNF-α-induced death, it was concluded that HRSV SH must also inhibit apoptosis via an alternative mechanism [66].

1.5.2 The polymerase complex and the transcription and replication of viral RNA

1.5.2.1 The polymerase complex proteins: L, P, N and M2.1

The HRSV L protein represents the catalytic component of the vRdRp, responsible for both the transcription and replication of the viral RNA, as well as the addition of the 5' cap and poly(A) tail to newly synthesised viral mRNA. The 2165 aa long L protein contains five conserved domains: vRdRp domain, poly-ribonucleotidyltransferase, connecting domain, methyltransferase, and the C-terminal domain (CTD).

The polymerase complex consists of L and its co-factor, P, which mediates the interaction between L and the encapsidated viral genome. P is a 241 aa protein containing an oligomerisation domain flanked by N- and C-terminal intrinsically disordered regions. P forms tetramers and structural studies have found that each P monomer adopts a different conformation when bound to L. The C-terminal domain of P binds the RNP [67], and an interaction site for M2-1 has also been identified, which allows the recruitment of M2-1 to the replication complex [68,69]. More recently, N-terminal binding sites which mediate the interaction between P

and M have also been identified [70], indicating a role for P in virion assembly and release.

N encapsidates the viral genome to form a nuclease-resistant nucleocapsid which is used as the template for RNA synthesis. The 391 aa protein contains a core region with N- and C- terminal domains (NTD/CTD) linked by a hinge region, and the RNA groove is situated at the interface of the NTD and CTD [39,40].

The role of the M2-1 protein is not certain, with proposed roles in transcription anti-termination, vRdRp processivity as well as a structural role in virion formation. Whatever the role of M2-1, it is an essential protein, as deletion of the M2-1 gene from the HRSV genome prevents viable virus rescue [71]. In terms of its role in transcription, M2-1 promotes the generation of full-length mRNAs, necessary for the synthesis of functional viral proteins, and current evidence suggests that this is achieved by direct binding to nascent mRNA transcripts [68,72,73] . In terms of its structural role, M2-1 is found within filamentous virions as a second matrix layer, positioned in between M and the RNP [41,42]. M2-1 is 194 aa in length and contains three domains separated by flexible linkers; an N-terminal zinc-binding domain, a central oligomerisation domain which allows the protein to form tetramers, and a core domain involved in RNA binding [73].

1.5.2.2 Transcription

Transcription is initiated when the vRdRp binds the 3’ end of the viral RNA [74] and then moves in a 3’ to 5’ direction along the genome to generate a short (~25 nucleotides) RNA transcript known as the leader RNA (*le*), followed by a single mRNA from each of the 10 HRSV genes (Figure 1-3, 6). HRSV transcription occurs according to a stop-start model [38,75] wherein the vRdRp responds to

GS and GE signals that flank each gene. The expression levels of each of the viral mRNAs is dictated by gene order, due primarily to a proportion of vRdRps disengaging from the RNA template after each gene junction, resulting in a gradient of expression where genes at the 5' end are transcribed less abundantly than those at the 3' end. The resulting mRNAs are both 5' capped and polyadenylated by the vRdRp, which allows them to co-opt the host cell ribosomal machinery for viral protein translation (Figure 1-3, 7).

1.5.2.3 Replication

As infection progresses, the predominant activity of the vRdRp switches from mRNA transcription to replication, which serves to amplify genomic RNA strands (Figure 1-3, 8). During replication, the vRdRp enters the genome at the extreme 3' end and as it transits along the template, it no longer responds to the transcription termination signals at either the leader/NS1 junction, or at any of the GE signals contained within the gene junctions. Instead, the vRdRp transcribes a full length, complementary copy of the viral RNA, known as the anti-genome, which then serves as a template for further cycles of replication, generating further genomes as templates for transcription or for assembly into new virions. In contrast to mRNAs generated during transcription, both genomes and anti-genomes are entirely encapsidated with N protein, thus forming RNPs [75].

1.5.2.4 Switching between transcription and replication

The vRdRp initiates viral RNA transcription and replication from the same promoter within the *le* region [74]. This promoter region contains two initiation sites, one for each process (Figure 1-4). Initiation at the +1 site results in encapsidated anti-genomes (replication), whereas initiation at the +3 site results

in the generation of viral mRNAs (transcription) [76,77]. If a polymerase has initiated at the +1 site when there are only low levels of N protein, the polymerase is released after production of the *le* transcript. Therefore, N expression represents a key determinant in the switch between transcription and replication. Another determinant appears to be the relative levels of available nucleoside triphosphates (NTPs). Minigenome studies revealed that the vRdRp has an innate affinity for adenosine triphosphate (ATP) and guanosine triphosphate (GTP) and these NTPs compete for binding at site 1 in the active site of the polymerase (NTP_1), and cytosine triphosphate (CTP) occupies NTP_2 [78]. The *le* sequence is such that the polymerase has the possibility to bind on two registers, depending on which NTP is bound at NTP_1. GTP bound at NTP_1 results in initiation at +3 and results in transcription, whereas ATP bound at NTP_1 pairs with the initiation site at +1 and leads to replication. Changing the relative levels of ATP and GTP in cells was sufficient to switch the initiation site and therefore the outcome of vRdRp activity [77,78].

Additionally, early studies suggested that M2-2 plays a role in the switch between transcription and replication. An accumulation of viral mRNAs was observed during infection with a M2-2 deletion mutant, as well as a corresponding reduction in genomic and anti-genomic RNA indicating that the switch from transcription to replication is unable to occur in the absence of M2-2 [79]. However, the mechanism by which this small (90 aa) accessory protein may regulate this process remains to be established.

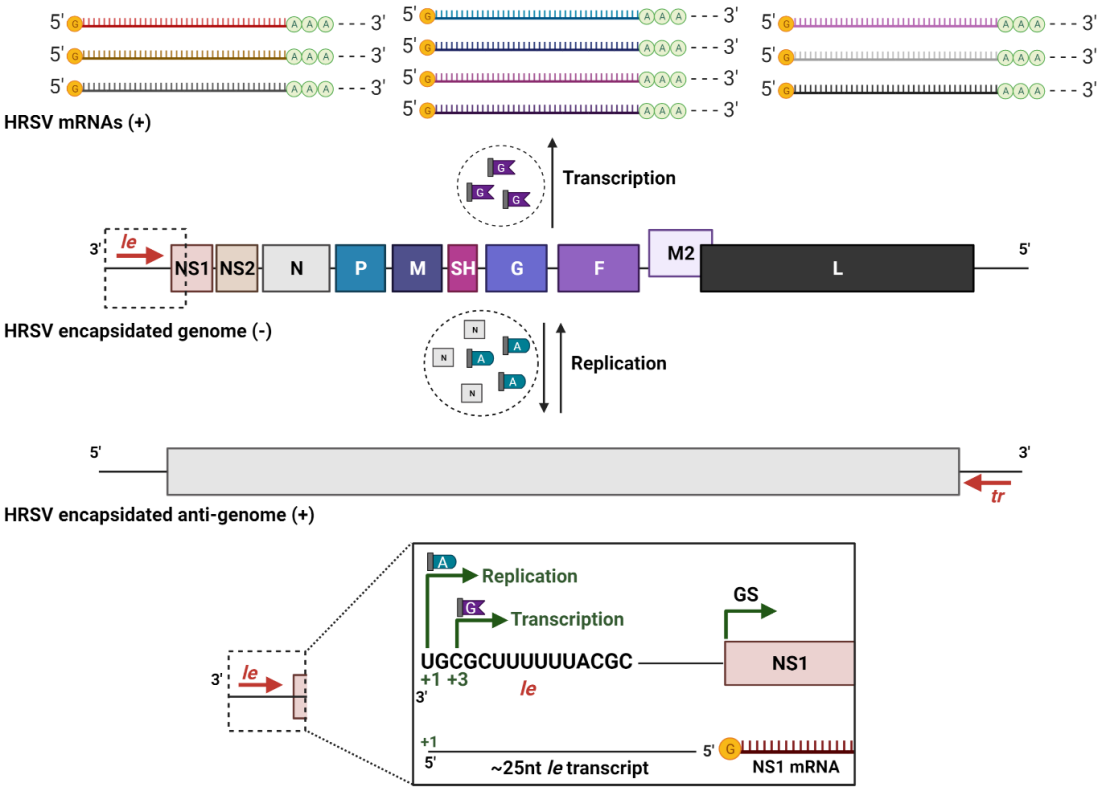

Figure 1-4 HRSV transcription and replication. The negative-sense genomic RNA is transcribed into positive-sense mRNA by the vRdRp complex from the 3' end. Transcription occurs according to a 'stop-start' model, wherein each gene is flanked by a GS and GE sequence. The vRdRp adds a 5' cap and 3' poly(A) tail to the viral mRNAs, which co-opt host translation machinery to produce viral proteins. High cellular levels of N protein cause the vRdRp to switch to viral replication, during which intermediate positive-sense anti-genomic copies are produced, which is encapsidated in N. This anti-genome is then used as a template to produce new genomic RNA. Both transcription and replication are initiated by a single promoter in the leader (*le*) region. The sequence of the leader region has similar repeats to the sequence of the GS, meaning that the vRdRp can bind on two registers. In an abundance of G nucleosides, the vRdRp binds at the +3 site and transcription begins, whereas in an abundance of A nucleosides, replication is initiated from the +1 site. The trailer (*tr*) region at the 3' end of the antigenome acts as the promoter of genome synthesis. Created in BioRender.com. Adapted from Noton *et al.*, 2019 [77].

1.5.3 Inclusion bodies; sites of viral RNA synthesis

In the cytoplasm, RNPs along with the L, P and M2-1 proteins that form the vRdRp complex congregate at inclusion bodies (IBs) (Figure 1-3, 9). IBs form on or near intracellular membranes such as the Golgi and can be visualised by both light and electron microscopy [80,81]. They are membrane-less structures which are granular, electron-dense and resemble liquid organelles such as stress granules (SGs) [82].

IBs are dynamic and highly ordered structures which play a multitude of roles within the HRSV life cycle. Firstly, they are considered to be the major site of viral RNA synthesis and mRNA sorting [83,84]. Immunofluorescence studies revealed that IBs form in the presence of N and P protein complexes [84] and the use of molecular beacons confirmed that they contain viral RNA [85]. More recently, 5EU labelling of newly synthesised viral RNA uncovered that IBs are the only sites of viral transcription, and also revealed the existence of distinct sub-compartments within IBs, termed inclusion body-associated granules (IBAGs) [83]. IBAGs contained only newly synthesised viral mRNA and the M2-1 protein, while N, P and L remained inside the IB but excluded from IBAGs, indicating that viral mRNA synthesis occurred in IBs, and were then stored in IBAGs until they were released into the cytosol by IBAG disassembly [83].

As well as being sites of RNA synthesis, IBs are thought to mediate several immune evasion strategies through the sequestration of cellular proteins involved in antiviral responses (discussed further in 1.5.5.4).

Other NSVs also produce cytoplasmic inclusions which are morphologically comparable to HRSV-induced IBs (reviewed in [86]). An example of these are

Negri bodies induced by rabies virus (RABV) infection. Negri bodies are the sites for RABV mRNA synthesis and, like HRSV IBs, can be formed by just the expression of viral N and P proteins [87]. Other examples of NSVs which use IBs as sites of viral RNA transcription and/or replication include Ebola virus (EBOV) [88], vesicular stomatitis virus [89] and human metapneumovirus [90], however this is not a universal phenomenon as Nipah virus was recently shown to induce two distinct populations of IBs, neither of which supported viral RNA replication [91].

1.5.4 Virion assembly and release

1.5.4.1 The driver of assembly: M

The HRSV M protein is known as the driver of assembly because it interacts with all the components required for virion formation; the RNP, M2-1, the G and F glycoproteins, and with cellular membranes [92]. Additionally, M exists as a dimer which self-assembles into higher order structures by the formation of NTD/NTD and CTD/CTD interfaces, allowing the formation of long, flexible structures, ideal for its role in budding [93] . The M monomer is a 256 aa protein which consists of two beta-sheet containing folded domains separated by a short, unstructured linker region [94]. The linker region confers the structural plasticity required by M for interactions with multiple binding partners. A large, positively charged area exists on the surface of M, spanning both domains and the linker region to enable its function in binding to membranes, likely through electrostatic interactions [94]. M is predicted to encode a zing-finger domain, two nuclear export signals and a nuclear localisation signal. Consistent with this, evidence suggests that M indeed localises within the nucleus at early stages of the life cycle and may inhibit host cell transcription [95].

1.5.4.2 Assembly

Upon viral protein synthesis, the glycoproteins are trafficked from their sites of synthesis in the endoplasmic reticulum (ER) to the apical surface of the cell and integrate into the host cell membrane (Figure 1-3, 10). The F protein undergoes its first of two cleavage events in the TGN, so that it is in the pre-fusogenic conformation when incorporated into new virus particles. M can bind to the cytoplasmic tails of both F and G, and, although G is dispensable for virus assembly, the M-F interaction is crucial for filament formation [96,97]. Additionally, it appears that P plays an important role in bringing M and F together, and the absence of P impacts the efficiency of assembly and the morphology of filaments produced.

The newly formed RNPs associate with M within IBs before entering the cytoplasm and trafficking along the actin filaments of the cytoskeleton towards the cell membrane to meet the glycoproteins (Figure 1-3, 10). In the absence of M, the RNP is unable to traffic to the cell membrane and accumulates in IBs [98], yet how M facilitates RNP trafficking remains unclear. Some studies have reported that M2-1 plays a crucial role in this by interacting with M and driving its localisation into IBs [99]. Conversely, others have suggested that M can be found in IBs in the presence of only N and P [96]. Whether M2-1 recruits M to IBs or not, structural studies have proven that M2-1 provides a crucial link between M and the RNP inside virions [41,42].

1.5.4.3 Release

Filamentous projections containing the structural proteins and RNP can be observed protruding from the cell surface during HRSV infection and are

important in virus release and syncytium formation [100,101]. Budding from these filaments produces infectious pleiomorphic virions with glycoproteins embedded within the viral membrane (Figure 1-3, 11). The M protein contributes to budding by oligomerising underneath the cell membrane to induce membrane curvature. Membrane scission is required to release the new infectious virus particles. Whilst many closely related viruses use the endosomal sorting complex required for transport (ESCRT) pathway, HRSV release has been shown to be ESCRT-independent [102], therefore, the mechanism by which HRSV virion release occurs requires further investigation. Released virions can then infect naive cells, advancing infection. Alternatively, HRSV can spread to neighbouring cells without exiting the infected cell. The expression of F on the surface of infected cells can mediate fusion with neighbouring cellular membranes, resulting in syncytia formation [5,103].

1.5.5 Pathogenesis and immune evasion

1.5.5.1 The non-structural proteins: NS1 and NS2

The non-structural proteins of HRSV are unique and do not have counterparts in other closely related viruses. They are accessory proteins which are considered non-essential for HRSV infection *in vitro*, however *in vivo* they contribute to the virus evasion of both the innate and adaptive immune responses (reviewed in [104]) and therefore are important for the pathology of the virus.

The NS1 and NS2 genes reside at the 3' end of the genome which means, due to the aforementioned stop-start strategy of HRSV transcription (1.5.2.2), the non-structural proteins are expressed the earliest and to the highest levels [38]. The NS1 protein is the more well-studied of the two non-structural proteins; it is

a 139 aa protein which is predominantly expressed as a monomer and traffics to the nucleus upon production [105]. Minigenome studies revealed that NS1 blocks viral transcription and replication [106], which may serve to help the virus evade the immune response very early in infection whilst its other immune evasion strategies are being established. NS2 on the other hand is slightly smaller at 124 aa and is not as stable, with an intracellular half-life of around 1 hour. Both homo- and heterodimers of NS1 and NS2 have been observed, with NS2 and NS1-NS2 complexes localising to the mitochondria [105], an organelle which is involved in the innate antiviral response [107].

1.5.5.2 Triggering the antiviral response

Infection with HRSV triggers the host antiviral type I interferon (IFN) response (Figure 1-5) [104,108]. Briefly, this involves the sensing of the viral RNA by cytosolic RNA helicase retinoic acid-inducible gene I (RIG-I) which then activates the mitochondrial antiviral-signalling protein (MAVS) [109,110]. MAVS then activates TNF-receptor-associated factor 3 (TRAF3), which in turn activates TRAF-associated NFκB activator (TANK), followed by IκB kinase ε (IKKε) and finally results in the activation of IFN regulatory factor 3 (IRF3) [107]. IRF3 triggers the production of NFκB, a transcription factor which switches on type I IFN gene expression. Alternatively, HRSV also induces the toll-like receptor (TLR) pathways of type I IFN production. The presence of viral ssRNA or dsRNA is detected by TLR7 or TLR3, respectively. Both TLR7 and TLR3 signal via distinct pathways resulting in the activation and nucleolar translocation of IRF3/7 or NFκB transcription factors; TLR7 via a Myeloid differentiation primary response 88 (MyD88)-dependent signalling cascade and TLR3 via TIR-domain-containing adapter-inducing interferon-β (TRIF) [104,108,109].

Upon the induction of IFN gene expression, they are secreted from the infected cell to alert neighbouring cells of the presence of the viral pathogen (Figure 1-5). To achieve this, IFNs bind to IFN receptors (IFNR) on the cell surface, triggering the Janus kinase (JAK)-signal transducer and activator of transcription (STAT) pathway (JAK-STAT) signalling cascade to stimulate the expression of interferon-stimulated genes (ISGs). This occurs via the formation of STAT-dimers complexed with IRF9, that translocate to the nucleus and bind to IFN-stimulated response elements (ISRE) within the promoter regions of ISGs [104,108,109]. These can go on to perform a variety of antiviral functions, for example reducing protein synthesis, promoting apoptosis of infected cells, upregulating the expression of major histocompatibility complex proteins to increase antigen presentation, and recruiting immune cells to the site of infection.

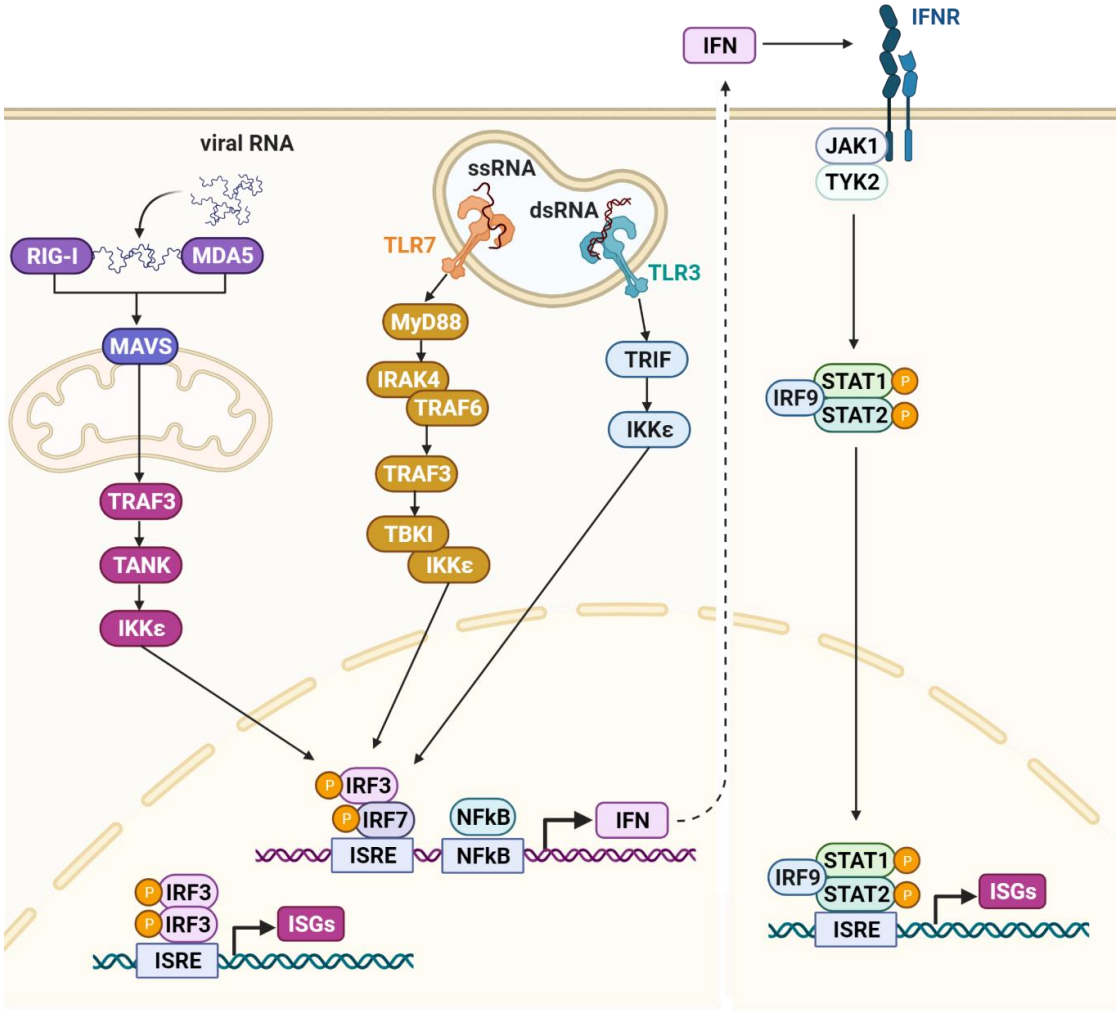

Figure 1-5 Schematic of the host antiviral IFN response triggered by HRSV. Viral RNA is detected by cytosolic RIG-I or endosomal TLRs. Distinct signalling cascades are subsequently activated which all result in the phosphorylation and nuclear translocation of IRF3 and IRF7. Once active, these transcription factors stimulate the expression of type I IFNs. They can also stimulate the expression of other ISGs. IFN's bind to IFNR on the cell surface (of the same cell or neighbouring cells) and signal through the JAK/STAT cascade to control the expression of ISGs. Adapted from [104,108], created using BioRender.com.

1.5.5.3 Subverting the antiviral response

Compared to other respiratory viruses such as influenza A virus (IAV) and human parainfluenza virus, infection with HRSV produces surprisingly low levels of IFN

[111]. The HRSV NS1 and NS2 proteins are crucial to the virus's ability to evade the cellular type I IFN response [104,108]. A key role of these proteins is the formation of the NS-degradosome which targets and destroys host proteins involved in the IFN response [112]. The NS-degradosome is a large, heterogeneous protein complex, the composition of which is currently unknown. It is located at the mitochondria and is thought to associate with MAVS, resulting in the proteasomal degradation of RIG-I, TRAF3, IKKε, IRF3/7 and STAT2 [112] therefore hampering these signalling pathways and the production of IFNs.

As well as their joint role, the NS proteins can also individually directly inhibit cellular proteins involved at each stage of the signalling pathways leading to IFN production (Figure 1-5). For example, co-immunoprecipitation studies suggested that NS2 bound to RIG-I [113], and upon solving its crystal structure, it was found that NS2 specifically binds to inactive RIG-I, preventing its ubiquitination, and therefore activation [114]. On the other hand, NS1 did not directly bind to RIG-I [113], but it was found to bind MAVS and prevent its interaction with RIG-I [115]. In both instances, inhibition of these early signalling steps reduced IFN production in response to HRSV infection.

In a similar fashion, it was found that the presence of recombinant NS1 and NS2 reduced the levels of TRAF3 expression, although the effect of NS2 was much weaker than NS1 [116]. TRAF3 is an important target for HRSV as it represents a convergence of both the RIG-I and TLR-induced pathways of IFN production (Figure 1-5). In the same study, NS1 was also found to decrease IKKε expression whereas NS2 had no effect, again highlighting the differences in the roles the NS proteins play during immune evasion.

The next stage of signalling involves the activation of IRF3/7 (or NFκB) transcription factors (Figure 1-5) and there is evidence that HRSV also targets these proteins, therefore preventing the induction of IFN gene expression. Using deletion mutants, a role for NS1 and NS2 in preventing the nuclear localisation of IRF3 was revealed [117]. This could have been, in part, due to the inhibition of upstream effectors, however, the use of constitutively active IRF3 overexpressing cells revealed that IRF3 levels were reduced in the presence of NS1, suggesting a specific effect on IRF3. Further investigation showed that NS1 inhibited the binding of IRF3 to the ISREs within IFN promoter by affecting the interaction between IRF3 and its co-activator CBP [118].

Upon the induction of IFN expression by the infected cell, JAK-STAT signalling pathways are triggered by IFN binding to IFNRs at the cell surface which ultimately leads to the expression of ISGs (Figure 1-5). HRSV has also evolved mechanisms against this by targeting proteins involved in this secondary pathway. For example, NS1 was shown to upregulate the expression of miR-29a, a microRNA which targets and suppresses the expression of IFN-α receptor 1 (IFNAR1) [119], thereby preventing the induction of IFN signalling. Additionally, NS2, but not NS1, was reported to potently decrease the level of STAT2 present in cells [116]. However, the role of NS proteins against STAT2 is debated and some groups have confirmed this finding [112,120,121] whereas others have reported that STAT2 levels were also reduced in the presence of NS1 [122]. Whilst further work is needed to fully elucidate the many mechanisms of immune evasion mediated by NS1 and NS2, it is clear that they play critical roles in HRSV pathogenesis.

1.5.5.4 Role of IBs in immune evasion

As previously mentioned (1.5.3), the HRSV replication complexes, or IBs, are known to sequester elements of the host immune response to prevent antiviral signalling. For example, HRSV sequestered the p65 subunit of NFκB in IBs where it was unable to interact with the rest of the NFκB complex [82]. Similarly, sequestration of melanoma differentiation-associated protein 5 (MDA5) and MAVS into IBs has also been observed during HRSV infection [110]. MDA5 is a member of the RIG-I-like-receptor family which senses the presence of dsRNA and activates MAVS. Sequestration of these critical proteins through interaction with HRSV N protein resulted in a decrease in IFN-β mRNA in infected cells [110].

Other proteins involved in the cellular stress responses are also sequestered into IBs. P38 mitogen-activated protein kinase (MAPK) recruitment into IBs in HRSV infected cells rendered the protein unable to interact with its downstream partner MAPK-activated protein kinase 2 (MK2), an essential component of the inflammatory response. Removal of p38 MAPK from the cytoplasm resulted in a depletion of MK2 levels, which was reversable upon the disruption of IBs [123]. The same study also observed that infected cells with large IBs did not contain SGs whereas cells with smaller IBs did also contain SGs. Evidence suggested that this was due to the sequestration of O-linked N-acetylglucosamine transferase, a key enzyme in the formation of SGs, within the IBs [123]. This highlights the efficiency of which HRSV can evade cellular antiviral responses.

1.6 Host cell ion channels

Ion channels are multimeric transmembrane proteins which form an aqueous pore through which charged ions are rapidly and selectively passed across cellular membranes. There are over 300 known channel subunits expressed within human cells. They generally exist in three states: open, inactivated closed, and resting closed, and the stimuli by which they are activated ('gating') include membrane potential (voltage), ligand binding, and environmental factors such as pressure, light, and temperature (Figure 1-6) [124–127]. For the purpose of this thesis, ion channels are classified by the type of ion they are selective for: potassium (K^+), sodium (Na^+), calcium (Ca^{2+}), and chloride (Cl^-) channels. Although, they are sometimes classified by their gating mechanism (e.g., 'voltage-gated channels') or their subcellular localisation (e.g., 'mitochondrial channels').

Ions move across membranes according to their electrochemical gradient, which is a combination of the ion concentration gradient and the electrical gradient (Figure 1-6) [124]. An unequal balance in the concentration of a particular ion drives the movement of those ions from the side of the membrane with the highest concentration to the side of the membrane with the lowest concentration, until an equilibrium is reached. However, as ions are charged particles, another layer of complexity is added in the form of an electrical gradient. If the overall charge at the two sides of the membrane is unequal, the difference in electrical potential drives the movement of ions to achieve a balanced charge [124]. Ion channels do not require an energy input to facilitate the flow of ions, thereby allowing the passage of between 10^6-10^8 ions per second [124]. This is extremely efficient, almost reaching the rate of diffusion in free solution. In contrast, ion transporters

(or pumps) utilise cellular energy to actively transport ions against their electrochemical gradients.

In 2003, Prof Roderick MacKinnon won the Nobel Prize in Chemistry (jointly with Prof Peter Agre) for his work on the structural and mechanistic studies of ion channels. In a landmark 1998 paper, MacKinnon's group outlined the principles underlying of the structure and operation of K^+ channels using x-ray crystallography [128]. They concluded that ion channels were able to achieve their high throughput and maintain the selectivity of ion flux due to their highly specialised structure. Some examples of this are: the entryways to the pore on both sides of the membrane are negatively charged to attract cations and repel anions; the channel pore lining is hydrophobic and relatively inert and the selectivity filter located within the pore is very short (12 Å), minimising the area over which K^+ ions interact with the channel which would slow them down; and, a large, internal, water-filled cavity surrounded by the C-termini of four helices lowers the electrostatic barriers imposed by the lipid bilayer [128].

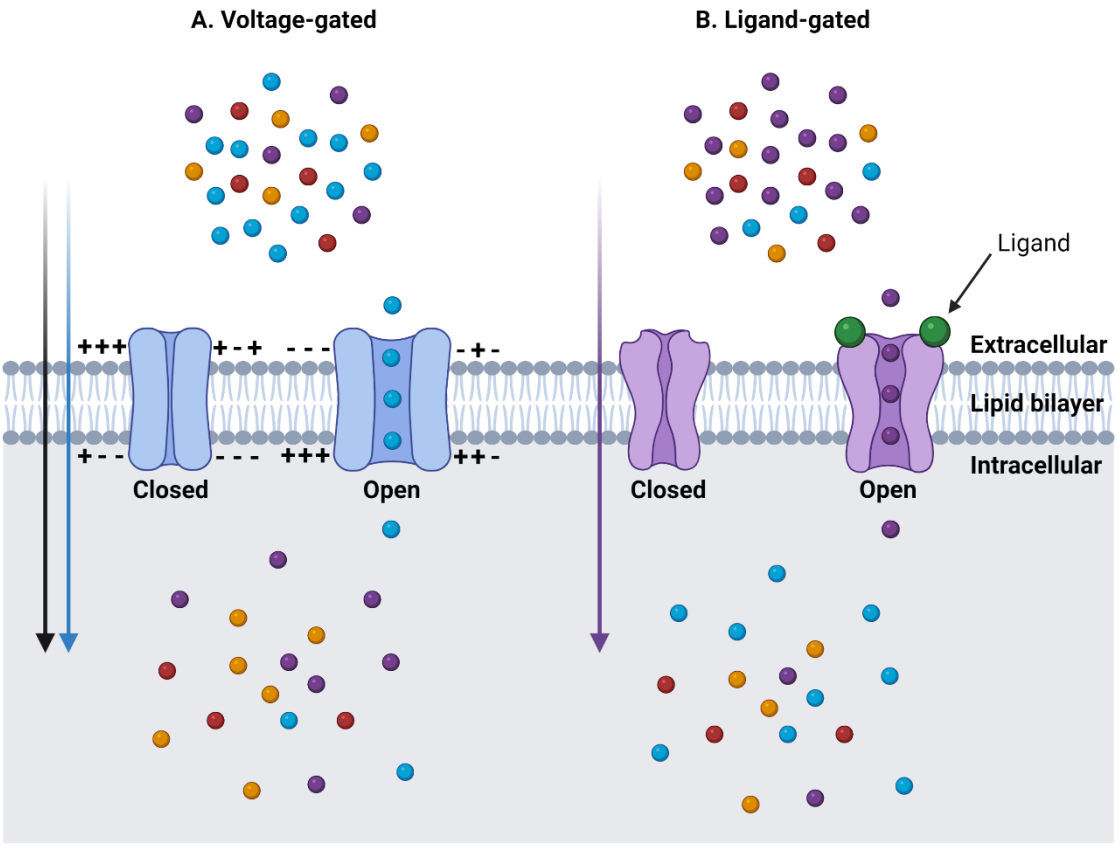

Figure 1-6 Ion channel gating. Ion channels are activated by stimuli such as a change in **(A)** voltage or **(B)** ligand binding (green). This switches the channel from a closed state to an open state, allowing the diffusion of selected ions (coloured circles) through the pore. The ions flow according to the electrochemical gradient, which is influenced by the concentration gradient of the selected ion (coloured arrows) and the electrical potential of the membrane (black arrow).

The most well-known role of ion channels is in the propagation of action potentials in excitable cells such as neurons, muscle cells and cardiac cells to transmit signals to neighbouring cells [124] (Figure 1-7). Briefly, upon the triggering of an action potential, voltage-gated Na^+ channels (Na_v) open and allow the rapid influx of Na^+, therefore depolarising the membrane. When the action potential reaches its peak, the inside of the cell has a net positive charge causing the Na_v channels to close. To repolarise the membrane, voltage-gated K^+ channels (K_v) open and

facilitate the efflux of K^+, causing the membrane potential to return to a negative value. Lastly, there is a refractory period in which the Na_v and K_v channels are inactivated. During this time, the membrane potential falls below the resting value and the Na^+/K^+ ATPase (or pump) actively transports 3 Na^+ out and 2 K^+ into the cell to restore the resting membrane potential [124].

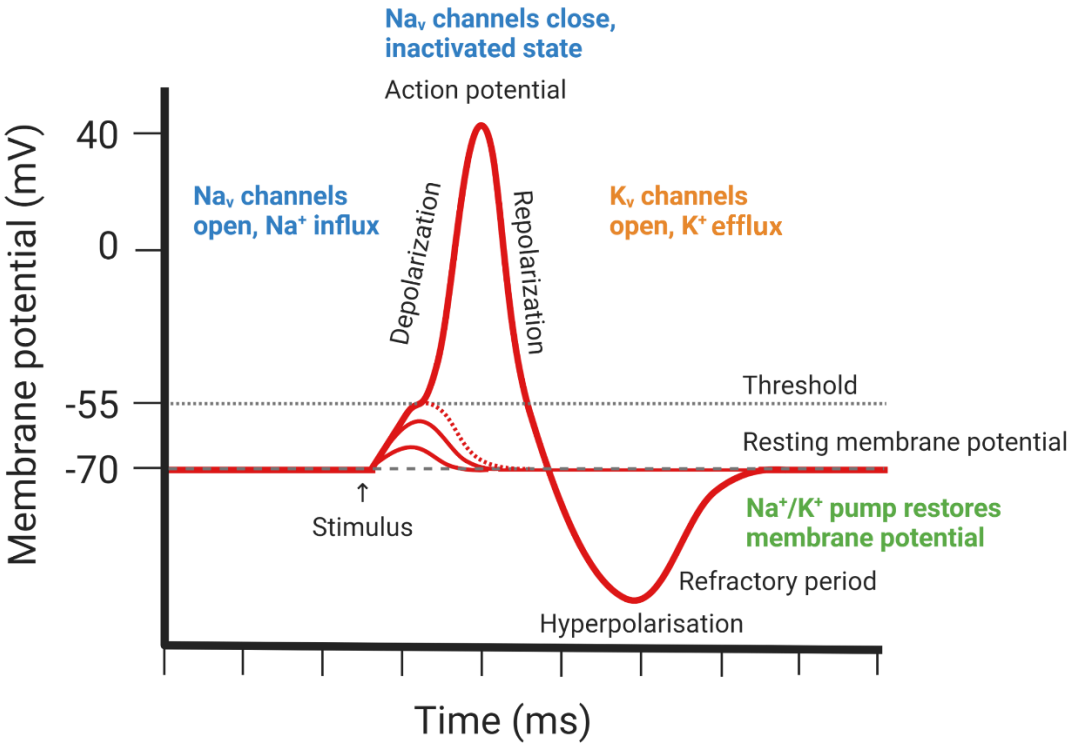

Figure 1-7 The role of ion channels during an action potential. In excitable cells, a stimulus above the threshold triggers the opening of Na_v channels and the rapid influx of Na^+, depolarising the membrane. At the peak of the action potential, the Na_v channels close, and the K_v channels open. K^+ ions move out of the cell, repolarising the membrane. The K_v channels remain open causing the membrane potential to drop below resting state (hyperpolarisation). The action of the Na^+/K^+ pump restores the membrane potential and during this time, another action potential cannot be triggered as the Na_v channels are inactive (refractory period). Created using BioRender.com.

Ion channel activation and activity, both at the cell surface and on intracellular membranes, is crucial for maintaining ionic homeostasis within cells, which is responsible for regulating a wide range of cellular functions. In non-excitable cells, ion channels play vital roles including in cell signalling pathways, volume regulation, transepithelial transport, inflammasome activation, and autophagy [129–133]. Due to their huge influence over cells and tissues, dysfunction in ion channels inevitably leads to diseases, termed channelopathies [134] (discussed further in 1.8). The consequences of such disease can be severe, and intense research has provided us with many chemical compounds that can modulate ion channel activity. As of 2017, approximately 18% of all FDA-approved drugs target ion channel activity [135], second only to those targeting G-protein coupled receptors (GPCRs, 30%), and a promising research avenue is to unlock the potential of these drugs against virus infection.

The subsequent sections give an introduction to each ion channel family. As the work in this thesis concerns Cl^- channels, a more detailed review of this family is provided.

1.6.1 Potassium ion channels

The K^+ ion channel superfamily is the largest and most widely studied channel family. All K^+ channels possess the TXGXG selectivity sequence within the pore domain to allow only K^+ ions to pass [128,136]. Due to the narrowness of the selectivity filter, K^+ ions must lose their associated water molecules to enter. Once dehydrated, carbonyl oxygen atoms associated with the glycine amino acids of the selectivity sequence are precisely positioned to interact with K^+ instead of the water oxygen atoms; this balances out the energy cost of dehydration and stabilises the ion within the pore. The carbonyl oxygens within the pore are also

spaced in such a way that means the presence of a second K^+ ion exerts enough repulsion upon the first K^+ ion that it is forced through the selectivity filter and out the opposite side of the pore. This explains why smaller cations such as Na^+ cannot simply diffuse through K^+ channels, as the carbonyl oxygens are too far apart for Na^+ to efficiently bind all four carbonyl oxygen atoms at the same time, therefore the energy cost of dehydration of Na^+ is not met, and it cannot escape the selectivity filter [128,136].

There are four K^+ channel subfamilies, classified by the number of transmembrane domains (TMDs) they possess as well as their gating properties. These are K_V, Ca^{2+}-activated (K_{Ca}), inwardly-rectifying (K_{IR}) and two-pore (K_{2P}) K^+ channels. The K_V channels are primarily involved in the efflux of K^+ to repolarise the membrane during an action potential (Figure 1-7) [124]. However, they also have roles in non-excitable cells in the regulation of cell volume, exocytosis (e.g., of hormones) and cell death [137–139]. The K_{Ca} channels are a small family which are regulated by intracellular Ca^{2+} concentration ($[Ca^{2+}]_i$), and play roles in cell volume regulation, proliferation (e.g., of lymphocytes) and secretion [140]. The K_{IR} channels are so-called because they facilitate the flow of K^+ into the cell, in contrast to the other K^+ channels which allow the diffusion of K^+ down the electrochemical gradient which is usually outwards. The K_{IR}'s tend to be voltage- or ligand-gated, and play roles in the regulation of action potentials, vasodilation, and muscle contraction [141]. Lastly, the K_{2P} channels possess a slightly different architecture in that two subunits must dimerise in order to form the pore domain (hence their name). Additionally, they are constitutively active and play an important role in the regulation of resting membrane potential by allowing K^+ efflux [142]. Further roles for K_{2P} channels have been described in cytoskeletal

organisation, nociception (the sensing of painful stimuli), cell proliferation (e.g., in prostate cancer cells) and hormone secretion [142,143].

1.6.2 Calcium ion channels

Ion channels which facilitate the movement of Ca^{2+} are generally voltage-gated (Ca_v) or ligand-gated. Ca^{2+} influx into cells through Ca_v not only affects the membrane potential, but also acts as a trigger for many downstream effector proteins and cell signalling pathways. This is because Ca^{2+} is an important intracellular messenger which controls crucial cellular functions including survival, gene expression, exo- and endocytosis, metabolism, muscle contraction and apoptosis [144–146]. Therefore, the $[Ca^{2+}]_i$ is tightly controlled and kept low by the action of various Ca^{2+} pumps which actively transport Ca^{2+} out of the cell. Stimulation by membrane depolarisation activates Ca_v on the plasma membrane and results in an increase in $[Ca^{2+}]_i$ [144]. The presence of high voltage activated, long lasting (L-type) and low voltage activated, transient (T-type) Ca_vs allows the cell to fine tune the $[Ca^{2+}]_i$ [147]. The remaining Ca_v family members are mainly expressed within the central nervous system (CNS): P-type, expressed in Purkinje neurones; N-type, expressed in nerves; and R-type, ‘residual’, expressed in cerebellar granule cells [147].

Extracellular or intracellular ligands of Ca^{2+} channels can also influence Ca^{2+} signalling. In non-muscle cells, the ER stores Ca^{2+} away from the cytoplasm, which can be released following the binding of secondary messengers to ligand-gated Ca^{2+} channels on the ER membrane [146]. This generally occurs through the binding of inositol trisphosphate (IP3) to its receptor (IP3R) [144,148]. In muscle cells, the Ca^{2+} stores are located within the sarcoplasmic reticulum (SR) and are released by ryanodine receptors [149]. Another example of a ligand-

gated Ca^{2+} channel is the two-pore Ca^{2+} channel 2 (TPC2) which is activated by the binding of the secondary messenger nicotinic acid adenine dinucleotide phosphate (NAADP) and facilitates the release of acidic Ca^{2+} stores (i.e., from endosomes, lysosomes, and other acidic organelles, rather than from the ER/SR) [150].

As the extracellular concentration of Ca^{2+} is lower than that of other ions such as Na^{+} which is of a similar size, Ca^{2+} channels must be highly selective. Like K^{+} channels, Ca^{2+} channels rely on precise spacing of Ca^{2+} binding sites to generate a repulsion force between two bound ions to facilitate rapid movement through the channel [151,152]. However, in contrast to K^{+} channels, the Ca^{2+} channel selectivity filter contains a highly conserved EEEE sequence, the side chains of which reach into the pore and bind Ca^{2+} [153]. Furthermore, Ca^{2+} is thought to remain hydrated during movement through the channel [152].

1.6.3 Sodium ion channels

The most well-known Na^{+} channels are the Na_vs associated with the membrane depolarisation during the propagation of action potentials in excitable cells. Na_vs are opened once the membrane potential passes a voltage threshold, this ensures that action potentials are only triggered when necessary (Figure 1-7) [124]. Another important feature of Na_vs is the inactivation gate, which essentially plugs the pore following membrane depolarisation to ensure the unidirectional movement of the action potential along the neurone or muscle fibre [124,154]. The specificity of Na_vs is mediated by a highly conserved DEKA amino acid sequence within the selectivity filter wherein the basic lysine side chain is thought to be the key factor in allowing Na^{+} movement whilst blocking K^{+} [155].

Ligand-gated Na^+ channels are expressed at the neuromuscular junction and play an important role in stimulating an action potential by depolarising the membrane in response to neurotransmitters such as acetylcholine transmitted from a neighbouring neurone [124]. These channels are referred to as nicotinic acetylcholine receptors and are less selective than Na_v, being permeable to K^+, and in some cases Ca^{2+}. However, due to the large electrochemical gradient of Na^+ that exists at resting membrane potential, the opening of these receptors triggers a large influx of Na^+ [124]. Roles for Na^+ channels have also been described in non-excitable cells, including in endocytosis and cell migration [156,157].

1.7 Chloride ion channels

Cl^- ion channels are less well understood than their cation counterparts, mainly due to a historic lack of interest and research [158]. It was previously assumed that Cl^- channels only served to maintain the electrochemical equilibrium across cell membranes, however, since the discovery of important Cl^- channelopathies such as cystic fibrosis (CF) and myotonia congenita (1.8), research into this channel family has increased and has consequently revealed that Cl^- is responsible for a myriad of functions within the cell.

In contrast to cation channels, Cl^- channels do not exhibit exclusive selectivity for Cl^- and are often permeable to other anions such as bromide (Br^-), iodide (I^-), thiocyanate (SCN^-) or bicarbonate (HCO_3^-) with the sequence of permeability differing between the Cl^- channel subfamilies [159–161]. For this reason, they are sometimes referred to as anion channels. At a physiological level, generally only Cl^- and HCO_3^- ions are present in substantial concentrations and most anion

channels have a preference for Cl^- over HCO_3^-, however discrimination between the two does not appear to be vital [160].

Categorisation of Cl^- channels into families is not universally standardised. Broadly speaking, five major families exist: cystic fibrosis transmembrane conductance regulator (CFTR), voltage-gated Cl^- channels (ClCs), ligand-gated Cl^- channels (LGCCs), Ca^{2+}-activated Cl^- channels (CaCCs) and volume-regulated anion channels (VRACs). Additionally, other types of Cl^- channels described include the Cl^- channel accessories (CLCA), and Cl^- intracellular channels (CLICs) [158].

1.7.1 Cystic fibrosis transmembrane conductance regulator

The *CFTR* gene encodes an anion channel which is a member of the ATP-binding cassette (ABC) transporter superfamily. As such, the CFTR protein structure (Figure 1-8 A) has two TMDs (1 and 2), consisting of six segments each, which form the channel pore. Each TMD is followed by a cytosolic nucleotide binding domain (NBD) which mediate the gating of the channel, and between the two TMD-NBD complexes lies a unique regulatory domain which is responsive to phosphorylation [162,163]. The regulatory domain is phosphorylated by protein kinase A which in turn increases the open probability of the channel. However, gating of CFTR is also controlled by the binding of ATP to the NBDs [164,165]. When open, the CFTR allows the passage of Cl^- and HCO_3^-.

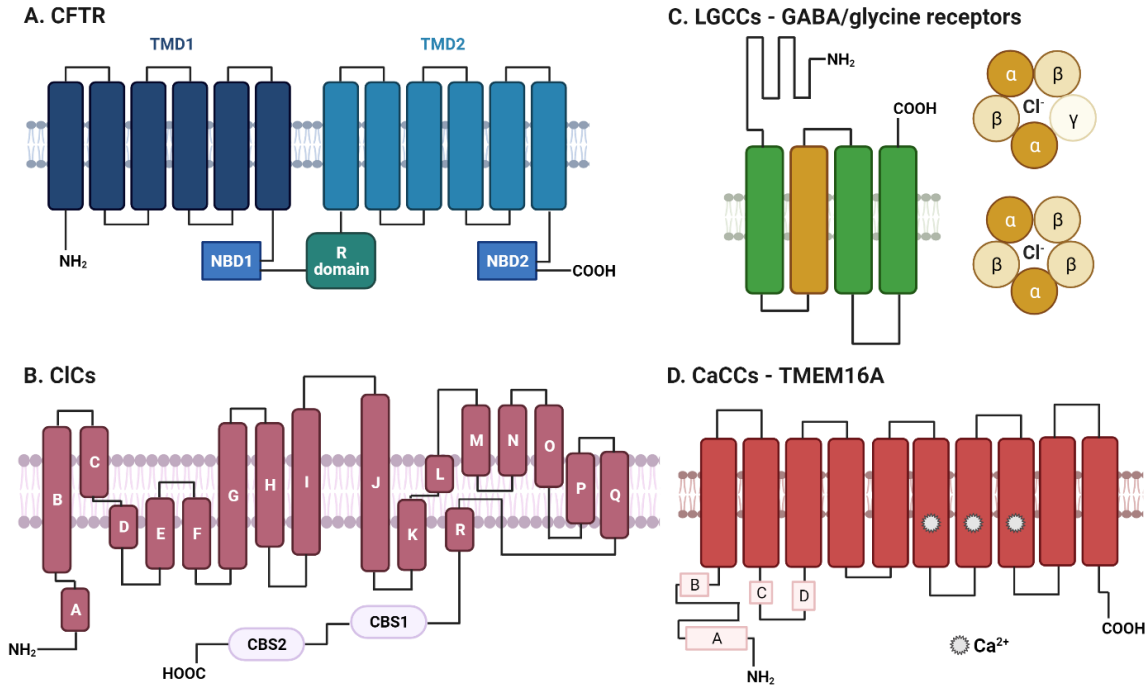

Figure 1-8 Schematic representation of the structures of Cl^- channels. **A)** The CFTR contains 12 membrane-spanning segments making up two transmembrane domains (TMD1/2). At the end of each TMD lies a nucleotide binding domain (NBD1/2) and a regulatory (R) domain lies in between the two TMDs. **B)** The ClC channels consist of 18 segments (A-R), 17 of which span the membrane at least partially. The cytosolic N-terminal A segment does not span the membrane. Two cystathionine-β-synthase (CBS1/2) domains are located at the C-terminus. **C)** LGCCs, or GABA and glycine receptors, consist of 4 transmembrane segments with a large N-terminus and short C-terminus at the extracellular side of the membrane. The second helices of each subunit (yellow) form the central pore within the pentameric conformation (yellow circles). GABA-A pentamers are made of 2α:2β:1γ subunits and glycine receptors of 2α:3β subunits. **D)** The CaCCs, exemplified by TMEM16A, have 10 membrane-spanning helices with structured cytosolic N and C termini. Ca^{2+} binds at sites located on helices 6, 7 and 8. Adapted from [166,167] and created using BioRender.com.

Expression of the CFTR occurs in epithelial cells in many organs of the human body, including the respiratory tract, gastro-intestinal tract, and reproductive tract,

as well as sweat and salivary glands. The active transport of Cl^- through the CFTR drives passive Na^+ transport out of the epithelium and ultimately creates an osmotic driving force resulting in water secretion [168]. This is essential in these tissues to produce digestive fluids, mucus and sweat. The opposite of secretion is a process called absorption in which Na^+ and other ions travel into the epithelium. The epithelial Na^+ channel (ENaC) is responsible for the active transport of Na^+ into the cell, which promotes passive Cl^- transport down an electrochemical gradient into the cells. The salt concentration gradient allows water to be absorbed through osmosis. Figure 1-9 depicts the processes of secretion and absorption in airway epithelial cells.

The CFTR is probably the most well-known Cl^- channel and this is because its dysfunction is the cause of CF. In the respiratory tract, the airway surface liquid (ASL) is a thin layer of liquid which lines the epithelial cells to protect them from air and help in the removal of microbes in a process called mucociliary clearance [168]. Through the secretion mechanism described above, the CFTR contributes to the balance of Cl^- and HCO_3^- in the ASL which, alongside the function of ENaC, is vital to maintain a healthy airway (Figure 1-9) [169]. When the CFTR is mutated, the ASL becomes dehydrated resulting in an increase in mucus viscosity and a reduction in antimicrobial functions, causing the symptoms of CF (further discussed in 1.8) [168,169].

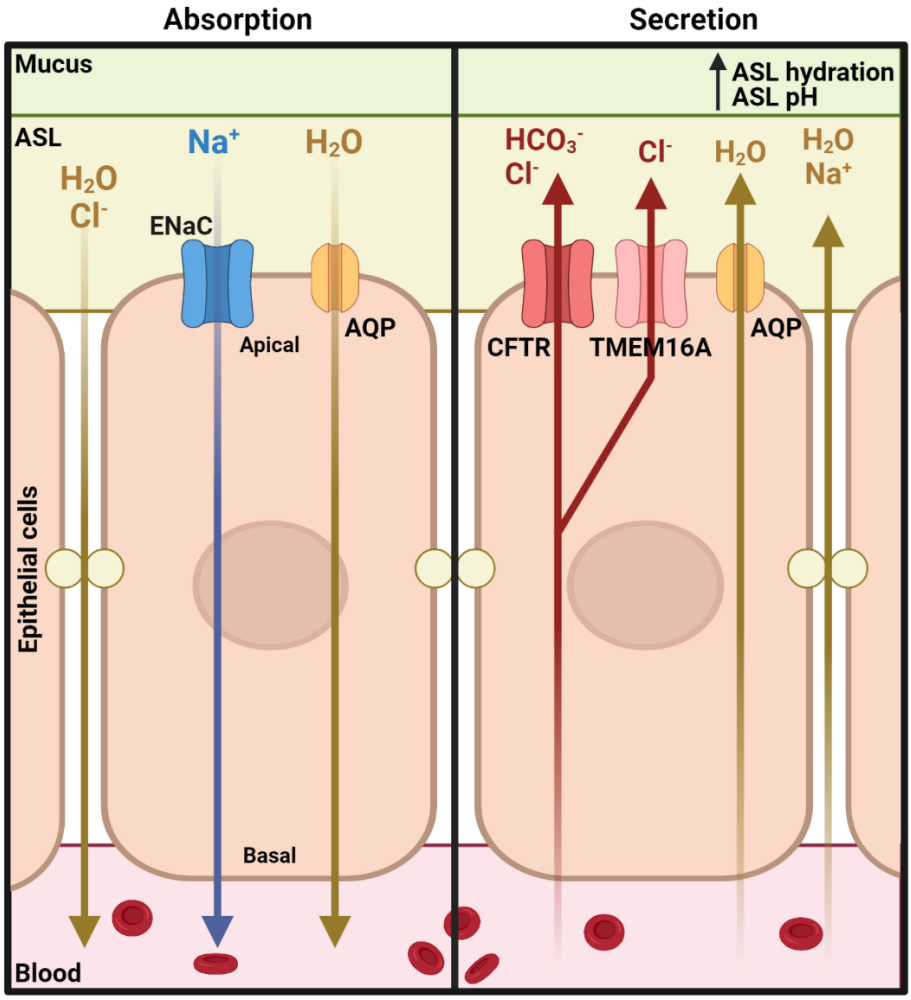

Figure 1-9 The processes of apical absorption and secretion in airway epithelial cells. Absorption: ENaC transports Na^+ into cells, driving absorption from the ASL and mucus lining to create an electrochemical gradient for paracellular passive Cl^- transport. Water is absorbed by osmosis though aquaporins (AQP) or paracellularly. Secretion: The CFTR drives secretion of Cl^-, helped by other Cl^- channels such as TMEM16A. The active transport of Cl^- out of the cells drives Na^+ movement paracellularly which causes water to move into the ASL by the para- or transcellular route. Adapted from [168].

1.7.2 Voltage-gated chloride channels

There are nine proteins that are recognised as ClC family members (Table 1-1) (reviewed in [170,171]). The first four, ClC-1, ClC-2, ClC-Ka, ClC-Kb, are voltage-

gated Cl^- channels that are expressed on cell membranes. The remaining family members, ClC-3 to ClC-7, are Cl^-/hydrogen ion (H^+) exchangers expressed on intracellular membranes which actively transport 2 Cl^- ions per H^+ [172]. The existence of ion channels and transporters within one family is rare, as the two are usually structurally distinct and require vastly different energy inputs, however the amino acid sequences of the ClC channels and transporters are remarkably similar.

The general ClC structure is complex, consisting of 18 helices (A-R), 17 of which span the membrane and two cystathionine-β-synthase (CBS1/2) domains follow at the cytosolic C-terminus [167] (Figure 1-8 B). The function of the CBS domains is thought to be regulatory but is not well understood [171]. The ClCs assemble as homodimers, each with the ability for independent ion transport, with either subunit or both contributing to conductance at one time, called double-barrel gating. Within the pore, there are three Cl^- binding sites: the internal site (S_{int}), the central site (S_{cen}) and the external site (S_{ext}) [173]. An important glutamate at position 148 (E148, helix F) known as the glutamate gate (or Glu_{gate}) is crucial for the distinction between Cl^- channel and transporter functions in ClCs [173]. In transporters the Glu_{gate} swings between S_{cen} and S_{ext} and competes with Cl^- for binding, resulting in 2 Cl^- ions moving through the pore. One H^+ from the cytosol protonates Glu_{gate} at S_{cen}, after which the Glu_{gate} swings to the extracellular side to release the H^+ [174]. A kinetic barrier present in the transporter stops the leakage of Cl^- through the pore when the Glu_{gate} is in the extracellular configuration. In contrast, structural analysis of ClC-1 (channel) has shown that the Glu_{gate} does not block the Cl^- pore in the depolarised membrane, allowing the fast flow of Cl^- [175]. In addition, the pore is also a little wider in ClC-1 than in the

transporters. At resting membrane potential, the Glu_{gate} may occupy the S_{cen} or S_{ext} sites of ClC-1, effectively closing the channel pore. This mechanism may also exist for ClC-2; however, the ClC-K proteins do not possess a Glu_{gate} and therefore the pore is not blocked and remains open. Mutation of the Glu_{gate} in ClC transporters renders them 'channel-like', producing constitutive activity [172].

As summarised in Table 1-1, the expression of the ClC channels ClC-1 and ClC-Ka/b are specific to the skeletal muscle, and the kidneys and inner ear respectively, whereas ClC-2 is widely expressed in numerous tissue types such as the brain, heart, lungs, kidney, pancreas, liver, skeletal muscle, and gastro-intestinal tract [170]. The physiological role of ClC-1 in the skeletal muscle is in the repolarisation of the muscle fibre following an action potential and mutation in ClC-1 leads to muscle disorders such as myotonia congenita, the most common skeletal muscle hereditary channelopathy in humans, for which there is no specific treatment [176] (discussed further in 1.8). The other three channels of the ClC family have roles in transepithelial transport. ClC-2 dysfunction is implicated in a variety of diseases such as azoospermia, leukodystrophy, degeneration of the retina, epilepsy and many more (reviewed in [177]) due to its ubiquitous expression. The ClC-K proteins are slightly different to the other channels in that they require an accessory protein – barttin - for their function, stability, and trafficking. Mutation of ClC-K proteins or barttin cause both renal salt loss (Bartter syndrome) and deafness, highlighting their importance in the tissues to which they are localised.

The ClC transporters are involved in the endosomal pathway: ClC-5 is expressed in early endosomes, ClC-3 and -6 are found in late endosomes and ClC-7 in lysosomes, with the sub-cellular localisation of ClC-4 being less clear. Along the

endosomal pathway, a pH gradient exists. The acidification of endosomes is achieved by the influx of protons through the H^+-ATPase (proton pump), and Cl^- provides the electrical shunt required for this. Perhaps counterintuitively, computational modelling revealed that the presence of $2Cl^-/H^+$ exchangers on endosomal membranes can facilitate a more acidic endosomal pH than a Cl^- channel [178] even though they require the loss of a proton from the endosome for every two Cl^- that enter, and it is thought that Cl^- may play a separate role in endocytosis.

ClC-5 is the most well-studied ClC transporter due to its role in Dent's disease [179], an x-linked kidney disorder characterised by poor absorption of low molecular weight proteins (proteinuria), dysregulation of Ca^{2+} transport (hypercalciuria), calcium deposits in the renal tissues (nephrocalcinosis) and renal failure [180]. It is expressed predominantly in the kidneys and plays a crucial role in receptor-mediated and fluid-phase endocytosis. Mutations in the gene encoding ClC-5 occurs in ~60% of Dent's disease patients, resulting in impaired endosomal acidification and decreased endocytosis of low molecular weight proteins in the proximal tubule cells. However, of the over 100 mutations associated with Dent's diseases, few have been functionally characterised and the mechanism by which ClC-5 contributes to disease is still debated [170,171,180].

ClC-7 is unique among the ClC transporters as it requires a β-subunit called Ostm1 for normal function [181]. ClC-7/Ostm1 mutation results in osteopetrosis, a disease characterised by increased bone density [182]. Osteoclasts are the cells responsible for the dissolution and absorption of bone and they mediate this using their acidic lysosomes. The lysosomes insert into the ruffled border of

osteoclasts and release their contents to acidify the resorption lacuna, which is the space between the osteoclast ruffled border and the bone [170]. Loss of ClC-7 impairs the acidification of the resorption lacuna, rendering the osteoclast unable to break down the bone leading to osteopetrosis [182].

The remaining three ClC transporters are not as well characterised and have not been linked to specific human diseases, however mouse models do exhibit important phenotypes such as retinal and brain degeneration (ClC-3 KO) and lysosomal storage disease (ClC-6 KO) (reviewed in [170,171]).

Table 1-1 Mammalian ClC channels and transporters. A summary of the tissue expression, functions and disease states associated with voltage-gated chloride channels (ClCs). Essential (/) and non-essential (±) subunits are shown. Adapted from ([170,171]).

Protein	Expression	Function	Human Disease
ClC-1	Skeletal muscle	Stabilisation of membrane potential	Myotonia congenita
ClC-2 ±glialCAM	Wide (brain, kidney, liver, heart, pancreas, skeletal muscle, lungs, GI tract)	Transepithelial transport, extracellular ion homeostasis, regulation of excitability	Leukodystrophy, azoospermia, Blindness, male infertility,
ClC-Ka /barttin	Kidney, inner ear	Transepithelial transport	
ClC-Kb /barttin	Kidney, inner ear	Transepithelial transport	Bartter syndrome type III (renal salt loss)
ClC-3	Wide (brain, retina, adrenal gland, pancreas, intestines, epididymis, kidney, liver, skeletal muscle, heart)	Acidification and ion homeostasis of late endosomes	
ClC-4	Skeletal muscle, brain, heart	Ion homeostasis of endosomes	Epilepsy
ClC-5	Kidney, intestine	Acidification and ion homeostasis of endosomes	Dent disease
ClC-6	Neurones	Ion homeostasis of late endosomes	
ClC-7 /Ostm1	Brain, kidney, liver, bone	Lysosomal ion homeostasis and acidification osteoclast resorption lacuna	Osteopetrosis, retinal degeneration, lysosomal storage disease

1.7.3 Ligand-gated chloride channels

The LGCC family comprises two types of receptors: γ-aminobutyric acid (GABA)-dependent channels and glycine-dependent channels which play important roles in the CNS [166]. Both channels form a pentameric structure, and each subunit consists of four transmembrane segments with a large extracellular N-terminal domain and a short extracellular C-terminus with the second segment in each subunit forming the central pore (Figure 1-8 C). For glycine receptors, there are four types of α subunit ($\alpha_{1–4}$) and one β subunit, with each pentamer comprising 2α:3β [183]. GABA receptors are a little more complex having a selection of 19 different subunits: $\alpha_{1–6}$, $\beta_{1–3}$, $\gamma_{1–3}$, δ, ε, π, θ and $\rho_{1–3}$. GABA-A receptors are formed by 2α:2β:1γ subunits, and GABA-C receptors are homo- or heteromers of the $\rho_{1–3}$ subunits only [166,184]. (GABA-B receptors are GPCRs and do not belong to the LGCC family). Consequently, there are many isomers of the GABA receptor.

In the CNS, GABA and glycine are inhibitory neurotransmitters which bind to their corresponding LGCC receptors in the brain and spinal cord respectively. The extracellular N-terminal domain of the channel is the target site for GABA and glycine, and binding triggers conformational changes firstly at the N-terminus, and then in the transmembrane domains, opening the channel pore [185]. This initiates an influx of Cl^- which results in membrane hyperpolarisation, therefore suppressing excitability of the target cell [186]. These inhibitory pathways are crucial to the function of the CNS and a loss of GABA-A receptor expression has been linked to prevalent neurological conditions such as Parkinson's [187], Alzheimer's [188] and Huntington's [189] diseases, and epilepsy [190]. Similarly,

glycine receptor dysfunction has been linked to hyperekplexia [191] and autism [192].

1.7.4 Calcium-activated chloride channels

As the name suggests, CaCCs are activated by intracellular Ca^{2+} ions leading to channel opening and flow of Cl^- ions. Two protein families have so far been identified as CaCCs; the bestrophins were described as CaCCs in 2003 [193], followed by the identification of the TMEM16 proteins, also called anoctamins, by three independent studies in 2008 [161,194,195]. The structures, physiological functions, and links to human disease of these channel families are outlined below.

1.7.4.1 Bestrophins

The human bestrophin family consists of four, structurally conserved members (Best1-4) which exhibit different expression patterns in humans. All four bestrophins are now thought to encode CaCCs [193]. The crystal structure of chicken Best1 reveals that the channels are pentameric, with each monomer comprising four transmembrane domains. Overall, a funnel configuration is described with an outer entryway, a narrow hydrophobic gate controlled by a 'Ca^{2+} clasp' and an anion selectivity filter within the neck region, and a large inner cavity [196].

Best1 is the most well-characterised member of the family; it was discovered as the protein product of the gene responsible for Best vitelliform macular dystrophy, a rare genetic form of macular degeneration which is characterised by the breakdown of the retinal pigment epithelium (RPE), eventually leading to a complete loss of central vision whilst the peripheral vision remains

unaffected [197]. The basolateral membrane RPE is the major site of high Best1 expression, where it has a role in anion flux, regulating intracellular Ca^{2+} signalling, and volume regulation [198,199]. Best1 is also expressed in other epithelial and non-epithelial cells and has since been associated with other retinal degenerative disorders named the bestrophinopathies, which are currently untreatable [200].

The other three bestrophins are less well studied and have not yet been linked to any human disease. Best2 is expressed in the colonic goblet cells and in sweat glands where it facilitates bicarbonate transport [201,202]. The expression of Best3 is more widely distributed and is thought to have protective roles against cellular stresses and inflammation [200,203]. Lastly, Best4 is also expressed in the colon, however its role there is yet to be elucidated [202].

1.7.4.2 TMEM16 proteins (Anoctamins)

The mammalian TMEM16 protein family consists of 10 members (TMEM16A-K, excluding I, or ANO1-10). Between the 1980s and 2008, Ca^{2+}-activated Cl^- currents had been identified in many cell types however the identity of the channels responsible remained elusive until three studies independently identified TMEM16A as a CaCC [161,194,195]. The following year, TMEM16B was also identified as a CaCC [204]. Rather intriguingly, despite being closely related, the rest of the TMEM16 proteins do not share this function. The majority of the TMEM16 family are Ca^{2+}-activated lipid scramblases which facilitate the bidirectional movement of lipids within the bilayer of membranes [205–207]. Furthermore, the TMEM16 scramblases have a dual functionality and have been shown to conduct ions in a non-selective manner. In contrast, the TMEM16A/B channels are highly selective for anions and do not function as scramblases [208].

Phylogenetic analysis predicts that the TMEM16 channels descended from a scramblase but have since lost this function [205]. Interestingly, a single point mutation has been shown to confer scramblase function to TMEM16A [209].

The TMEM16 channels comprise 10 transmembrane helices with structured cytosolic N and C termini (Figure 1-8 D) and exist as homodimers on the cell membrane. TMEM16A is the best characterised protein of the family, and the structure of the mouse analogue (mTMEM16A) has been resolved by cryo-electron microscopy in the presence and absence of Ca^{2+} allowing the study of the gating mechanism of the channel [210–212]. Structural analysis revealed residues on helices α6, α7 and α8 that are important for Ca^{2+} binding. When two Ca^{2+} are bound on α7 and α8, the resulting positive charge density attracts the lower half of α6 which moves via a hinge mechanism towards the bound Ca^{2+}. This movement closes access to the Ca^{2+}-binding sites whilst simultaneously opening the Cl^- pore to allow the flow of ions across the membrane [210]. Alternative splicing of segments A-D produces various isoforms of TMEM16A which can alter properties of the channel [213]. For example, isoforms containing segment B have a higher Ca^{2+} sensitivity, whereas segment C influences the voltage-dependence of the channel.

Due to its wide distribution, TMEM16A is involved in many physiological functions throughout the body. The channel is expressed in a wide range of cell types, including epithelial cells, smooth muscle cells, neuronal cells, and myocardial cells [214–216] and many functions have been reported in each instance [158,208,217], examples of which are detailed below.

The physiological role of TMEM16A in the airway is complex (Figure 1-10). TMEM16A is primarily expressed at the apical surface of secretory airway

epithelial cells (as well as some intracellular and basolateral expression) where it facilitates the release of Cl^-, contributing to the maintenance of the ASL (Figure 1-10 A) [218,219]. Ca^{2+} signalling is important in the airway epithelia as it drives the activity of both TMEM16A and CFTR as well as inhibiting the absorption of Na^+ via ENaC. As previously outlined in section 1.7.1, the balance of ions in the ASL determines the direction of the osmotic driving forces to control its hydration. There is evidence to suggest that TMEM16A regulates local Ca^{2+} signalling by co-localising with ATP-activated receptor P2Y at the apical cell surface (Figure 1-10 C) [220,221]. When P2Y is stimulated by free ATP in the mucosal lining of the airway, it sends signals to the IP3R on the ER, which stimulates Ca^{2+} release from stores. TMEM16A tethers the ER to the apical surface of the membrane through interaction with IP3R to create a compartment in which it can control local Ca^{2+} signalling [222]. The increase in local Ca^{2+} drives CFTR activity by stimulating the production of cAMP [219], therefore the activity of CFTR is dependent on TMEM16A.

In goblet cells, intracellular Ca^{2+} signalling stimulates the exocytosis of mucin from the apical surface into the airway linings (Figure 1-10 B). TMEM16A is greatly upregulated in mucus-producing goblet cells during airway inflammation, CF and asthma, and a role for the channel in both mucus production and secretion in goblet cells has been suggested [223–225], but is controversial [226]. Therefore, whilst some studies conclude that potentiation of TMEM16A to compensate for abolished CFTR function is necessary for CF patients (reviewed in [227]), others suggest that inhibition of TMEM16A would prevent the thickening of the mucus layer and provide a therapeutic benefit for CF patients (reviewed in [220]). Further investigation into the role of TMEM16A in the airway is warranted.

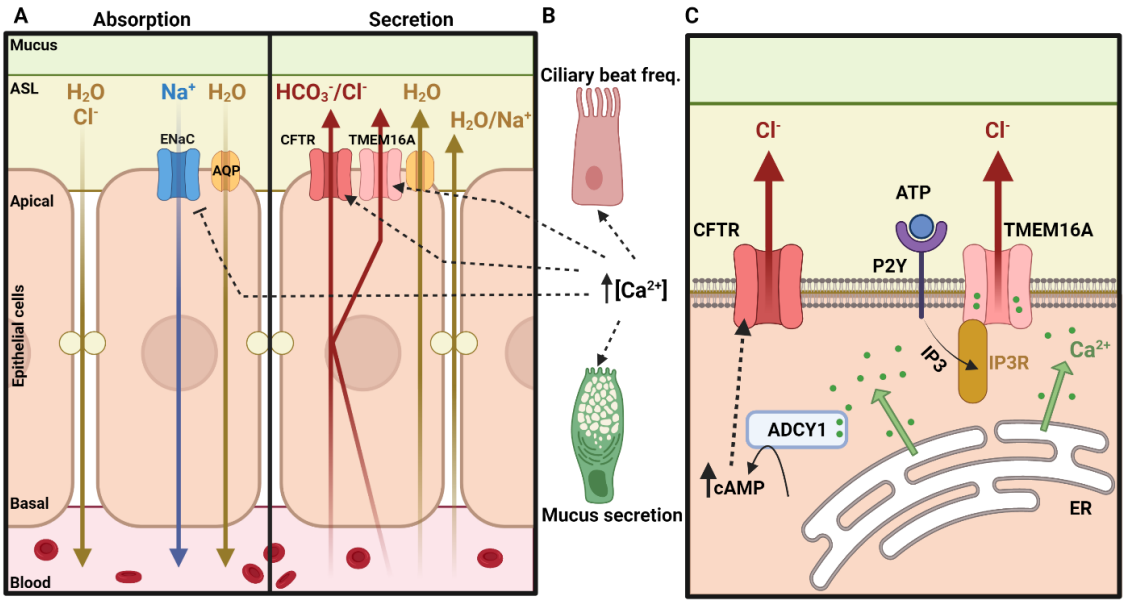

Figure 1-10 The role of TMEM16A in the airway. **A)** The processes of apical absorption and secretion in airway epithelial cells, as shown in Figure 1-9. **B)** The role of intracellular Ca^{2+} signalling in the airway. Increasing intracellular Ca^{2+} hydrates the ASL by inhibiting Na^+ absorption through ENaC, and by activating Cl^- secretion via TMEM16A and CFTR. The increased Ca^{2+} also initiates mucin exocytosis from goblet cells, which forms a mucus gel lining the airway and regulates mucociliary clearance. Ciliated cells move the mucus along the airway, the rate of which increases in response to Ca^{2+}. Adapted from [227]. **C)** Regulation of intracellular Ca^{2+} signalling by apical TMEM16A. TMEM16A interacts with P2Y receptors and IP3 receptors (IP3R) on the ER, which tethers it to the apical membrane. Free ATP binding to P2Y triggers cell signalling pathways causing Ca^{2+} release from ER stores. This creates a local high-Ca^{2+} environment which stimulates the production of cAMP through adenylate cyclase type 1 (ADCY1) and activates the CFTR via protein kinase A. Adapted from [220,222]. Created with BioRender.com.

TMEM16A activity is also important in smooth muscle cells; including vascular cells that line blood vessels, and the interstitial cells of the Cajal (ICC) which are the pacemaker cells of the gastrointestinal (GI) tract. TMEM16A facilitates Cl^- outflux in response to an intracellular build-up of Ca^{2+}, which results in membrane

depolarisation and ultimately smooth muscle contraction. In rat models of pulmonary hypertension, increased expression of TMEM16A was observed [228]. The rats were sensitive to CaCC modulation and furthermore, TMEM16A specific blockers were shown to induce vasorelaxation in mouse and human arteries [229], implicating this channel as a potential target for treatment of pulmonary hypertension. In the GI tract, smooth muscle contractions are controlled by slow waves generated by the ICC. TMEM16A knockout resulted in diminished slow wave activity in mice [214], and TMEM16A activators have been shown to promote smooth muscle cell contractions in guinea pig ileum [230], highlighting potential for TMEM16A modulation to treat GI disorders.

Another role for TMEM16A is described in nociceptors, which are the peripheral nerve endings of dorsal root ganglion (DRG) neurones that detect potentially harmful stimuli such as heat, mechanical or chemical stress and convert them into electrical signals for the CNS [231]. There are various stimuli that can increase intracellular [Ca^{2+}] in DRG neurones leading to TMEM16A activation [232]. These include inflammatory mediators such as bradykinin, serotonin or proteases which are released in response to tissue damage [233]. These mediators activate GPCRs on the surface of DRG neurones which signal through IP3R to trigger the release of ER Ca^{2+} stores. Upon TMEM16A activation and Cl^- efflux, the membrane becomes depolarised, and more action potentials can be propagated, leading to an amplification of pain sensation [232]. CaCC inhibitors have been shown reduce acute and inflammatory nociception in animal models [234,235], leading to the possibility of their use in pain management.

It is necessary for cells to regulate their volume under changing conditions. In hypertonic environments, cell volume initially increases due to osmotic uptake,

and volume-regulated Cl^- currents cause regulatory volume decrease (RVD) back to their original size [236]. In mice lacking TMEM16A, these Cl^- currents are reduced and RVD is impaired [237]. Cell volume regulation is critical for processes such as cell proliferation, migration, and apoptosis.

Perhaps most surprising is the role that TMEM16A plays in tumorigenesis. This is an extensive field of research that has been recently reviewed [238,239]. TMEM16A is overexpressed in many human cancers including head and neck squamous cell carcinomas, breast, brain, colorectal, oesophageal, endometrial, gastric, liver, lung, pancreatic, parotid, and prostate cancers [238–252]. The chromosome which harbours the TMEM16A gene in humans – 11q13 – is amplified in many of these cancers [253,254], however this is not the only mechanism of overexpression. This leads to the dysregulation of several signalling pathways resulting in enhanced cell proliferation, apoptosis resistance, tumour growth and migration. The role of TMEM16A in cancer is multifaceted, and a wide range of cancer-related functions have been proposed including roles for both the TMEM16A protein itself, as well as TMEM16A channel activity.

The physiological roles of TMEM16B are less well characterised. Expression of TMEM16B has been reported within the CNS, including in the olfactory epithelium [255], hippocampus [256], thalamus [257], cerebellar cortex [258] and amygdala [259] where it plays an important role in action potential firing in response to Ca^{2+} signalling in neuronal cells. Mice lacking TMEM16B show impaired motor control and learning, longer displays of aggression, and a reduction in anxiety and fear, indicating an important role for TMEM16B in the regulation of these behaviours [260–262].

1.8 Channelopathies

As previously alluded to, due to their crucial roles in a variety of cellular functions, the dysfunction of ion channels is a major cause of human disease [134]. Channelopathies can result from genetic or acquired factors which contribute to defective channel function. In excitable cells, defects in ion channel function impair the ability of the cell to regulate action potential firing. An example of this is long QT syndrome, wherein action potentials in cardiac muscle cells are slowed down due to an inability to repolarise the membrane. Loss-of-function mutations in the genes encoding $K_V7.1$ (also known as K_VLQT1) [263] or $K_V11.1$ (also known as hERG) [264] prevent the K^+ influx during repolarisation. Gain-of-function mutations in $Na_V1.5$ delay channel inactivation following depolarisation, also resulting in long QT syndrome [265]. This causes cardiac arrythmia (irregular heartbeat) which can lead to symptoms such as fainting, seizures or even sudden death. Conversely, gain-of-function mutations in $K_V7.1$ [266], $K_V11.1$ [267], or $K_{IR}2.1$ [268] result in short QT syndrome in which action potentials occur more quickly, causing atrial fibrillation (abnormally fast heartbeat) and symptoms such as breathlessness, palpitations and fatigue.

Channelopathies of the CNS include skeletal muscle disorders, epilepsy, migraines, blindness, deafness, and peripheral pain syndromes [134]. For example, myotonia congenita is a the most frequent skeletal muscle channelopathy and it is caused by loss-of-function mutations in the gene encoding ClC-1 [176,269]. When K^+ leaves the cell during the repolarisation stage of an action potential, it creates a large K^+ concentration gradient which could depolarise the membrane, therefore Cl^- influx through ClC-1 compensates for this, stabilising the repolarisation of the membrane (Figure 1-7). When this is

impaired, spontaneous repetitive firing of action potentials and a slower rate of repolarisation occur, causing the muscle stiffness associated with this disease. Moreover, certain types of epilepsy are caused by dysfunctional channels in GABAergic neurones [134,270]. Loss-of-function mutations in $Na_V1.1$ [271] or gain-of-function mutations in GABA-A [272] both lead to a reduction in the excitability of GABAergic neurones by preventing Na^+ influx and therefore membrane depolarisation, or by enhancing Cl^- influx and therefore increasing membrane hyperpolarisation, respectively. This results in a type of epilepsy called Dravet syndrome which is the most severe form of epilepsy and is characterised by prolonged seizures, behavioural disorders, cognitive impairment, and motor defects [134,270].

The most well-studied channelopathy is CF, with causative mutations within the *CFTR* gene identified in 1989 [273]. Before then, CF was defined “the most common life-threatening inherited disorder of children in Caucasian populations”. However, thanks to the implementation of genetic screening policies, as well as the development of CFTR modulator therapies, patients are now surviving well into adulthood and the global incidence of CF has decreased from 1/2500 live births to between 1/3000-1/6000 live births [274]. More than 2,000 mutations in the gene encoding CFTR have now been identified (according to the Cystic Fibrosis Mutation Database [275]), however around two-thirds of CF cases are caused by just one of these mutants, ΔF508, which cannot fold properly and is consequently not trafficked to the plasma membrane [276,277]. As previously detailed in 1.7.1, a lack of CFTR function results in the loss of Cl^- secretion from cells, which is important for the hydration of the ASL. In CF patients, the ASL becomes a thick, sticky mucus layer which can block up the airways and lead to

difficulty breathing [168,169]. Furthermore, due to the impairment of mucociliary clearance, CF patients are prone to recurrent bacterial infections which they struggle to clear naturally. Dysfunctional CFTR can also cause the build-up of mucus in other organs such as the liver, pancreas, and intestines by a similar mechanism, leading to a wide range of complications. Importantly, there is currently no cure for CFTR dysfunction, and CF patients are treated symptomatically.

There is growing evidence that Na_v channel dysfunction plays a key role in certain types of cancer [156]. One example of this is the observation that $Na_v1.5$ was overexpressed in breast cancer biopsies (compared to non-cancer biopsies) and this was associated with metastasis, lymph node invasion, and decreased survival [278,279]. Similarly, $Na_v1.4$ or $Na_v1.7$ overexpression has been linked to the invasiveness of prostate cancer cells [280]. The molecular mechanisms underpinning the role of Na^+ channels in cancers of non-excitable cell types are not well understood.

The above examples are a selected few of the many known human channelopathies and as our knowledge of the structure and functions of ion channels continues to expand, so too will our understanding of the mechanisms behind these important diseases. This is necessary to enable the identification of new cellular targets for therapeutic interventions.

1.9 Viral requirement for ion channels

1.9.1 Viroporins

Many viruses encode their own ion channels, termed ‘viroporins’, which allow them to modulate the ionic balance within specific cellular environments and

therefore manipulate both cellular and viral processes (reviewed in [281,282]). For a virus to use its limited genetic code to produce an ion channel, one can predict that manipulating the ionic homeostasis is critical during infection. Viroporins are often more simplistic than host cell ion channels, generally lacking gating mechanisms and showing weak selectivity [282].

The matrix protein 2 (M2) proton channel encoded by IAV is probably the most well-studied viroporin [282]. It is more similar to a classic ion channel than many other viroporins, showing selectivity for H^+ as well as being gated by H^+ [283]. IAV enters cells via receptor-mediated endocytosis and subsequently traffics through the endocytic pathway [284,285]. The environment inside endosomes is highly acidic and IAV uses this to its advantage. The expression of the M2 proton channel on the virion surface facilitates movement of H^+ into the virion interior, lowering the pH [286]. This triggers confirmational changes in the viral surface proteins and also acts to dissociate the viral RNPs from the matrix protein, promoting fusion of the viral and endosomal membranes and the release of the RNPs into the cytoplasm [286–288]. Drugs targeting M2 (such as amantadine and rimantadine) were historically used to successfully treat IAV infection, however due to the rise of drug-resistant strains, these therapies are no longer in use [289].

Another well-documented viroporin is the viral protein U (Vpu) encoded by human immunodeficiency virus (HIV). Unlike IAV M2 and HRSV SH, the HIV viroporin is not a structural component of the virion, however it is still essential for efficient infection [282]. Vpu has two important roles during HIV infection: firstly, it promotes the degradation of cell surface protein CD4 [290,291] in order to avoid triggering the immune response; and secondly, it enhances virion release by

antagonising the cell surface protein tetherin, which, in the absence of Vpu, prevents the diffusion of viral particles away from the cell [292]. However, neither of these roles utilise the channel activity of Vpu, which is selective for monovalent cations (Na^+ and K^+) [293]. Whilst a role for Vpu in membrane depolarisation to trigger virus release was suggested [294], not all of the experimental evidence supports this. Therefore, the role of Vpu channel activity during HIV infection is still unclear [295].

Other viruses which encode viroporins include members of the *Picornaviridae* such as poliovirus [296,297], some *Flaviviridae* including HCV [298] and Dengue virus (DENV) [299], rotavirus [300], *Coronaviridae* including Middle Eastern respiratory syndrome coronavirus (MERS-CoV) and SARS-CoV-1/2 [301–303], and small tumour-causing DNA viruses such as simian virus 40, JC ('John Cunningham') virus and human papillomavirus (HPV)-16 [281,282,304].

On the other hand, many viruses do not encode their own viroporins and have instead evolved mechanisms to manipulate host cell channels. Recent evidence has highlighted the extent to which many viruses rely on and/or regulate host ion channels (reviewed in [305,306]), revealing the potential for repurposing licensed ion channel drugs as antiviral therapeutics.

1.9.2 Host ion channels in virus entry

Endocytosis is vital for many viruses as a pathway into the cell. Host ion channels are present at each stage of the endosomal network to facilitate the necessary changes in endocytic ionic milieu [307] and several important pathogenic human viruses have been shown to rely on these changes for successful infection [306].

Bunyaviruses, such as BUNV and Hazara virus (HAZV), rely on the increasing concentration of K^+ that occurs with passage through endosomes to allow activation of their fusion machinery, which subsequently mediates endosomal escape [308,309]. Treating cells with specific K^+ ion channel inhibitors blocked virus entry, leading to abrogation of infection [310]. In the case of BUNV, a panel of K^+ channel modulators were used to determine that K_{2P} family members were required for BUNV infection, and are likely involved in the endosomal K^+ regulation [310]. Furthermore, when BUNV virions were pre-treated directly, or 'primed', with buffers at pH 6.3 containing a high [K^+], virions were able to enter cells and begin viral gene expression at an accelerated pace, compared to those treated at low pH alone [308]. For HAZV, structural studies also revealed a conformational change in primed viruses that was mediated by K^+ alone [309]. High K^+ resulted in extensive spike conformational changes, and caused extended spikes to interact with membranes, reminiscent of the formation of the 'extended intermediate' in which the virus spike bridges both viral and endosomal envelopes. Furthermore, both viruses showed a dependency on cellular cholesterol as a component of the endosomal membrane, however this dependency could be overcome through priming with high [K^+] [311], suggesting that the role of cholesterol and K^+ channel activity may be linked. Furthermore, another study recently found that the treatment of cells with valinomycin, a K^+ ionophore (which reversibly binds to K^+ and disrupts K^+ gradients in the endocytic pathway), displayed antiviral activity against three bunyaviruses; La Crosse virus, Rift Valley fever virus and Keystone virus [312]. This was also observed for some enteroviruses (coxsackievirus, rhinovirus), Zika virus (ZIKV, flavivirus), and some coronaviruses (HCoV-229E and MERS-CoV), further highlighting the importance

of K^+ for virus infectivity and potentially revealing K^+ channels as broad antiviral targets [312].

Similarly, three important human pathogens have recently been shown to rely on K^+ channels for entry. Overexpression of the $K_v1.3$ channel inhibited the entry of HCV, DENV and ZIKV [313]. All three of these viruses enter cells through the endocytic pathway and rely on a low pH for membrane fusion to allow entry into the cytoplasm. It was revealed that $K_v1.3$ overexpression led to an increase in the pH of acidic organelles which resulted in an accumulation of virions, indicating that virus endosomal escape had been prevented. Furthermore, *in vivo* work confirmed $K_v1.3$ as a host factor for ZIKV infection as mice overexpressing the channel were protected against infection [313]. In contrast, Sendai virus, which fuses at the cell membrane requiring a neutral pH, was not affected by $K_v1.3$ manipulation; further indicating a role for $K_v1.3$ in virus entry via endosomes.

Ca^{2+} channels are also known to be required for virus entry. IAV entry is initiated by one of its surface glycoproteins, hemagglutinin (HA), which binds to sialic acid-containing glycolipids on the cell surface [284]. This, in combination with the binding of the second viral glycoprotein, neuraminidase (NA) with its cellular receptor, mediates IAV internalisation via endocytosis. It was discovered that IAV infection caused Ca^{2+} oscillations in cells through interaction of HA with $Ca_v1.2$, a voltage-gated Ca^{2+} channel [314]. This interaction was inhibited through use of the clinically available Ca^{2+} channel blocker diltiazem, thereby blocking IAV entry into cells [314]. Importantly, $Ca_v1.2$ is sialylated, which could explain its involvement during IAV entry. Interestingly, similarly to bunyaviruses, IAV also requires the endocytic increase in both H^+ (pH) and K^+ through endosomes for efficient fusion and entry. However, for IAV this is mediated through the virally

encoded M2 viroporin which it uses to transport endosomal H^+ and K^+ inside the virion to destabilise the core and ensure efficient uncoating [315]. Although this process has not yet been linked to specific K^+ ion channels, a clear requirement for regulating the endosomal ionic balance has been demonstrated for IAV and therefore represents a potential antiviral target.

EBOV enters cells through macropinocytosis and travels through the endocytic pathways until it meets the intracellular receptor Niemann-Pick C1 (NPC1) in the acidic late endosomes/lysosomes. The EBOV glycoprotein (GP) consists of two subunits; GP1 initiates attachment of EBOV to the cell and GP2 mediates the fusion of viral and endosomal membranes during entry. The NPC1 receptor-binding site on GP1 is only accessible in acidic compartments due to the action of cathepsins. The inhibition of Ca^{2+} channel TPC2 was shown to inhibit EBOV entry between the points of GP1 binding to NPC1 and the GP2-mediated fusion of the virion and endosomal membranes [316], indicting a role for Ca^{2+} channels in fusion. It was later revealed that the three factors pH, Ca^{2+} and NPC1 binding, synergistically contribute to a conformational change in GP2 to mediate fusion [317]. Blockade of TPC2 through FDA-approved small molecule inhibitors attenuated EBOV infection [318,319], further emphasising the power of repurposing licenced ion channel modulators for antiviral therapies.

A third family of ion channels has also been implicated in viral entry; Cl^- channels. Specifically, blockade of the CFTR with small molecule inhibitors or through genetic knockdown reduced BK polyomavirus (BKPyV) infection in primary kidney cells [320]. Time-of-addition assays revealed that CFTR was involved in the early stages of infection. Further investigation revealed that the CFTR modulators did not affect BKPyV binding or internalisation, however they did

reduce virus entry into the ER, evidenced by a reduction in the number of viral protein (VP)2/VP3 puncta visible in drug treated cells compared to non-treated controls. The VP2/VP3 minor capsid proteins are only exposed once the virus reaches the ER, therefore indicating that CFTR modulation acts at a stage between virus entry and trafficking to the ER [320].

1.9.3 Host ion channels in viral replication

Whilst virus entry through the endosomal network relies on changes in the cellular environment mediated by ion channels, the specific role of these channels in viral replication is less clear. Many RNA viruses induce the formation of replication complexes as a means of replicating their own genomes in distinct areas of the cell and therefore evading RNA sensing pathways. These complexes vary in nature depending on the sense of the genome; generally, positive-sense RNA viruses (PSVs) induce membrane-associated complexes, whereas NSVs tend to recruit collections of interacting proteins to membrane-less replication sites, and double stranded RNA (dsRNA) viruses utilise subviral particles as a means of replicating their genomes in a secure environment [321]. Recently, evidence has emerged that ion channels play a vital role within the replication complexes of many RNA viruses.

Infectious bursal disease virus (IBDV) is a dsRNA virus which has been shown to upregulate voltage-dependent anion channel 1 (VDAC1) during infection [322]. The IBDV RNP complex is composed of VP1 (the vRdRp), VP3 (the scaffolding protein which binds to dsRNA), and the genomic RNA segments. Co-immunoprecipitation experiments identified interactions between VDAC1 and VP1, and VDAC1 and VP3. These interactions were shown to enhance the stability of the RNP complex and increase the activity of the vRdRp. Minigenome

assays confirmed that knocking down VDAC1 had a detrimental effect on IBDV replication [322] indicating that VDAC1 is a critical host factor for the efficient replication of this virus.

Chikungunya virus (CHIKV) is a PSV which replicates its genome within membrane bound replication complexes formed at the plasma membrane. Small molecule Cl^- channel modulators had an inhibitory effect on CHIKV infection in both human and mosquito cells (the vector of disease) and genetic knockdowns identified Cl^- intracellular channels 1 and 4 (CLIC1 and CLIC4) as pro-viral host factors [323]. The absence of CLIC1 and CLIC4 in human cells inhibited CHIKV replicon replication. Additionally, affinity pull down of strep-tagged non-structural protein 3 (nsP3) of CHIKV revealed that nsP3 was in complex with CLIC1, but not CLIC4. As nsP3 is an essential component of the CHIKV replication complex [323], these results were suggestive of channel involvement in the formation and/or maintenance of these complexes.

Cl^- ion channels have also been linked to the PSV HCV infection [324]. Small molecule inhibitors of Cl^- channels were used to inhibit HCV replicon replication. Through use of an intracellular fluorescent dye (MQAE) which is quenched by high $[Cl^-]$, it was revealed that HCV replication increased intracellular $[Cl^-]$ which was suppressed upon treatment with Cl^- channel inhibitors. Furthermore, through genetic knockdowns, the authors identified two channels involved in HCV replication: ClC2 and ClC3 [324]. It was suspected that HCV manipulated the flow of Cl^- ions through ClC2 and ClC3 to alter the environmental conditions within early/late endosomes during the process of building its viral replication complexes. However, it is still unclear however why Cl^- is essential for HCV replication.

A role for Ca^{2+} channels has been described for the replication of members of the *Flaviviridae* family of PSVs [325]. A screen of FDA-approved drugs against Japanese encephalitis virus (JEV) uncovered several inhibitors of Ca_v's that had a potent effect on infection, including manidipine. Time of addition studies alongside the use of a replicon system confirmed that the drugs acted upon the replication stage of JEV infection. Furthermore, DENV, ZIKV and West Nile virus (WNV) were all sensitive to Ca_v modulation, whereas yellow fever virus (YFV) was insensitive. The selection and sequencing of a manidipine-resistant JEV mutant revealed a site on the non-structural protein NS4B which appeared to confer sensitivity to Ca_v modulation. A substitution at Q130 in transmembrane domain 3 of NS4B rendered the viruses insensitive to manidipine, and interestingly, this site was conserved in JEV, DENV, ZIKV and WNV but not in YFV [325]. NS4B is an essential component of the flavivirus replication complex and keeps the complex anchored to the ER. The exact role of Ca_v's in flavivirus replication remains to be determined, however it is clear that intracellular Ca^{2+}, the majority of which is stored in the ER, is crucial for their infection.

1.10 Project outline and aims

This thesis examines the role of Cl^- channel families during HRSV infection. A novel role for the CaCC channel, TMEM16A, during HRSV infection is revealed (Chapter 3), followed by an investigation into the mechanistic details underpinning this relationship (Chapter 4). Of note, data in Chapter 3 has been published by the candidate [326].

The aims of this project were:

1. To assess the role of host Cl^- channels during HRSV infection
2. Reveal the molecular identity of Cl^- channels involved in HRSV infection
3. To investigate the stage of the viral life cycle at which HRSV requires Cl^- channels
4. To assess the role of TMEM16A in the inflammatory response to HRSV infection

Chapter 2 Materials and Methods

2.1 Cell culture

2.1.1 Cell lines and continuous cell culture

A549 (adenocarcinoma human alveolar basal epithelial cells), HEp-2 (human epithelial cells) and SHSY-5Y (human neuroblastoma cells) cells were maintained in Dulbecco's Modified Eagle's Medium (DMEM) substituted with 10% foetal bovine serum (FBS) and 1% penicillin/streptomycin (P/S; 100 U/mL and 100 µg/mL, respectively); henceforth called complete media. Cells were incubated at 37°C and 5% CO_2 in a humidified incubator and sub-cultured once 70-80% confluent using 1x phosphate buffered saline (PBS) and 1% trypsin-ethylenediaminetetraacetic acid (EDTA). Cells were washed and trypsinised for 5 mins at 37°C. BSR-T7 cells (baby hamster kidney 21 – BHK-21 – cells constitutively expressing T7 RNA polymerase) were cultured in the same way with the addition of 1 mg/mL G418 into complete media every other passage.

2.1.2 Cell stocks

All cell lines were stored at -80°C, or liquid nitrogen for long term storage. For start-up, cells were rapidly thawed in a 37°C water bath. Once defrosted, the 1 mL suspension was added to 14 mL warm, complete DMEM in a 15 mL falcon and gently mixed to dilute out the DMSO. Cells were pelleted by centrifugation at 300 x *g* for 5 mins and the supernatant discarded. The pellet was resuspended in 5 mL complete media and added to a T-25 cell culture flask. After incubation overnight, the cells were washed in PBS and the media changed. Once cells reached confluency they were moved into a T-75 cell culture flask.

Healthy cells at the lowest passage number possible were used to freeze down to maintain cells stocks. Cells were grown to confluency in a T-175 cells culture flask. Then, cells were washed in PBS and detached from the flask using 3 mL trypsin as described in section 2.1.1 and collected in 12 mL complete media. The cells were gently pelleted by centrifugation at 300 x *g* for 5 mins and the supernatant was discarded. The cells were resuspended in 4 mL complete media containing 10% sterile-filtered dimethyl sulfoxide (DMSO) and aliquoted into cryo-vials for storage.

2.1.3 Cell viability assays

To assess cell viability following treatment with ion channel modulators or other drugs (2.3.2), the treated media was removed and replaced with 100 µL serum-free DMEM. CellTiter®96 AQueous One Solution (Promega, G3580) was added (20 µL per well) and incubated at 37^{o}C for 1-4 hrs in the dark. A measurement of the absorbance at 492 nm was taken using a microplate reader. This was used to compare cell health of drug-treated cells compared to the solvent-treated control cells. Compounds were considered non-toxic if an average of ≥80% cell viability compared to solvent-treated controls was observed after 3 biological repeats [326].

2.1.4 Cell lysis

To generate lysates to be used in western blot or ELISA analysis, cells were incubated in ice cold Leeds Lysis Buffer (25 mM glycerol phosphate, 20 mM tris(hydroxymethyl)aminomethane (Tris), 150 mM NaCl, 1 mM EDTA, 1% Triton, 10% glycerol, 50 mM NaF, 5 mM $Na_4O_7P_2$ - pH 7.4) supplemented with Halt Protease Inhibitor Cocktail (Thermo Scientific, 78429) for 20 min at 4^{o}C. Cells

were detached from the plate using a cell scraper and lysates collected in 1.5 mL tubes. Lysates were centrifuged for 10 mins at 17 x *g* to pellet cell debris and an equal volume of each protein-containing supernatant was transferred to fresh tubes for storage at -20^{o}C [326].

2.2 Virus culture

2.2.1 Virus strains

Wild type (WT) HRSV strain A2 was obtained from the National Collection of Pathogenic Viruses (NCPV) of Public Health England (PHE). Green fluorescent protein (GFP)-expressing HRSV was purchased from ViraTree (RSV-GFP1) in which the *gfp* gene had been inserted as an independent transcriptional unit in the first position in the HRSV gene order. GFP-PA (polymerase acidic protein) labelled IAV (H1N1 WSN/33 strain) which was rescued as described in Neumann *et al*., 1999 [327], was kindly gifted by Eleanor Todd (on behalf of Dr JN Barr's lab, University of Leeds). WT-BUNV and WT-HAZV were generously provided by Dr Samantha Hover (on behalf of Dr J Mankouri's lab, University of Leeds).

2.2.2 HRSV propagation

HEp-2 cells were seeded at a density of 5x10^{5} cells/well in a 6-well plate and left to adhere and grow overnight. The monolayer was then washed with PBS and infected with WT-HRSV at a multiplicity of infection (MOI) of 0.01 in a total of 200 µL of DMEM containing 2% FBS and 1% P/S; henceforth called infection media. The plate was incubated for 2 hrs, with gentle manual rocking every 15 mins to allow the virus to bind cells and prevent cells drying out. Following the

binding period, the wells were topped up to a total of 2 mL using infection media. The infection was left for 5 days with manual rocking daily.

2.2.2.1 Harvesting HRSV

All procedures for harvesting the virus were conducted strictly at 4^{o}C or on ice. The virus was harvested to produce the P1 stock. To achieve this, the media containing extracellular virus was collected and the cells were manually collected using a cell scraper into 10 mL PBS. The scraped cells underwent three rounds of quick-freeze/thaw cycles (using a dry ice/ethanol slushy, and a 37^{o}C water bath) to release the cell-associated virus. The harvested virus and sonicated cells were combined and clarified by centrifugation at 4000 x *g* for 7 min. The pelleted cell debris was discarded, and the virus supernatant (VSN) was stored at -80^{o}C.

The P1 virus was used to propagate HRSV further. Multiple T-75 cell culture flasks of HEp-2 cells were seeded at a density of 3x10^{6} cells/flask, and the following day were infected with 100-200 µL P1 virus in a total volume of 1 mL infection media. As before, virus was allowed a 2 hr binding step with manual rocking before the flasks were topped up to a final volume of 10 mL infection media. The infection was left for 5 days with daily rocking. If >50% cytopathic effect (CPE) was observed before 5 days, the amount of P1 virus was reduced. If no CPE was observed at 5 days, P2 virus was passaged a further time. P2 virus was harvested in the same way as P1.

Once the extracellular virus and cell-associated virus had been harvested and combined, the VSN was clarified firstly by centrifugation for 40 min at 3250 xg and discarding the pelleted cell debris, then secondly by passing the virus supernatant through a 0.45 nm filter (allowed virus to pass through).

2.2.2.2 Concentrating HRSV

All procedures for concentrating the virus were conducted strictly at 4°C or on ice. The clarified P2 virus supernatant was adjusted to 100 mM $MgSO_4$ to stabilise the virus [328], and 100 mM Tris-HCl, pH 7.5. To concentrate the virus, 50% (w/v) polyethylene glycol (PEG)-6000 was added to the VSN to a final concentration of 10% (w/v) and the mixture was left stirring overnight. The virus was pelleted via centrifugation at 4000 xg for 30 min. Following resuspension of the pellet into a small volume of serum-free DMEM (1 mL per 50 mL of VSN concentrated), the virus was aliquoted, quick-frozen and stored at -80°C. This concentrated P2 virus was titred and used as the working stock, and P1 was used to propagate more virus when necessary.

2.2.3 Virus titration by immunostaining-based plaque assay

To determine the titre of WT-HRSV or HRSV-GFP, HEp-2 cells were seeded at a density of $2x10^5$ cells/well in a 12-well plate and left to adhere and grow overnight. Serial dilutions of virus from 10^{-1} to 10^{-8} were prepared in serum-free DMEM. The cell monolayer was washed with PBS and infected with 100 µL of each virus dilution in duplicate for 1 hr, with manual rocking every 15 mins to disperse the virus and prevent the cells from drying out. Following the binding stage, non-internalised virus was aspirated, and cells were overlayed with 1 mL 0.5% (v/v) methylcellulose: infection media. The infection proceeded for 4-7 days at 37°C with no movement. Ice cold 4% paraformaldehyde (PFA) was used to fix cells by adding directly on top of the overlay for 1 hr at 4°C. The cells were then gently washed in PBS and permeabilised using cold methanol: acetone for 10 mins at 4°C. Following another PBS wash step, cells were incubated in blocking buffer (5% milk in PBS) for 30 mins. Plaques were detected by incubation

overnight at 4ºC with a primary polyclonal antibody targeting HRSV followed by horseradish peroxidase (HRP)-conjugated secondary antibody for 1 hr at room temperature (for antibody details see Table 2-4 and Table 2-5). Antibodies were made up in blocking buffer and cells were washed with PBS between each step. Following incubation with 4-chloro-1-naphthol (4-CN, Pierce, 1:10) and 30% H_2O_2 (Sigma) purple plaques were revealed [326]. Plaques were counted and the titre calculated according to Equation 2-1.

$$Virus\ titre\ \left(\frac{PFU}{mL}\right) = \frac{number\ of\ plaques}{\left(dilution\ factor\ \times\ volume\ of\ virus\ added\ (mL)\right)}$$

Equation 2-1 Calculating the titre (plaque forming units (PFU)/mL) of virus stocks from a plaque assay.

2.2.4 Virus titration by $TCID_{50}$

HRSV titre was also determined by measuring the median tissue culture infectious dose ($TCID_{50}$) following the method outlined in Sun and Lopez, 2016 [329]. Briefly, this involved infecting HEp-2 cells seeded at $2x10^4$ cells/well in a 96-well plate with serially diluted virus in a total volume of 25 µL/well in infection media. All infections were performed in triplicate and proceeded for 2 hrs before the volume was topped up to 100 µL/well and incubated for 4-5 days. The virus/media was removed and 100 µL of crystal violet working solution (40 mL of stock solution (1 g crystal violet, 20 mL 100% ethanol, 80 mL dH_2O), 80 mL methanol, 180 mL dH_2O) was added. After 15-30 mins, the plate was washed by submerging in dH_2O and left to dry. To calculate the titre, the last dilution in which CPE was observed was given a score, and the titre calculated according to

Equation 2-2.

$$\text{'+++'}\ 10^X\ TCID_{50} = 10^{X+0.7}/25\ \mu L$$

$$\text{'++-'}\ 10^X\ TCID_{50} = 10^{X+0.4}/25\ \mu L$$

$$\text{'+--'}\ 10^X\ TCID_{50} = 10^{X-0.1}/25\ \mu L$$

Equation 2-2 Calculating the titre of virus stocks from a $TCID_{50}$ assay. (X= dilution of the virus).

2.3 Virological assays

2.3.1 Virus infection

A549 cells (unless otherwise stated) were seeded into 6-well plates ($3x10^5$ cells/well), 12-well plates ($1x10^5$ cells/well), or 96-well plates ($1x10^4$ cells/well) and left to adhere and grow for 24 hrs at 37°C. Cells were washed with PBS and infected with WT-HRSV or HRSV-GFP in infection media at MOI 0.1 (unless otherwise stated) for 24 hrs. To analyse infection, cells were either lysed for western blotting (2.4.2) or fixed for immunofluorescence analysis (2.4.4). Infections with IAV-GFP, WT-BUNV and WT-HAZV were carried out in a similar manner, substituting infection media for complete media.

2.3.2 Ion channel inhibitor assays

A549 or SH-SY5Y cells were seeded in 96-well plates. Cl^- channel inhibitors (Table 2-1) were made up in infection media to working concentrations alongside solvent-only controls (sterile-filtered DMSO or autoclaved distilled H_2O). Cells were washed with PBS and pre-treated with 100 µL inhibitor per well for 45 min prior to infection. Each condition was performed in duplicate on the same plate. Infection with HRSV-GFP, IAV-GFP, WT-BUNV or WT-HAZV was carried out (2.3.1) in the presence of the inhibitors and analysed at 24 hours post-infection (hpi) by IncuCyte ZOOM (2.4.5) or western blot (2.4.2) analysis [326].

Table 2-1 Details of ion channel modulators and other drugs used.

Drug	Source	Target
DIDS (4,4'-diisothiocyanostilbene-2,2'-disulfonic acid)	Sigma Aldrich, D3514	Broad spectrum Cl^- channel inhibitor
NPPB (5-nitro-2-(3-phenylpropylamino) benzoic acid)	Sigma Aldrich, N4779	Broad spectrum Cl^- channel inhibitor
R(+)IAA-94 (R(+)-[(6,7-Dichloro-2-cyclopentyl-2,3-dihydro-2-methyl-1-oxo-1H-inden-5-yl)-oxyacetic acid)	Sigma Aldrich, I117	Broad spectrum Cl^- channel inhibitor
DCPIB (4-(2-butyl-6,7-dichlor-2-cyclopentylindan-1-on-5-yl) oxobutyric acid)	Sigma Aldrich, SML2692	VRAC inhibitor
CFTRinh-172	Sigma Aldrich, C2992	CFTR inhibitor
Chromanol 293B	Sigma Aldrich, C2615	CFTR inhibitor
Glibenclamide	Tocris Biosciences, 0911	CFTR inhibitor
CaCCinh-A01	Sigma Aldrich, SML0916	CaCC inhibitor
Niflumic acid	Sigma Aldrich, N0630	CaCC inhibitor
Talniflumate	Sigma Aldrich, SML1710	CaCC inhibitor
Tannic acid	Sigma Aldrich, 403040	CaCC inhibitor
T16Ainh-A01	Merck Chemicals Ltd, 613551	TMEM16A inhibitor
MONNA	Sigma Aldrich, SML0902	TMEM16A inhibitor

Ribavirin	Sigma Aldrich, R9644	Broad spectrum viral replication inhibitor (including HRSV)
Ammonium chloride	Sigma Aldrich, A9434	Endosomal acidification inhibitor
Eact	Sigma Aldrich, SML1157	TMEM16A activator

2.3.3 Virion treatments

Channel inhibitors were made up to 2x working concentrations in infection media and added to an equal volume of WT-HRSV supernatant (MOI 0.2). The virus was incubated with the inhibitor for 45 min at room temperature. The treated virions were then used to infect A549 cells in a total volume of 3 mL/well in a 12-well plate (MOI 0.2; final inhibitor concentration on cells ≥400-fold dilution from active concentration). Cells were lysed (2.1.4) at 24 hpi and HRSV protein expression was assessed via western blotting (2.4.2) [326].

2.3.4 Virus entry assays

A549 cells were prepared in a 6-well plate. Cells were pre-treated with channel inhibitors for 45 mins prior to infection with WT-HRSV (or WT-BUNV) at MOI 0.2. At 3 hpi, the drug and any non-internalised virus was removed by washing with 0.1% trypsin in PBS three times and replaced with complete media. The cells were lysed (2.1.4) at 24 hpi and infection was assessed via western blot analysis (2.4.2).

2.3.4.1 Virus binding assay

For the BUNV binding assay, tannic acid was made up in pre-chilled complete media. A549 cells in a 6-well plate were placed on ice for 30 mins to chill prior to

drug addition. The cells were infected with WT-BUNV at MOI 0.1 in a total volume of 350 µL and were incubated for 1 hr on a rocker at 4°C, with manual shaking every 10 mins to prevent the cells drying out. Reduced temperature was used to prevent endocytosis of bound virions and thus separate the binding stage from entry. Cells were then brought back up to 37°C to allow infection to proceed. The drug and any unbound virus were washed away by three 0.5% trypsin washes. Tannic acid was added and removed to the appropriate wells every hour for the first 4 hrs of infection. Lastly, cells were lysed at 24 hpi (2.1.4) and infection was analysed via western blotting (2.4.2).

2.3.5 Virus release assay

Cells were infected with HRSV-GFP at MOI 0.1 in infection media for 16-18 hrs. Infected cells were washed three times with PBS and media was replaced containing the appropriate inhibitors at a total volume of 0.5 mL (in a 12-well plate). After 4 hrs, the VSN was removed from each well and collected into pre-chilled 1.5 mL tubes on ice. The VSN was clarified by centrifugation at 300 x *g* for 5 mins to collect any cell debris, and with the pellet removed, the VSN was kept on ice to keep the virus stable. A new plate of cells was washed with PBS and 4 mL infection media was added. The 0.5 mL VSN was added to the fresh cells which were incubated for 24 hrs. This diluted the inhibitor by 9-fold and allowed assessment of the amount of released virus present in the VSN by quantifying the number of HRSV-GFP expressing cells in the re-infection (2.4.5).

2.3.6 Post-infection time of addition assay

Channel inhibitors were prepared at 2x working concentration in 50 µL infection media and added to a 96-well plate of cells alongside an equal volume of

HRSV-GFP supernatant (MOI 0.1, T=0 hr). For post-infection treatments, inhibitors were freshly prepared for each time point and added to infected cells at 3, 6 and 9 hpi, resulting in a total volume of 100 µL per well and a dilution of the inhibitor to 1x. At 24 hpi, HRSV-GFP expression was analysed via IncuCyte ZOOM analysis (2.4.5) [326].

2.3.7 HRSV minigenome assay

A 6-well plate of BSR-T7 cells grown overnight. Cells were transfected (2.5.4) with pN, pP, pL and pM2-1 support plasmids alongside a plasmid expressing RNA minigenome pM/SH-GFP, able to express GFP (for further details of these plasmids refer to 2.5.1.1). At 6 hours post-transfection (hpt), the transfection mixture was removed, cells were washed with PBS and TMEM16A channel inhibitors in complete media were added. After 24 hrs (i.e., 30 hpt), the replication of the minigenome was assessed through quantification of GFP fluorescence via IncuCyte ZOOM (2.4.5).

2.3.8 Blind passaging HRSV in the presence of T16Ainh-A01

Cells were pre-treated for 45 min with either T16Ainh-A01 (15 µM), ribavirin (40 µM) or DMSO (solvent control) prior to infection with HRSV-GFP at MOI 0.1 in a total volume of 1 mL (6-well plate). Infection proceeded for 72 hrs before the VSN was collected into pre-chilled 1.5 mL tubes. The subsequent steps were performed on ice or at 4^{o}C to maintain virus stability. The VSN was clarified via centrifugation at 300 x *g* for 5 mins to pellet the cell debris, after which the pellet was discarded. The VSN was then used to infect a fresh plate of pre-treated cells: 250 µL of the T16Ainh-A01 and ribavirin VSN was transferred and 100 µL of the DMSO VSN into a total volume of 1 mL. After passaging, the old plate (P1) was

analysed for HRSV-GFP fluorescence via IncuCyte ZOOM (2.4.5) and then the cells were lysed for western blot analysis (2.1.4 and 2.4.2). The remaining VSN was stored at -80ºC for future use. The newly infected plate (P2) was incubated for 72 hrs and passaged in the same way, for a total of 10 passages.

2.3.9 IP-10 release assays

2.3.9.1 Collection of samples

Cells were pre-treated with inhibitors prior to infection (2.3.2). Following this, cells were infected or mock infected with HRSV (MOI 0.5). Alternatively, cells were transfected (2.5.4) with 400 ng poly(I:C) per well in a 6-well plate or treated with IFN-α/γ (100 ng per well). The drug remained present in all conditions. After 24 hrs, the cell supernatants were collected into separate 1.5 mL tubes, clarified by centrifugation at 300 x *g* for 5 mins, and stored at -80ºC. Cells were washed in PBS and lysed (2.1.4). Lysates were stored for short term at -20ºC.

2.3.9.2 Enzyme-linked immunosorbent assay (ELISA)

The concentration of interferon γ-induced protein 10 (IP-10) or interleukin-8 (IL-8) in the cell supernatants and lysates was measures by ELISA. The assays were carried out according to the manufacturers' protocols (Human CXCL10/IP-10 DuoSet ELISA, R&D Systems, DY266 and ELISA MAX™ Deluxe Set Human IL-8, BioLegend, 431504). Briefly, this involved binding the capture antibody (provided) to a 96-well plate overnight before washing the plate by submerging in wash buffer (0.1% TWEEN-20 in PBS) three times. Non-specific binding was prevented by a blocking step for 1 hr using 1% BSA in PBS (IP-10) or the provided blocking buffer (IL-8). Alternating incubation and wash steps were performed with the detection antibody (provided), streptavidin-HRP (provided), substrate solution

(Pierce TMB Substrate Kit, 34021) and stop solution (H_2SO_4). All steps were carried out at room temperature. The optical density of each well was determined using a microplate reader set to 450 nm. The reading at 540 nm was subtracted from this to correct for optical imperfections in the plate. A standard curve was generated and used to quantify the concentration of protein within each sample.

2.4 Biochemical methods

2.4.1 SDS-PAGE

Polyacrylamide gels were cast consisting of a 10% resolving gel and 5% stacking gel (Table 2-2). Lysates were prepared for sodium dodecyl sulphate (SDS)-polyacrylamide gel electrophoresis (PAGE) by the addition of Laemmli sample buffer (Bio-Rad, 1610747) supplemented with β-mercaptoethanol followed by incubation at 95^{o}C for 10 min, then centrifugation at 17 x *g* for 5 min. Samples were loaded and electrophoresed at 180V for around 70 min in SDS-PAGE running buffer (0.25 M Tris, 2.5 M glycine, 1% (w/v) SDS) [326].

Table 2-2 SDS-PAGE gel recipes. Volumes are to make 1 gel. Sodium dodecyl sulphate (SDS), ammonium persulphate (APS), tetramethylethylenediamine (TEMED).

	10% Resolving gel	5% Stacking gel
Tris-HCl	2.5 mL (1.5 M, pH 8.8)	0.125 mL (1 M, pH 6.8)
dH_2O	4 mL	1.495 mL
30% acrylamide	3.3 mL	0.33 mL
10% SDS	0.1 mL	0.02 mL
10% APS	0.1 mL	0.02 mL
TEMED	0.016 mL	0.01 mL

2.4.2 Western blotting

Proteins were resolved by SDS-PAGE (2.4.1) and transferred to a methanol-activated polyvinylidene difluoride (PVDF) membrane (Millipore) using the Trans-blot Turbo (BioRad) semi-dry transfer system – 25 V – 1.0 A – 30 min in transfer buffer (0.25 M Tris, 0.89 M glycine, 20% (v/v) methanol).

Non-specific antibody binding was blocked by incubating membranes in 10% milk in Tris-buffered saline (TBS)-T (0.25 M Tris, 1.37 M NaCl – pH 7.5, 0.1% (v/v) Tween-20) for a minimum of 1 hr before antibody staining. Proteins were labelled by incubation of primary antibodies (Table 2-4) in 5% milk overnight at 4^{o}C. HRP-conjugated secondary antibodies (Table 2-5) were made up in 5% milk and added to the membrane for 1 hr at room temperature. Membranes were washed for 5 mins three times between each antibody using 1x TBS-T, and four times prior to detection. Antibody binding was detected using the enhanced chemiluminescence system (ECL; Advansta WesternBright™ ECL-Spray) and developed on an xograph compact X4 processor using light-sensitive film (Thermo Scientific CL-Xposure). For quantification of band densities, blots were scanned and analysed using ImageJ. In each instance, bands of interest were normalised to the loading control [326].

2.4.3 Silver staining after SDS-PAGE

Samples of purified WT-HRSV and HRSV-GFP were resolved by SDS-PAGE (2.4.1). Following this, the proteins within the gel were fixed by incubation in solution A for 30 mins (Table 2-3). All incubations were performed at room temperature with gentle agitation. Solution A was removed, and solution B added for 15 mins. The gel was subjected to three wash steps in dH_2O for 5 mins each

before solution D was added. The sodium thiosulphate in solution D helped to reduce background and enhance staining. Another round of wash steps followed, for 30 secs each. The addition of solution E for 20 mins imbued the gel with silver which interacts with functional groups within proteins. Solution E was washed away by three wash steps for 30 secs each. The bands were developed through the addition of solution F which converted the silver ions into metallic silver. Solutions E and F included formaldehyde as an enhancer by causing chemical crosslinking of the proteins in the gel. Lasty, when the bands were visible, solution G was added to stop the reaction and prevent any further development.

Table 2-3 Solutions used in silver stain.

Solution	Components (total volume 100 mL)
A	50% (v/v) ethanol, 10% (v/v) acetic acid
B	5% (v/v) ethanol, 1% (v/v) acetic acid
C	0.2 g sodium thiosulphate
D	10 mL solution C
E	0.2g silver nitrate, 75 µL formaldehyde
F	6g sodium carbonate, 50 µL formaldehyde, 0.2 mL solution C
G	5% (v/v) acetic acid

2.4.4 Immunofluorescence

For analysis of GFP-tagged virus infection in live cells, plates were scanned at stated time points using IncuCyte ZOOM imaging system (2.4.5) within a 37^{o}C, 5% CO_2, humidified incubator.

For immunofluorescent staining, cells were washed with PBS and fixed by incubation with ice cold 4% PFA whilst rocking for 10 mins at 4^{o}C. The fixed cells were permeabilised using ice cold methanol: acetone for 10 mins at 4^{o}C. After a PBS wash, cells were incubated in blocking buffer (1% BSA in PBS) for 15 mins at room temperature. Primary antibodies (Table 2-4) were made up to the appropriate working dilutions in 1% BSA and added to cells at room temperature for 1 hr, or overnight at 4^{o}C. After three PBS wash steps, fluorescent secondary antibodies (Table 2-5) were used to stain cells for 2 hrs at room temperature, protected from light. Cells were imaged using the IncuCyte ZOOM (2.4.5), or via confocal microscopy (2.4.6).

2.4.5 IncuCyte ZOOM analysis

The IncuCyte ZOOM was used to generate widefield images of 2.15mm^2 at 10x magnification in phase and green or red channels. The accompanying software (2018A) was used to analyse the number of fluorescent cells (count 1/well) or average fluorescence intensity (green calibration unit (GCU) x µm^2). In each instance, data was normalised to solvent-treated control cells.

2.4.6 Confocal microscopy

A549 cells, which were seeded onto coverslips, were transfected (section 2.5.4) with pTMEM16A-mycDDK (for further details of this plasmid refer to 2.5.1.2). At 24 hpt, cells were infected or mock infected with WT-HRSV for a further 24 hrs. Cells were then fixed and stained for immunofluorescence analysis (2.4.4) using primary antibodies targeting the DDK tag as well as various subcellular markers, and Alexa Fluor® labelled secondary antibodies (Table 2-4 and Table 2-5). Stained coverslips were mounted onto microscope slides using ProLong Gold

Antifade Mountant with DAPI (Thermo Fisher, P36941) and allowed to cure overnight. Slides were imaged using a Zeiss LSM880 + Airyscan Upright Confocal Microscope. The images were captured using the Plan-Apochromat 40x and 63x/1.4 Oil DIC objectives with the diode 405 nm, argon 488 nm and DPSS 561 nm lasers. Individual fluorescent signals were acquired independently to produce multicolour images and ensure that no bleed through between channels was observed. Images were analysed using Zen Blue software (Zeiss) and co-localisation line scan analysis was performed using ImageJ.

2.4.7 Antibodies

Table 2-4 Details of primary antibodies used in western blot (WB) and immunofluorescence (IF) experiments.

Antibody	Target/ Localisation	Concentration	Species	Source
HRSV	Polyclonal Ab targeting tissue, cells or virus corresponding to HRSV. Viral lysate of HRSV isolate.	WB 1:1000 IF 1:500	Goat	Abcam, Ab20745
GAPDH	α-glyceraldehyde 3-phosphate dehydrogenase (loading control)	WB 1:1000	Mouse	Santa Cruz, sc47724
BUNV-N	Bunyamwera virus nucleoprotein	WB 1:5000	Sheep	In house
HAZV-N	Hazara virus nucleoprotein	IF 1:5000	Sheep	In house
DDK (FLAG)	FLAG-tagged TMEM16A	WB 1:1000 IF 1:1000	Mouse	OriGene, TA50011-100
GM130	Golgi (cis)	IF 1:500	Rabbit	Cell signalling technologies, D6B1
EEA1	Early endosomes	IF 1:100	Rabbit	Invitrogen, PA5-17228

EIF4G	Stress granules	IF 1:200	Rabbit	Cell signalling technologies, 2469
LAMP1	Lysosomes	IF 1:100	Rabbit	Cell signalling technologies, 9091
Concanavalin A (Alexa Fluor 594 conjugate)	Endoplasmic reticulum	IF 1:30 (stock 5 mg/mL)	-	Invitrogen, C11253

Table 2-5 Details of secondary antibodies used in western blot (WB) and immunofluorescence (IF) experiments.

Antibody	Concentration	Species	Source
Goat IgG-HRP	WB 1:5000	Rabbit	Sigma, A8919
Mouse IgG-HRP	WB 1:5000	Goat	Sigma, A4416
Sheep IgG-HRP	WB 1:5000	Donkey	Sigma, A3415
Goat IgG-594	IF 1:500	Donkey	Invitrogen, A-11058
Mouse IgG-488	IF 1:500	Chicken	Invitrogen, A-21200
Sheep IgG-594	IF 1:500	Donkey	Invitrogen, A-11015
Rabbit IgG-594	IF 1:500	Chicken	Invitrogen, A-21442

2.5 Molecular biology

2.5.1 Plasmids

2.5.1.1 HRSV minigenome assay plasmids

Plasmids expressing HRSV (strain Long) N, P, L and M2-1 under the control of a T7 promoter, designated pN, pP, pL and pM2-1, have been described previously [330]. The fifth component of the HRSV minigenome assay (2.3.7) was the RNA minigenome, which consisted of terminal HRSV promoter regions flanking two transcriptional units (the second encoding eGFP) separated by the M/SH gene junction [331], henceforth termed pM/SH-GFP. These plasmids have been used previously to probe the roles of HRSV proteins in viral transcription [68,332,333]. All plasmids were generously gifted by Eleanor Todd on behalf of Dr JN Barr's lab.

2.5.1.2 TMEM16A mammalian cell expression plasmid

A plasmid encoding human TMEM16A ORF with a C-terminal 'mycDDK' tag within the pCMV6-Entry vector was purchased from OriGene (RC229400). The pCMV6-Entry vector is a functional mammalian expression vector. The 'mycDDK' tag contains myc-tag sequence (EQKLISEEDL) and the DDK (or FLAG) tag sequence (DYKDDDDK) separated by 18 nucleotides. This plasmid is henceforth termed 'pTMEM16A-mycDDK' and was used to study the localisation of TMEM16A within A549 cells by confocal microscopy (2.4.6).

2.5.2 Bacterial cell transformation

All work involving bacterial cells was performed under sterile conditions next to a Bunsen burner. To generate plasmid stocks, gifted or purchased plasmid DNA

was transformed into *E. coli* DH5-α competent cells (New England Biosciences). Cells were thawed on ice and incubated with 5 µL plasmid DNA on ice for 30 min. The heat shock method was used to transform cells at 42^{o}C for 45 secs before being placed back on ice for 5 mins. Room temperature lysogeny broth (LB) media was added, and cells were allowed to recover for 1 hr at 37^{o}C before being plated on LB agar plates containing 100 µg/mL ampicillin (pN, pP, pL, pM2-1, pM/SH-GFP) or 50 µg/mL kanamycin (pTMEM16A-mycDDK). Plates were incubated at 37^{o}C overnight to allow colonies to form.

2.5.3 Plasmid cDNA amplification

A single colony was selected to inoculate 5 mL LB media containing the appropriate antibiotic in a 50 mL falcon tube. This was incubated at 37^{o}C in a shaking incubator (160-200 RPM) for approximately 8 hrs. The 5 mL culture was added to 100 mL LB media containing antibiotic in a 500 mL conical flask and left to grow overnight. Bacterial cells were harvested, lysed and the DNA extracted using QIAGEN Maxi-prep kits following the manufacturers protocol. The concentration and purity of extracted DNA was checked using a NanoDrop One Microvolume UV-Vis Spectrophotometer (Thermo Scientific). To confirm the identity of the plasmid, a sample was sent for sequencing (Genewiz). The pN, pP, pL and pM2-1 plasmids were sequenced using T7 forward primer (5’ TAATACGACTCACTATAGGG 3’) and pTMEM16A-mycDDK was sequenced using the VP1.5 forward (5' GGACTTTCCAAAATGTCG 3') and XL39 reverse (5' ATTAGGACAAGGCTGGTGGG 3') primers (OriGene).

2.5.4 Mammalian cell transfections

Transfections were carried out using FuGENE HD transfection reagent (Promega, E2311). For HRSV minigenome studies (2.3.7), a total of 3.3 µg DNA was transfected per well (6-well plate) at a plasmid ratio of 1:1:1:1:1 unless otherwise stated, and for TMEM16A localisation studies (2.4.6), a total of 1 µg DNA was used per well (12-well plate). Plasmid DNA was mixed with Opti-MEM (Thermofisher) in a 1.5 mL tube and the transfection reagent was added to the centre of the liquid (avoiding the edges of the tube). The transfection reagent (µL):DNA (µg) ratio was 3:1. The transfection mixture was mixed by pipetting 15 times and incubated for 15 mins at room temperature to allow the formation of transfection complexes. The mixture was then added to cells containing 450 µL (12-well plate) or 850 µL (6-well plate) serum-free media for a total volume of 0.5 mL or 1 mL, respectively. After incubation at 37^{o}C for 6 hours, the transfection mix was removed, cells were washed with PBS and the media was replaced with complete DMEM.

2.6 Precision-cut lung slices (PCLS)

All practical work involving PCLS detailed below was carried out by members of Dr C Hesse's lab (Fraunhofer Institute, Germany) except for the western blot analysis of HRSV proteins in PCLS lysates, which was carried out by the author of this thesis according to section 2.4.2. All members of this collaboration contributed to the analysis and interpretation of the data and are recognised as co-authors in the resulting publication [326].

2.6.1 Preparation of Precision-Cut Lung Slices (PCLS)

Primary human lung tissue was provided by KRH Klinikum Siloah-Oststadt-Heidehaus (Hannover, Germany) from cancer patients who underwent lung

resection. Human PCLS were generated from disease-free tissue as previously described [334]. Briefly, lobes were filled with 2 % agarose (Sigma Aldrich) in DMEM/F12 (Gibco) via the bronchi. Solidified tissue was punched into cores of 8 mm diameter and cut into slices of 300-350 µm on a microtome (Krumdieck Tissue Slicer, Alabama Research and development, Muniford, AL, USA). PCLS containing airways were microscopically checked for ciliary movement and cultured in a 24-well plate in DMEM/F12 supplemented with 1% P/S (10,000 U/ml, Gibco) at 37°C with 5% CO_2 overnight [326].

2.6.2 Ex vivo infection experiments using human PCLS

PCLS were drug-treated for 40 min in DMEM/F12 (1% P/S) and subsequently infected with HRSV ($2.5x10^5$ PFU/well) or ultraviolet (UV)-inactivated virus. Supernatants were collected after 24 hrs, and tissues were lysed in 1 % Triton X-100 (Sigma Aldrich) in PBS (Lonza). Supernatants and lysates were supplemented with 0.02% Protease Inhibitor Cocktail (P1860, Sigma Aldrich). For viability assessments, lactate dehydrogenase (LDH) release was assayed in the supernatants using Cytotoxicity Detection Kits (Roche). IP-10 secretion was measured by ELISA (2.3.9.2). Total protein content was measured from the lysates via bicinchoninic acid (BCA) assays (Thermo Scientific). Virus protein expression was assessed by western blot (2.4.2) [326].

2.6.3 Ethics Statement

The use of human lung tissue was approved by the ethics committee (number 2701–2015) of the Hannover Medical School, Hannover, Germany. Experiments complied with the Code of Ethics of the World Medical Association (Declaration of Helsinki) involving human subjects. The privacy rights of human subjects were

observed, and written consent was obtained from all patients. Personal data were not recorded to protect anonymity [326].

2.7 Statistical analysis

IncuCyte ZOOM quantification (2.4.5) or western blot densitometry (2.4.2) analysis of virus infection, as well as cell viability (2.1.3) data were compared using a one-way analysis of variance (ANOVA) Bonferroni multiple comparison test (Cl^- channel inhibitor-treated cells vs solvent-treated controls). Data were analysed using Microsoft Excel (V.2013). Assays were verified using the HRSV inhibitor ribavirin (and additional controls where stated). Averages and statistical analysis were performed where $n \geq 3$. P values ≤ 0.05 were considered statistically significant (*). For PCLS (2.6) data, statistical analysis was performed using a one-way ANOVA Dunnett's multiple comparison test or an unpaired Mann-Whitney one-tailed test using GraphPad Prism (V.8.3.1). P values of ≤ 0.05 were considered significant (*) [326].

Chapter 3 Discovery of a novel role for TMEM16A during HRSV infection

3.1 Introduction

Human Cl^- channels are a family of poorly understood, largely overlooked ion channels. Until relatively recently, it was thought that their only role was the regulation of action potentials in excitable cells, however it is now becoming apparent that Cl^- channels have many more equally important functions within cells [158]. With the emergence of a wealth of research implicating other host ion channel families (e.g., K^+ channels) as viable antiviral targets [305,306], a need to assess the potential role of Cl^- channels became apparent. HRSV was described 65 years ago, however there are still currently no effective treatment options available. A role for Cl^- channels as host factors during HRSV infection was yet to be investigated, and a need for novel antiviral targets was evident. Therefore, the aim of this chapter was to assess a potential role of host Cl^- channels during HRSV infection. To achieve this, a pharmacological approach was adopted wherein an ion channel inhibitor screen was performed to test the sensitivity of HRSV to selected and increasingly specific modulators of Cl^- channels. For this, the use of a GFP-labelled HRSV A2 strain to assess infection was firstly validated. Following the screen, hits were investigated further using physiologically relevant models of infection. Lastly, other NSVs were tested for their sensitivity to the Cl^- channels of interest.

3.2 HRSV propagation, purification, and quantification

The experiments described in this thesis involved two genetically distinct HRSV isolates, which were the wild type A2 strain (WT-HRSV) and a derivative in which the GFP gene had been inserted as an independent transcriptional unit in the first

position in the HRSV gene order (HRSV-GFP). To generate purified stocks of these viruses for use in subsequent experiments, an optimal HRSV propagation protocol was established based methods described by Sun and Lopez, 2016 [329], Gias et al., 2008 [328], Vasou, 2016 [335], alongside in-house protocols written by Dr Samantha Hover, and Eleanor Todd. To propagate the virus, HEp-2 cells were infected with HRSV at MOI 0.01 for 5 days, or until CPE was observed. HEp-2 cells are known to produce high yields of HRSV and are the most common cell type used for this purpose [336] and a low MOI is required to prevent the formation of defective viral particles [329].

HRSV spreads from cell-to-cell through release of infectious virions, but also through the creation of large, multinucleated cells known as syncytia [337]. Therefore, to gain the highest yield of virus, the supernatant containing the released virus and the cell-associated virions were collected separately and later combined. Infection with HRSV produces substantial cytokine release from cells therefore purification of HRSV stocks is critical to prevent these from interfering with future experiments [338]. WT-HRSV was harvested from supernatant and from cell lysates, and each was recovered after purification through a 30% sucrose cushion. Samples were additionally collected throughout purification to test the efficiency of the process (i.e., the post-ultracentrifugation media, the sucrose cushion, and the interface between the two). Infectious virions were identified in samples by applying to naïve A549 cells (alongside an MOI of 1 or 0.5 infection controls) and assessing the number of infected cells by immunofluorescence (Figure 3-1 Ai). Fluorescence images (Figure 3-1 Aii) were taken, and the number of infected cells was quantified using an IncuCyte ZOOM cell imaging system. For WT-HRSV, the purification process was efficient and

only minimal amounts of virus were found in the post-ultracentrifugation test samples (Figure 3-1 A; sucrose, interface, and media), compared to the cells infected with the purified virus samples (clarified) and infection controls.

Next, the second HRSV isolate, HRSV-GFP, was purified using the optimised method outlined above using a sucrose cushion. Again, naïve cells were infected with the purified virus stock to check for infectious virions, and GFP-expressing cells were detected using the IncuCyte. Initially, the virus yield appeared greatly reduced owing to the lack of GFP-fluorescent cells upon re-infection with the total purified sample compared to the control infection (MOI 0.5) (Figure 3-1 B, green cells). However, upon staining with the α-HRSV antibody, it was revealed that most of the cells were infected, however did not contain GFP (Figure 3-1 B, red cells). The images in Figure 3-1 B show the contrast in the number of green (HRSV-GFP expressing) cells and the number of red cells (positive for α-HRSV staining) infected with the virus purified by sucrose cushion. This indicated that the HRSV-GFP isolate had lost the ability to express GFP following propagation and purification by ultracentrifugation.

By comparison, when HRSV-GFP was purified by PEG precipitation rather than by sucrose cushion, all the infected cells displayed GFP expression. The images in Figure 3-1 C show cells infected with HRSV-GFP purified via PEG and the α-HRSV staining (red) co-localised perfectly with HRSV-GFP expressing cells (green). This showed that when HRSV-GFP was propagated and purified by PEG-precipitation, it retained GFP expression and therefore, this was the method taken forward for virus purification (2.2.2).

Silver staining was used to check the purity of WT and GFP virus preparations using PEG. A sample of each virus prep was resolved by SDS-PAGE and silver

staining revealed bands corresponding to viral proteins (Figure 3-1 D). Minimal non-viral bands were identified in the samples, confirming samples were relatively pure.

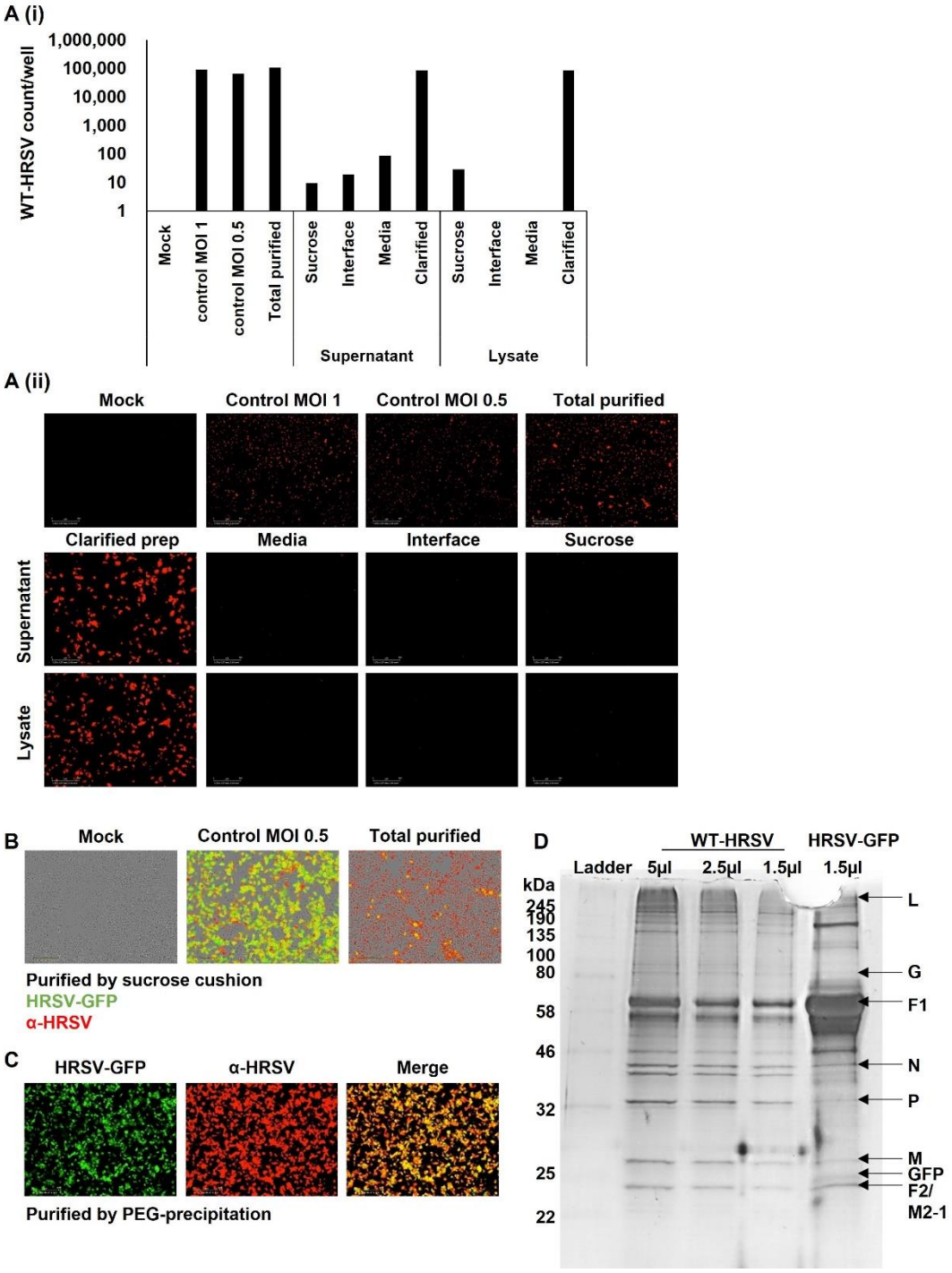

Figure 3-1 Optimisation of HRSV purification. A) WT-HRSV stocks were purified using ultracentrifugation through a 30% sucrose cushion and fractions taken at each step. The amount of virus present in each fraction was assessed

by re-infecting cells and staining with anti-HRSV (red). IncuCyte ZOOM analysis quantified the number of fluorescent cells. **B-C)** IncuCyte images of A549 cells infected with HRSV-GFP (green) following purification by (B) sucrose cushion or (C) PEG-precipitation. Cells were co-stained for anti-HRSV (red). **D)** Samples of WT-HRSV and HRSV-GFP were resolved by SDS-PAGE and silver stained revealing the labelled viral bands.

To quantify the titre of the virus produced, several methods were assessed including a crystal violet-based plaque assay, immunostaining-based plaque assay, focus forming assay (FFA) and median tissue culture infectious dose ($TCID_{50}$) assays. The crystal violet plaque assays were less accurate due to the ability of HRSV to spread without lysing the infected cells, thus often producing poorly defined, or non-existent, plaques, resulting in a lower estimate of virus quantity. The FFA and $TCID_{50}$ assays had the benefit of speed, giving a measure of virus titre within a couple of days, although the difficulty in accurately identifying HRSV-mediated CPE or foci of infection was a possible source of inaccuracy. Measurement of titre using the immunostaining-based plaque assay resulted in similar findings to the $TCID_{50}$ assay and provided the additional important benefit of increased certainty of HRSV foci detection, due to the HRSV antibody specificity. An example of this is shown in Figure 3-2, wherein titration of the same WT-HRSV virus stock resulted in similar estimations of virus titre of between $1\text{-}7x10^{7}$ PFU/mL via immunostaining-based plaque assay (Figure 3-2 A) and $TCID_{50}$ (Figure 3-2 B). Samples of the unpurified virus supernatant and cell pellet taken when the virus was harvested were also titred via both methods. The immunostaining-based plaque assay displayed plaques from the virus supernatant in the first three dilutions (10^{-1}-10^{-3}, Figure 3-2 A), however in the $TCID_{50}$, CPE was only observed in the first dilution (10^{-1}, Figure 3-2 B), indicating

the lower sensitivity of the $TCID_{50}$ compared with the immunostaining-based plaque assay. Moreover, the cell pellet, which contained the leftover cellular debris after harvesting the virus and therefore should not contain any virus, displayed zero plaques on the immunostaining-based plaque assay (Figure 3-2 A) but CPE was observed in the $TCID_{50}$ assay up to the 10^{-5} dilution (Figure 3-2 B), indicating inaccuracy. For these reasons, the immunostaining-based plaque assay was deemed the most accurate and reliable assay and so this was used routinely to check virus titres (2.2.3).

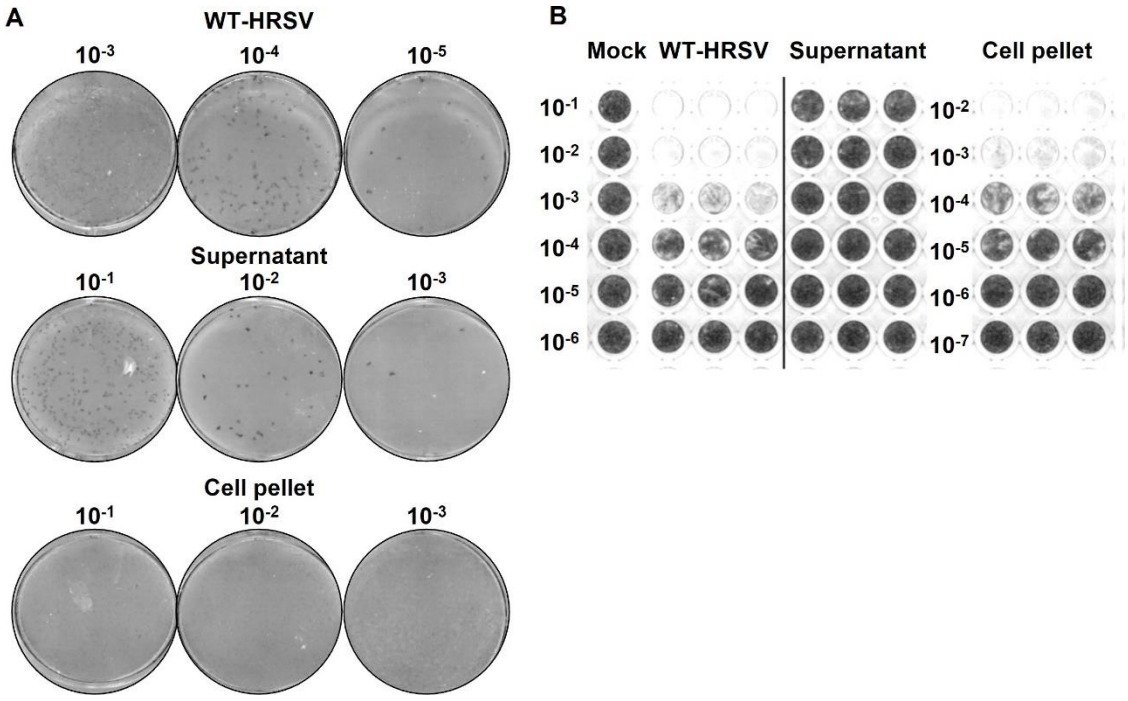

Figure 3-2 Comparison of techniques used to quantify HRSV stocks. A-B) Purified WT-HRSV, along with samples of the supernatant and cell pellet taken whilst harvesting the virus were quantified using (A) an immunostaining-based plaque assay or (B) $TCID_{50}$ assay and the results were compared.

3.3 Assessment of HRSV infection

The GFP-tagged HRSV strain was used for the rapid detection of HRSV infected cells, and quantification of HRSV gene expression in live cells. To verify the use of HRSV-GFP as a surrogate for WT-HRSV, the growth kinetics and plaque morphologies of the two viruses were compared. These, and the subsequent drug experiments, were performed in A549 adenocarcinomic human alveolar basal epithelial cells as a physiologically relevant, HRSV-permissive cell line. To analyse the growth of HRSV-GFP, the IncuCyte ZOOM was used to visualise and quantify GFP fluorescence within live infected cells over 48 hrs. HRSV-GFP expression was first observed at 9 hpi indicating the start of viral gene expression and ensuing protein production (Figure 3-3 A). Newly infected cells became observable at around 25 hpi, therefore as the primary round of infection was first detected at 9 hpi the time of release was likely ~9 hrs earlier, at ~16 hpi. This was comparable to what is known for WT-HRSV [339]. The number of HRSV-GFP infected cells continued to increase, roughly doubling between 24 and 48 hpi. As expected, infection of a MOI of 1 resulted in a larger number of HRSV-GFP expressing cells than did infection at MOI 0.1 at all time points, although the rate of infection was consistent for both MOIs. In addition, plaque morphologies of WT-HRSV and HRSV-GFP showed no differences (Figure 3-3 B), being of a similar size and shape, and both viruses were able to be grown to a similar titre. Taken together, these results suggest that introducing an additional transcriptional unit in HRSV-GFP resulted in no distinguishable differences in virus growth with the parental HRSV-WT, in agreement with previous work [339].

To further validate the utility of the IncuCyte/HRSV-GFP detection system to act as a surrogate for HRSV-specific gene expression and growth, ribavirin, a known

HRSV inhibitor and the only current FDA-approved treatment for HRSV LRTI was assessed for its antiviral efficacy against HRSV-GFP. Ribavirin is known to inhibit WT-HRSV in a concentration-dependent manner *in vitro* [340]. A549 cells were treated pre-infection (pre-treated) with ribavirin (10-80 µM) to allow the drug to act upon the cells, after which cells were infected with HRSV-GFP for 24 hrs with drug maintained throughout. Infection was assessed at 24 hpi and a concentration-dependent decrease was observed in HRSV-GFP fluorescence from a 35.5% reduction with 10 µM ribavirin relative to solvent-treated controls, to a 92.7% reduction with 80 µM ribavirin (Figure 3-3 C(i), black bars). Representative IncuCyte images of HRSV-GFP expression within these cells are shown in Figure 3-3 C(ii), which revealed a decline in the number of GFP expressing cells with increasing concentrations of ribavirin. The toxicity of ribavirin was determined by measuring the viability of drug-treated cells via MTS assays. In these and all future assays, an average of ≥80.0% cell viability relative to the solvent-treated controls was considered non-toxic. In ribavirin-treated cells, cell viability remained over the threshold at all concentrations (95.9% of solvent-control at 80 µM) indicating that the decrease in HRSV-GFP expression and thus HRSV infection, was not due to toxic effects on the cells (Figure 3-3 C(i), grey bars). Taken together, these data validated the HRSV-GFP virus as a surrogate marker of HRSV infection in cell culture assays.

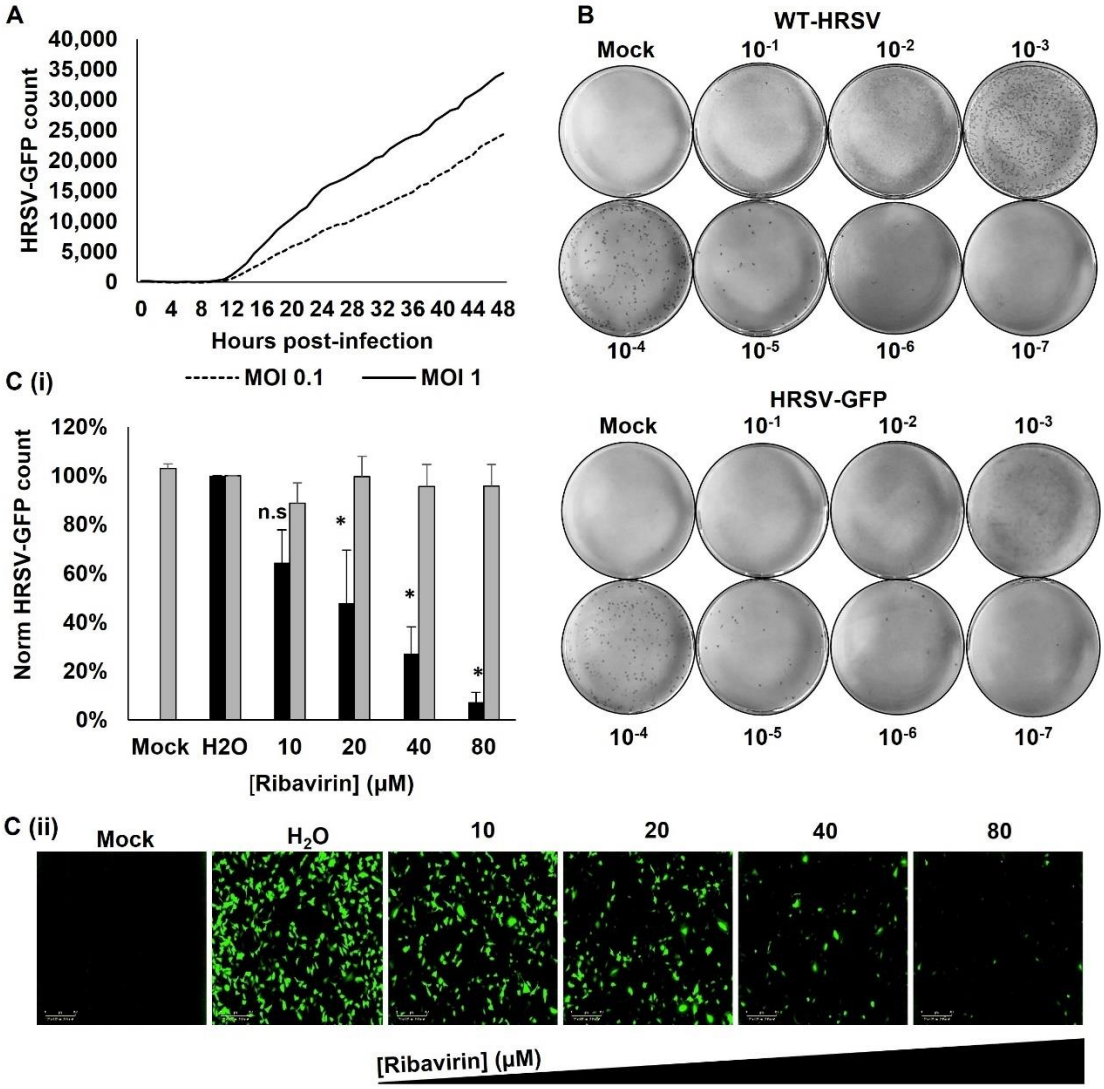

Figure 3-3 Using HRSV-GFP expression as a marker of infection. A) A549 cells were infected with HRSV-GFP at MOI 0.1 or 1 for 48 hrs and the number of fluorescent cells was quantified in live cells every hour via IncuCyte ZOOM analysis. **B)** Comparison of the plaques formed by WT-HRSV and HRSV-GFP. HEp-2 cells were infected with a serial dilution of either virus for 5 days under a methylcellulose overlay. Cells were fixed and plaques visualised by staining with anti-HRSV with an HRP-conjugated secondary antibody and incubation with 4-CN. **C(i)** A549 cells were pre-treated with ribavirin (10-80 µM) for 45 min prior to infection with HRSV-GFP. Quantification of HRSV-GFP expression by IncuCyte ZOOM took place at 24 hpi (black bars). Cell health was measured by MTS assay and was compared to solvent (H_2O)-treated controls (grey bars). Mean of n=4 ± SE, *p≤0.05, n.s = non-significant. **C(ii)** Representative IncuCyte images showing HRSV-GFP expressing cells in the presence of ribavirin.

3.4 Blocking Cl^- channels inhibits HRSV

To investigate the effects of Cl^- channel inhibition on HRSV infection, classical broad-spectrum Cl^- channel inhibitors 4,4'-diisothiocyanostilbene-2,2'-disulfonic acid (DIDS), 5-nitro-2-(3-phenylpropylamino) benzoic acid (NPPB), and R(+)-[(6,7-Dichloro-2-cyclopentyl-2,3-dihydro-2-methyl-1-oxo-1H-inden-5-yl)-oxyacetic acid (R+IAA-94) were added to A549 cells prior to HRSV-GFP infection. These compounds were selected as they have been shown to block a multitude of Cl^- family members (Figure 3-4 A), and thus any effects would reveal a general role for this ion channel family during virus infection. Open-channel blockers, such as DIDS and NPPB, work by binding within and occluding the channel pore therefore preventing the flow of Cl^- ions. DIDS is known to modulate Cl^-/HCO_3^- exchanger, VDACs, ClCs, CaCCs and VRACs [341–343]. NPPB inhibits CaCCs, most ClCs, CFTR and VRACs [342,344]. R+IAA-94 modulates CLIC1 [345,346], CLIC4 and CLIC5 [347] through an unknown mechanism. It has been speculated that R+IAA-94 binds the soluble form of CLIC1, reducing its enzymatic activity and ultimately its channel activity [346]. However, direct binding of R+IAA-94 to the membrane bound form of CLIC1 has not been ruled out. R+IAA-94 has been exploited for the isolation and reconstitution of CLIC3 and CLIC4 [347], indicating a direct interaction between the drug and these channels occurs within cells.

Treatment with both DIDS (10-50 µM) and NPPB (40-100 µM) resulted in a concentration-dependent reduction in HRSV-GFP expression of up to 85.7% (50 µM) and 94.7% (100 µM) respectively, compared to solvent-treated controls (Figure 3-4 B and C; black bars). MTS assays confirmed that there was no adverse effect on cell viability at the concentrations tested as this remained

above 80% of the viability of solvent-treated controls (Figure 3-4 B and C; grey bars). In contrast to DIDS and NPPB, treatment with R+IAA-94 at non-toxic concentrations (10-25 µM) did not elicit an inhibitory effect on HRSV-GFP expression compared to the solvent-treated control (Figure 3-4 D).

Figure 3-4 E shows representative IncuCyte images of HRSV-GFP infected cells treated with all three inhibitors, in which the concentration-dependent inhibition of DIDS and NPPB from left to right is clearly visible [326].

These results were confirmed using WT virus. Cells were pre-treated with Cl^- channel inhibitors and infected as in the previous experiments. To measure WT-HRSV infection, cells were lysed at 24 hpi and the lysates were resolved by SDS-PAGE. WT-HRSV glycoprotein (G) was used as a marker of infection, and expression levels were analysed by western blot. In agreement with the results obtained for HRSV-GFP, WT-HRSV-G expression decreased in a concentration-dependent manner in the presence of NPPB and DIDS as well as the positive control ribavirin, with no loss of viral protein expression observed in R+IAA-94 treated cells (Figure 3-4 F). This ruled out any impact of the drugs on GFP expression alone and indicated a HRSV-specific effect.

Taken together, these data strongly indicated a requirement for Cl^- channels during HRSV infection, specifically Cl^- channel family member(s) that are sensitive to NPPB and DIDS, but not R+IAA94. From this inhibitory profile, a role for CLICs during HRSV infection was ruled out, however the sensitivity of HRSV to DIDS and NPPB implicated CaCCs, ClCs, VRACs and CFTR as channel families of interest (Figure 3-4 A). The following sections describe further experiments to examine the role of these remaining Cl^- channel families.

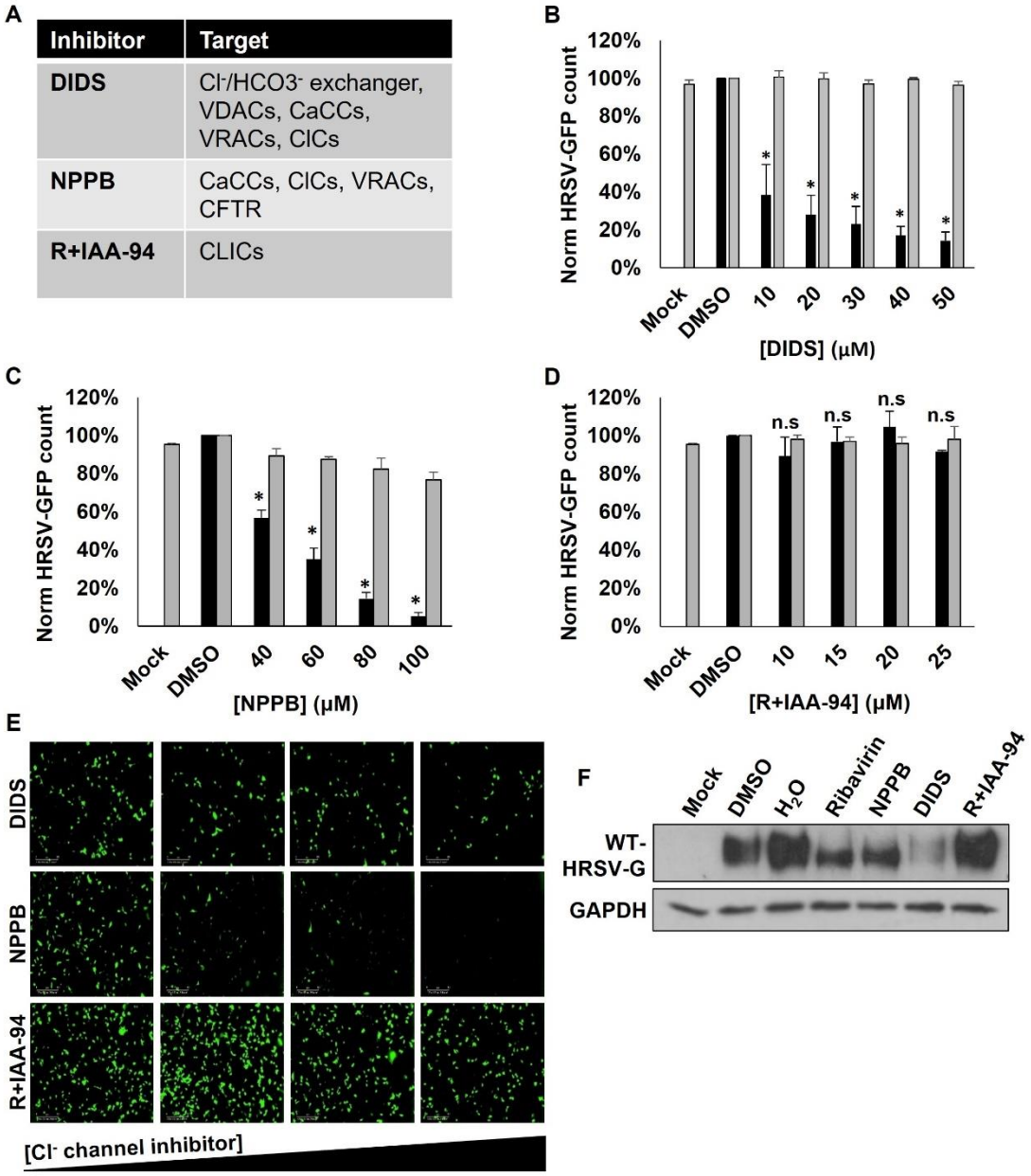

Figure 3-4 Blocking Cl^- channels inhibits HRSV infection. A) Broad spectrum Cl^- inhibitors and their known targets. **B-D)** A549 cells were pre-treated with broad spectrum Cl^- channel inhibitors (B) DIDS 10-50 μM, (C) NPPB 40-100 μM or (D) R+IAA-94 10-25 μM for 45 mins prior to HRSV-GFP infection. Quantification of HRSV-GFP expression by IncuCyte ZOOM took place at 24 hpi (black bars). Cell health was measured by MTS assay and was compared to solvent (DMSO)-treated controls (grey bars). Mean of n=4 ± SE, *p≤0.05, n.s = non-significant. **E)** Representative IncuCyte images showing HRSV-GFP expressing cells in the presence of indicated Cl- channel inhibitors. **F)** A549 cells were pre-treated with the indicated inhibitors and infected with WT-HRSV. Cell lysates were taken 24

hpi and analysed by western blot. WT-HRSV-G was used as a marker of infection and GAPDH loading control is shown.

3.5 Inhibiting CFTR does not influence HRSV infection

CFTR is a Cl^- channel that is highly expressed in the epithelial cells of the respiratory tract, the major site of HRSV infection. Several CFTR-specific inhibitors exist, including CFTRinh-172, chromanol 293B and glibenclamide. CFTRinh-172 is an allosteric inhibitor of CFTR that interacts with the NBD-1 resulting in maintenance of the closed state [348,349]. The mechanism of action of chromanol 293B is not well understood although it is thought to be more complex than a simple pore blocker; evidence suggests that the mechanism is voltage-independent and may depend on the phosphorylation state of CFTR [350]. CFTR is activated by various phosphatases and can be classed as dephosphorylated, partially-, moderately-, or highly phosphorylated; it appears that chromanol 293B can only inhibit CFTR whilst it is moderately phosphorylated. Glibenclamide is an open-channel blocker that occludes Cl^- flow by binding residues deep within the pore [351]. Evidence suggests that a key charged residue (K978) on cytoplasmic loop 3, which is situated close to the pore and is involved in channel opening [352], acts as an initial interaction point to drive glibenclamide into the pore [353].

Despite the known importance of this channel in lung epithelial cells, treatment of A549 cells with the highest non-toxic concentrations of CFTRinh-172 (25 µM) elicited a small reduction in HRSV-GFP expression of 8.9% relative to solvent-treated controls, however was statistically non-significant (Figure 3-5 A). Moreover, chromanol 293B and glibenclamide treatments also had no significant

adverse impact on HRSV-GFP expression. In fact, cells treated with chromanol 293B showed a small but significant increase in HRSV-GFP expression (12.8% increase at 30 µM compared to solvent-treated control), however this was not maintained at higher concentrations of chromanol 293B (Figure 3-5 B). Lastly, glibenclamide (40 µM) showed a 10.0% reduction in HRSV-GFP expression and this also did not reach statistical significance (Figure 3-5 C). The representative images in Figure 3-5 D confirm that the number of GFP-expressing cells does not change with increasing concentrations of the CFTR modulators. As the drugs had varying mechanisms of inhibition of the CFTR, based on these data, it was concluded that the CFTR does not play a role during the HRSV lifecycle, at least in the cell culture system used here [326].

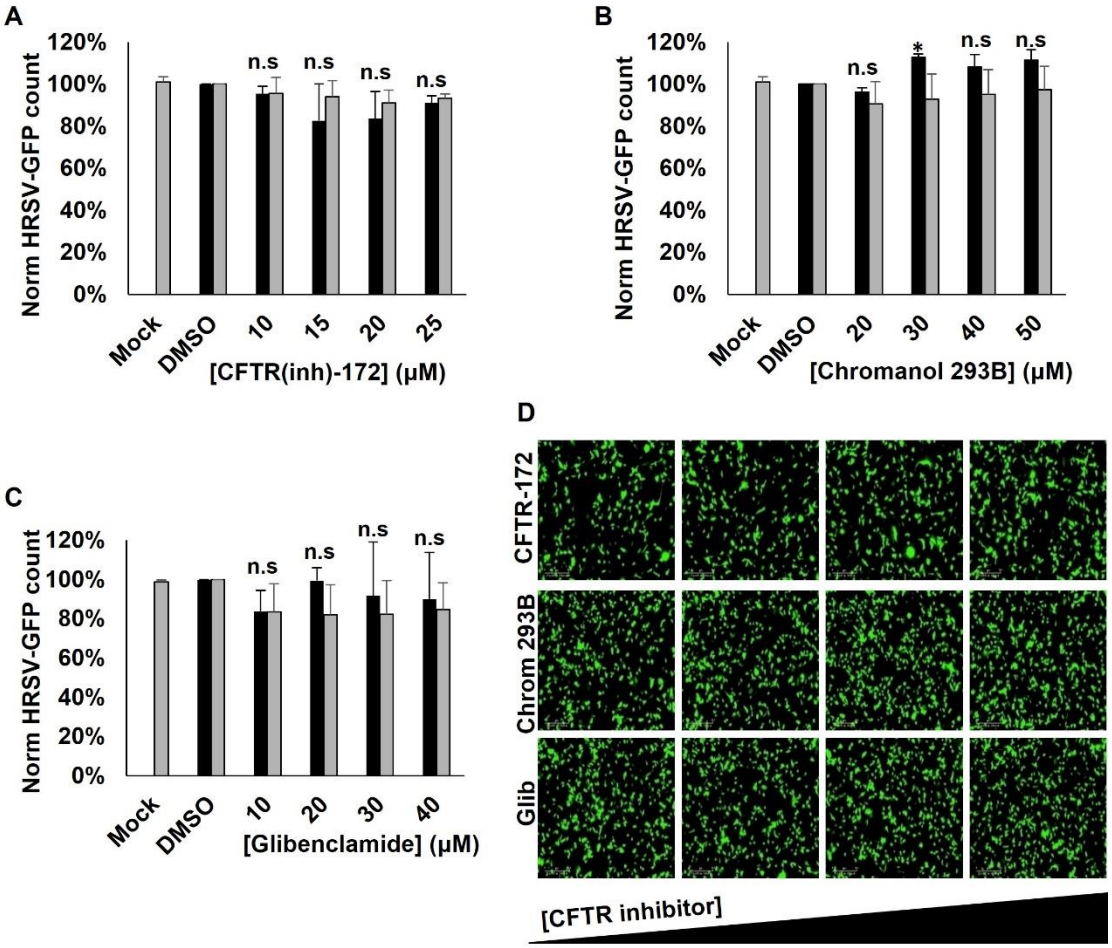

Figure 3-5 Inhibiting CFTR does not influence HRSV infection. A-C) A549 cells were pre-treated with CFTR inhibitors (A) CFTRinh-172 10-25 μM, (B) chromanol 293B 20-50 μM or (C) glibenclamide 10-40 μM for 45 mins prior to HRSV-GFP infection. Quantification of HRSV-GFP expression by IncuCyte ZOOM took place at 24 hpi (black bars). Cell health was measured by MTS assay and was compared to solvent (DMSO)-treated controls (grey bars). Mean of n=4 ± SE, *p≤0.05, n.s = non-significant. **D)** Representative IncuCyte images showing HRSV-GFP expressing cells in the presence of indicated CFTR inhibitors.

3.6 VRACs do not play a key role during HRSV infection

Mammalian cells respond to cell swelling by increasing swelling-activated Cl^- currents, which play key roles in cell volume, apoptosis, and membrane potential regulation. Swelling-activated currents are mediated by ubiquitously expressed

volume-regulated anion channels (VRACs) [354]. The functional significance of VRACs during HRSV infection was evaluated by studying the effects of their known small molecule pharmacological inhibitor 4-(2-Butyl-6,7-dichloro-2-cyclopentyl-indan-1-on-5-yl) oxobutyric acid (DCPIB) [355]. Structural studies have revealed that DCPIB blocks VRACs through a 'cork in a bottle' mechanism where it binds within the channel selectivity filter [356].

In cells treated with DCPIB (2-10 µM), HRSV-GFP expression was reduced by up to 30.0% at 8 µM, compared to the solvent-treated control (Figure 3-6 A, black bars). DCPIB was not toxic to cells at these concentrations and the cell viability remained above 91.6% of the solvent-treated control (Figure 3-6 A, grey bars). Despite the modest decrease in infection, this compound failed to recapitulate the concentration-dependent and potent effects of NPPB and DIDS, as shown in the representative IncuCyte images in Figure 3-6 B, suggesting that VRACs are unlikely to represent the key Cl^- channel family required for HRSV infection. The result was also confirmed using WT-HRSV. As previously, WT-HRSV-G was used to assess infection and in the presence of DCPIB, expression levels were slightly reduced (Figure 3-6 C). Based on this data, a minor role for VRACs during infection could not been discounted but was not investigated further in this study.

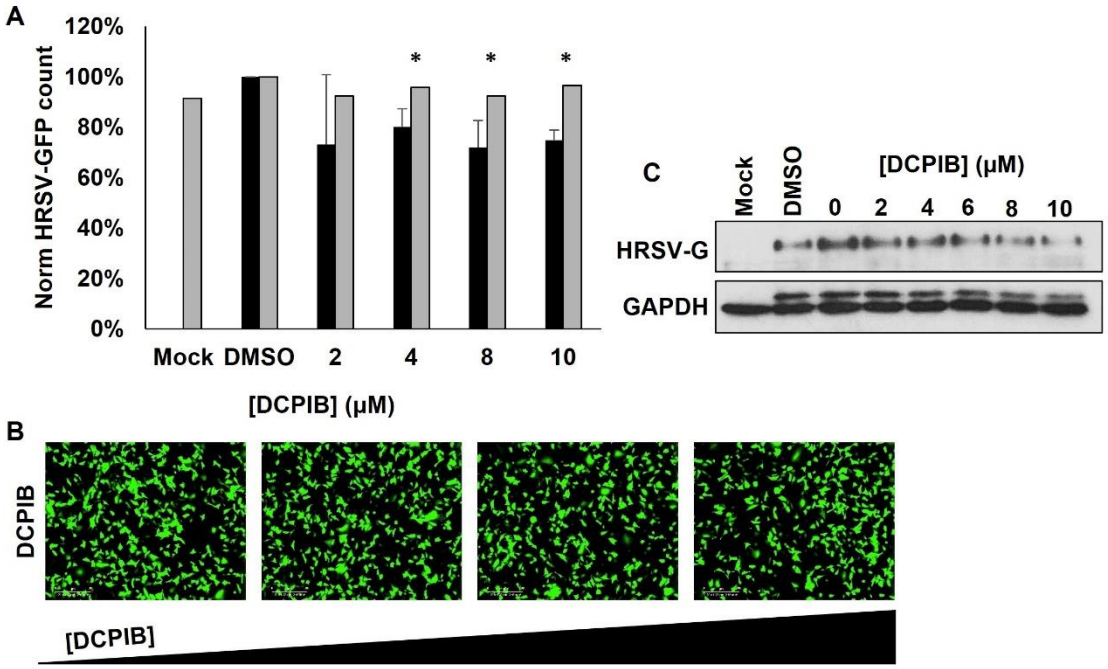

Figure 3-6 VRACs do not play a key role during HRSV infection. A) A549 cells were pre-treated with VRAC inhibitor DCPIB 2-10 µM for 45 mins prior to HRSV-GFP infection. Quantification of HRSV-GFP expression by IncuCyte ZOOM took place at 24 hpi (black bars). Cell health was measured by MTS assay and was compared to solvent (DMSO)-treated controls (grey bars). Mean of n=4 ± SE, *p≤0.05, n.s = non-significant. **B)** Representative IncuCyte images showing HRSV-GFP expressing cells in the presence of DCPIB 2-10 µM. **C)** Cells were treated as in (A) and infected with WT-HRSV for 24 hrs. Cell lysates were analysed by western blot using WT-HRSV-G as a marker of infection and a GAPDH loading control.

3.7 Blocking CaCCs inhibits HRSV infection

CaCCs are activated by intracellular Ca^{2+} ions leading to channel opening and flow of Cl^- ions. Several inhibitors of this family have been identified, including CaCCinh-A01, niflumic acid, talniflumate and tannic acid (Figure 3-7 A). Whilst these inhibitors have been used abundantly in studies of CaCC currents, the mechanisms of action have largely remained unknown. The recent revelation of

the structure of TMEM16A [210,357] has allowed the first insights into the mechanisms of some of these compounds. Computational analysis suggested that CaCCinh-A01 inhibited CaCC currents through directly binding the upper pocket of the pore, therefore occluding ion flow through the channel. Furthermore, this interaction caused the collapse of the pore [358]. However, an earlier study had described a mechanism of inhibition wherein CaCCinh-A01 facilitated the proteasomal degradation of the TMEM16A protein, therefore reducing expression levels within the cell [359]. The mechanism of CaCC inhibition by niflumic acid and its pro-drug talniflumate remain to be elucidated but have been shown to be voltage-dependent [360], with the level of blockade being lessened when the membrane potential is negative. Furthermore, both are known non-steroidal anti-inflammatory drugs clinically approved for the treatment of rheumatoid arthritis, and chronic obstructive pulmonary disease (COPD) and asthma, respectively. Lastly, tannic acid is another classical CaCC inhibitor which has been used historically to inhibit TMEM16A/B through a yet unknown mechanism. Interestingly, tannic acid is a natural ingredient in green tea and red wine and is thought to mediate the health benefits of these drinks due to its ability to inhibit CaCC channels involved in aortic smooth muscle contraction and epithelial Cl^- secretion [361].

Upon the assessment of HRSV-GFP expression in cells pre-treated with CaCC modulators, CaCCinh-A01 (5-40 µM) treatment resulted in a concentration-dependent decrease in HRSV-GFP expression by up to 59.8% (40 µM) relative to solvent-treated control cells (Figure 3-7 B, black bars). Similarly, niflumic acid (10-40 µM) and talniflumate (10-40 µM) inhibited HRSV-GFP expression significantly, up to 93.5% (40 µM) and 75.4% (40 µM) respectively (Figure 3-7 C-

D, black bars). Tannic acid treatment (5-20 µM) also inhibited HRSV-GFP expression by 91.2% of the control at 20 µM (Figure 3-7 E). MTS assays confirmed that the CaCC modulators did not impact cell health, and at all concentrations the cell viability was over the threshold of 80% of the solvent-treated controls (Figure 3-7 B-E, grey bars). Representative IncuCyte images in Figure 3-7 F show visually the significant decrease in HRSV-GFP fluorescence in drug-treated cells.

These data were validated through western blot analysis of WT-HRSV-G expression in the presence of each CaCC modulator. A potent decrease in viral protein expression was observed in response to treatment with CaCCinh-A01, niflumic acid, talniflumate and tannic acid compared to the solvent-treated controls (Figure 3-7 G-J). This confirmed that the concentration-dependent decrease observed in the GFP signal acted at the level of protein expression, rather than an unspecified direct effect of the inhibitors on GFP fluorescence, such as quenching. Therefore, based on of the potency and concentration-dependency of virus inhibition, it was concluded that the CaCCs represented the major Cl^- channel family on which HRSV relies for efficient infection (summarised in Table 3.1) [326].

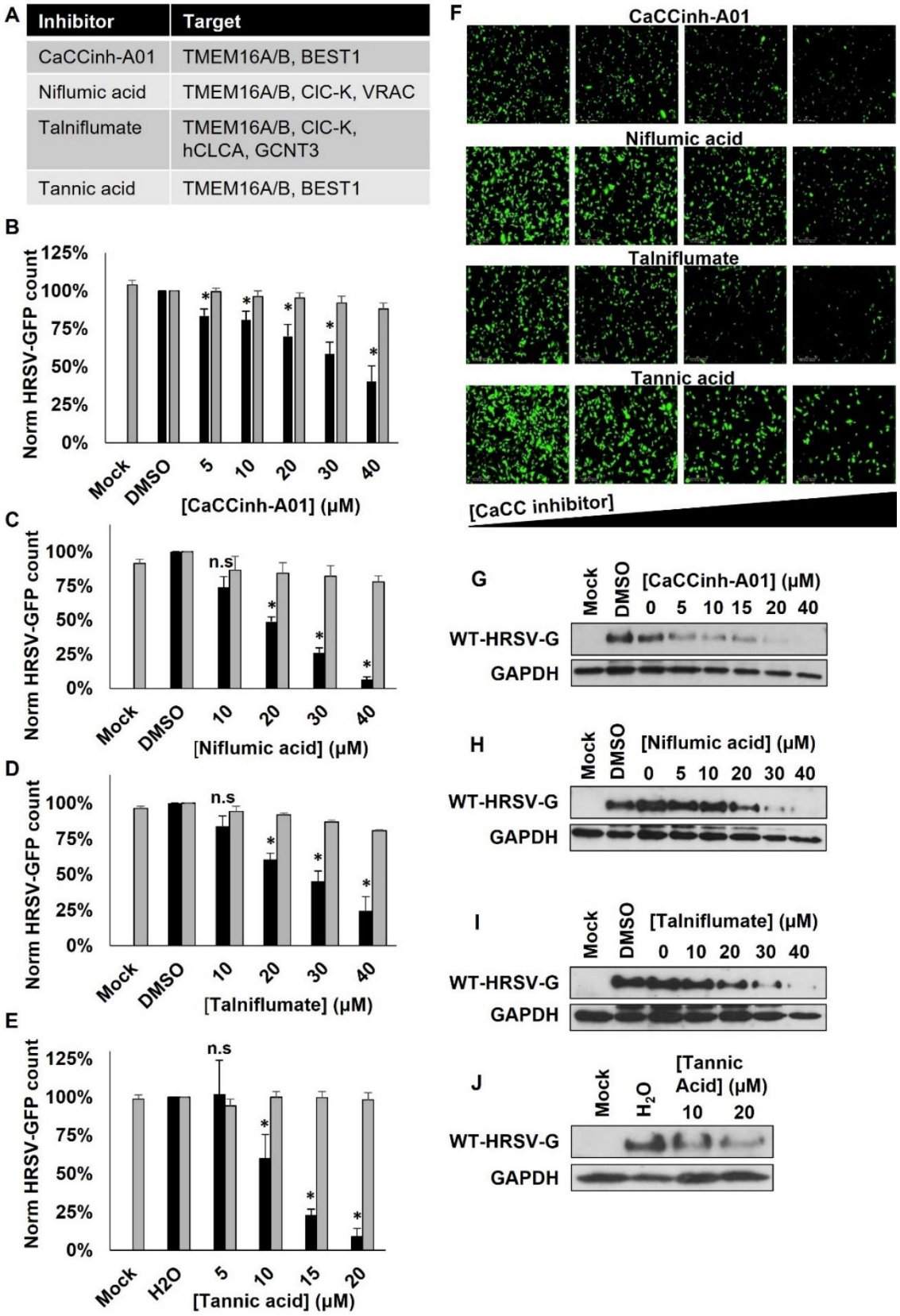

Figure 3-7 Blocking CaCCs inhibits HRSV infection. A) Known targets of the selected CaCC inhibitors. **B-E)** A549 cells were pre-treated with CaCC inhibitors

(B) CaCCinh-A01 5-40 µM, (C) niflumic acid 10-40 µM, (D) talniflumate 10-40 µM or (E) tannic acid 5-20 µM for 45 mins prior to HRSV-GFP infection. Quantification of HRSV-GFP expression by IncuCyte ZOOM took place at 24 hpi (black bars). Cell health was measured by MTS assay and was compared to solvent (DMSO or H2O)-treated controls (grey bars). Mean of n=4 ± SE, *p≤0.05, n.s = non-significant. **F)** Representative IncuCyte images showing HRSV-GFP expressing cells in the presence of indicated CaCC inhibitors. **G-H)** Cells were treated as in (B-E) and infected with WT-HRSV for 24 hrs. Cell lysates were analysed by western blot using WT-HRSV-G as a marker of infection and a GAPDH loading control.

Table 3.1 Summary of the sensitivity of HRSV to modulation of Cl^- channel families.

Cl^- channel family	HRSV sensitivity?	Reasoning
CFTR	No	CFTRinh-172, chromanol 293B and glibenclamide insensitive
ClCs	Potentially ClC-2, others unlikely	Tissue specific expression (ClC-1 – skeletal muscle, ClC-Ka and -Kb – kidney and inner ear) ClC-2 widely expressed and sensitive to DIDS and NPPB
LGCCs	Unlikely	Tissue specific expression (GABA and glycine receptors – CNS)
CaCCs	Yes	Sensitive to CaCCinh-A01, niflumic acid, talniflumate and tannic acid
VRACs	Potentially a minor role, but unlikely to play a major role	Partial sensitivity to DCPIB, but not concentration-dependent
CLCAs	Unlikely	Tissue specific expression (CLCA1 – intestines, CLCA2 – Trachea and mammary glands, CLCA3 – truncated pseudogene, CLCA4 – Neural tissue)
CLICs	No	R+IAA-94 insensitive

3.8 TMEM16A is the CaCC required during HRSV infection

Within the CaCC channel family, two subgroups exist: anoctamins (TMEM16 proteins) and bestrophins. Of the anoctamins, only TMEM16A and B have highly selective Cl^- channel activity whilst other family members are dual function lipid scramblases and non-selective ion channels. The bestrophins all show Cl^- channel activity; however, they are mainly expressed in the eye and colon and so are unlikely involved in HRSV infection (1.7.4.1) [199,202]. TMEM16A (anoctamin 1, ANO1) is highly expressed within the respiratory tract, and it is a common target for all the CaCC inhibitors that displayed anti-HRSV activity. Furthermore, due to its overexpression in many cancers, TMEM16A has been widely studied and as a result, several potent and specific small molecule inhibitors that target this channel are available. For these reasons, TMEM16A was the channel of interest in the following studies.

To investigate a role for TMEM16A during the HRSV lifecycle, the effects of specific inhibitors of this channel upon HRSV-GFP infection were assessed. Benzbromarone [223], T16Ainh-A01 [362] and MONNA [363] were all identified as TMEM16A-inhibitors by high-throughput screening strategies and inhibit the channel with half-maximal inhibitory concentrations (IC50s) of 9.97 µM, 1.10 µM and 1.27 µM, respectively. Benzbromarone is thought to work via a pore-blocking mechanism [223], and interestingly, is used clinically in the treatment of gout. For T16Ainh-A01, inhibition occurs independently of voltage, and without affecting calcium signalling, indicating it likely acts on the TMEM16A protein directly in an unspecified manner and without affecting the expression levels of the protein [359,362]. The mechanism for MONNA is less clear but it is highly selective for

TMEM16A and elicits no inhibitory effects on other Cl^- channels including CFTR, CLC-2 and BEST1 [363] .

The pre-treatment of HRSV-GFP infected cells with each of these TMEM16A inhibitors recapitulated the results of the CaCC inhibitors and showed a significant, concentration-dependent reduction of GFP expression (Figure 3-8). Benzbromarone modulation caused a decrease in HRSV-GFP expression between 14.0% and 53.3% (10-20 µM) relative to the solvent-treated control, whilst cell viability remained over 81.2% (Figure 3-8 A). Additionally, T16Ainh-A01 treatment elicited a potent decrease in HRSV-GFP expression by up to 79.3% (30 µM) whilst retaining an 88.6% cell viability compared to the solvent-treated control (Figure 3-8 B). TMEM16A modulation with MONNA resulted in a significant 66.2% (30 µM) decrease in HRSV-GFP expression compared to solvent controls, and the cells retained 96.1% viability (Figure 3-8 C). The potency of the TMEM16A-speciffic modulators against HRSV-GFP is shown visually by the representative images of each condition (Figure 3-8 D). Western blot analysis of WT-HRSV-G expression in drug-treated cells confirmed the reduced levels of WT-HRSV gene expression in the absence of TMEM16A activity (Figure 3-8 E). These data provided the first description of a crucial role for TMEM16A during HRSV infection [326].

Genetic silencing of TMEM16A has been shown to inhibit cell proliferation in cancer cells [247,359], and indeed in the present study siRNA and CRISPR approaches led to a loss of cell viability in our chosen cell lines (data not shown). Furthermore, the TMEM16 proteins are known to play additional roles within the cell, including lipid scramblase functions and participation in many cell signalling pathways (see 1.7.4.2). A pharmacological approach, as adopted here, allowed

the study of Cl^- channel activity without affecting other key roles carried out by TMEM16A.

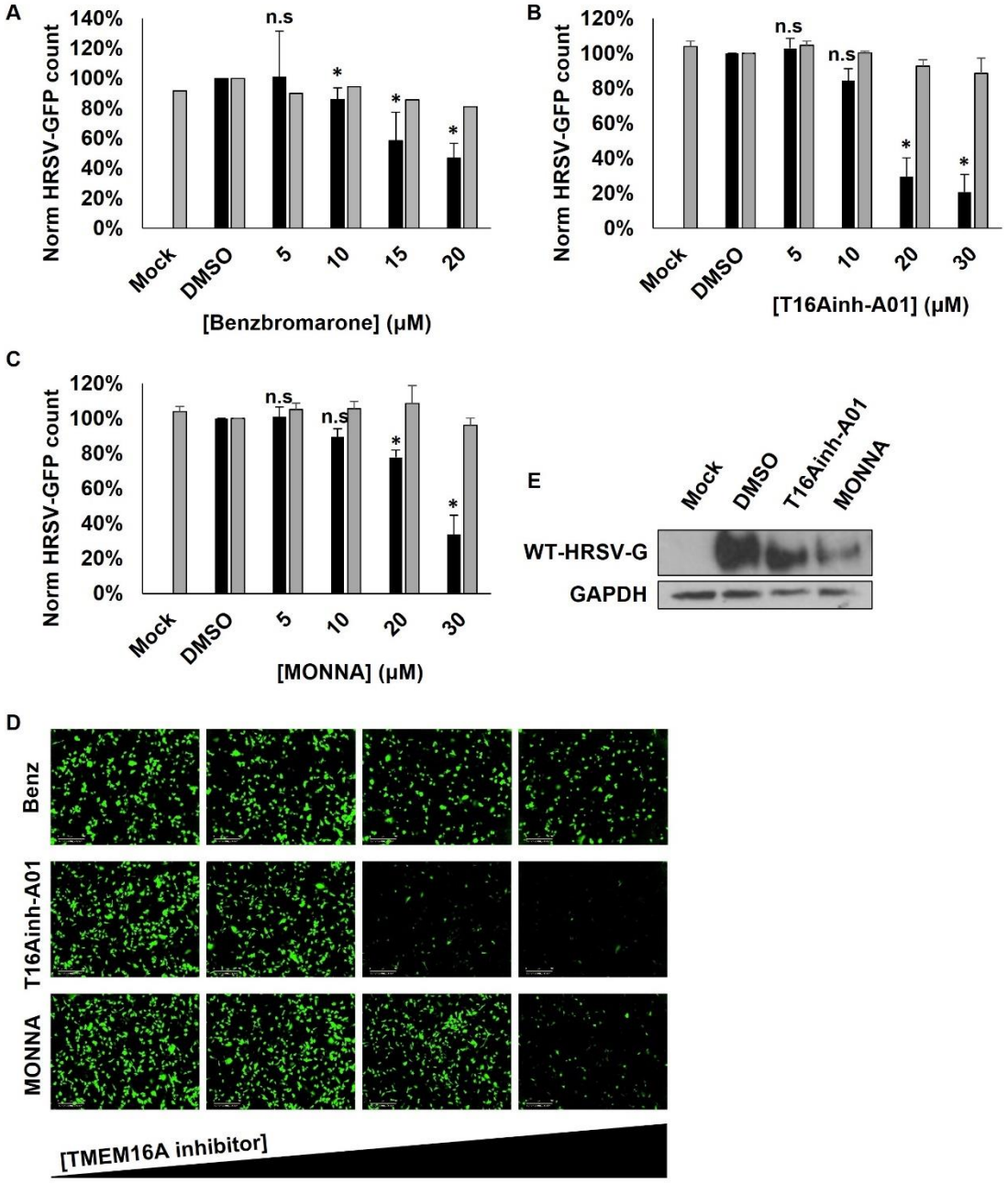

Figure 3-8 TMEM16A is the CaCC required during HRSV infection. A-C) A549 cells were pre-treated with TMEM16A-specific inhibitors (A) benzbromarone 5-20 μM, (B) T16Ainh-A01 5-20 μM or (C) MONNA 5-30 μM for 45 mins prior to HRSV-GFP infection. Quantification of HRSV-GFP expression by IncuCyte ZOOM took place at 24 hpi (black bars). Cell health was measured by MTS assay and was compared to solvent (DMSO)-treated controls (grey bars). Mean of n=4 ± SE, *p≤0.05, n.s = non-significant. **D)** Representative IncuCyte images showing

HRSV-GFP expressing cells in the presence of indicated TMEM16A-specific inhibitors. **E)** Cells were treated as in (A-C) and infected with WT-HRSV for 24 hrs. Cell lysates were analysed by western blot using WT-HRSV-G as a marker of infection and a GAPDH loading control.

3.9 Inhibitory effects of TMEM16A modulators on HRSV are not through direct effects on HRSV virions

Within the HRSV virion envelope, three transmembrane proteins are encoded; including SH which forms a pentameric ion channel [62]. To ensure the small molecule inhibitors were not affecting the function of SH, or having any unknown effect on the HRSV virions, WT-HRSV virions were treated directly with ribavirin, CaCCinh-A01, T16Ainh-A01 or MONNA for 45 mins. The drugs were then diluted in media (≥400-fold dilution from active concentration) and the treated virions applied to untreated cells. Western blot analysis of WT-HRSV-G expression at 24 hpi showed similar levels of infection from drug- and solvent-treated virions (Figure 3-9 A(i)), and the quantification of WT-HRSV-G expression (Figure 3-9 A(ii)) revealed there was no significant differences between them. These data indicated that the drugs were not viricidal and that the previously observed reduction in HRSV infection in response to CaCC and TMEM16A modulation was not due to any direct effect on the virion, but rather due to cell-mediated effects. This supported the hypothesis that the inhibition of TMEM16A channel activity disrupts HRSV infection [326].

Additionally, the effect of each inhibitor was independent of MOI; the percentage reduction of HRSV-GFP expression following drug treatments relative to solvent-treated controls was not significantly altered when an MOI of 0.5 or 1 was used

(Figure 3-9 B), compared to MOI 0.1 used in the previous experiments. This indicated that the inhibitory effects of TMEM16A modulation within cells could not be overcome simply with a higher viral load. This corroborated the idea that the inhibition of HRSV observed was due to modulation of a host factor (of unchanging concentration) rather than an effect on the virion (which changed concentration with increasing MOI) [326].

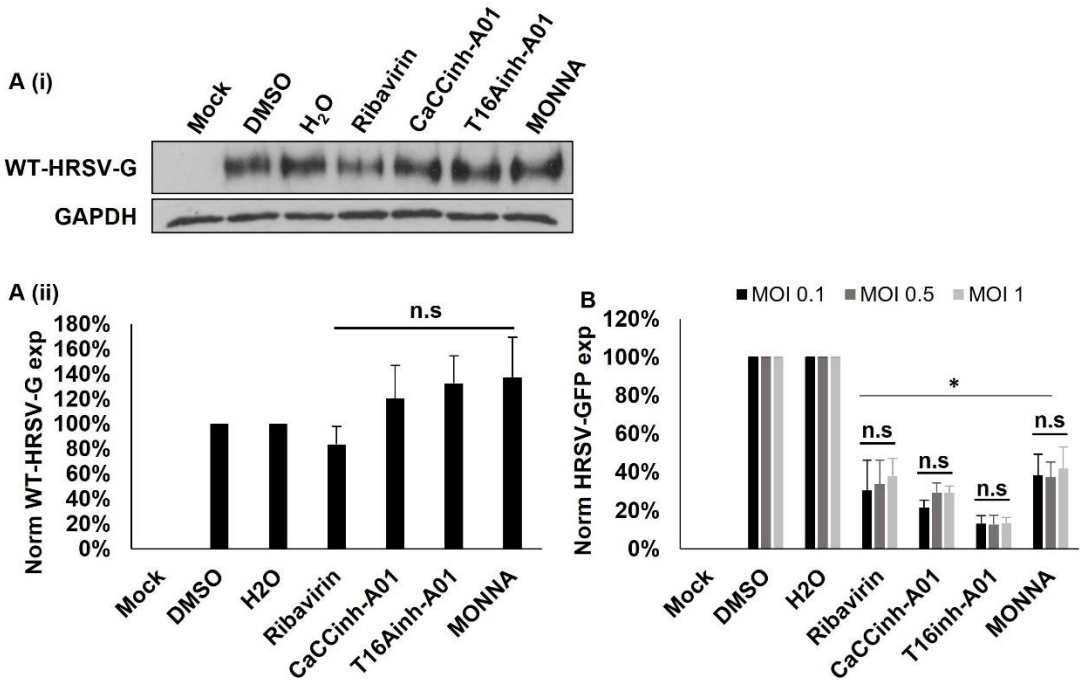

Figure 3-9 TMEM16A-modulators exert cell-mediated effects on HRSV. A (i) WT-HRSV virions were treated directly with ribavirin (40 µM), CaCCinh-A01 (40 µM), T16Ainh-A01 (30 µM), MONNA (30 µM), or the appropriate solvent control (DMSO or H_2O) for 45 min. The drugs were diluted in media and the treated virions were used to infect cells. After 24 hrs infection was analysed by western blot utilising WT-HRSV-G as a marker of infection. The GAPDH loading control is shown. **A (ii)** Quantification of three biological repeats by densitometry. WT-HRSV-G expression was normalised to GAPDH expression and then to solvent-treated controls. Mean of n=3 ± SE. **B)** Cells were pre-treated with ribavirin (40 µM), CaCCinh-A01 (40 µM), T16Ainh-A01 (30 µM), MONNA (30 µM) for 45 mins prior to HRSV-GFP infection at MOI 0.1 (black bars), 0.5 (dark grey

bars) or 1 (light grey bars). HRSV-GFP expressing cells were quantified by IncuCyte ZOOM analysis at 24 hpi. Mean of n=3 ± SE, *p≤0.05, n.s not significant.

3.10 The requirement for TMEM16A during HRSV infection is conserved in neuronal cells

In addition to the respiratory system, HRSV is known to infect the CNS where it is thought to elicit neurological symptoms including seizures [364,365]. TMEM16A is expressed within neuronal cells [215], and so the effects of TMEM16A channel inhibition in SH-SY5Y neuronal cells upon HRSV infection were examined.

Firstly, using the three broad spectrum Cl^- channel inhibitors which were previously tested in A549 cells (Figure 3-4 F), the effect of Cl^- channel modulation in SH-SY5Y cells was assessed by western blot analysis. The results in SH-SY5Y cells mirrored those in A549 cells; a decrease in WT-HRSV-G expression was observed for both NPPB and DIDS, and R+IAA94 had no detectable effect on WT-HRSV-G expression (Figure 3-10 A). This indicated that the anti-HRSV effect of Cl^- channel modulation was not cell type-specific and that HRSV relied on a similar profile of Cl^- channel in the CNS as in the respiratory tract.

To investigate whether the Cl^- channel required by HRSV in the CNS was indeed TMEM16A, SH-SY5Y cells were pre-treated with TMEM16A-specific modulators prior to infection with HRSV-GFP. Like A549 cells, a concentration-dependent reduction in HRSV-GFP expression was observed following treatment of SH-SY5Y cells with 30 µM T16Ainh-A01 and 40 µM MONNA (87.1% and 88.1% decrease relative to solvent-treated controls, respectively) (Figure 3-10 B and C, black bars). The positive control, ribavirin also inhibited HRSV-GFP infection by

up to 85.2% at 80 µM (Figure 3-10 D, black bars). Representative IncuCyte images (Figure 3-10 E) show visually the stark contrast in HRSV-GFP expression in cells treated with a low vs high concentration of each of these compounds. All three compounds were checked for toxic effects and used at non-toxic concentrations (≥80% cell viability of solvent-treated controls; Figure 3-10 B-D, grey bars). Western blot analysis of WT-HRSV-G expression in treated SH-SY5Y cells also showed a HRSV-G decrease in T16Ainh-A01 or MONNA treated cells compared to untreated, infected control cells (Figure 3-10 F) [326]. These data have important implications for the treatment of not only the respiratory symptoms of HRSV infection but also the neurological symptoms, of which less is currently known.

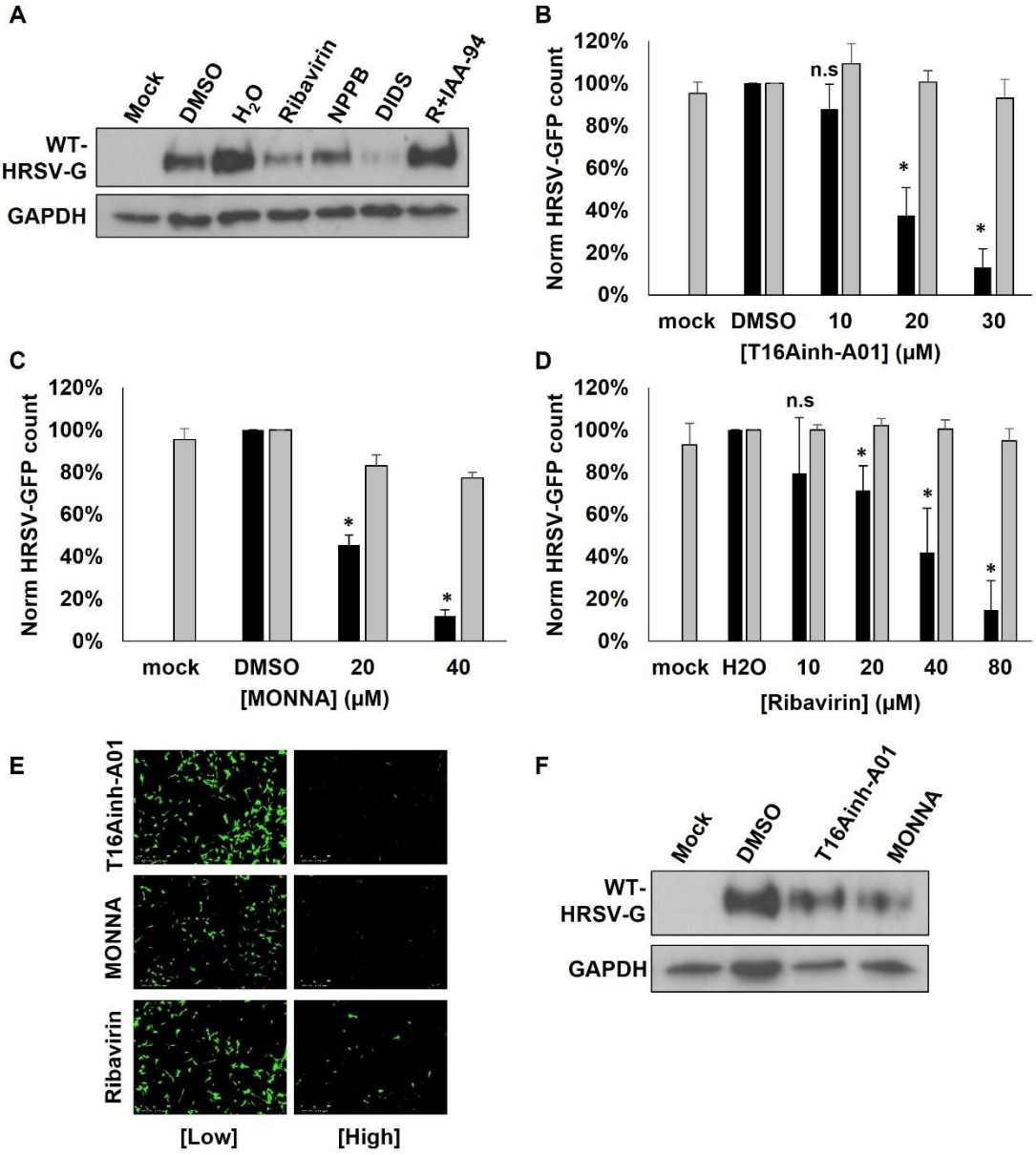

Figure 3-10 The requirement for TMEM16A during HRSV infection is conserved in neuronal cells. A) SH-SY5Y cells were pre-treated with the indicated broad spectrum Cl^- channel inhibitors and infected with WT-HRSV. Cell lysates were taken at 24 hpi and analysed by western blot. WT-HRSV-G was used as a marker of infection and GAPDH loading control is shown. **B-D)** SH-SY5Y cells were pre-treated with TMEM16A-specific inhibitors (B) T16Ainh-A01 1-30 μM or (C) MONNA 20-40 μM, or (D) HRSV replication inhibitor ribavirin 10-80 μM for 45 mins prior to HRSV-GFP infection. Quantification of HRSV-GFP expression by IncuCyte ZOOM took place at 24 hpi (black bars). Cell health was measured by MTS assay and was compared to solvent (DMSO or H_2O)-treated controls (grey bars). Mean of n=3 ± SE, *p≤0.05, n.s = non-

significant. **E)** Representative IncuCyte images showing HRSV-GFP expressing cells in the presence of low or high concentrations of the indicated inhibitors. **F)** As in (A) using TMEM16A-specific inhibitors.

3.11 TMEM16A is a viable target for HRSV inhibition in primary human lung tissue

The data so far was generated using the A549 cell line, which is derived from adenocarcinomic human alveolar basal epithelial cells. Often, cell lines have dysregulated cell signalling pathways, and therefore, a more physiologically relevant model of infection was sought. In collaboration with Dr Hesse at The Fraunhofer Institute for Toxicology and Experimental Medicine, precision-cut lung slices (PCLS) generated from disease-free human tissue were used to assess the requirement of TMEM16A during HRSV infection.

To validate the use of PCLS, their permissibility to HRSV infection was firstly assessed. Interferon gamma-induced protein 10 (IP-10) had been previously shown to be released in airways in response to respiratory virus infection, including HRSV [366], and was therefore assessed as a marker of HRSV infection in the present study. PCLS were infected with HRSV for 72 hrs, after which the supernatants were collected and the amount of IP-10 released into the supernatant was assessed by ELISA. It was found that in PCLS, IP-10 was specifically released in response to active HRSV infection, but not ultraviolet (UV)-inactivated HRSV (Figure 3-11 A). The permissibility of PCLS to HRSV infection was further confirmed using confocal imaging, wherein specific HRSV staining was observed throughout the tissue, including in ciliated cells (Figure

3-11 B). IP-10 was therefore considered to be a suitable surrogate marker of HRSV infection which was quantifiable by ELISA.

PCLS from three independent donors were pre-treated with T16Ainh-A01 (10-20 µM) or CaCCinh-A01 (10-20 µM) for 40 mins prior to infection with HRSV. After 24 hrs, the cell supernatants and lysates were collected. The level of IP-10 released into the supernatants was assessed by ELISA and in all three donors, T16Ainh-A01 treatment resulted in a significant 0.35-fold decrease at 10 µM and 0.07-fold decrease at 20 µM compared to untreated, infected tissue (Figure 3-11 C). To check for any potential toxicity associated with the T16Ainh-A01 treatment in these samples, LDH release assays were performed. In these assays, the amount of LDH released into the supernatant was indicative of the level of plasma membrane damage. There was no significant difference observed in LDH release from T16Ainh-A01 treated PCLS compared to untreated tissue, and all samples showed ≤20.0% LDH release compared to the triton-lysed (high) controls (Figure 3-11 D) indicating minimal effects of both compounds on cell membrane integrity. However, the concentrations at which the inhibitors were non-toxic were lower in PCLS than in A549 or SH-SY5Y cell lines. These results demonstrated that T16Ainh-A01 maintains its anti-HRSV activity in physiologically relevant models of HRSV infection [326].

T16Ainh-A01 (20 µM) treatment similarly reduced WT-HRSV-G and WT-HRSV-N expression in PCLS by 17.4% and 69.0%, respectively, as determined by western blot (Figure 3-11 E). This is shown for one donor in Figure 3-11 E, but unfortunately, there was not enough sample remaining to analyse virus protein expression in every donor via western blotting, therefore statistical analysis was unable to be performed.

Treatment of PCLS with CaCCinh-A01 led to a similar decrease in IP-10 in two out of three donors, yet these values did not quite reach statistical significance (Figure 3-11 F). This is likely due to the lower specificity of this drug for TMEM16A. Additionally, whilst there was no significant difference in LDH levels between CaCCinh-A01 treated and untreated PCLS (Figure 3-11 G), the LDH levels overall were higher relative to the triton-lysed controls than was seen with T16Ainh-A01 (≤30.0%), hence the use of a lower concentrations of CaCCinh-A01 than was previously used in cell lines (maximum of 20 µM in PCLS compared with 40 µM in cell lines). In A549 cells, 20 µM CaCCinh-A01 resulted in a modest 30.0% reduction in HRSV-GFP expression relative to solvent-treated controls (Figure 3-7 B).

Taken together, these data validated the use of PCLS as a model of HRSV infection and showed that TMEM16A-modulation by T16Ainh-A01 significantly inhibited HRSV infection, confirming the previous data to be representative of a physiologically relevant phenomenon. The use of IP-10 as a marker of infection in PCLS was useful in these experiments, however it was not a perfect solution. The question of whether the inhibition of IP-10 release in PCLS by T16Ainh-A01 was indeed a direct result of the action of the drug on the virus remained. This was further probed in Chapter 4 (4.8).

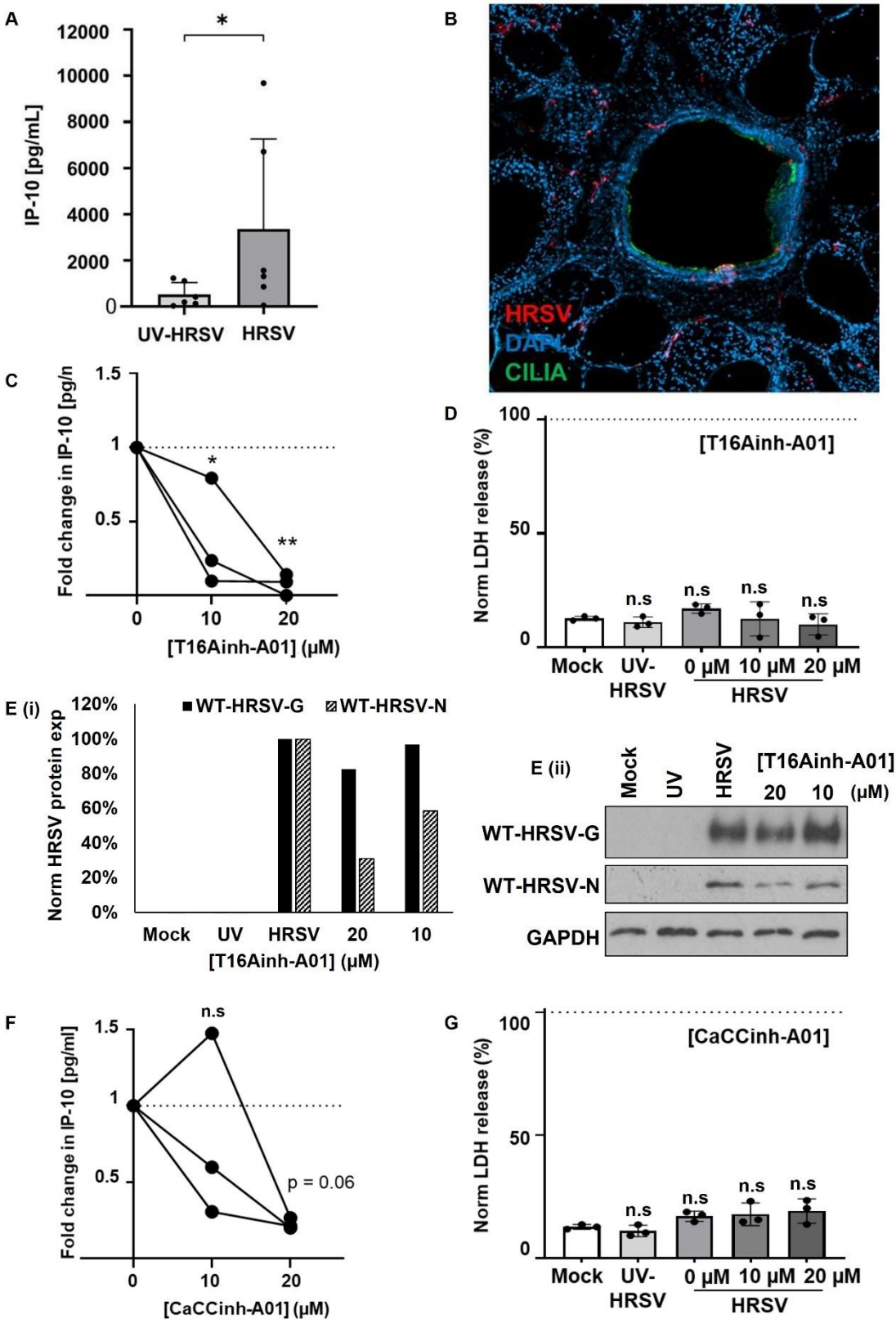

Figure 3-11 TMEM16A is a viable target for HRSV inhibition in primary human lung tissue. A) Extrinsic IP-10 levels in the supernatants of PCLS infected with HRSV or UV-inactivated HRSV. Samples were infected for 2 hours

and extrinsic levels of IP-10 in the supernatants at 72 hpi were measured by ELISA. Individual values (dots) of six independent donors are shown. Data were compared using an unpaired Mann-Whitney one-tailed test, *p<0.05. **B)** Immunofluorescence image of HRSV-infected PCLS inoculated for 2 hours. Slices were fixed 72 hpi and stained for HRSV (red), cilia (green) and DAPI (nuclear marker, blue). **C)** Extrinsic IP-10 in the supernatants of T16Ainh-A01 (10–20 µM) pre-treated HRSV-infected PCLS 24 hpi. Values are the fold changes of cytokine values (normalised to pg/mg total protein) compared with respective untreated HRSV-infected tissue. Individual values (dots) of three donors are shown. Connecting lines represent data sets from the same donor. Data was analysed using a one-way ANOVA with Dunnett's multiple comparison test, *p<0.05 or **p<0.01. **D)** Released LDH is shown normalised to respective Triton-lysed untreated, uninfected tissue (mock). Mean values (bars) and individual values (dots) of three donors are shown. n.s, non-significant. **E (i)** Quantification of western blot **(E (ii))** analysing the expression of WT-HRSV-G, WT-HRSV-N and GAPDH (loading control) in the lysates of PCLS samples treated with T16Ainh-A01 (in C). **F-G)** As in (C) and (D) using CaCCinh-A01 (10-20 µM).

3.12 CaCCs may be required for other negative sense RNA viruses

3.12.1 Influenza virus

Influenza A virus (IAV), belonging to the *Orthomyxoviridae* family, is a segmented, single-stranded, negative-sense RNA virus [367]. Usually infecting birds, IAV can spread to and cause disease in other hosts, including humans. There are many subtypes of IAV, designated according to the type of HA and NA proteins displayed on the virions surface. Several subtypes of IAV cause severe disease in humans and there are examples of severe outbreaks scattered

throughout history. The most pathogenic subtype in humans, H1N1, was the causative agent of the 1918 ‘Spanish flu’ and the 2009 ‘swine flu’ pandemics which resulted in ~50 million and ~284,000 deaths, respectively [368].

Like HRSV, IAV is a respiratory pathogen which causes similar symptoms; fever, cough, sore throat, runny nose, and headaches, accompanied by muscle and joint pain and severe malaise. In severe cases, IAV infection can lead to breathing problems and pneumonia. Another similarity to HRSV is the seasonality of cases, with both viruses circulating at the same time of year in temperate climates. Globally, seasonal IAV infection is thought to severely affect 3-5 million people annually, resulting in approximately 290,000-650,000 deaths (according to the WHO [369]). The transmission of IAV occurs via the same routes as HRSV: inhalation of infectious droplets, or direct contact with fomites. The greatest risk factors for severe IAV disease are age and underlying health conditions.

To explore the potential for a pan-virus effect of TMEM16A channel modulation of NSVs, a GFP-labelled IAV strain (2.2.1) was obtained. In a similar fashion to HRSV-GFP, IAV-GFP was used to quantify infection in the presence of CaCC inhibitors. Treatment with CaCCinh-A01 resulted in a modest but significant reduction in IAV-GFP expression at 5 and 10 µM of 29.6% and 30.0%, respectively, relative to solvent-treated controls. However this was not a concentration-dependent effect with the higher concentrations (20 - 40 µM) showing lower levels of virus inhibition (25.6% – 12.8% reduction, Figure 3-12 A). MONNA treatment led to a similarly small and concentration-independent inhibition of IAV-GFP expression of between 20.2% (30 µM) and 35.9% (20 µM) of the solvent-treated control (Figure 3-12 B).

However, treatment with T16Ainh-A01 did recapitulate the effect previously observed on HRSV and showed a concentration-dependent decrease in IAV-GFP expression from 27.9% - 65.5% at 5 - 30 µM (Figure 3-12 C). Additionally, as ribavirin is a known inhibitor of IAV it was utilised here as a positive control. Ribavirin treatment (10 - 80 µM), resulted in a significant reduction of 24.9% - 85.9% in IAV-GFP expression compared with solvent-treated controls (Figure 3-12 D). This was more effective than any of the CaCC inhibitors assessed (shown visually in Figure 3-12E) [326].

These results suggested that whilst TMEM16A appears crucial for HRSV infection, it may play a less important role in IAV infection. However, IAV-GFP expression was limited to the nucleus as the site of IAV replication, whereas HRSV-GFP was expressed throughout the cytoplasm. Therefore, the variability of the results for IAV-GFP may have been partly due to a flaw within the assay: it was more difficult to detect IAV-GFP by IncuCyte analysis due to the smaller area of expression.

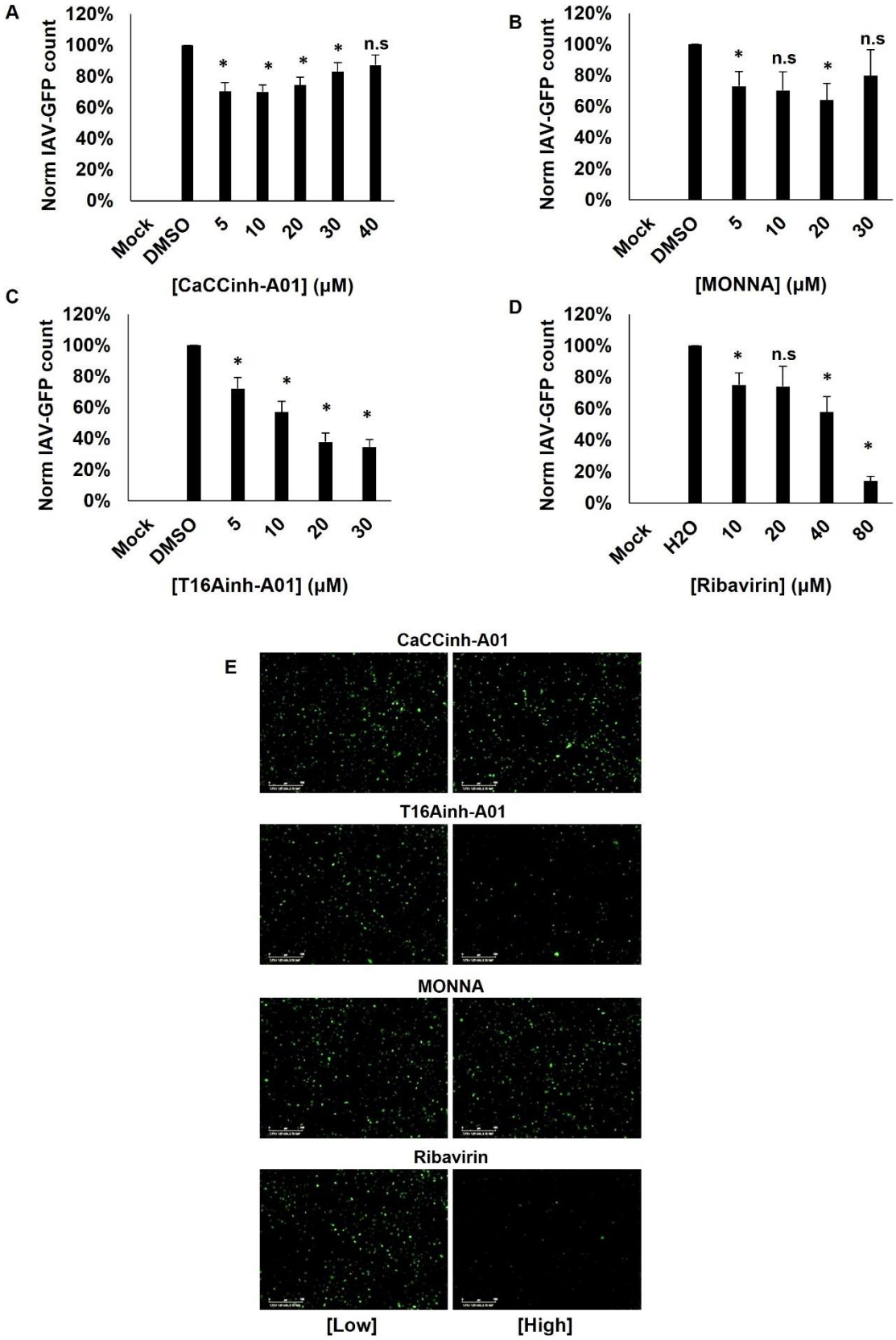

Figure 3-12 TMEM16A may play a role during IAV infection. A-D) A549 cells were pre-treated with (A) CaCC inhibitor CaCCinh-A01 5-40 μM, TMEM16A-

specific modulators (B) MONNA 5-30 µM or (C) T16Ainh-A01 5-30 µM or (D) positive control ribavirin (10-80 µM) for 45 mins prior to IAV-GFP infection. Quantification of HRSV-GFP expression by IncuCyte ZOOM took place at 24 hpi. Mean of n=3 ± SE, *p≤0.05, n.s = non-significant. **E)** Representative IncuCyte images showing IAV-GFP expressing cells in the presence of low or high concentrations of the indicated inhibitors.

3.12.2 Bunyaviruses

The *Bunyavirales* are a large order of segmented, single-stranded, negative-sense RNA viruses [370]. These vector-borne viruses can infect plants, insects, and animals as well as humans. Bunyamwera virus (BUNV) is the prototypic member of the *Bunyavirales* order and belongs to the *Peribunyaviridae* family. It is carried by mosquitos (*Aedes aegypti)* and causes a febrile illness in humans known as Bunyamwera fever. Hazara virus (HAZV) is another member of the *Bunyavirales* order of NSVs, belonging to the *Nairoviridae* family. It is carried by *Ixodes redikorzevi* ticks, and whilst it does not cause disease in humans, it mirrors the symptoms of Crimean-Congo haemorrhagic fever virus (CCHFV) in mice [371]. CCHFV is highly pathogenic in humans with a fatality rate of up to 40% and is endemic in Africa, the Middle East and Asia. Symptoms of CCHF include fever, dizziness, photophobia, muscle-, neck-, back- and headaches and can progress to bleeding of internal mucosal surfaces and organ failure [372]. Due to the dangerous nature of this pathogen, combined with the lack of preventative or therapeutic treatment options, research must be carried out under bio-safety level (BSL)-4 conditions. The close similarity between HAZV and CCHFV allows the use of HAZV as a model virus in the study of CCHFV without the need for high containment facilities [373].

To further investigate the potential pan-viral effect of TMEM16A modulation on NSVs, BUNV and HAZV were investigated. Of note, both viruses infect respiratory cells, though the respiratory tract is not thought to represent the major sites of virus infection.

WT-HAZV was used in these studies and infection was assessed through quantification of immunofluorescent staining of the nucleoprotein (WT-HAZV-N). CaCC modulation through treatment with CaCCinh-A01 (5 - 40 µM) caused a statistically significant, concentration-dependent reduction in WT-HAZV-N expression from 29.2% up to 84.4% of the solvent-treated control (Figure 3-13 A). Treatment with T16Ainh-A01 and MONNA also had a profound effect on HAZV infection demonstrated by a significant reduction in WT-HAZV-N expression up to 88.4% and 75.5%, respectively (Figure 3-13 B-C). Furthermore, the broad antiviral ribavirin was also highly effective against HAZV, eliciting a 94.7% reduction in WT-HAZV-N at 80 µM (Figure 3-13 D). Images of infected cells treated with the highest and lowest drug concentrations demonstrate the potent inhibitory effects of each of these compounds on WT-HAZV-N expression (Figure 3-13 E).

For BUNV, the nucleoprotein (WT-BUNV-N) was also used as a marker of infection which was analysed by western blot. CaCCinh-A01 treatment resulted in a 58.8% reduction in protein expression relative to solvent-treated controls (40 µM, Figure 3-13 F). However, specific TMEM16A modulation through T16Ainh-A01 treatment resulted in a small and non-significant 20.4% reduction in WT-BUNV-N expression (20 µM, Figure 3-13 G).

Altogether, these data suggest that the role for TMEM16A is not conserved for all NSVs. BUNV was inhibited by CaCC modulation but was unaffected by

TMEM16A-specific modulation by T16Ainh-A01, suggesting another channel may be involved. However, HAZV shared the same requirement for TMEM16A as HRSV and IAV, indicating some conserved mechanism between different virus families.

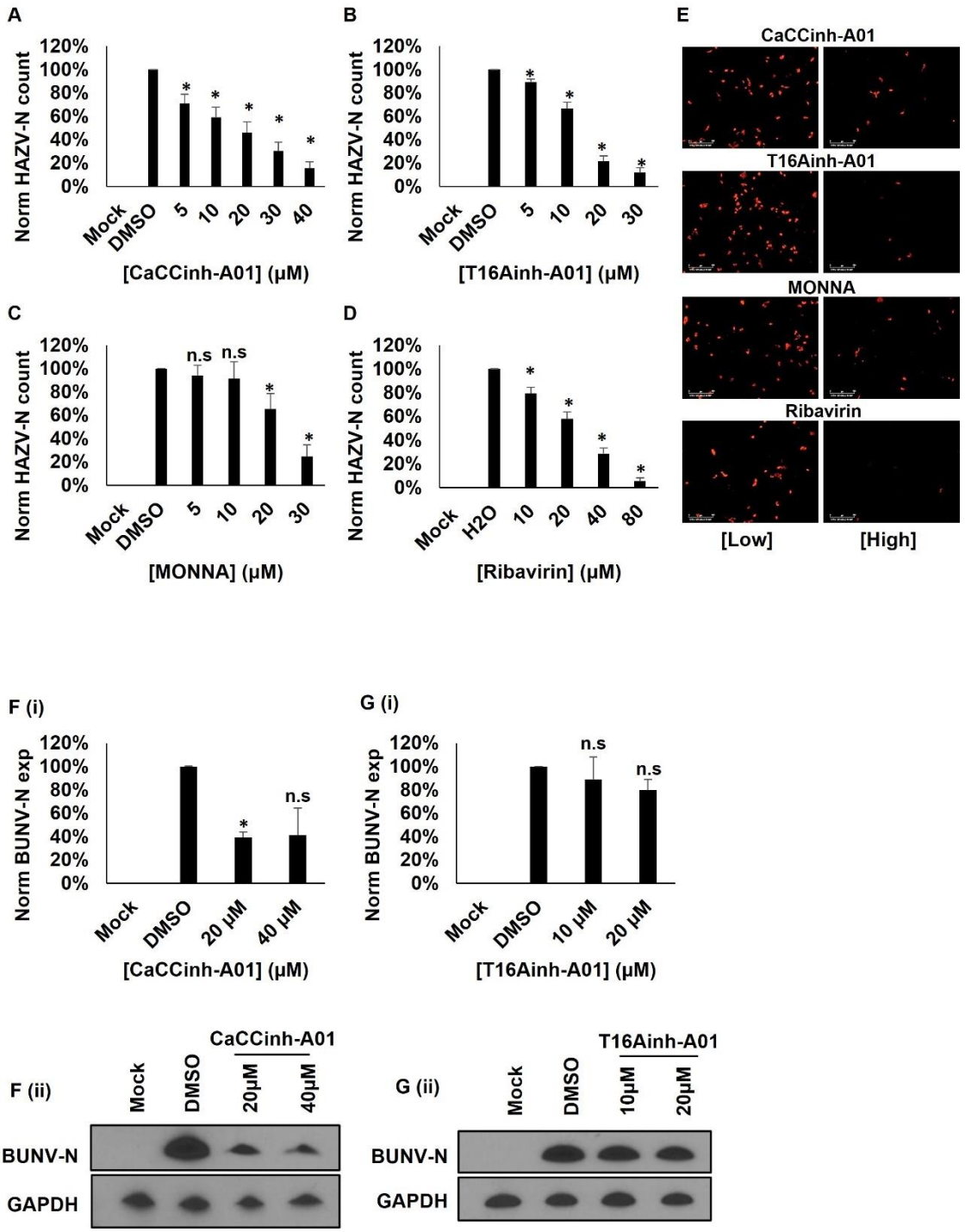

Figure 3-13 The role of TMEM16A during Bunyavirus infection. A-D) A549

cells were pre-treated with (A) CaCC inhibitor CaCCinh-A01 5-40 µM, TMEM16A-specific modulators (B) T16Ainh-A01 5-30 µM or (C) MONNA 5-30 µM or (D) positive control ribavirin (10-80 µM) for 45 mins prior to WT-HAZV infection. Quantification of WT-HAZV-N expression by IncuCyte ZOOM took place at 24 hpi. Mean of n=4 ± SE, *p≤0.05, n.s = non-significant. **E)** Representative IncuCyte images showing cells fluorescently labelled with anti-HRSV-N in the presence of low or high concentrations of the indicated inhibitors. **F-G)** A549 cells were pre-treated with (F) CaCCinh-A01, 20-40 µM or (G) T16Ainh-A01 (10-20 µM) and infected with WT-BUNV. Cells were lysed 24 hpi and infected assessed by western blot analysis. Representative blots are shown, and expression of WT-BUNV-N was quantified by densitometry. N expression was normalised to GAPDH loading control and to solvent (DMSO)-treated cells. Mean of n=2 ± SE, *p≤0.05, n.s = non-significant.

3.13 Summary of the aims and key findings in Chapter 3

This chapter sought to find novel host factors for HRSV infection by utilising the new wealth of knowledge surrounding viral modulation of ion channels and the roles of Cl^- channels in cells. One major benefit of identifying ion channels as host factors is the potential for drug repurposing (discussed in Chapter 5). Therefore, the aim of this chapter was to assess the potential role of host Cl^- channels during HRSV infection.

To determine the role of Cl^- channels during HRSV infection, the sensitivity of HRSV-GFP to pharmacological inhibitors of Cl^- channels was assessed. Two of the three broad spectrum Cl^- channel inhibitors potently inhibited HRSV-GFP infection by over 85% compared to untreated controls, implicating a role for Cl^- channels during HRSV infection. Of the five major Cl^- channels families, modulation of one family recapitulated this potent inhibitory effect: the CaCCs. Through a combination of logical reasoning and experimental evidence,

TMEM16A was highlighted as a channel of interest. Modulation of TMEM16A with inhibitors T16Ainh-A01, MONNA and benzbromarone indeed potently reduced HRSV-GFP infection by up to 79%. Treatment of HRSV virions directly with TMEM16A channel modulators did not influence infection, indicating that the drugs did not inhibit the virus directly and therefore that the previous inhibition observed was due to the action of the drug on cells. Furthermore, this relationship was conserved in other cells lines as well as in primary human lung tissue. Therefore, the aim of Chapter 3 was successfully achieved by the identification of a Cl^- channel, TMEM16A, which was crucial to HRSV infection and represented a potential therapeutic target [326]. Following on from this finding, Chapter 4 explores the mechanisms underpinning this relationship.

An in-depth interpretation of the results of Chapter 3, along with an analysis of the approaches taken and suggestions for future work are provided in the Discussion (Chapter 5).

Chapter 4 Investigation into the mechanisms underpinning the requirement for TMEM16A during HRSV infection

Following on from Chapter 3 in which the CaCC TMEM16A was identified as a novel host factor for HRSV infection, the studies in this chapter sought to elucidate the mechanisms underpinning this relationship. To achieve this, an analysis of the HRSV life cycle was undertaken to determine at which stage TMEM16A was required. Furthermore, confocal microscopy was utilised to probe the subcellular localisation of TMEM16A and where it might facilitate HRSV infection. Lastly, based on the PCLS data presented in 3.11, an investigation into the mechanism by which T16Ainh-A01 inhibited HRSV-induced IP-10 release was undertaken in order to investigate the role of TMEM16A in the inflammatory response to infection.

4.1 TMEM16A is not required for HRSV cell entry

To investigate the role of TMEM16A during HRSV infection, the viral life cycle stage at which the channel was required was determined. As discussed in 1.5.1.3, HRSV binds target host cells by attaching to CX3CR1 via its G protein, allowing F to interact with cellular receptors such as nucleolin, and triggering the uptake of the virion by actin-dependent macropinocytosis [48,374–376]. An approximate timeline of HRSV infection is shown in Figure 4-1 A(i), with virus binding and entry occurring within the first 3 hrs. Using the broad-spectrum CaCC inhibitors CaCCinh-A01 (40 µM) and tannic acid (15 µM), and TMEM16A-specific inhibitors T16Ainh-A01 (30 µM) and MONNA (20 µM), the role of TMEM16A during the entry stage of the HRSV life cycle was examined. Pre-treated cells were challenged with WT-HRSV in the presence of each inhibitor for the first 3 hrs, after which any uninternalized virus was washed away. Infection was

assessed via western blot analysis of lysates collected at 24 hpi, probing for WT-HRSV-G as a marker of infection.

The virus entry assays showed no significant difference in WT-HRSV-G expression in solvent-treated cells and CaCCinh-A01, T16Ainh-A01 or MONNA-treated cells (Figure 4-1 B), suggesting that TMEM16A was not involved in HRSV entry. However, there was a significant reduction in WT-HRSV-G expression when cells were treated with tannic acid during the entry stage of infection (65.3% decrease compared to solvent control). This effect was consistent with the ability of this compound to prevent virus-receptor interactions as reported for HCV [377] and norovirus [378], and was likely independent of its TMEM16A-modulating activity. Lastly, the replication inhibitor ribavirin (40 µM) did not inhibit WT-HRSV-G expression when present during the same 3 hr window. This was expected as the mechanism of action of ribavirin occurs later in the viral life cycle (1.3.2), therefore this result validated the entry assay.

4.2 HRSV does not require TMEM16A for assembly and release stages of infection

To further assess the role of TMEM16A within the life cycle stages of HRSV, virus release assays were performed in which cells were infected with HRSV-GFP and at 16-18hpi the supernatant was removed and any uninternalized virus was washed away. Cells were treated with the TMEM16A modulators for 4 hours at the time point corresponding to virion assembly and release (Figure 4-1 A(i)), and after this time, the supernatants were collected and tested for the presence of any released virus. This was achieved by diluting the viral supernatants 10-fold in media to dilute any remaining drug and applying these to untreated cells.

Therefore, analysis of the subsequent infection through quantification of GFP fluorescence revealed the amount of virus released from the initial, drug-treated cells.

The level of subsequent infection following treatment with T16Ainh-A01 (30 µM) or MONNA (20 µM) during HRSV release stages was not significantly different to solvent-treated control cells (Figure 4-1 C). This implied that the amount of released virus from treated cells was roughly equivalent to untreated cells, indicating that TMEM16A did not play a role during the later life cycle stages of HRSV infection. Similarly, ribavirin (40 µM) treatment did not affect the level of released virus in these assays, as expected from the well-documented activity of this compound as an inhibitor of virus multiplication [26].

Interestingly, the use of broad-spectrum inhibitor tannic acid (15 µM) in release assays resulted in a 43.8% reduction in HRSV-GFP expression in re-infected cells compared to the solvent-treated control, indicating that significantly less virus was released from the tannic acid-treated cells. Like the virus entry assay described above, this effect was probably related to additional activities of the tannic acid compound other than TMEM16A-modulation, however this warranted further investigation.

Somewhat unexpectedly, the use of the other broad-spectrum inhibitor, CaCCinh-A01 (40 µM) in these release assays also resulted in a statistically significant 28.0% reduction in HRSV-GFP expression in re-infected cells, also indicating a reduction in released virus compared to solvent-treated controls. The most likely explanation for this is that CaCCinh-A01, like tannic acid, targets other CaCCs, and so may influence multiple HRSV-life cycle stages. In contrast, inhibitors T16Ainh-A01 and MONNA are specific to TMEM16A. Therefore, on the

basis that neither of these specific inhibitors significantly decreased assembly and release of HRSV, it was concluded that TMEM16A was not required for these processes.

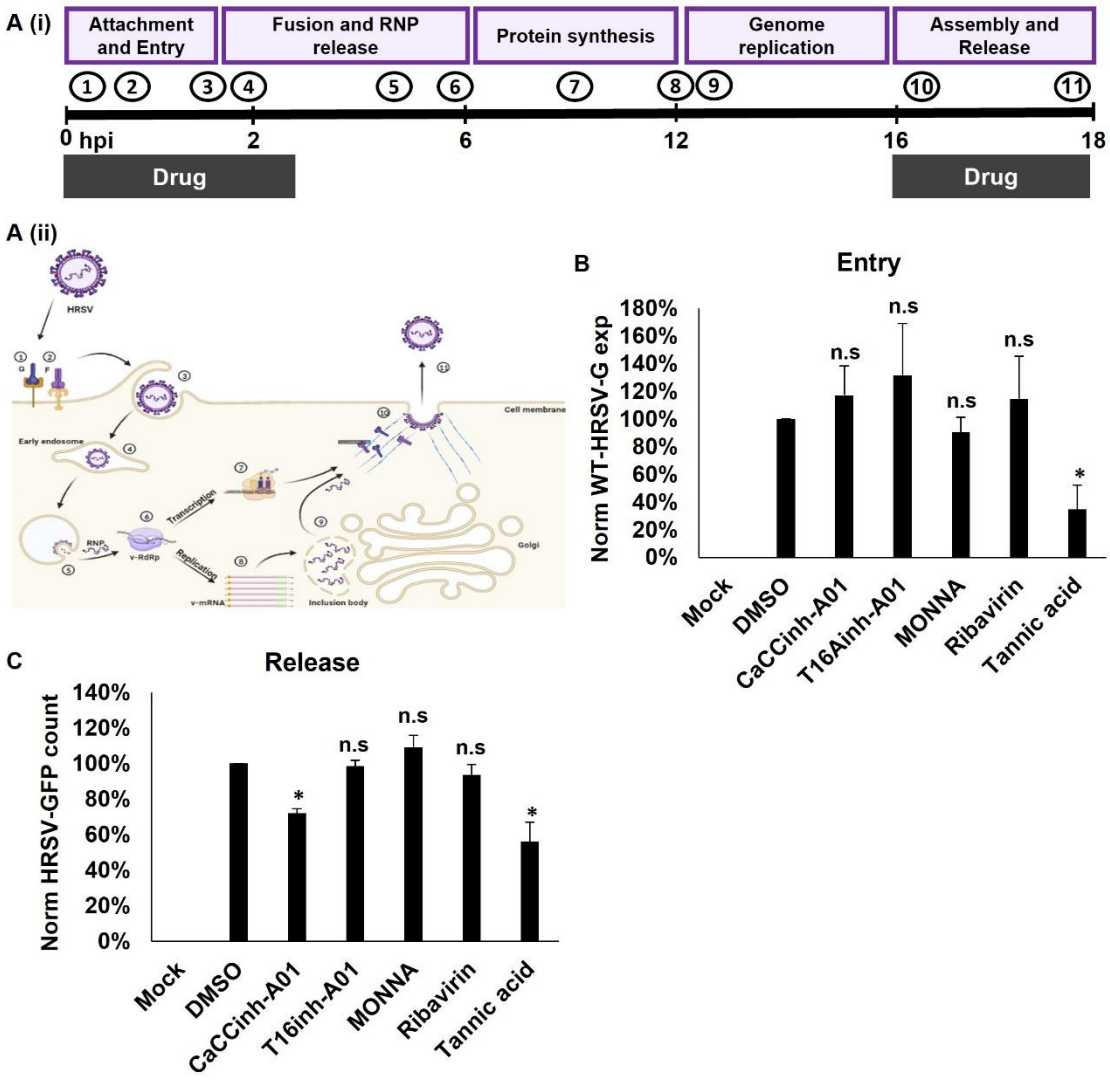

Figure 4-1 TMEM16A in not required for the cell entry or release of HRSV. **A (i)** Schematic depiction of HRSV infection timeline indicating when the drugs were present in the following assays. The circled numbers represent the stages of the HRSV life cycle as depicted in **A (ii)**, as in Figure 1-3. **B)** A549 cells were infected with WT-HRSV for 24 hrs. Broad-spectrum CaCC inhibitors CaCCinh-A01 (40 µM) and tannic acid (15 µM), TMEM16A-specific inhibitors T16Ainh-A01 (30 µM) and MONNA (20 µM), or positive control ribavirin (40 µM) was added for the initial three hours and then removed. Infection was assessed by western blot using WT-HRSV-G as a marker of infection. WT-HRSV-G expression was

normalised to GAPDH expression and then to solvent (DMSO)-treated controls. Mean of n=5 ± SE, *p≤0.05, n.s not significant. **C)** A549 cells were infected with HRSV-GFP and treated with the same panel of drugs as 16 hpi. Released virus within cell supernatants was collected at 24 hpi and the drug diluted out. The presence of HRSV-GFP in supernatants was determined by infecting new cells and quantifying GFP expression by IncuCyte ZOOM analysis relative to solvent (DMSO)-treated controls. Mean of n=3 ± SE, *p≤0.05, n.s not significant.

4.3 Time-of-addition assays reveal that TMEM16A is required during early, post-entry stages of HRSV infection

After ruling out a role for TMEM16A during HRSV entry and release, post-entry time of addition assays were performed to define the life cycle stage requiring TMEM16A functionality more clearly. As mentioned previously, in infected cells HRSV-GFP expression was first observed at 9 hpi (Figure 3-3 A) suggesting that this was the time taken for the virus to enter cells, establish viral replication complexes and synthesize mRNAs resulting in viral protein translation [374]. The ability of a compound to inhibit HRSV-GFP expression when added 9 hpi would therefore be suggestive of a role in blocking HRSV gene expression, whereas no effect on HRSV-GFP gene expression at this time point would be indicative of a role prior to this. To test this, A549 cells were infected with HRSV-GFP and a panel of broad-spectrum Cl^- channel inhibitors, CaCC inhibitors and TMEM16A-specific inhibitors, as well as ribavirin and NH_4Cl controls, were added at 0, 3, 6 or 9 hpi (shown schematically in Figure 4-2 A) and infection was assessed at 24 hpi by quantifying HRSV-GFP expression. The levels of GFP expression were compared to solvent-treated cells, and to each of the other time-of-addition points.

The positive control, ribavirin (40 µM), was active against HRSV when added at 0, 3, 6 or 9 hpi, as demonstrated by a significant reduction in HRSV-GFP expression at each time point compared to the solvent-treated control (Figure 4-2 B). The difference between the expression of HRSV-GFP when ribavirin was added at 0 hpi vs 9 hpi was also statistically significant, suggesting that ribavirin was most potent against HRSV when added at earlier time points. However, there was still a significant reduction of 36.8% in HRSV-GFP expression when ribavirin was added at 9 hpi, implying this drug inhibited gene expression processes, as expected.

Endosomal acidification is a process which occurs through the co-ordination of ion channel families to decrease the pH of the subcellular compartment. H^+ ions are pumped into endosomes by H^+ ATPase, and this requires a charge balance facilitated by the outward flow of K^+, or an influx of Cl^- through the appropriate ion channels [178]. Preventing this pH change by treatment of HRSV infected cells with NH_4Cl (10 µM) did not affect HRSV-GFP expression at any time point (Figure 4-2 C). This suggested that HRSV did not rely on endosomal acidification and therefore the requirement for TMEM16A by the virus was not due to a role in endosomal acidification process.

Treatment of cells with tannic acid (15 µM) at 0 hpi showed a substantial 91.8% reduction in HRSV-GFP expression relative to the solvent control. However, a reduced antiviral efficacy was observed when the drug was added at ≥ 3 hpi (38.8% to 13.0% reduction from 3 to 9 hpi, Figure 4-2 D). Statistical analysis confirmed that HRSV-GFP expression was significantly lower when tannic acid was added at 0 hpi compared to all other time points. This complemented the entry assay data and confirmed an inhibitory effect independent of the

TMEM16A-modulating abilities of this compound. However, there was still a significant reduction in HRSV-GFP expression when tannic acid was added at 3, 6 or 9 hpi compared to the solvent-treated control which was likely due to the blockade of TMEM16A.

The Cl^- channel blocker NPPB (80 µM), along with the CaCC inhibitors CaCCinh-A01 (40 µM) and talniflumate (30 µM), all maintained their ability to inhibit HRSV-GFP expression when added up to 9 hpi, resulting in a 69.2%, 63.2% and 40.0% reduction respectively compared to solvent-treated controls (Figure 4-2 E-G). For NPPB and talniflumate, no significant differences in the inhibition of HRSV-GFP expression were observed between the times of addition, implying that the drugs are equally effective at all early points of infection. However, statistical analysis showed that addition of CaCCinh-A01 at 9hpi resulted in a less potent inhibition of HRSV-GFP expression than addition at the earlier time points (0-3 hpi, 81.4%-75.9% reduction, Figure 4-2 F).

Lastly, TMEM16A-specific modulators T16Ainh-A01 (30 µM) and MONNA (40 µM) were also able to inhibit HRSV-GFP expression potently when added up to 9 hpi compared to solvent-treated controls (80.4% and 84.2% reduction respectively at 9 hpi, Figure 4-2 H-I). Furthermore, there was a significant difference between HRSV-GFP expression levels when the inhibitors were added at 0 or 3 hpi than at 9 hpi (T16Ainh-A01 94.8% reduction when added at 0 hpi, MONNA 95.7-96.9% reduction when added at 0-3 hpi). This was a similar effect to the results of the ribavirin and CaCCinh-A01 time-of-addition assays.

Taken together, the time-of-addition data suggested that TMEM16A was required within the first 9 hrs of infection during a viral life cycle stage that predominantly takes place early post-infection. The potent activity of these modulators displayed

when added at 9 hpi suggested that TMEM16A plays a role HRSV gene expression. These data highlight the potential of TMEM16A modulators as post-entry inhibitors of HRSV infection in infected individuals [326].

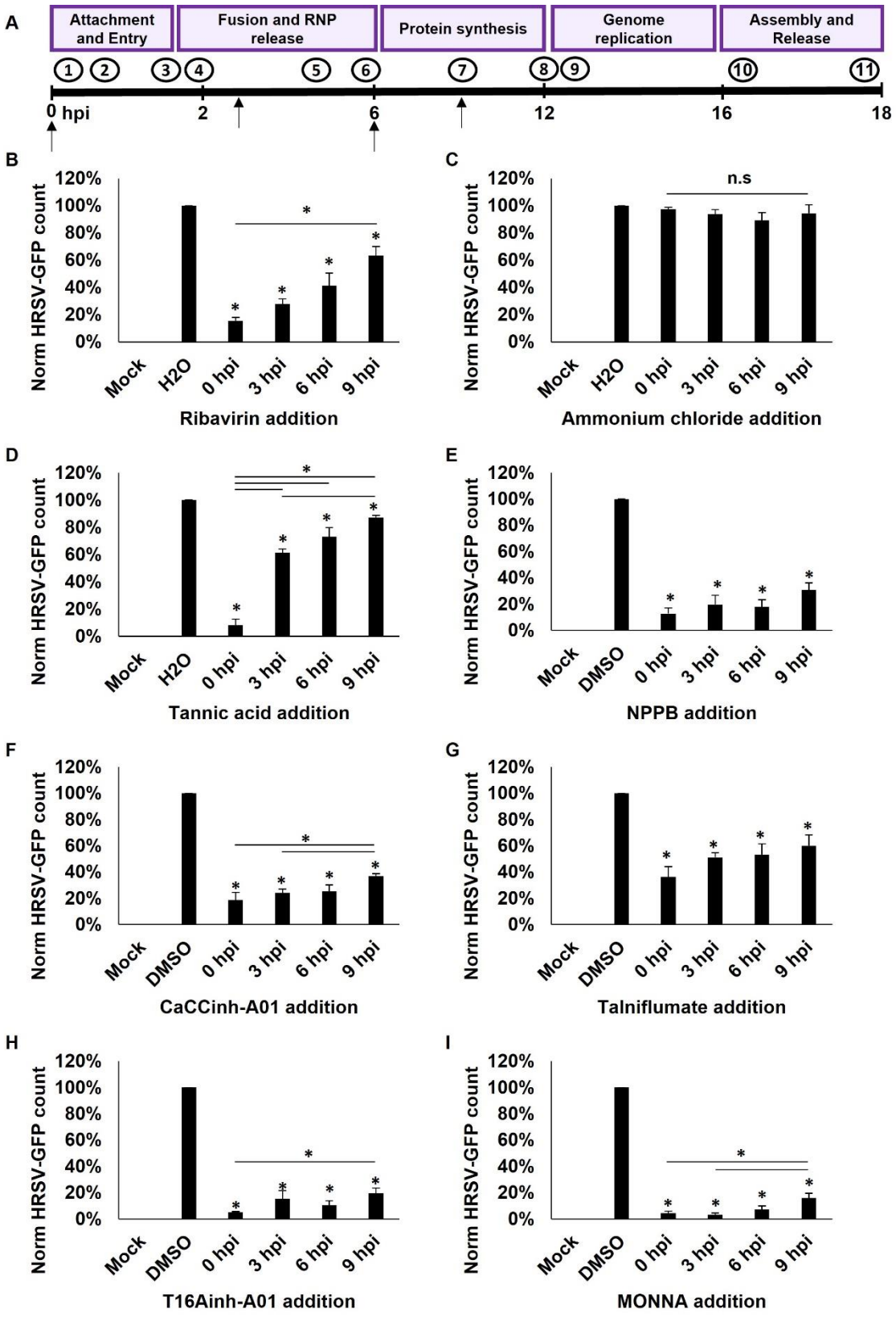

Figure 4-2 TMEM16A is required for early, post-entry stages of HRSV infection. A) Schematic depiction of HRSV infection timeline indicating when the drugs were added in the time-of addition assays (arrows). The circled numbers

represent the stages of the HRSV life cycle as depicted in Figure 4-1 A (ii). **B-I)** Time-of-addition assays in which (B) positive control ribavirin (40 µM), (C) negative control ammonium chloride (10 µM), (E) Cl- channel blocker NPPB (80 µM), CaCC inhibitors (D) tannic acid (15 µM), (F) CaCCinh-A01 (40 µM) or (G) talniflumate (30 µM) or TMEM16A-specific inhibitors (H) T16Ainh-A01 (30 µM) or (I) MONNA (40 µM) were added to HRSV-GFP infected A549 cells at 0, 3, 6 or 9 hpi. Infection was assessed by IncuCyte ZOOM quantification of fluorescent cells at 24 hpi and is shown relative to solvent (DMSO or H_2O)-treated controls. Mean of n=3 ± SE, *p≤0.05, n.s not significant

4.4 T16Ainh-A01-treatment causes a delay in HRSV viral protein synthesis

To characterise HRSV-GFP infection in the presence of TMEM16A modulators, a time course of HRSV-GFP expression was generated using the IncuCyte live cell imaging system (Figure 4-3 A). In agreement with the previous data presented in Figure 3-3 A, HRSV-GFP expression began at 9 hpi in solvent-treated cells and the number of GFP-expressing cells rose steadily until 24 hpi (Figure 4-3 A, dark grey line). However, in the presence of replication inhibitor ribavirin (40 µM), a delay in HRSV-GFP expression was observed of around 4 hours, with fluorescence first being observed at 13-14 hpi (Figure 4-3 A, black dash). The viral genomic RNA must be transcribed into mRNA before viral protein synthesis occurs, therefore the delay in HRSV-GFP expression, which is representative of viral protein translation, was likely due to inhibition of a viral step prior to this. Interestingly, treatment with T16Ainh-A01 (15 µM) also resulted in a similar delay in HRSV-GFP expression (Figure 4-3 A, black line), suggesting a role for TMEM16A prior to viral protein translation. Despite the delay, the number

of HRSV-GFP expressing cells increases at a similar, steady rate in ribavirin- and T16Ainh-A01-treated cells as in solvent-treated cells.

Within the same time-course, data regarding the intensity of fluorescence in HRSV-GFP expressing cells was obtained (Figure 4-3 B). Under all conditions, the intensity of HRSV-GFP fluorescence increased at a consistent, steady rate. It was observed that the level of HRSV-GFP intensity correlated with the number of HRSV-GFP expressing cells (e.g., in T16Ainh-A01-treated cells, the number of infected cells was lower than solvent-treated cells, and therefore so was the HRSV-GFP intensity) under all conditions except tannic acid treatment.

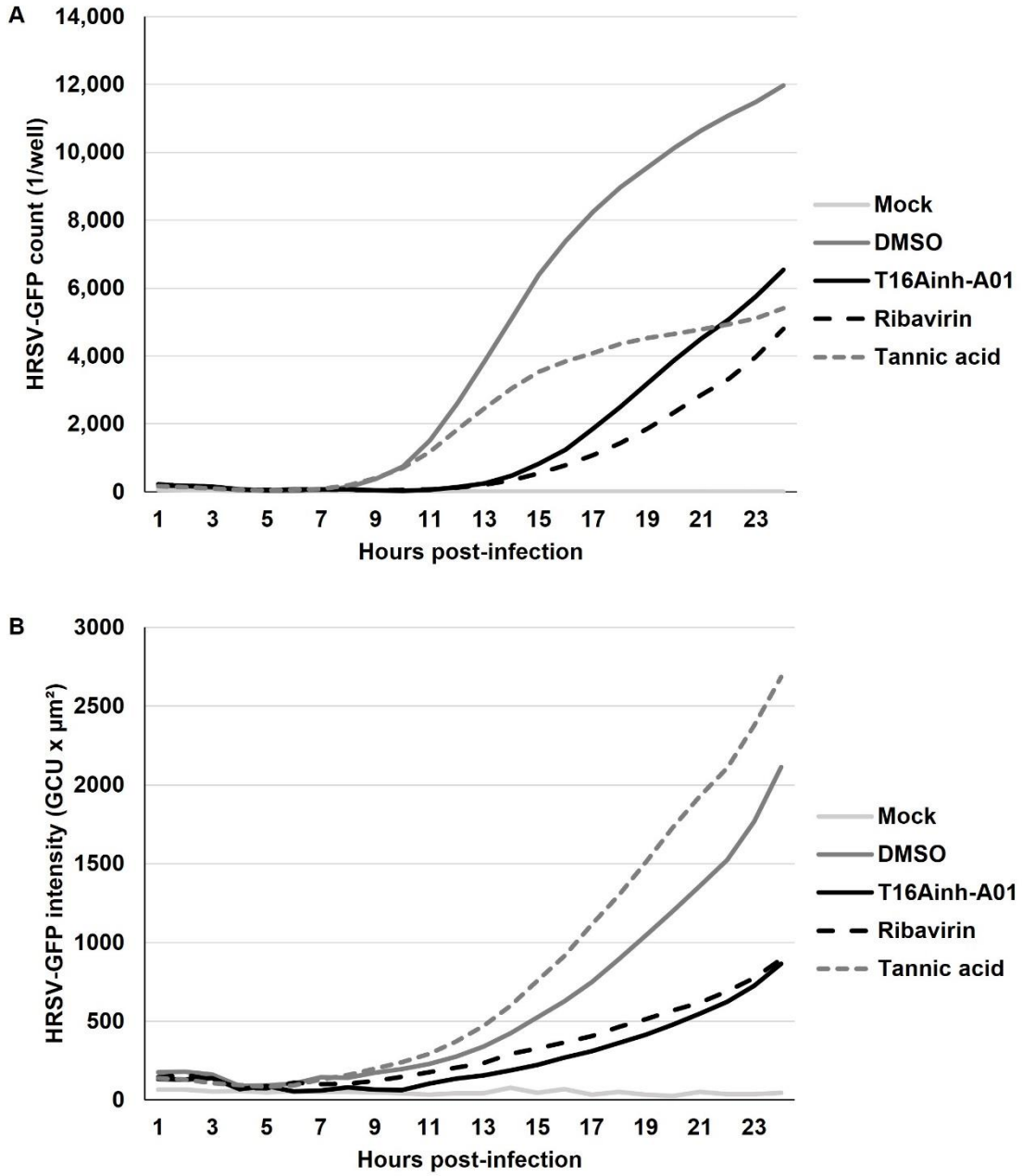

Figure 4-3 Time course of HRSV-GFP infection in the presence of TMEM16A-modulators. A-B) A549 cells were pre-treated with TMEM16A-specific modulator T16Ainh-A01 (15 µM, black solid line), HRSV replication inhibitor ribavirin (40 µM, black dashed line), CaCC modulator tannic acid (15 µM, grey dashed line) or solvent (DMSO, grey solid line) control for 45 mins prior to infection with HRSV-GFP at MOI 0.1. The number of GFP-expressing cells per well (A) or a quantification of the intensity of GFP fluorescence (B) was analysed every hour for 24 hrs.

4.4.1 Tannic acid inhibits HRSV entry and release via a TMEM16A-independent mechanism

Conversely, tannic acid (15 µM) treatment, which was suggested to inhibit HRSV entry and/or release in the previous assays, did not display the same delay in HRSV-GFP expression as in T16Ainh-A01- or ribavirin-treated cells. In the presence of tannic acid, HRSV-GFP expression began at 8/9 hpi but did not proceed at the same rate as in solvent-treated control cells (Figure 4-3 A, light grey dash). At approximately 14-15 hpi, the number of HRSV-GFP expressing cells began to plateau, indicating that fewer virions were entering tannic acid-treated cells, consistent with previous experiments. Although the number of HRSV-GFP expressing cells was fairly consistent between 16-24 hpi, the HRSV-GFP fluorescence intensity was the highest in tannic acid cells throughout the time-course (Figure 4-3 B, light grey dash), indicating that these few infected cells were responsible for the majority of the HRSV-GFP signal. This may support the hypothesis that tannic acid inhibits both the entry and release of HRSV, as the increase in HRSV-GFP intensity could be due to a build-up of release-deficient virions, however further investigations are necessary to draw this conclusion.

4.4.1.1 Tannic acid also inhibits BUNV cell entry by preventing the virus from binding to the cell

As tannic acid appeared to inhibit HRSV by a different mechanism to the TMEM16A-specific modulators, its ability to block another virus, BUNV, was investigated in more detail. Previously, in 3.12.2, it was discovered that BUNV was sensitive to CaCCinh-A01 (20-40 µM) but not T16Ainh-A01 (10-20 µM). Therefore, entry assays were performed on BUNV using these two inhibitors plus tannic acid (20 µM). Pit stop 2 (30 µM), an inhibitor of clathrin-mediated

endocytosis, was also used as a positive control. As shown in the western blot in Figure 4-4 A(i) and quantified from three independent repeats in Figure 4-4 A(ii), there was no significant difference in WT-BUNV-N expression in cells treated with CaCCinh-A01 or T16Ainh-A01 compared to the solvent treated control indicating that the presence of these drugs did not affect BUNV entry. However, an 87.9% reduction in N expression was observed in those treated with tannic acid, indicating a potent inhibition of BUNV entry. Similarly, pit stop 2 was able to inhibit BUNV entry as shown by a relative 61.1% reduction in N expression.

As previously mentioned, tannic acid has been implicated in the entry of several other viruses. During HCV infection, tannic acid inhibited entry by blocking the docking of the virus onto cells [377]. In this study, the authors suggested that this was likely due to the ability of tannic acid to form macromolecular complexes on the surface of cells. To investigate whether tannic acid was able to block the binding of BUNV onto cells, a virus binding assay was performed. This involved binding BUNV onto the surface of cells at 4^{o}C for 1 hr in the presence or absence of tannic acid (20 µM). The cold temperature inhibited endocytosis to ensure that any bound virus could not enter the cell. After the binding step, any unbound virus was washed away, and the infection continued at 37^{o}C. Tannic acid was then present during the first or second hour of BUNV entry before being replaced with drug-free media. Infection was assessed by the quantification of WT-BUNV-N expression after 24 hrs (Figure 4-4 B(i)). When tannic acid was present during the binding stage only, there was a 96.0% drop in N expression compared to the solvent-treated control (Figure 4-4 Bii), indicating that tannic acid was potently preventing the binding of BUNV onto cells. In contrast, when the virus could bind to cells in the absence of tannic acid, but the drug was present for the first or

second hour of entry at 37°C, WT-BUNV-N expression was not significantly different to the solvent treated control. These data indicated that only the binding and not the internalisation of BUNV was affected by tannic acid treatment.

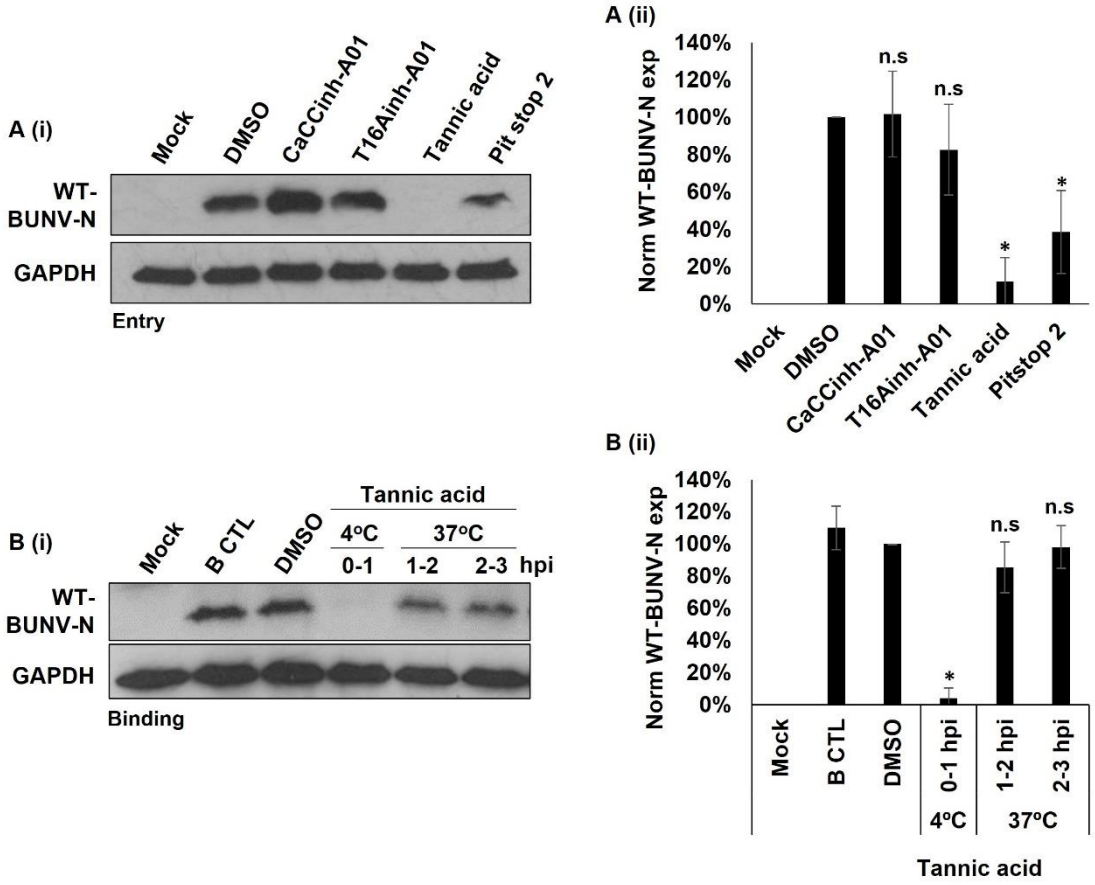

Figure 4-4 Tannic acid prevents BUNV docking onto cells. A) BUNV entry assay in which A549 cells were infected with WT-BUNV for 24 hrs. Broad-spectrum CaCC inhibitors CaCCinh-A01 (40 µM) and tannic acid (20 µM), TMEM16A-specific inhibitor T16Ainh-A01 (20 µM) or positive control entry inhibitor pit stop 2 (30 µM) was added for the initial three hours and then removed. Infection was assessed by western blot using WT-BUNV-N as a marker of infection. Representative blot shown in A (i). A (ii) Densitometry analysis of WT-BUNV-N expression was normalised to GAPDH and then to solvent (DMSO)-treated controls. Mean of n=3 ± SE, *p≤0.05, n.s not significant. **B)** Binding assay in which BUNV was bound to A549 cells at 4°C for 1 hours in the presence or absence of tannic acid (20 µM). Non-internalised virus was washed away, and virus entry proceeded at 37°C with the drug present during the first or second hr

of entry. At 24 hpi, infection was analysed by western blot as above. Mean of n=2 ± SE, *p≤0.05, n.s not significant.

4.5 Minigenome assay reveals a role for TMEM16A during HRSV replication

A HRSV minigenome assay was utilised to further investigate the role of TMEM16A during replication. Minigenome assays have been used previously to probe the roles of HRSV proteins in viral transcription [68,332,333]. Plasmids expressing the minimal requirements for genome replication were transfected into BSR-T7 cells (depicted in Figure 4-5 A). These plasmids encoded the genes for P, L, N, M2-1 under the control of a T7 RNA polymerase promoter and the fifth plasmid encoded a minigenome, which consisted of HRSV terminal promoter regions flanking two transcriptional units (the second encoding eGFP) separated by an authentic M/SH gene junction (pM/SH-GFP). In BSR-T7 cells, the endogenous T7 polymerase drove the transcription of all five plasmids and subsequent expression of the HRSV replication complex proteins as well as the minigenome, which were able to assemble into transcriptionally competent minigenome RNPs, with the expression of GFP. A negative control was included in all experiments, in which the L plasmid was omitted and replaced with an empty plasmid, to ensure all GFP expression was HRSV RdRp-dependent.

Optimisation of the transfection was required with respect to plasmid and transfection reagent quantities, as successful reconstitution of the active minigenome was only possible when cells received a copy of all five plasmids. Previous work [332] indicated that a ratio of 1:1:0.5:0.25:0.25 for the five plasmids pN: pP: pL: pM2-1: pM/SH-GFP was optimal, and this was compared to an

alternative ratio of 1:1:1:1:1. A ratio of 1:1:1:1:1.5 was also tested to examine whether transfecting more of the minigenome would increase the efficiency of the assay. After 24 hrs, the number of GFP-expressing cells was similar in all conditions, between 2098 and 2905 cells (Figure 4-5 B). At 48 hpt, the number of GFP-expressing cells was highest for the 1:1:1:1:1 transfection with 11,679 cells, compared to 9661 and 9849 cells in the 1:1:0.5:0.25:0.25 and 1:1:1:1:1.5 conditions, respectively, therefore this was deemed the most efficient transfection protocol, which was adopted throughout.

The transfection reagent used in these experiments was FuGENE HD (Promega) and next, according to the manufacturers protocol, varying amounts of total DNA were used in the transfection with a DNA:transfection regent ratio of 1:3 and a plasmid ratio of 1:1:1:1:1 (Figure 4-5 C). The number of GFP expressing cells was assessed at 24, 48 and 72 hpt. At each time point, 3.3 µg DNA resulted in the highest number of GFP-expressing cells, and so this amount was used in future experiments. The largest number of cells expressing GFP occurred at 48 hpt and the background GFP signal from the negative (-pL) control was minimal. A time course of GFP expression in cells transfected with the minigenome system revealed that GFP expression begins to rise above background fluorescence levels at around 18 hpt (Figure 4-5 D).

To test the effect of TMEM16A modulation on HRSV replication, BSR-T7 cells were transfected with the minigenome plasmids for 6 hrs before treatment with TMEM16A modulators. The level of HRSV replication was assessed 24 hrs after the addition of the drugs (30 hpt) through measurement of the intensity of GFP fluorescence within transfected cells. Treatment with the replication inhibitor ribavirin (80 µM) as a positive control resulted in an 80.2% reduction in GFP

intensity compared to solvent treated control cells (Figure 4-5 E). Treatment with the broad-spectrum channel inhibitor CaCCinh-A01 (40 µM) also resulted in a decrease in HRSV minigenome replication, with a 55.3% reduction in GFP intensity, whereas treatment with the specific TMEM16A inhibitor T16Ainh-A01 (20 µM) resulted in a more potent effect, with a 64.1% reduction in GFP expression. Surprisingly, the other TMEM16A-specific drug MONNA (30 µM) did not elicit a significant reduction upon the replication of the HRSV minigenome, and neither did tannic acid (15 µM), the broad spectrum CaCC inhibitor, which had previously inhibited HRSV entry and release.

Taken together, the outcome of treatment with CaCCinh-A01 and T16Ainh-A01 implicated a role for TMEM16A during HRSV genome replication. The use of BSR-T7 cells in this assay may account for the inconsistent results of the two TMEM16A-specific modulators T16Ainh-A01 and MONNA. Although MONNA did not significantly inhibit HRSV replication, an average of 43.9% reduction in GFP intensity was observed in MONNA-treated cells, indicating some inhibition of the compound of HRSV minigenome replication. The inconstancy here may be due to the use of a non-human cell line in which the mechanism of action of the compounds may differ. However, unfortunately due to time constraints, a more physiologically relevant cell line expressing T7 polymerase was unable to be generated.

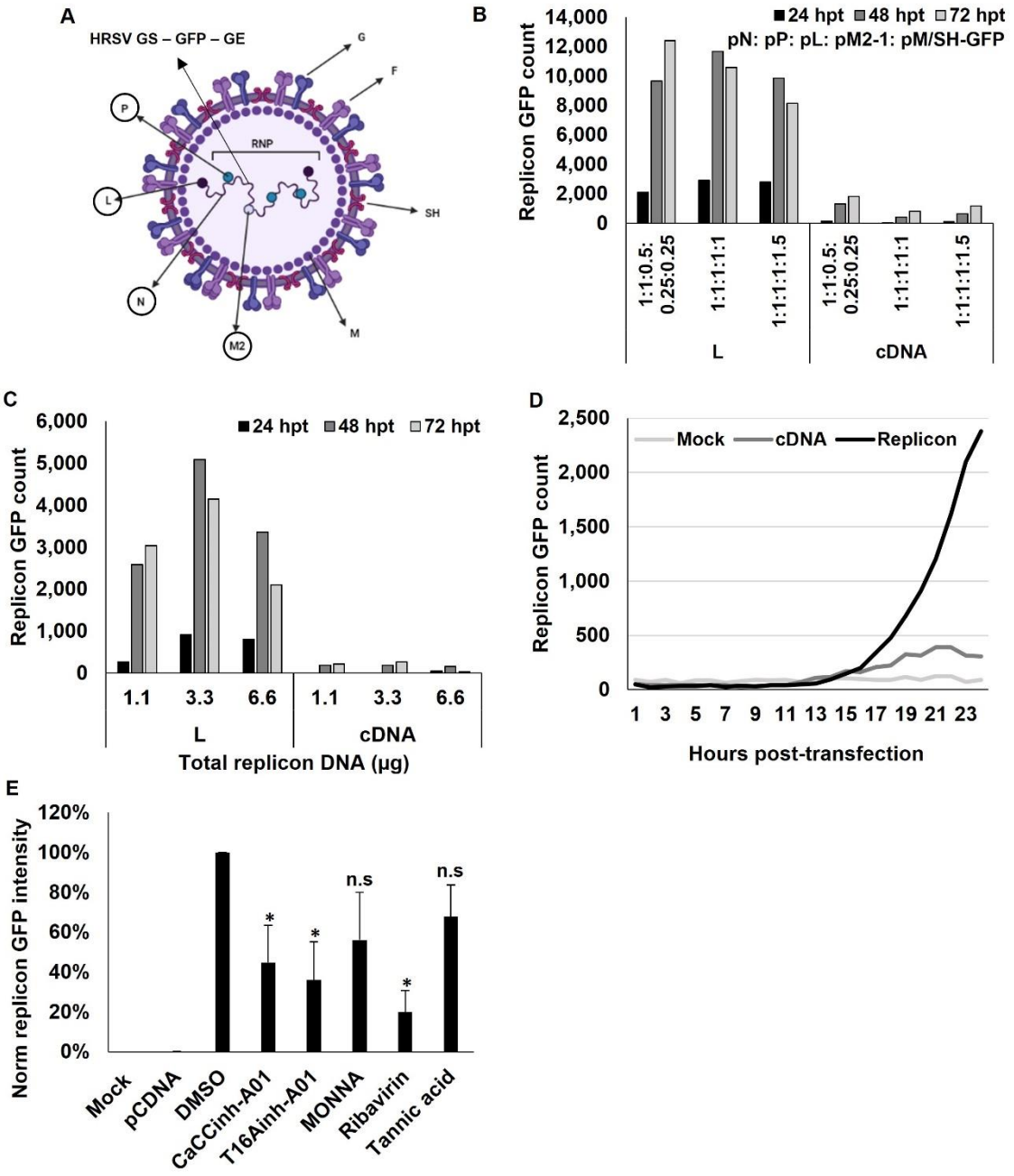

Figure 4-5 TMEM16A is required during HRSV genome replication and/or transcription. A) Schematic of the HRSV virion to demonstrate the minimal requirements for HRSV genome replication/transcription (circled). **B)** Optimisation of the ratio of plasmids used in the HRSV minigenome system. BSR-T7 cells were transfected with pN, pP, PL, pM2-1, and pM/SH-GFP at the indicated ratios for 24, 48 or 72 hrs. Quantification of GFP-expressing cells was performed using IncuCyte ZOOM. As a specificity control, pL was replaced with an empty plasmid. **C)** Cells were transfected with a total of 1.1, 3.3 or 6.6 µg DNA at a plasmid ratio of 1:1:1:1:1 and analysed as in (B). **D)** Time course of GFP

expression in cells transfected with the HRSV minigenome as in (C), with a total of 3.3 µg DNA. **E)** BSR-T7 cells were transfected with the HRSV minigenome plasmids as in (D). At 6 hpt, the CaCC inhibitors CaCCinh-A01 (40 µM) or tannic acid (15 µM), TMEM16A-specific modulators T16Ainh-A01 (20 µM) or MONNA (30 µM), or the HRSV replication inhibitor (positive control) ribavirin (80 µM) were added for 24 hr. HRSV replication and/or transcription was quantified at 30 hpt by IncuCyte ZOOM analysis of GFP intensity. Mean of n=4 ± SE, *p≤0.05, n.s not significant.

4.6 HRSV cannot easily develop resistance to TMEM16A modulators

The generation of viral ‘escape’ mutants that can evade pharmacological inhibition is often useful in determining the mechanisms of inhibitor action during infection. Therefore, the generation of a HRSV mutant with resistance to TMEM16A-specific modulator T16Ainh-A01 was attempted by sequentially blind passaging the virus in the presence of the drug. Firstly, the toxicity of T16Ainh-A01 in A549 cells at different concentrations was tested at 24 hr intervals up to 96 hrs to select an appropriate concentration and time point for passaging (Figure 4-6 A). Concentrations of 20 µM and above were considered too toxic as the cell viability fell below 80% of the solvent treated control cells. A drop in cell health in drug treated cells was observed at 48 hrs at all concentrations, which then recovered at later time points, suggesting the drug may be metabolised by 72-96 hrs. To be able to leave a longer time between passages, a lower concentration of drug had to be used, and 15 µM from 72 hrs was deemed a good compromise between the health of the cells and a good inhibitory effect on the virus.

Another variable which required optimisation was the volume of virus supernatant (VSN) to transfer between passages. It is well known that HRSV infection induces release of many cytokines [338] which could be transferred in the supernatant negatively affect the fresh cells. To test this, cells were infected in the presence or absence of 15 µM T16Ainh-A01 for 24 or 72 hrs, after which the VSN was removed and clarified. Then varying volumes of VSN were transferred to fresh cells (P2) to assess the level of infection achieved as well as the health of the cells. In the P2 cells passaged for 24 hrs, the viability of the drug-treated and control cells was similar and all above 80% irrespective of volume VSN transferred (Figure 4-6 B), however, no viral bands were detected on the western blot analysis indicating that this passage time was too short (data not shown). Conversely, in the P2 cells passaged for 72 hrs, the health of the solvent-treated control cells was much lower than that of the drug-treated cells (Figure 4-6 Ci). This was likely due to more virus being present in the VSN of the control cells which caused more damage to the P2 cells. When the different volumes of VSN were compared, it was revealed that transferring higher volumes of VSN resulted in less infection in the drug-treated cells despite there being more virus in the VSN (Figure 4-6 Cii). It was concluded that transferring 250 µL of VSN in drug-treated cells offered the best balance of infection against cell health. However, because of the higher viral load of the VSN from control cells, only 100 µL was transferred from these samples to keep the MOI somewhat consistent between control and drug treated cells during the blind passaging.

Following optimisation, HRSV-GFP was passaged in the presence of T16Ainh-A01 (15 µM), ribavirin (40 µM), or solvent control (DMSO) for 10 passages with 72 hrs between each passage. During this time, the levels of infection in the

DMSO and ribavirin passaged virus gradually recovered to eventually reach a level that was comparable to the initial passage. However, virus levels in the T16Ainh-A01 treated cells dropped immediately, such that no GFP-expression was detected after passage 10 (Figure 4-6 D). This indicated that HRSV was not easily able to escape the effect of TMEM16A modulation. While this was unfortunate in that it did not provide information of the requirement of TMEM16A for HRSV multiplication, it revealed that HRSV escape mutants were not readily generated, which is a critical attribute of any combination of virus and a potential antiviral inhibitor.

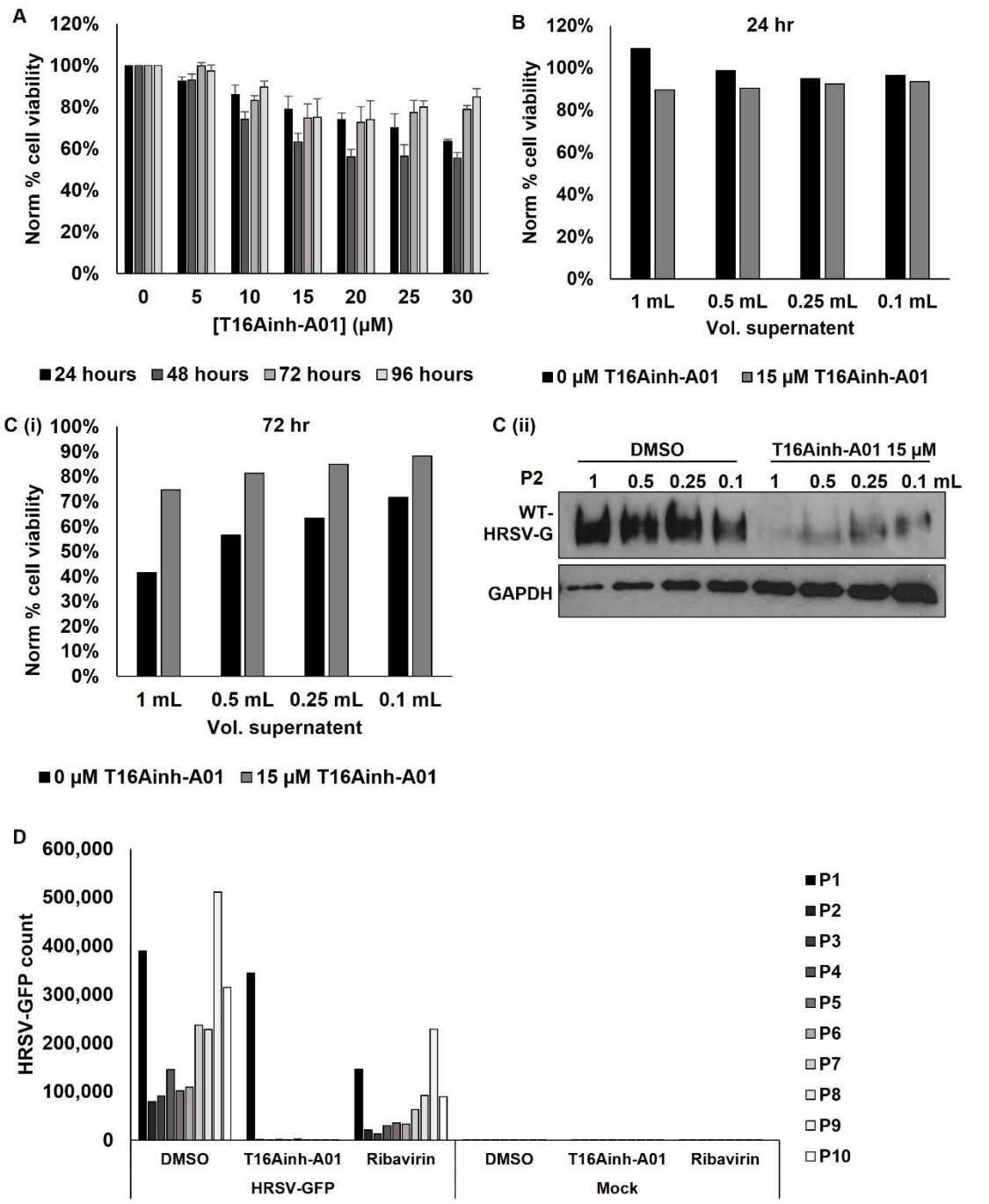

Figure 4-6 Attempt to generate T16Ainh-A01-resistant HRSV escape mutants. A-C) Optimisation of blind passage of HRSV in the presence of T16Ainh-A01. **A)** MTS assay to measure the cell viability of A549 cells treated with T16Ainh-A01 (5-30 μM) for 24, 48, or 72 hrs. Results shown relative to solvent-treated controls (0 μM). Mean of n=3 ± SE. Cell viability ≥80% of the control was considered non-toxic. **B)** MTS assays to measure the cell viability of cells after 24 hr incubation with 0.1-1 mL virus supernatant from cells infected with HRSV and treated with 0 or 15 μM T16Ainh-A01. **C (i)** as in (B), incubated

for 72 hrs. **C (ii)** Analysis of HRSV infection in the cells from C (i) by western blot. WT-HRSV-G is used as a marker of infection and GAPDH is shown as a loading control. **D)** Quantification of HRSV-GFP expressing cells in sequential passages in the presence of DMSO (solvent-control), T16Ainh-A01 (15 µM) or ribavirin (40 µM). Cells were incubated for 72 hrs with 250 µL (inhibitors) or 100 µL (DMSO control) VSN from the previous passage in a total of 1 mL. Infection was assessed in live cells by IncuCyte analysis just prior to passaging.

4.7 Investigation into TMEM16A localisation in A549 cells

TMEM16A is expressed on the plasma membrane, however its intracellular localisation is not well described. In order to learn more about the role of TMEM16A during HRSV infection, the localisation of the channel was investigated using confocal microscopy. The antibodies which target TMEM16A are often unreliable (Appendix A, Figure A-1), therefore an alternative method of detecting the channel in cells was sought. A plasmid encoding the TMEM16A ORF with a C-terminal mycDDK tag was purchased from OriGene, henceforth termed ‘pTMEM16A-mycDDK’. Varying amounts of plasmid DNA were used to transfect A549 cells and expression of TMEM16A-mycDDK was confirmed by western blot analysis using an anti-DDK (FLAG tag) antibody (Figure 4-7 A). A band was present at the expected molecular weight of approximately 115 kDa, which did not appear in the mock transfected cell lysates. Transfected cells were also fixed and stained for immunofluorescent analysis using the same anti-DDK antibody (Figure 4-7 B). From the two methods of analysis, it was confirmed that TMEM16A-mycDDK could be detected in cells transfected with 1 µg plasmid DNA by both western blotting and immunofluorescence techniques.

For analysis by confocal microscopy, transfected cells were fixed at 24 hpt and stained with anti-DDK. The expression of TMEM16A-mycDDK appeared to take two phenotypes: diffuse staining throughout the cell with some cell surface expression, or distinct puncta within the cell (examples shown in Figure 4-7 C).

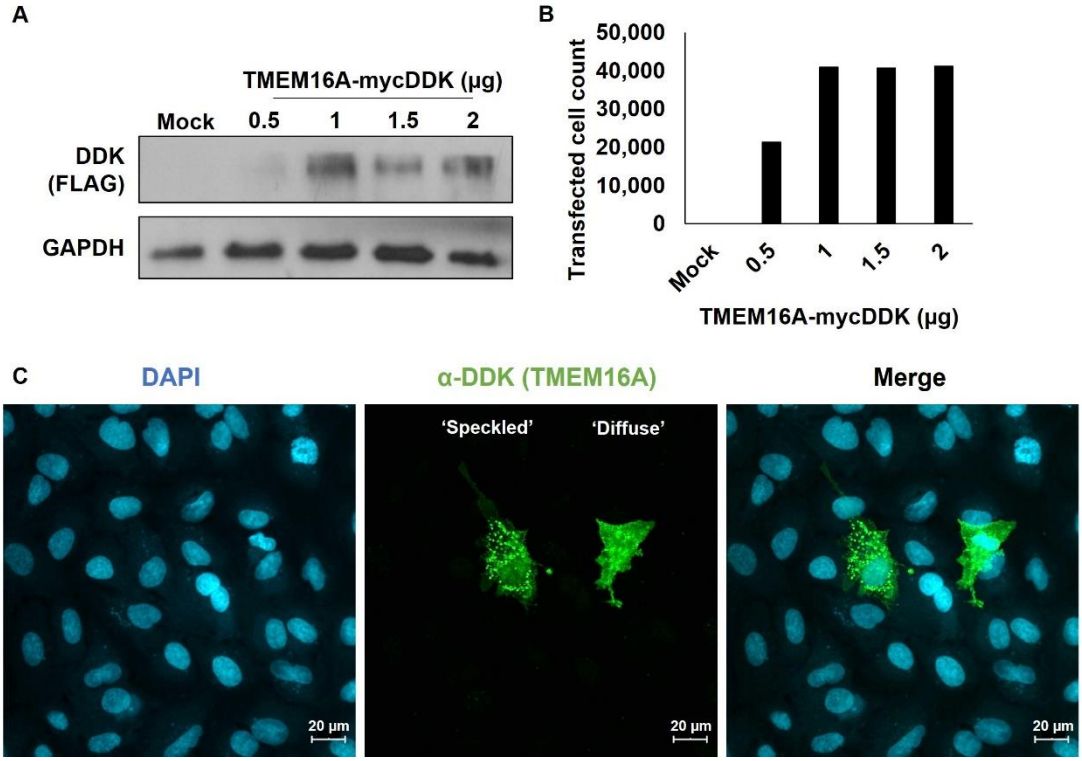

Figure 4-7 Overexpression of TMEM16A in A549 cells. A) Cells were transfected with 0.5-2 µg of pTMEM16A-mycDDK. Western blotting was used to detect the presence of tagged TMEM16A using anti-DDK (FLAG). GAPDH is shown as a loading control. **B)** Cells transfected as in (A) and TMEM16A was detected by immunofluorescent staining of the DDK tag. IncuCyte analysis was used to quantify to number of TMEM16A-mycDDK expressing cells. **C)** Confocal microscopy images of cells transfected with pTMEM16A-mycDDK. DAPI was used to visualise the nucleus (cyan) and the DDK tag of TMEM16A was labelled with Alexa-Fluor-488 (green). Images captured on Zeiss LSM880 at 40x magnification, scale bar 20 µM.

In the following sections, A549 cells expressing TMEM16A-mycDDK were co-stained with antibodies targeting various subcellular organelles to investigate the localisation of the channel. Co-localisation between the TMEM16A (green) and the cellular markers (magenta) was assessed by line scan analysis using ImageJ. This technique was recently used to study ion channel localisation in the context of viral infection [313].

4.7.1 TMEM16A is not expressed within the endocytic pathway

As HRSV enters cells via macropinocytosis and subsequently passes through the endosomal network, the possibility that TMEM16A was expressed in endosomes was investigated. Cells were transfected with pTMEM16A-mycDDK and stained with anti-EEA1, a marker for early endosome compartments (Figure 4-8) and as expected, small and distinct cytoplasmic puncta were observed. In cells with speckled TMEM16A staining, no co-localisation with early endosomes was observed and line scan analysis confirmed the peaks of EEA1 and TMEM16A expression were in different locations (Figure 4-8 A-B).

To examine whether TMEM16A might localize to later compartments of the endosomal system, an antibody targeting lysosomal marker LAMP1 was also used (Figure 4-9). Lysosomal staining was observed as many very small puncta dotted throughout the cytoplasm and revealed no clear co-localisation with TMEM16A, in agreement with the line scans that show peaks corresponding to TMEM16A and LAMP1 expression did not coincide (Figure 4-9 A-C). These results suggested that TMEM16A was not highly expressed within the endocytic pathway.

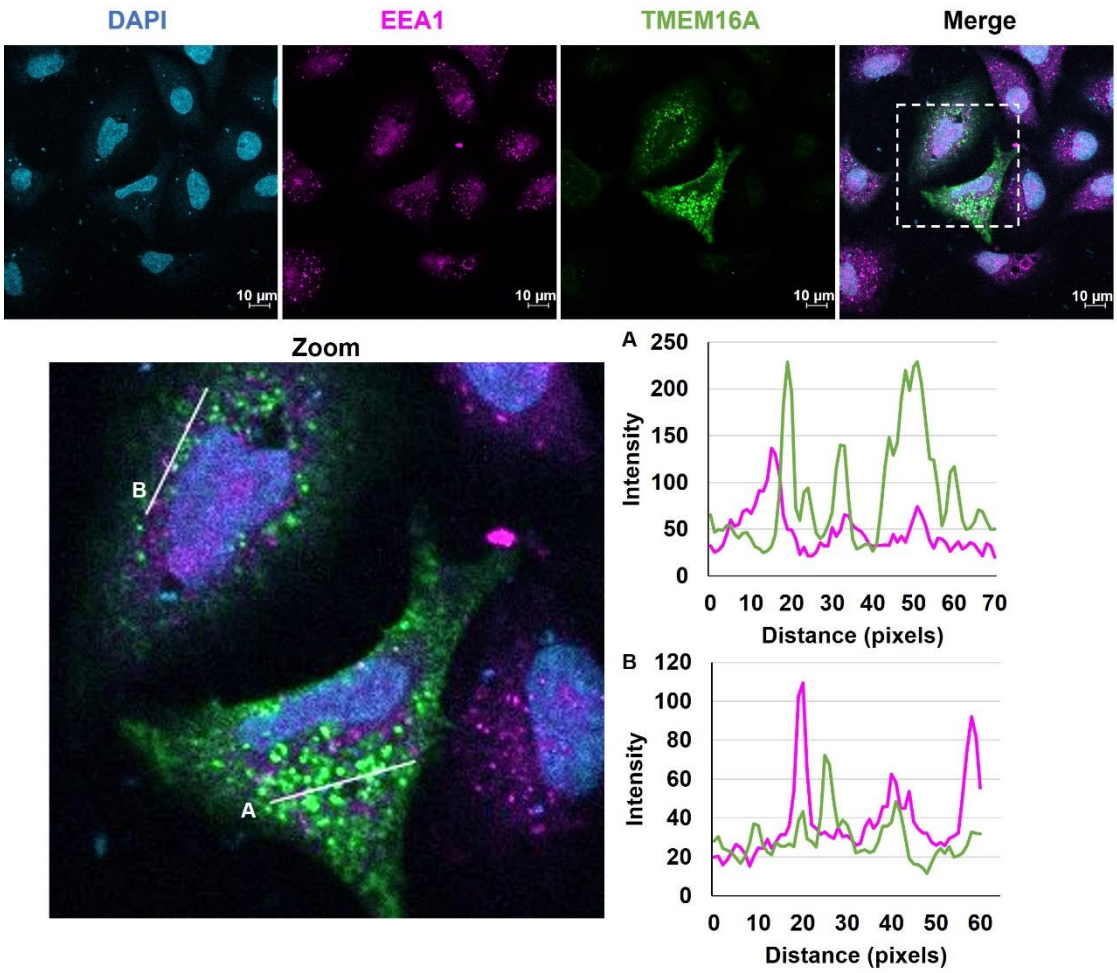

Figure 4-8 TMEM16A is not expressed in early endosomes. A549 cells were transfected with 1 µg pTMEM16A-mycDDK for 24 hrs. Cells were analysed by confocal microscopy at 63x magnification on Zeiss LSM880 microscope. DAPI was used to visualise the nucleus (cyan). TMEM16A was detected using antibodies against the DDK tag (green). Cells were co-stained for early endosomal marker EEA1 (magenta). **A-B)** Fluorescent line scans to analyse the spatial distribution of TMEM16A-mycDDK and EEA1 taken using ImageJ.

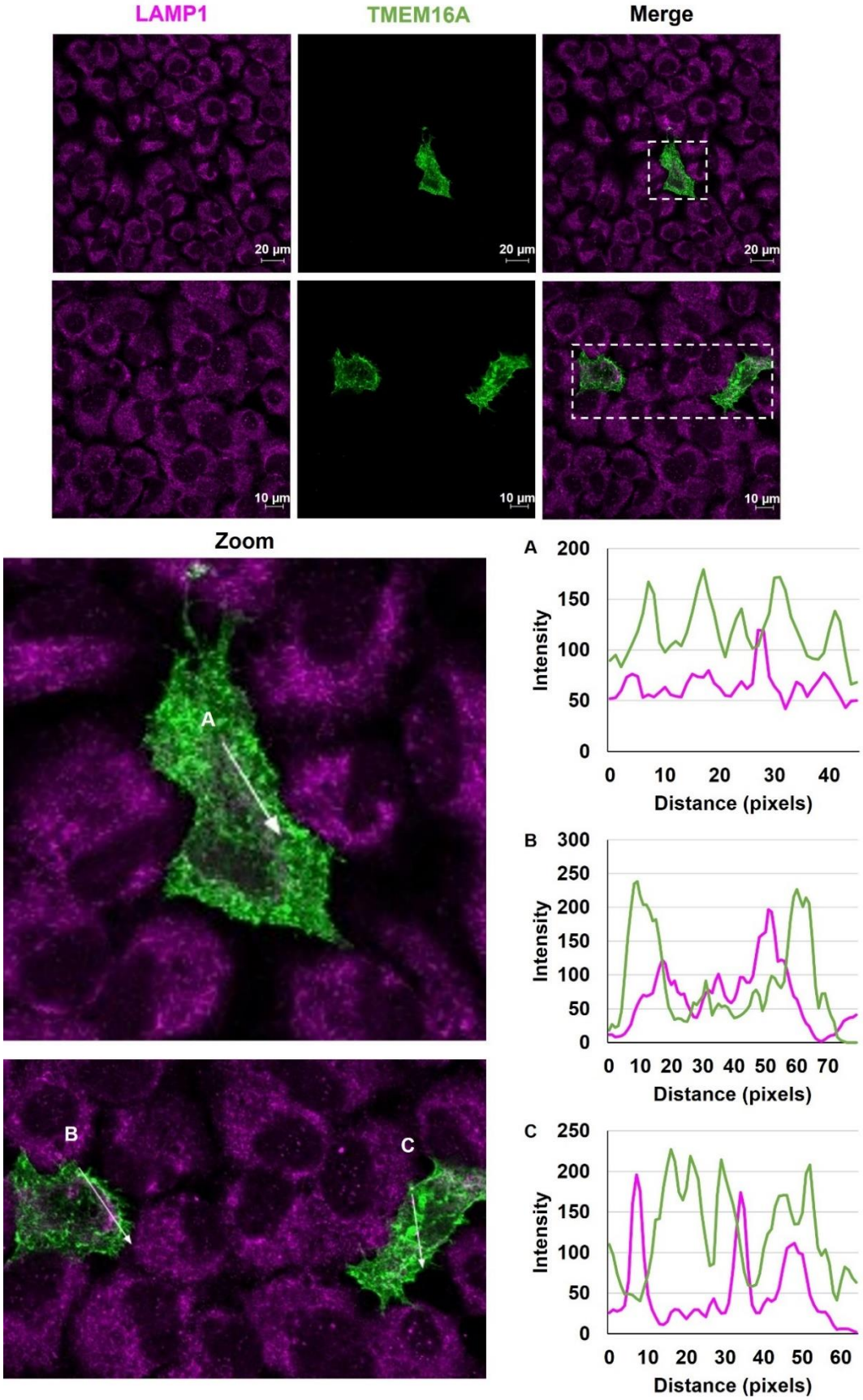

Figure 4-9 TMEM16A is not expressed in lysosomes. A549 cells were transfected with 1 µg pTMEM16A-mycDDK for 24 hrs. Cells were analysed by

confocal microscopy on the Zeiss LSM880 at 40x magnification (top row) or 63x (bottom row), scale bars 20/10 µM. TMEM16A was detected using antibodies against the DDK tag (green). Cells were co-stained for lysosomal marker LAMP1 (magenta). **A-C)** Fluorescent line scans to analyse the spatial distribution of TMEM16A-mycDDK and LAMP1 taken using ImageJ.

4.7.2 TMEM16A co-localises with membranous sub-cellular structures

In cells transfected with pTMEM16A-mycDDK and stained with the fluorescently labelled ER stain concanavalin A (conA), co-localisation was observed between TMEM16A-mycDDK and the ER. ConA is a lectin which binds to α-mannopyranosyl and α-glucopyranosyl residues in the ER. The microscopy images in Figure 4-10 show an example of cells demonstrating each phenotype of TMEM16A staining (speckled and diffuse). ER staining by conA displayed characteristic cytoplasmic staining surrounding the nucleus and more diffuse towards the plasma membrane. The puncta of TMEM16A in the speckled phenotype co-localised well with the ER stain, and line scan analysis (Figure 4-10 A) revealed coincident peaks of TMEM16A and ER staining at the same locations, indicating a high level of co-localisation. In cells with more diffuse TMEM16A staining, co-localisation was also observed (Figure 4-10 B). Based on some of the known functions of TMEM16A in the control of intracellular Ca^{2+} signalling (1.7.4.2, [221,222]) it is perhaps not surprising that the channel would be expressed in close association with the ER, which houses the cellular Ca^{2+} stores.

Next, the Golgi body was stained with antibodies targeting the Golgi marker GM130, showing the characteristic peri-nuclear expression clustered to one side

of the nucleus (Figure 4-11). In cells with both speckled and diffuse TMEM16A staining, co-localisation was observed with GM130 in many instances. The associated line scan analysis confirmed these observations, revealing several coincident peaks corresponding to both TMEM16A and GM130 (Figure 4-11 A-C). In agreement with the confocal images, line scan peaks corresponding to TMEM16A and GM130 did not always align, with several isolated peaks, indicating expression of only one of the two proteins. It is interesting to speculate that TMEM16A resides at the Golgi considering that HRSV IBs are also known to form in close proximity to the Golgi [80,81].

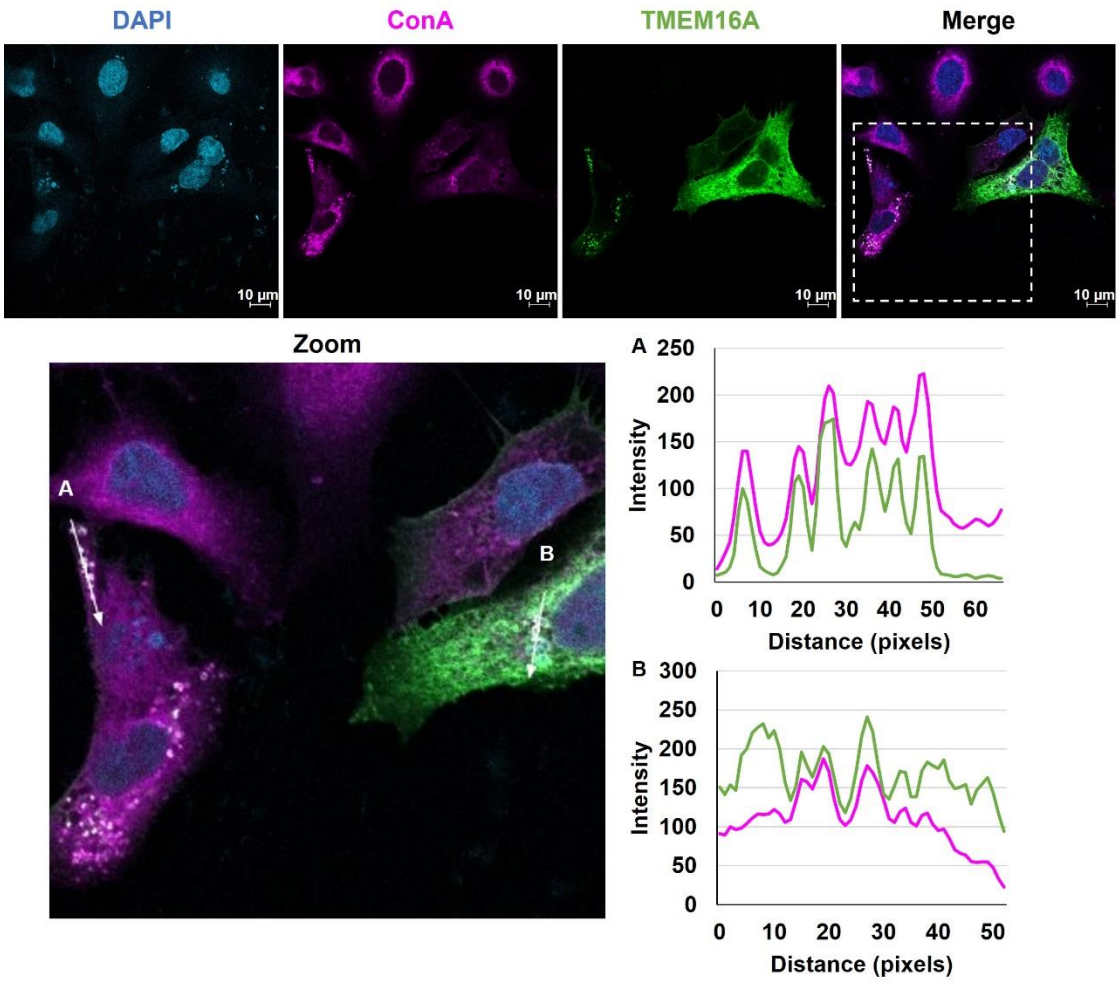

Figure 4-10 TMEM16A partially co-localises with the ER. A549 cells were transfected with 1 µg pTMEM16A-mycDDK for 24 hrs. Cells were analysed by confocal microscopy at 63x magnification on the Zeiss LSM880 microscope. DAPI was used to visualise the nucleus (cyan). TMEM16A was detected using antibodies against the DDK tag (green). Cells were co-stained with the fluorescently labelled ER stain conA (magenta). **A-B)** Fluorescent line scans to analyse the spatial distribution of TMEM16A-mycDDK and conA taken using ImageJ.

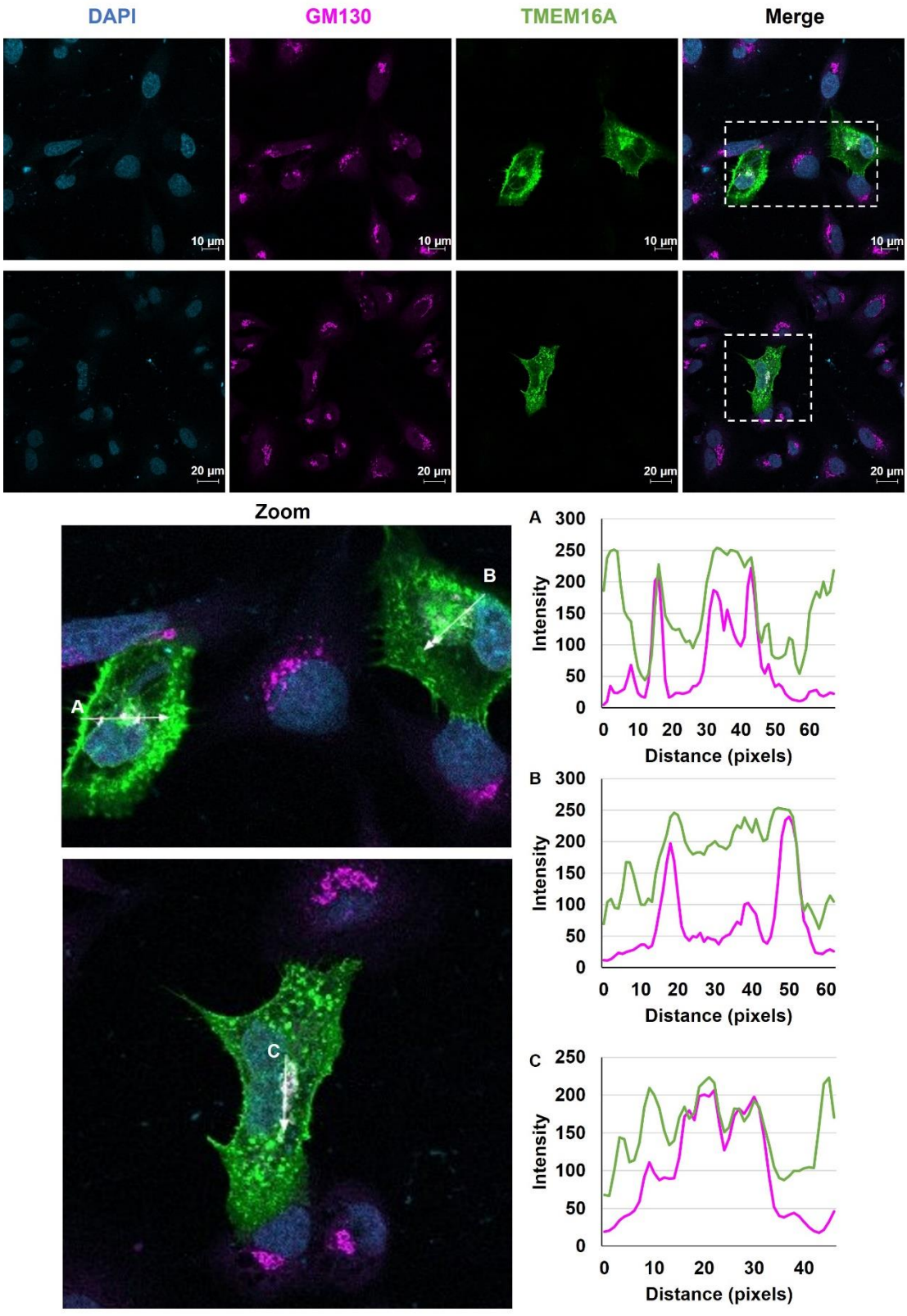

Figure 4-11 TMEM16A co-localises with the Golgi. A549 cells were transfected with 1 µg pTMEM16A-mycDDK for 24 hrs. Images captured on Zeiss LSM880 microscope at 63x magnification (top) or 40x magnification (bottom), scale bars 10/20 µM. DAPI was used to visualise the nucleus (cyan). TMEM16A was

detected using antibodies against the DDK tag (green). Cells were co-stained for Golgi marker GM130 (magenta). **A-C)** Fluorescent line scans to analyse the spatial distribution of TMEM16A-mycDDK and GM130 taken using ImageJ.

4.7.3 TMEM16A may be involved in stress granule formation

In stressed cells, untranslated mRNAs accumulate into SGs. Many cellular proteins have been reported to be recruited into SGs, including the translation initiation factor EIF4G [379]. HRSV infection is one such trigger for SG formation, however it is thought that the virus is largely able to prevent this induction [123]. A potential role for TMEM16A within SGs was investigated. In cells transfected with pTMEM16A-mycDDK, EIF4G staining was punctate, however, the surrounding untransfected cells displayed a diffuse EIF4G stain indicating that SGs had formed within the transfected cells (Figure 4-12). However, from this data it was difficult to determine whether this was due to the expression of TMEM16A specifically or due to the presence of the foreign plasmid. In the cells analysed in Figure 4-12 A, the SGs were located near the nucleus and there was no co-localisation observed between the SGs and TMEM16A. However, in the cell analysed in Figure 4-12 B-C, there were more SGs in the cytoplasm, and some co-localisation was observed between these SGs and TMEM16A.

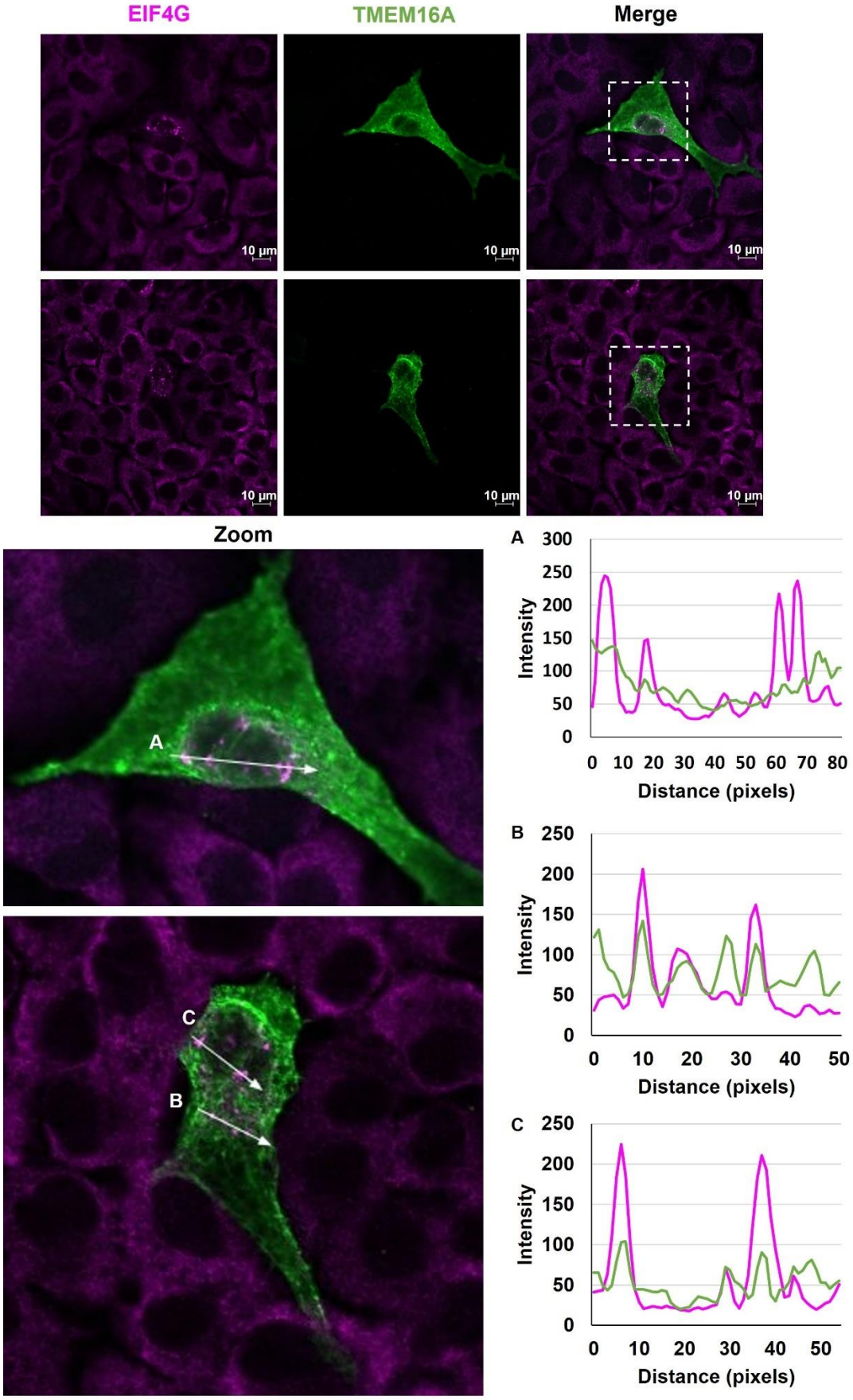

Figure 4-12 Cells transfected with TMEM16A form SGs. A549 cells were

transfected with 1 µg pTMEM16A-mycDDK for 24 hrs. Images captured on Zeiss LSM880 at 63x magnification, scale bar 10 µM. TMEM16A was detected using antibodies against the DDK tag (green). Cells were co-stained for SG marker EIF4G (magenta). **A-C)** Fluorescent line scans to analyse the spatial distribution of TMEM16A-mycDDK and EIF4G taken using ImageJ.

4.7.4 HRSV and TMEM16A may interact within cells

Finally, an interaction between HRSV and TMEM16A was investigated, however this proved challenging as there were relatively few cells which were both transfected with pTMEM16A-mycDDK and infected with HRSV at MOI 1 (example shown in Figure 4-13). A polyclonal antibody against HRSV viral lysate was used and staining was observed either throughout the whole cytoplasm, or in smaller, more distinct areas, potentially representing IBs (white triangles). In the cell analysed in Figure 4-14 A-B, the expression of HRSV viral proteins was observed throughout the cytoplasm and TMEM16A in puncta. Line scan analysis showed that some TMEM16A puncta did contain viral proteins, but others did not. In contrast, in the second example, HRSV proteins were expressed in small distinct areas of the cell and TMEM16A expression was diffuse. Line scan analysis (Figure 4-14 C-D) revealed some co-localisation between the areas of high viral protein expression and TMEM16A but again this was not perfect correlation.

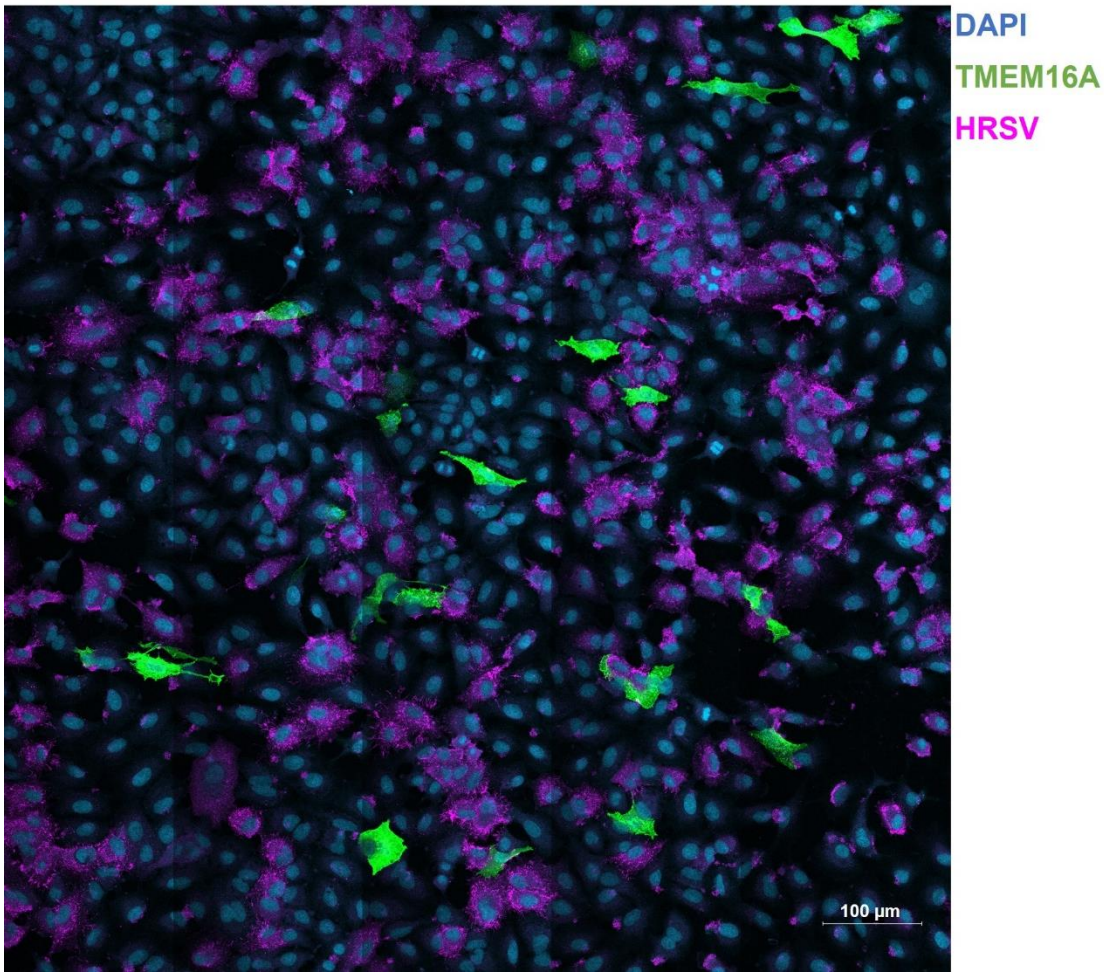

Figure 4-13 Detection of HRSV and TMEM16A dual-labelled cells. A549 cells were transfected with 1 µg pTMEM16A-mycDDK, and infected with WT-HRSV at MOI 1 for 24 hrs. Cells were analysed by confocal microscopy (Zeiss LSM880) and the tile scan was captured at 40x magnification, scale bar 100 µM. DAPI was used to visualise the nucleus (cyan). TMEM16A was detected using antibodies against the DDK tag (green). Infected cells were identified using anti-HRSV (magenta).

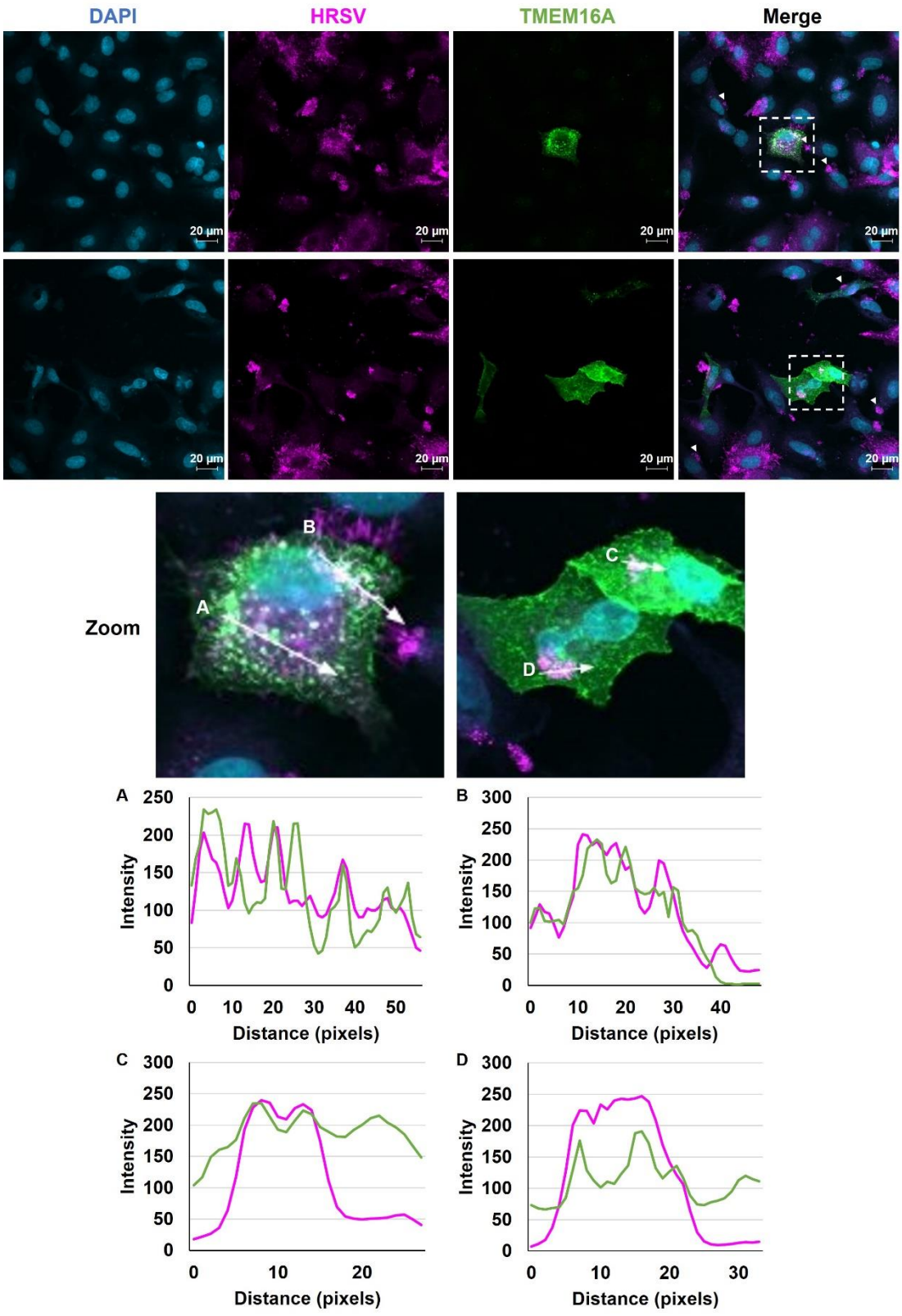

Figure 4-14 HRSV and TMEM16A may interact within cells. A549 cells were transfected with 1 µg pTMEM16A-mycDDK and infected with WT-HRSV at MOI 1 for 24 hrs. Cells were analysed by confocal microscopy at 40x magnification

(Zeiss LSM880), scale bar 20 µM. DAPI was used to visualise the nucleus (cyan). TMEM16A was detected using antibodies against the DDK tag (green). Anti-HRSV was used to detect presence of the virus (magenta). White triangles in merged images highlight areas resembling HRSV IBs. **A-D)** Fluorescent line scans to analyse the spatial distribution of TMEM16A-mycDDK and HRSV taken using ImageJ.

4.7.5 The localisation of TMEM16A summarised

To summarise the TMEM16A localisation studies, although none of the subcellular locations investigated correlated perfectly with TMEM16A expression, areas of high co-localisation between TMEM16A and highly membranous structures such as the ER and Golgi were observed, indicating that the channel was expressed to some degree within these compartments. This highlights potential sites at which TMEM16A may facilitate HRSV infection, particularly as HRSV IBs form in close proximity to the Golgi [80,81].

In contrast, organelles associated with the endocytic pathway such as endosomes and lysosomes did not co-localise with TMEM16A, indicating that the channel was not expressed there. This corroborated the previous data suggesting that HRSV did not require TMEM16A during entry by confirming that the virus would not encounter TMEM16A within the endocytic pathway. However, a role for TMEM16A in late endosomes was not investigated in these studies.

It is likely that the EIF4G-positive SGs observed in the transfected cells were a result of the transfection process rather than being specifically induced by the overexpression of TMEM16A. However, there was expression of the channel observed within some of the SGs. This could indicate a role for TMEM16A during

SG formation and it would be interesting to see whether TMEM16A is expressed in HRSV-induced SGs.

In HRSV infected cells, some co-localisation was observed between areas of high viral protein expression and TMEM16A. It was possible that these areas represented viral replication factories or IBs however as a polyclonal anti-HRSV antibody was used, it was difficult to distinguish the IBs. IBs are generally observed as large, spherical, cytoplasmic puncta often in close proximity to the nucleus or the Golgi [83]. Staining resembling this was observed in Figure 4-14 (examples highlighted by white triangles), however they were not as spherical and less distinct. IBs contain the replication complex proteins N, P, L and M2-1 [83], therefore it is likely that the visualisation of other viral proteins such as G and F in these cells obscured the IBs. Utilisation of monoclonal anti-bodies targeting N, P, L or M2-1 would help to establish whether TMEM16A is indeed recruited into HRSV-induced IBs.

4.8 Inhibition of IP-10 by TMEM16A modulators is not HRSV-specific

IP-10 is a chemokine that is released in airways in response to HRSV infection [366]. In 3.11, IP-10 release was validated and utilised as a surrogate marker for HRSV infection in PCLS and it was revealed that T16Ainh-A01 treatment of PCLS resulted in a decrease in HRSV-mediated IP-10 release (Figure 3-11). To investigate whether this effect was a result of cell-mediated action of the drug on the virus, or a direct effect of the drug on IP-10 production, A549 cells were transfected with a synthetic analogue of dsRNA, poly(I:C), to mimic a viral infection and the concentration of IP-10 released into the cell supernatant was measured by ELISA. In mock A549 cells, no IP-10 release was observed,

however, both HRSV infection (MOI 0.5) and poly(I:C) transfection (400 ng) stimulated IP-10 release. Treatment of these cells with T16Ainh-A01 (20 µM) completely abolished both HRSV- and poly(I:C)-stimulated IP-10 release back to mock levels (Figure 4-15 A). Similarly, another TMEM16A-specific modulator MONNA (30 µM) also eliminated HRSV- and poly(I:C)-mediated release of IP-10. Conversely, the level of IP-10 released from ribavirin-treated cells (80 µM) was not significantly different to the control cells when stimulated with HRSV or poly(I:C), indicating that the inhibitory effect of T16Ainh-A01 and MONNA on IP-10 release could be independent of their inhibitory effects on HRSV replication. Therefore, these data suggested that firstly, IP-10 secretion was not specific to HRSV as it was also induced by poly(I:C), and was a marker for the cellular antiviral response. Secondly, the blockade of TMEM16A with T16Ainh-A01 or MONNA prevented the antiviral response to HRSV and poly(I:C) resulting in the inhibition of IP-10 release from cells.

To test whether T16Ainh-A01 and MONNA were non-specific blockers of cytokine secretion or whether they were specifically inhibiting the release of IP-10, the secretion of IL-8, a cytokine known to be stimulated by HRSV and poly(I:C) [380,381], was measured. As expected, an increase in IL-8 release was observed in HRSV-infected and poly(I:C)-transfected cells compared to mock infected controls (Figure 4-15 B). Treatment with T16Ainh-A01 or MONNA had no effect on HRSV- or poly(I:C)-induced IL-8 release compared to solvent-treated controls, indicating that inhibition of cytokine secretion by TMEM16A-modulation did not inhibit the general release of cytokines, but likely inhibited a process involved in IP-10 secretion.

As the release of IP-10 was inhibited by TMEM16A-modulation, the expression of IP-10 within these cells was measured next. To distinguish IP-10 release from IP-10 expression, the concentration of intracellular IP-10 (from cell lysates) was compared to secreted IP-10 (from cell supernatants). As in the previous experiment, A549 cells were stimulated by either HRSV infection or poly(I:C) transfection, followed by treatment with TMEM16A modulators or ribavirin, and the cell lysates were collected and analysed for IP-10 expression by ELISA. The results mirrored that of the supernatants; IP-10 expression was induced by HRSV infection and poly(I:C) transfection but treatment with T16Ainh-A01 or MONNA completely inhibited this (Figure 4-15 C). Ribavirin treatment did not inhibit HRSV- or poly(I:C)-mediated IP-10 expression and levels of IP-10 in these cells were roughly equal to solvent-treated controls. Taken together, these data suggested that the TMEM16A-modulators specifically inhibit antiviral responses that are triggered by HRSV and poly(I:C) and that result in IP-10 and potentially other ISG expression (rather than inhibiting general protein secretion).

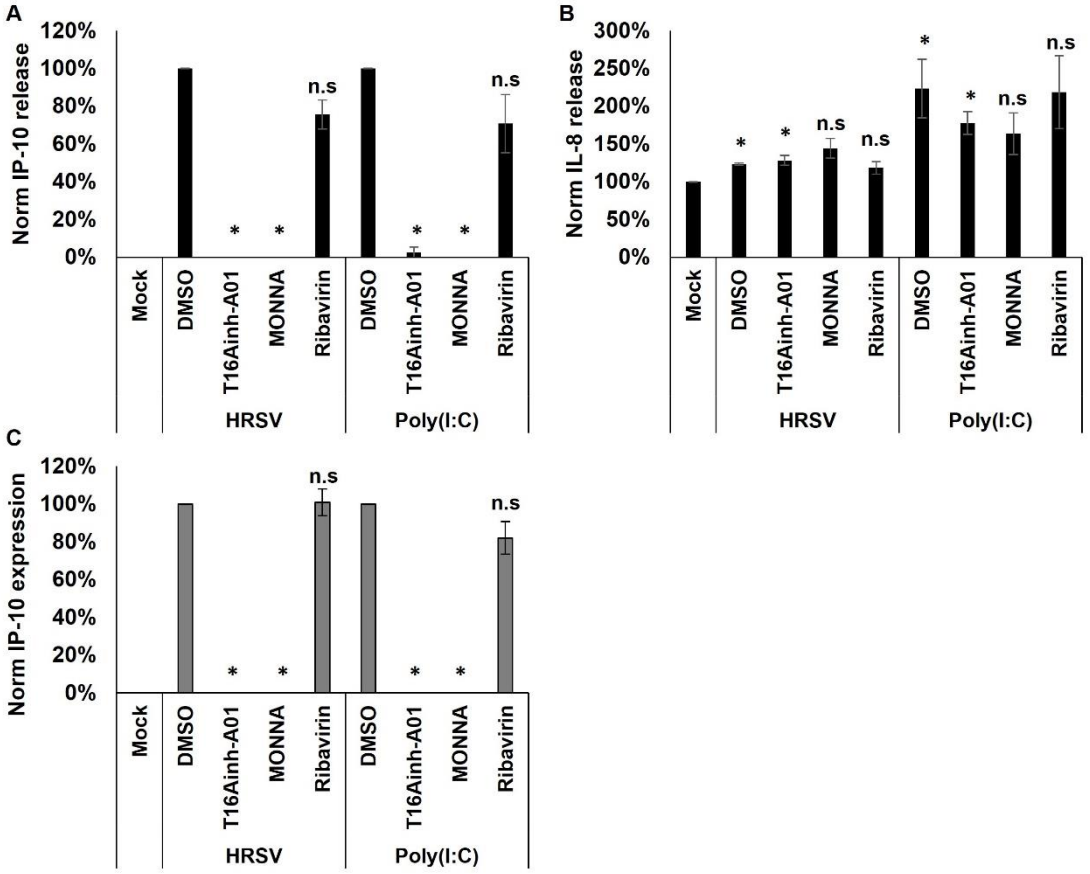

Figure 4-15 IP-10 production is blocked by TMEM16A-modulators in a non-specific manner. A) A549 cells were pre-treated with T16Ainh-A01 (20 µM), MONNA (30 µM), ribavirin (80 µM), or solvent control (DMSO) for 45 mins prior to infection with HRSV (MOI 0.5) or transfection with poly(I:C) (400 ng) for 24 hrs. The level of IP-10 was measured in the cell supernatants by ELISA and are shown relative to the solvent-control in each treatment. **B)** Levels of IL-8 in the cell supernatants from (A) were assessed by ELISA and are shown relative to the untreated mock (basal secretion). **C)** Cells treated as in (A) and cell lysates were collected. IP-10 expression was measured by ELISA and are shown relative to solvent-treated controls. Mean of n=3 ± SE, *p≤0.05, n.s not significant.

4.9 TMEM16A modulators inhibit expression and release of antiviral protein IP-10 via interferon-dependent pathways

In HRSV infected cells, the antiviral response triggers IP-10 expression via two main signalling pathways (Figure 4-16). The cell detects the presence of dsRNA

through sensing proteins such as RIG-I and MDA5, which then bind to MAVS on the mitochondrial membrane, activating it [109,110]. MAVS activation triggers many signalling cascades which result in the phosphorylation of various transcription factors involved in the expression of pro-inflammatory cytokines, including type I IFN [107]. Two of these transcription factors, IRF3 or NFκB, can induce IP-10 expression directly by binding to an ISRE within the promoter of the *CXCL10* gene which encodes IP-10 [382–384]. The second pathway to IP-10 expression is dependent on IFN expression. When type I or II IFNs bind to their appropriate cell receptors, they trigger a JAK-STAT signalling cascade which results in the activation of IP-10 expression through the binding of STAT dimers to ISRE or gamma activation site (GAS) elements within the *CXCL10* promoter [382].

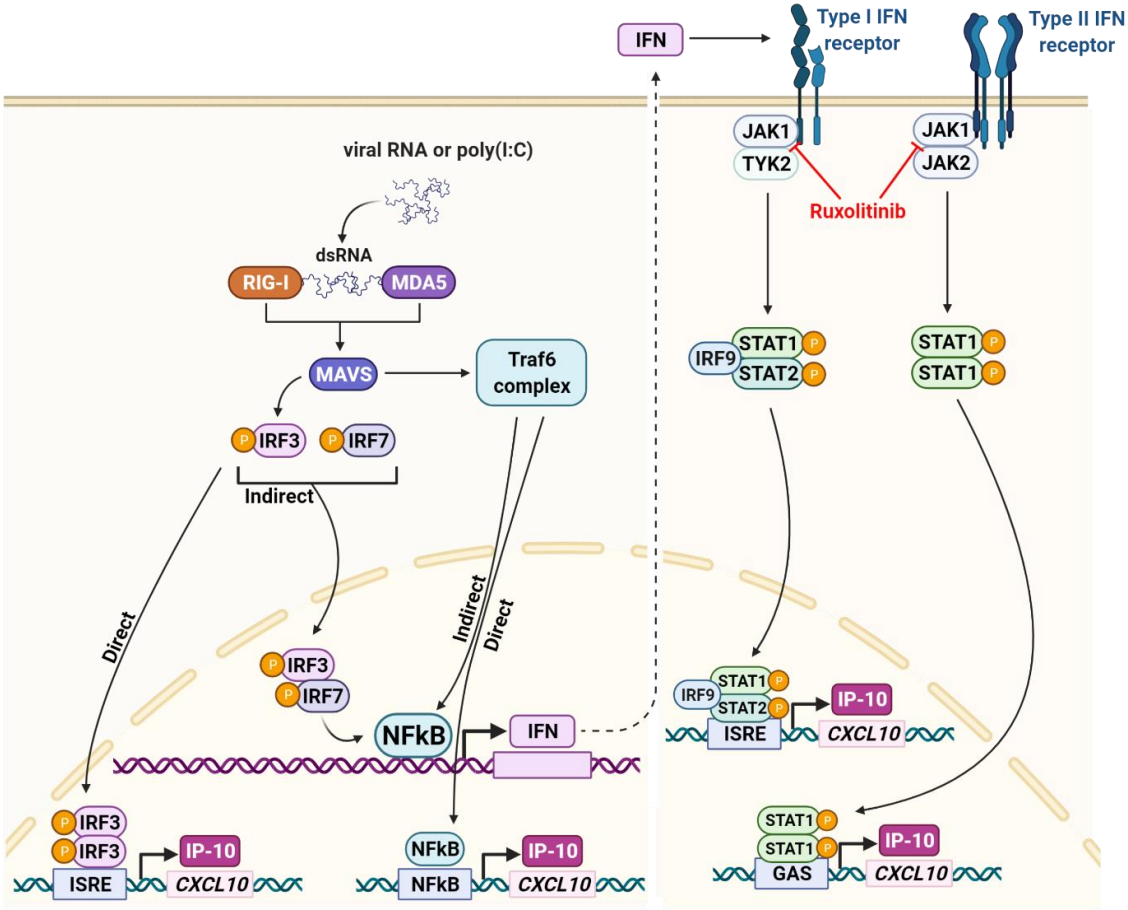

Figure 4-16 Pathway of IP-10 production induced by HRSV infection or poly(I:C) transfection. RNA helicases (RIG-I and MDA5) sense the presence of dsRNA in cells and signal via MAVS, resulting in the phosphorylation and activation of regulatory proteins (IRF3, IRF7, cJun) or the Traf6 complex, a signal transducer for the NFκB pathway. The IP-10/CXCL10 gene promoter contains elements such as ISRE, GAS or NFκB binding sites. Direct induction of IP-10 expression can be via the transcription factors IRF3 (homodimer) or NFκB which bind to ISRE and NFκB elements, respectively. Alternatively, IP-10 expression can be induced by an indirect pathway in which the activated regulatory proteins stimulate the production of type I and type II IFNs. These activate a JAK-STAT signalling cascade in neighbouring cells which ultimately drives IP-10 expression through the binding of STAT dimers to ISRE or GAS elements in the CXCL10 gene promoter. Created in BioRender.com.

To investigate which pathway of IP-10 production was inhibited by T16Ainh-A01 and MONNA, cells were stimulated with a type I and a type II IFN (IFN-α and IFN-γ, 100 ng each) before treatment with the TMEM16A-modulators or ribavirin, and IP-10 expression and release were measured. Stimulation with both IFNs resulted in IP-10 expression and release (Figure 4-17 A and B, respectively), however treatment with T16Ainh-A01 and MONNA completely abolished this, and ribavirin treatment was also moderately inhibitory (74.8% and 40.0% reduction in IP-10 expression in IFN-α and IFN-γ stimulated cells respectively, Figure 4-17 A). This suggested that the IFN-dependent pathway of IP-10 production was blocked by TMEM16A-modulation.

To investigate further, ruxolitinib, a JAK inhibitor which prevents the phosphorylation and activation of STAT [385], was used to inhibit the IFN-dependent IP-10 production. To ensure that ruxolitinib fully blocked the expression and release of IP-10 via the IFN-dependent JAK-STAT signalling pathway, cells were stimulated with IFN-α and then treated with ruxolitinib. As expected, ruxolitinib treatment eliminated IP-10 expression and release in these cells, which validated the use of the JAK inhibitor in the following assays (Figure 4-17 C-D). HRSV-induced IP-10 expression was significantly inhibited by 92.9% and 88.1% in the presence of 5 and 10 μM ruxolitinib, respectively, compared to the no drug control (Figure 4-17 E). A similar effect was observed for poly(I:C)-induced IP-10 expression, which was reduced by 80.8% and 76.8% when treated with 5 and 10 μM ruxolitinib, respectively (Figure 4-17 G). Consequently, the release of IP-10 from HRSV and poly(I:C) stimulated cells was also reduced, or absent, in the presence of ruxolitinib (Figure 4-17 F/H). These data indicated that

the IFN-dependent pathway of IP-10 production was the dominant pathway stimulated by HRSV and poly(I:C).

In summary, these preliminary data revealed that blocking the IFN-dependent JAK-STAT pathway of IP-10 production rendered HRSV and poly(I:C) unable to stimulate IP-10 expression and release, implying that this was the main route of IP-10 production in these cells. However IP-10 expression was not completely inhibited by ruxolitinib, suggesting that the direct (IRF3) signalling pathway may also contribute to IP-10 production in a minor capacity. The TMEM16A-modulators also inhibited this pathway, as evidenced by the disruption of IP-10 expression and release in IFN-α and IFN-γ stimulated cells. Taken together, this suggests a role for TMEM16A in the antiviral response and IP-10 production, which is mediated downstream of dsRNA sensing, likely within the IFN-dependent JAK-STAT signalling pathway. This role is possibly independent of its role in HRSV replication and may contribute to the pathogenesis of HRSV infection.

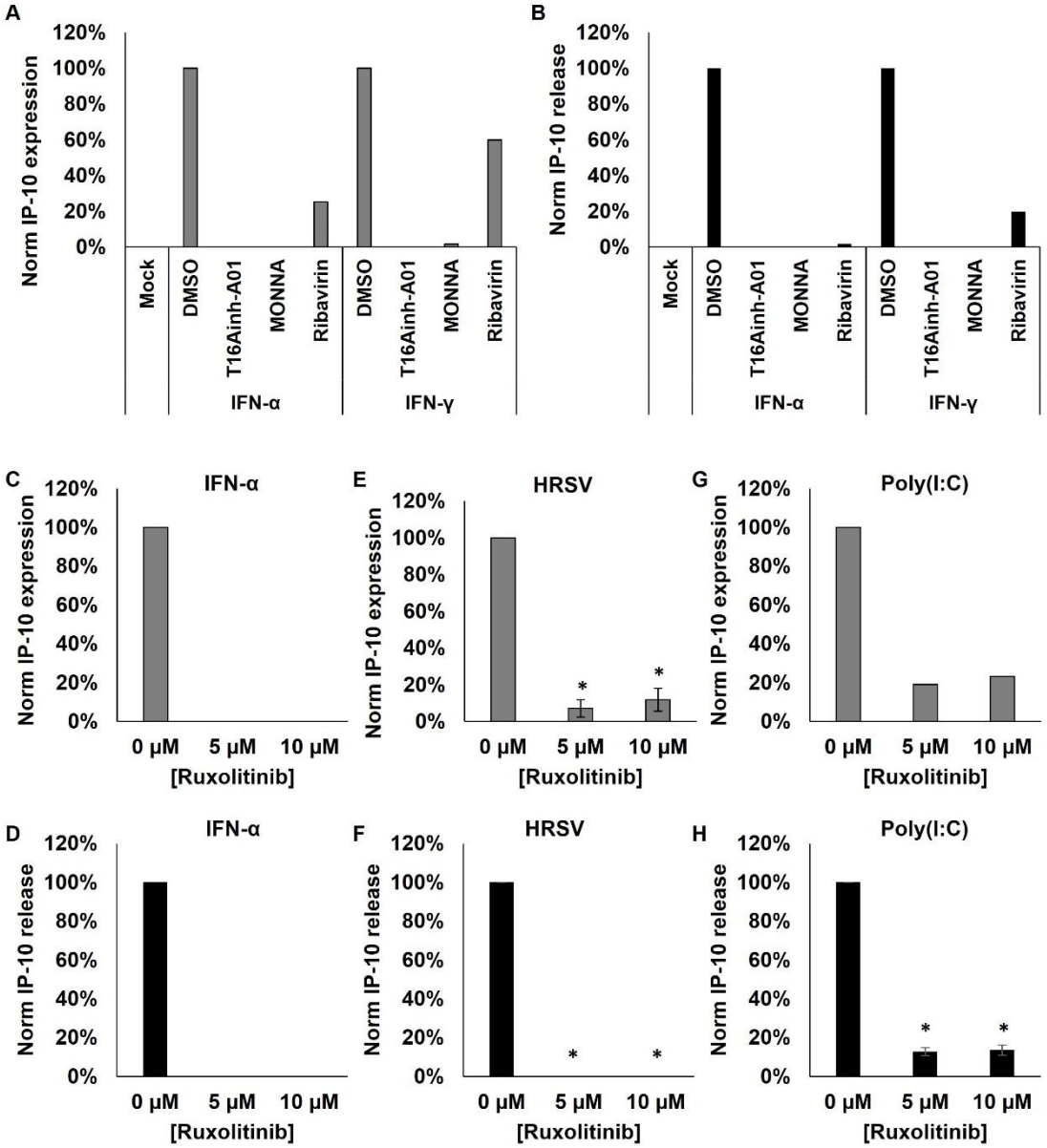

Figure 4-17 Inhibition of TMEM16A effects the production of IP-10 by an IFN-dependent pathway. A-B) IP-10 production was stimulated in A549 cells by treatment with IFN-α or IFN-γ (100 ng each) for 45 mins. Cells were treated with T16Ainh-A01 (20 μM), MONNA (30 μM), ribavirin (80 μM), or solvent control (DMSO) for 24 hrs. IP-10 levels were measured in the cell supernatants (release, A) or cell lysates (expression, B) by ELISA and are shown relative to solvent-treated controls (n=1). **C-H)** IP-10 production was stimulated by treatment with IFN-α (100 ng), HRSV infection (MOI 0.5) or poly(I:C) transfection (400 ng) for 45 mins, followed by treatment with JAK-inhibitor ruxolitinib (5-10 μM). IP-10 levels were measured in the cell lysates (C, E, G) or supernatants (D, F, H) by

ELISA and are shown relative to solvent-treated controls. C, D, G, n=1. E, F, H, mean of n=2 ± SE, *p≤0.05.

4.10 Increased TMEM16A channel activity has no effect on HRSV infection but may affect IP-10 signalling

As TMEM16A inhibition had such a potent effect on HRSV infection and on HRSV-induced IP-10 expression, it was hypothesised that TMEM16A agonism might also affect these processes. Eact is a small molecule activator of TMEM16A which binds directly to the channel and maintains its open state without affecting cellular [Ca^{2+}] [386]. Cells were pre-treated with Eact (5-20 µM) and infected with HRSV-GFP for 24 hrs. Quantification of fluorescence in these cells revealed no significant difference between HRSV-GFP expression in cells treated with Eact compared to the solvent-treated control (Figure 4-18 A, black bars). The level of HRSV-GFP expression ranged from 108.4% (5 µM) to 86.0% (20 µM) of the solvent-treated control, whilst MTS assays confirmed that the cell viability was ≥80% compared to the solvent-treated control (Figure 4-18 A, grey bars). It was previously found that TMEM16A inhibition delayed HRSV-GFP expression by around 4 hrs (Figure 4-3 A), therefore a time course was performed in the presence of Eact to test whether TMEM16A activation would have the opposite affect and allow the virus life cycle to progress more quickly. The growth curve of the virus was not affected by TMEM16A activation and HRSV-GFP expression occurred at the same rate in the presence and absence of Eact (Figure 4-18 B). Therefore, although the inhibition of TMEM16A activity had a significant negative impact on HRSV infection, the activation of TMEM16A appeared to have little effect on the virus. Eact increases the channel activity of

TMEM16A by maintaining an open state [386], however there is no evidence to suggest that the expression of TMEM16A is altered in cells treated with Eact.

The effect of TMEM16A activation on IP-10 expression and release was also investigated, however due to time limitations only preliminary data was obtained ($n \leq 2$). Similar to previous experiments, IP-10 expression was stimulated by HRSV infection, poly(I:C) transfection or IFN-α treatment in the presence or absence of Eact for 24 hrs, and the concentration of IP-10 in the supernatant and cell lysates was measured by ELISA. HRSV-induced IP-10 expression was reduced in a concentration-dependent manner by up to 41.6% when treated with 10 µM Eact, relative to the solvent-treated control (Figure 4-18 C). A similar trend was observed for poly(I:C)-induced IP-10 expression, which was reduced by 31.0% in the presence of 10 µM Eact (Figure 4-18 E). As expected, the amount of secreted IP-10 in these cells followed the same trend as IP-10 expression (Figure 4-18 D and F). When IFN-α was used to stimulate the expression of IP-10, Eact also had an inhibitory effect, reducing IP-10 expression by 53.01% (10 µM) and completely stopping IP-10 release (Figure 4-18 G-H). This data indicated that both the inhibition and activation of ion flux through TMEM16A prevented the IFN-dependent pathway of IP-10 production. Whilst more work is needed to draw conclusions from this preliminary data, it may suggest that the induction of IP-10 is, in some part, governed by ionic balance and therefore requires a precise level of TMEM16A channel activity. This could explain why IP-10 production is less efficient when the channel activity is pushed over or under the required amount and the concentration of Cl^- (or other anions) is changed. If confirmed, this would

strengthen the hypothesis that TMEM16A is required for HRSV replication and IP-10 production via separate mechanisms.

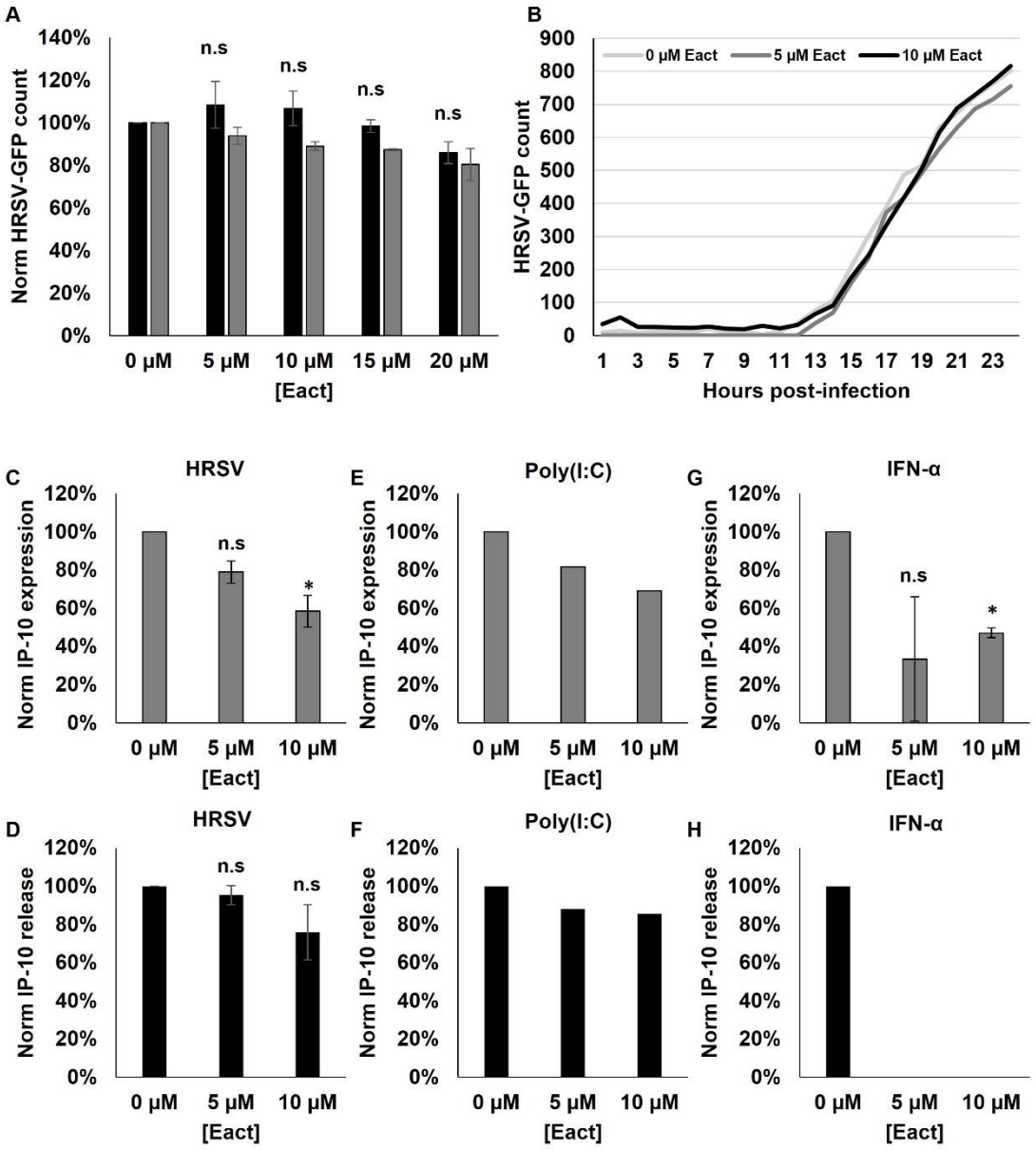

Figure 4-18 TMEM16A agonism does not affect HRSV infection but may inhibit IP-10 signalling. A) A549 cells were pre-treated with TMEM16A-agonist Eact (5-20 µM) for 45 mins and infected with HRSV-GFP in the presence of the drug for 24 hrs. Infection was analysed by quantification of GFP-expression in live cells via IncuCyte and is shown relative to solvent-treated controls (black bars). Cell viability was assessed in these cells by MTS assay (grey bars). mean

of n=3 ± SE, n.s not significant. **B)** HRSV-GFP growth curve in the presence of Eact (5-10 µM) or solvent control. GFP-expression was quantified every hour for 24 hrs. **C-H)** Cells were pre-treated with Eact for 45 mins prior to HRSV infection (MOI 0.5), poly(I:C) transfection (400 ng) or treatment with IFN-α (100 ng) to stimulate IP-10 production. IP-10 levels were measured in the cell lysates (C, E, G) or supernatants (D, F, H) by ELISA and are shown relative to solvent-treated controls. E,F,H, n=1. C,D,G, mean of n=2 ± SE, *p≤0.05, n.s not significant.

4.11 Summary of the aims and key findings in Chapter 4

Having isolated a single channel of interest, the studies in this chapter sought to investigate the mechanistic role of TMEM16A during HRSV infection. The aims of this chapter were to identify at which stage of the virus life cycle the channel was required, and to investigate the role of TMEM16A in the inflammatory response to infection using IP-10 as a marker.

Assays in which each stage of the virus life cycle was targeted by TMEM16A-specific modulators indicated that the channel was not required for virus entry into, or release from cells. Time of addition studies confirmed that TMEM16A activity was important for early, post-entry events and finally, a HRSV minigenome was used to reveal that TMEM16A was required for HRSV genome transcription and/or replication. Analysis of the localisation of TMEM16A suggested that the channel was expressed in membranous regions of the cell, including the ER and Golgi, and also raised the possibility that HRSV interacts with the channel in IBs. The first aim of Chapter 4 was therefore successfully attained.

Lastly, the role of TMEM16A in the antiviral response was investigated further by analysing the production of IP-10 during HRSV infection. It was discovered that

TMEM16A modulation inhibited the expression of IP-10 not only in HRSV-infected cells, but also in cells transfected with poly(I:C) to mimic viral infection. The fact that this inhibition was not HRSV-specific lead to the hypothesis that TMEM16A may play dual roles in HRSV infection, in genome replication and pathogenesis. Although only preliminary data was obtained, it suggested that TMEM16A may play a role in the antiviral response to HRSV via the IFN-dependent, JAK-STAT signalling pathway that results in IP-10 expression. These data have increased our understanding of the many cellular roles of TMEM16A and contributed to the partial fulfilment of the second aim of Chapter 4.

An assessment of the strategies used in this chapter, along with an interpretation of the results and suggestions for future work are given in the Discussion (Chapter 5). Hypotheses for the role of TMEM16A during HRSV replication, the HRSV-induced antiviral response and how these may link together are proposed in the concluding remarks.

Chapter 5 Discussion

5.1 Introduction

This thesis examined the role of Cl^- channels during HRSV infection, utilising HRSV-GFP in combination with an extensive panel of pharmacological inhibitors of ion channels. A novel role for TMEM16A as a host-factor for HRSV infection was revealed and the channel was implicated as a post-exposure antiviral target. An investigation into the mechanisms underpinning the relationship between HRSV and TMEM16A revealed that the channel was involved in the genome replication and/or transcription stage of infection, and evidence suggested that this interaction occurred at or near the Golgi, in HRSV IBs. Lastly, a role for TMEM16A was described within the antiviral response, specifically, in the IFN-dependent, JAK-STAT signalling pathway resulting in IP-10 production.

This final chapter provides an analysis of the experimental approaches undertaken, alongside an interpretation of the results. The evidence presented in this thesis supports a model wherein HRSV sequesters TMEM16A for replication, and simultaneously prevents the cellular antiviral response.

5.2 Analysis of the pharmacological approach used

In cancer cells, genetic knockdown of TMEM16A inhibits cells proliferation and is often lethal [359]. Indeed, in our hands, siRNA- and CRISPR-mediated knockdown of TMEM16A resulted in cell death in A549 cells (data not shown), however modulation of channel activity using pharmacological inhibitors did not affect cell viability, confirming that a reduction in TMEM16A protein but not functionality induces growth defects [326]. TMEM16A knockout has been achieved in primary cells in the literature [387] therefore the use of cancer cell

lines was a limitation of this study. Future experiments should include the use of genetic knockouts in primary cells and *in vivo* models to investigate the function of TMEM16A during HRSV infection. Nevertheless, the use of *ex vivo* PCLS in this study represented a physiologically relevant model in which TMEM16A modulation inhibited HRSV gene expression and virus-mediated IP-10 release.

A benefit of the pharmacological approach was that it allowed individual life cycle stages to be investigated by having the inhibitors present during particular points during infection. This data was crucial for identifying the role that TMEM16A plays during HRSV infection. Time of addition assays revealed that TMEM16A-specific modulators maintained their potent inhibitory effect on HRSV when added up to 9 hpi, the time when viral gene expression would have already been initiated [326,339].

A drawback to using a pharmacological approach was the potential for off-target effects. Whilst T16Ainh-A01 and MONNA display potent activity against TMEM16A [362,363], some reports suggest that other channels may also be modulated by their use. For example, T16Ainh-A01 reportedly inhibits Ca_V's in rat fibroblast (A7r5) cells [388]. The same study also found that MONNA could induce membrane hyperpolarisation in rat arteries, suggesting that a K^+ conductance had been activated, however the identity of such a channel was not identified [388]. A 2021 review of the pharmacology of TMEM16A inhibitors summarised the reported off-target effects of each drug (Table 5.1, [389]). The only channel, other than TMEM16A, to be inhibited by both T16Ainh-A01 and MONNA was TMEM16B (Table 5.1). TMEM16B is closely related to TMEM16A, however it is mainly expressed in cells within the CNS (see 1.7.4.2) and it has been reported that TMEM16B is not expressed in the airway smooth muscle cells

of mice, whereas TMEM16A is [390]. Furthermore, TMEM16B is not thought to be expressed in A549 or SH-SY5Y cells [391,392]. Therefore, although this study did not experimentally rule out a role for TMEM16B during HRSV infection, it is unlikely that this is the case. Future experiments should include assessing the expression of TMEM16B in the cells used in this study, generating genetic knockouts of both channels in primary cells, or the use of knockout mouse models, to examine the role of both TMEM16A and B in HRSV infection.

Table 5.1 Reported off target effects for TMEM16A modulators used in this study. Adapted from [389]. –, inhibitory effect. /, no effect. +, activating effect.

Inhibitor	Selectivity
T16Ainh-A01	TMEM16B (-) VDCC (-, 50 nmol/L) CFTR (/) $[Ca^{2+}]_i$ (/) hBest1 (/) xBest2a (/)
MONNA	VRAC (-) TMEM16B (-) mBest1 (/) hBest1 (/) mClC2 (/) CFTR (/) xBest2a (/)
Benzbromarone	TMEM16B (-) CFTR (/) ENaC (/)
CaCCinh-A01	hBest1 (-, 7 µmol/L) TMEM16B (-) VRAC (-) CFTR (/) $[Ca^{2+}]_i$ (/) xBest2a (/)
Niflumic acid	Kv4 channel (-) VRAC (-) ANO6 (-) $[Ca^{2+}]_i$ (+) KCa channel (+)
Tannic acid	hBest1 (-, 15 µmol/L) TMEM16B (-) CFTR (/) ENaC (/)

5.3 Use of PCLS as a model of HRSV infection

To determine the physiological relevance of TMEM16A as a host factor in HRSV infection, PCLS were used as a model of infection. PCLS are three-dimensional lung tissue slices that contain all the cell types found in the lung and retain the

tissue structure. The preparation of PCLS (Figure 5-1) involves the gentle infusion of the lung with warm, low-melting point agarose to inflate the lung, followed by immersion into ice-cold buffer to solidify the agarose. This process adds rigidity to the soft tissue and ensures the structures within the lung remains intact during slicing. Specialised coring tools are then used to generate cylindrical cores of tissue, which are sliced into thin sections using a tissue slicer or microtome to generate uniform and reproducible slices for downstream applications [393].

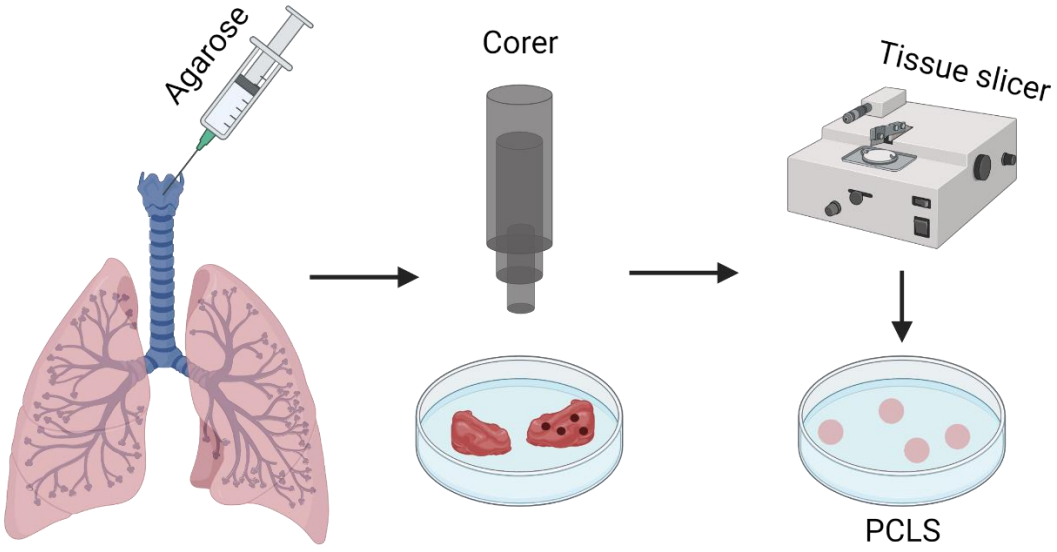

Figure 5-1 Generation of precision-cut lung slices (PCLS). Firstly, the lung is solidified by careful infusion of low-melting point agarose. Cylindrical cores of tissue are prepared using specialised coring tools. Lastly, these cores are cut using a tissue slicer to generate PCLS of the same thickness and diameter. Adapted from [393]. Created using BioRender.com.

The use of PCLS as disease models has been successful in previous studies on asthma, COPD, and other inflammatory respiratory diseases. The Fraunhofer ITEM have used PCLS disease models to test the toxicity and efficacy of new drugs [394,395]. A benefit of this is that it reduces the need for animal

experimentation, to comply with the 3Rs principle (replace, reduce, and refine). The drawback of using PCLS rather than animal models is that only the responses of the resident immune cells can be studied as there is no recruitable immune response. Whilst this may hinder experiments focussed on disease models and immune responses, it did not impact the aim of the experiments in this study.

PCLS have also been used to study innate responses to viral infections. For example, the cytokine response to IAV strains H1N1 and H3N2 during infection of PCLS were compared [396]. The use of PCLS allowed the researchers to determine the source of release of various cytokines, as well as to measure the strength of the immune response to the different strains. They found that although these strains exhibited large differences *in vitro* and in egg culture systems, only subtle differences were observed during the *ex vivo* infection [396], highlighting the importance of using multi-cellular systems in the study of respiratory viruses. Furthermore, the effects of virus infection on pre-existing disease can also be studied using PCLS. The efficacy of β-adrenoceptor agonists in the treatment of COPD was shown to be partially limited by exposure to cigarette smoke, and completely limited by exposure to cigarette smoke followed by IAV (H3N1) infection, through different mechanisms [397]. Respiratory viruses are particularly severe in patients with underlying lung disease, and so this type of research can have extremely useful applications in the clinic.

The use of PCLS to study HRSV infection was validated in Chapter 3. The PCLS used in these studies were generated from disease-free tissue isolated from cancer patients who underwent lung resection. Confocal analysis of infected PCLS showed HRSV-specific staining in both ciliated and non-ciliated lung cells

(Figure 3-11 B). Furthermore, in WT-HRSV infected PCLS, but not in PCLS infected with UV-inactivated HRSV, viral proteins G and N were detected by western blot analysis (Figure 3-11 E), indicating that PCLS were capable of supporting HRSV replication. IP-10 secretion, measured by ELISA, was used as a surrogate marker of infection in PCLS in this study. Whilst not necessarily specific for HRSV, IP-10 release is a useful marker of viral infection (discussed further in 5.10). In PCLS infected with WT-HRSV, significantly high amounts of IP-10 were secreted compared to infection with UV-inactivated HRSV indicating an active infection is required to produce large quantities of IP-10 (Figure 3-11 A). This system was therefore able to detect changes in HRSV infection in response to TMEM16A modulation and represented a reliable addition to the *in vitro* experiments.

A limitation of this study was that tissue from only 3 donors were able to be used, and some donor-to-donor variability was evident, however the general outcomes were the same. Additionally, PCLS were more sensitive than A549 or SH-SY5Y cells were to T16Ainh-A01, therefore a lower concentration had to be used to avoid toxicity. Future work could include a larger scale study of the efficacy of TMEM16A-modulators for HRSV infection, which should use tissue from many donors from diverse backgrounds. These studies could also include the use of additional inhibitors such as benzbromarone, which is already clinically approved for the treatment of gout and therefore may be better tolerated by PCLS.

Overall, this data was the result of a successful collaboration with Dr Hesse and her lab group at the Fraunhofer ITEM and added invaluable data to this thesis.

5.4 Tannic acid antiviral mechanisms

In the initial ion channel inhibitor screen at the start of this thesis, tannic acid was used as a broad-spectrum CaCC inhibitor and showed an extremely potent, concentration-dependent reduction in HRSV-GFP expression by up to 91% compared to solvent controls (Figure 3-7 E). In fact, tannic acid was the most potent of all the broad-spectrum CaCC inhibitors tested against HRSV (i.e., CaCCinh-A01, niflumic acid and talniflumate). However, in the life cycle studies detailed in Chapter 4, it became apparent that tannic acid was inhibiting HRSV infection by a different mechanism to the other CaCC modulators. In the virus entry assay, tannic acid was the only CaCC inhibitor to significantly affect HRSV entry into cells (Figure 4-1 B). Similarly, tannic acid appeared to inhibit the release of HRSV (Figure 4-1 C). In the time of addition assays, addition of tannic acid at 0 hpi recapitulated the 91% reduction in HRSV-GFP expression, however the efficacy of the drug was significantly reduced when added 3 hrs later once the initial entry stages had passed (Figure 4-2 D). The later in infection that tannic acid was added, the less of an inhibitory effect it had until only a 13% reduction in HRSV-GFP expression was observed at 9 hpi. This contrasted with the other CaCC inhibitors tested which retained most of their potency against HRSV when added up to 9 hpi, well after virus entry was complete.

Moreover, the time course of HRSV-GFP expression in live cells treated with T16Ainh-A01, ribavirin, or tannic acid, also highlighted differences in the mode of action of tannic acid against HRSV. Whilst treatment with T16Ainh-A01 and ribavirin resulted in a delay of HRSV gene expression of around 4 hrs compared to solvent-treated controls, tannic acid did not affect the timing of HRSV gene expression (Figure 4-3 A). Instead, the number of HRSV-GFP expressing cells

plateaued around 15 hpi (Figure 4-3 A), however the intensity of GFP fluorescence continued to rise until 24 hpi (Figure 4-3 B), again contrasting the effects of T16Ainh-A01 and ribavirin. Taken together these data supported a hypothesis that tannic acid inhibits the entry or release of HRSV from cells, or both. The inhibition of virus entry could explain the plateau in the number of HRSV-GFP-expressing cells, as progeny virus would be unable to initiate a new round of infection.

The HRSV minigenome studies further added to this hypothesis as tannic acid treatment resulted in a small but non-significant effect on HRSV replicon replication (32% reduction compared to solvent-treated control, Figure 4-5 E). Therefore, whilst tannic acid did partially inhibit HRSV replication through its TMEM16A-modulating activity, it was clear that its potency against HRSV infection was independent of this.

Further work is needed to fully characterise the mechanism of action of tannic acid against HRSV; if it does indeed act as an entry or release inhibitor, it may have potential therapeutic benefits for HRSV sufferers. Tannic acid is a natural product derived from plants and is considered safe by the FDA when used as a food additive. Historically, tannic acid was widely used to treated other ailments due to its broad protective properties. One example of this was in World War I, where burns were wrapped in ‘tannic acid dressings’ [398,399]. However, the use of tannic acid as an antiviral drug would require further assessment and approval.

Several other viruses have been reported to be sensitive to tannic acid treatment, some examples of which follow: From a screening study of Chinese medicinal herbs, tannic acid was found to potently inhibit the entry of norovirus (NoV) into cells by blocking the interaction of the protruding (P) domain of the virus capsid

protein with the cellular histo-blood group antigen (HBGA) receptors [378]. Tannic acid was also found to inhibit the entry of HCV into Huh7.5 cells, but not the replication of an HCV sub-genomic replicon [377]. Binding assays revealed that tannic acid prevents the docking of HCV onto cells and the authors hypothesised that this was due to the ability of tannic acid to form macromolecular complexes on the cell surface [377]. Furthermore, IAV and HPV were also shown to be sensitive to tannic acid treatment [400]. Both viruses were inhibited at the attachment stage of entry and the inhibition occurred whether the viruses or the cells were pre-incubated with tannic acid, indicating an effect on cell surface proteins. However, this was not an unspecific effect, as adenovirus attachment and entry were not inhibited by the treatment, and neither was signalling through host cell surface protein TNF-α [400]. More recently, tannic acid prevented the entry of SARS-CoV-2 by inhibiting the cell surface protease transmembrane protease serine 2 (TMPRSS2) which plays a crucial role in activating the virion spike protein during the entry process [401].

In Chapter 3, CaCCinh-A01, but not T16inh-A01, was shown to inhibit BUNV infection (Figure 3-13 F-G), therefore in Chapter 4, entry assays were also performed on BUNV (Figure 4-4 A). CaCCinh-A01 did not affect BUNV entry, however tannic acid potently inhibited BUNV entry by 87.9% compared to solvent-treated controls. This was a stronger effect than was seen with the positive control pit stop 2, a known inhibitor of receptor-mediated endocytosis. Additionally, binding assays similar to those performed on HCV [377] revealed that tannic acid inhibited the attachment of BUNV to A549 cells by 96% compared to solvent-treated controls (Figure 4-4 B). This was the first description of the ability of tannic acid to inhibit the attachment and entry of a bunyavirus. As BUNV

represents the prototypic member of the *Bunyavirales*, an order of viruses containing almost 500 species, it is interesting to speculate how many more bunyaviruses may be sensitive to tannic acid treatment. Future work could include a large-scale screening study of the effects of tannic acid on bunyavirus family members.

A deeper investigation into the effect of tannic acid on HRSV entry was beyond the scope of this thesis. Future work could expand on this and see whether it is appropriate to add HRSV to the growing list of viruses which are prohibited from binding and/or entering cells treated with tannic acid. Combining the knowledge of these viruses could help determine the mechanism of action of tannic acid on virus attachment and entry.

Interestingly, earlier reports described the use of tannic acid to inhibit viral gene transcription. Through its inhibition of poly (ADP-ribose) glycohydrolase, an enzyme important for the regulation of DNA transcription in cells, tannic acid treatment suppressed transcription of mouse mammary tumour virus [402] and HIV [403] genes by negatively regulating response elements within the promoter region. This alludes to the fact that tannic acid has a broad range of effects within cells, and more antiviral mechanisms than a simple entry inhibitor.

5.5 Use of the HRSV minigenome system to study genome replication and transcription

In Chapter 4, data from the life cycle studies combined with the minigenome assay strongly indicated a role for TMEM16A within HRSV replication and/or transcription. The utility of the mini-genome assay in the context of this study was that its establishment did not rely on virus entry stages since all components were supplied by transfection. Thus, any modulation of mini-genome activity by

pharmacological inhibition could be directly attributed to RNA synthesis stages of the viral life cycle, rather than prior entry. BSR-T7 cells were transfected with plasmids encoding the HRSV N, P, L and M2-1 proteins, which are the minimal requirements for HRSV genome replication and transcription, along with the GFP-labelled minigenome (pM/SH-GFP). As the minigenome encoded the HRSV promoter region and gene junction signals, this allowed the HRSV replication complex expressed by the N, P, L and M2-1 plasmids, to transcribe and artificially encapsidate the minigenome. This viral sense genome RNA (vRNA) then underwent replication as per a natural infection via a complementary anti-genome RNA intermediate (cRNA). The newly synthesised, encapsidated vRNAs then acted as a template for transcription, which produced mRNAs that could be translated by the cellular machinery, resulting in the expression of the GFP reporter protein. Therefore, measurement of GFP fluorescence intensity by IncuCyte ZOOM was used as an assessment of the replication and transcription processes of the HRSV minigenome. The positive control, ribavirin, known to inhibit HRSV replication, resulted in an 80% reduction in GFP fluorescence compared to the solvent-treated control (Figure 4-5 E). Similarly, treatment with TMEM16A-modulator T16Ainh-A01 resulted in a 64% decrease in GFP fluorescence. This, along with the data from the life cycle studies, indicated that TMEM16A most likely plays a role in HRSV genome replication and/or transcription.

Minigenome systems are powerful tools for studying the life cycles of viruses (reviewed in [404]). They have been successfully used to study the roles of individual viral proteins during replication and transcription as well as in the characterisation of non-coding regions within the viral genome. For example, the

role of M2-1, which was required for transcription but not replication, was probed using minigenome systems [68,333]. Furthermore, minigenome systems have been used in the screening of antiviral agents [405], which sets a precedent for testing the sensitivity of the HRSV minigenome system to ion channel inhibitors in this thesis.

Whilst this thesis has successfully implicated TMEM16A-activity as crucial during HRSV replication and transcription, future work should aim to characterise this further. The use of a replication-deficient minigenome would enable the separation of these two processes to determine whether the channel function is required during replication or transcription. One such mutant was described by Peeples and Collins, 2000, in which point mutations within the 5' trailer region of a HRSV minigenome stopped the production of newly synthesised vRNAs without affecting encapsidation [406]. In this version of the minigenome system, the initial vRNA produced from the plasmid-supplied minigenome was still encapsidated and the production of the cRNA still occurred. Although this cRNA was not be copied into new vRNAs (i.e., no genome replication occurred). However, transcription of the initial vRNA still took place. A disadvantage of this system was that fewer vRNAs were available for transcription resulting in a lower GFP signal, however, the GFP reporter could be replaced for something more sensitive such as luciferase.

5.6 The role of Cl^- channels in RNA virus replication

The replication of RNA viruses requires the assembly of viral proteins into a replication complex in which the RdRp transcribes and replicates the vRNA. This usually occurs at defined replication sites within the cell, often involving the

recruitment of both cellular proteins and endo-membranes. Characterising these replication sites can reveal important antiviral targets.

As described in 1.9.3, Cl^- channels have been implicated in the replication of RNA viruses. During HCV infection, replication occurs at intracellular membrane-associated replication complexes. HCV replication produced an increase in intracellular [Cl^-] through ClC-2 and -3, which was inhibited by small-molecule Cl^- channel inhibitors and genetic knockdowns [324]. As ClC-2 and -3 have roles in endosomal acidification, it was suggested that HCV utilises ion influx through these channels to drive the formation of membrane-associated replication complexes, or viral factories.

In Chapter 4, upon revealing a dependence on Cl^- channels during HRSV infection, the role of endosomal acidification was assessed. When an inhibitor of endosomal acidification, NH_4Cl, was used in time of addition assays, no effect on HRSV-GFP expression was observed at any time point compared to the solvent-treated control (Figure 4-2 C). These data agreed with previous work and implied that HRSV did not rely on endosomal acidification for any stages of its lifecycle, suggesting that the virion fuses with the endosomal membrane early within the endocytic pathway, or it did not require an acidic pH to escape the endosome, as is the case for other viruses. Furthermore, it indicated that the requirement by the virus for TMEM16A was not related to alteration of the ionic balance within cellular compartments, as was suggested for HCV [324].

Others have reported of roles for Cl^- channels in the formation and/or maintenance of RNA virus replication complexes (1.9.3). During IBDV infection, protein interactions were observed between VDAC1 and viral replication complex proteins VP1 and VP3 which enhanced the stability of the whole complex and

increased the activity of the RdRp [322]. Similarly, CLIC1 was shown to interact with CHIKV NSP3, an essential component of the replication complex [323]. In both cases, minigenome/replicon assays were used to show a negative impact on replication in the absence of the relevant Cl^- channels.

The results described in this thesis have similarly shown that inhibition of TMEM16A channel activity negatively impacts HRSV minigenome replication, however, no data on potential protein interactions between the channel and the replication complex was obtained. This represents a limitation of this study and future work should aim to investigate any potential interactions between TMEM16A and HRSV proteins. This could include co-immunoprecipitation experiments utilising HRSV-infected cells transfected with the TMEM16A-mycDDK plasmid described in this thesis, and anti-myc or anti-FLAG antibodies.

The co-localisation experiments described in Chapter 4 attempted to discern by confocal microscopy whether HRSV and TMEM16A interacted in infected and transfected A549 cells. In cells with a punctate TMEM16A-staining pattern, some of these puncta were also positive for HRSV protein expression, however some were not (Figure 4-14, see 5.9 for further discussion). Although only partial co-localisation was observed in most cells, these data provide preliminary evidence for an interaction between TMEM16A and HRSV. Additional studies utilising monoclonal antibodies targeting individual HRSV proteins to check for co-localisation with TMEM16A would complement the co-immunoprecipitation experiments described above. Furthermore, using cells fixed at different time points post-infection may provide a clearer picture of the interaction between TMEM16A and HRSV as it may be transient or time dependent.

In Chapter 3, it was revealed that the NSVs IAV and HAZV shared a similar sensitivity towards T16Ainh-A01 (Figure 3-12 C and Figure 3-13 B), implicating a role for TMEM16A within the life cycle of these viruses. Like HRSV, both of these viruses must transcribe their negative-sense genome into positive-sense mRNAs to produce viral proteins and use a positive-sense cRNA anti-genome intermediate to replicate their genomes. HAZV replicates in the cytoplasm, however how it forms its virus factories is currently unknown. By analogy to the prototypic bunyavirus BUNV, it is possible that HAZV forms its virus factories near the Golgi [407]. It is interesting that HAZV and BUNV share similar life cycles, yet BUNV did not depend on TMEM16A for productive infection in this study, shown by its insensitivity to T16Ainh-A01 (Figure 3-13 G). Perhaps this indicates differences within the life cycles of these bunyaviruses that remain to be discovered. It must be noted that BUNV was indeed significantly sensitive to CaCCinh-A01 treatment (Figure 3-13 F), suggesting that other members of the CaCC family are required during infection such as BEST1, which is also modulated by CaCCinh-A01 [389,408] and is thought to be expressed at low levels in A549 cells [392,409]. On the other hand, IAV completes its replication stages within the nucleus of the cell [285,410]. Whilst nuclear expression of TMEM16A is not described in the literature, TMEM16A is involved in signalling pathways such as the NFκB and MAPK/ERK pathways [411] which may affect nuclear proteins. Future studies should investigate whether these viruses, like HRSV, require TMEM16A for replication stages of infection or if there is a different mechanism of action acting on HAZV and IAV. These experiments could resemble the life cycle and minigenome studies detailed within this thesis.

5.7 The role of other host ion channels during HRSV infection

This thesis (and the associated publication [326]) has documented the first assessment of the role of Cl^- channels during HRSV infection and described a novel role for CaCCs during HRSV genome replication/transcription, thus combining two rapidly growing areas of research: the functions of Cl^- channels and the emergence of ion channels as host factors during virus infection. As previously mentioned, host cation channels have been studied extensively. Consequently, previous publications have examined the importance of cation channels during HRSV infection.

Firstly, HRSV encodes its own viroporin, SH. SH is known to form pentameric channels within host cell membranes that are selective for monovalent cations (Na^+ and K^+) [62,63,412]. Whilst the reason for this is not yet understood, the function of these channels play an important role during HRSV infection as inhibition of SH is detrimental to the virus.

A role for K^+ channels during HRSV infection was ruled out in 2016 when the treatment of A549 cells with broad spectrum K^+ channel blocker tetraethylammonium (TEA) had no effect on HRSV infection [310]. In the same year, a role for Ca^{2+} during HRSV genome replication/transcription was described when drugs inhibiting the Ca^{2+} ATPase and Ca^{2+} ionophores both inhibited HRSV replicon replication [413]. Inhibition of the Na^+/K^+ ATPase elicited the same effect on the HRSV replicon. However, inhibition of the plasma membrane associated Ca^{2+} channels using nifedipine or nimodipine had no effect on HRSV infection. Likewise, blockade of TPCs with tetrandrine also did not influence HRSV infection. Furthermore, inhibition of Na^+ channels using DP salt or lidocaine, or inhibition of K_v channels using 4-AP did not hinder HRSV infection. Overall, roles

for Ca^{2+}, Na^{+} and K_V channels during HRSV infection were ruled out and the authors concluded that the anti-HRSV effects of both Ca^{2+} ATPases inhibitors and Ca^{2+} ionophores were mediated by their ability to elevate $[Ca^{2+}]_i$.

The Na^{+}/K^{+} ATPase was implicated in HRSV infection again in later papers [414,415]. Cardiac glycosides, which block Na^{+}/K^{+} ATPase functionality, inhibited the replication of the HRSV replicon [414]. Furthermore, genetic knockout of ATP1A1, the major subunit of the Na^{+}/K^{+} ATPase, also inhibited HRSV infection [415]. However, this was found to be preventative of virus entry rather than genome replication/transcription.

In summary, the literature to date indicates that HRSV relies upon the balance of Na^{+} and K^{+} within cells through the regulation of Na^{+}/K^{+} activity or via its viroporin SH. However, infection does not rely on the function host Na^{+} or K^{+} channels. Furthermore, the $[Ca^{2+}]_i$ appears to be important for HRSV replication. The Na^{+}/K^{+} ATPase has a documented role in the regulation of $[Ca^{2+}]_i$ and it is generally accepted that inhibition of the Na^{+}/K^{+} ATPase results in an increase in $[Ca^{2+}]_i$, however whether this is via an ionic model or through signalling cascades is still debated [416]. As TMEM16A both regulates and is regulated by Ca^{2+} (Figure 1-10, [221,222]) perhaps these observations and the data presented within this thesis are linked. Whilst the mechanism of action of drugs such as T16Ainh-A01 and MONNA have yet to be fully recognised, it has been reported that they do not interfere with Ca^{2+} signalling [362]. However, future investigations could assess the impact of blocking TMEM16A channel activity on $[Ca^{2+}]_i$ during HRSV infection to test the model that TMEM16A-modulation inhibits HRSV through a Ca^{2+} signalling-dependent mechanism.

5.8 Lack of resistance to T16Ainh-A01 reveals promise as an anti-HRSV therapeutic

During the characterisation of novel antiviral drugs, the generation of viral escape mutants through serial passage of the virus in the presence of the drug can help discern the mechanism of action. Identification of the gene or protein in which mutations arise resulting in a resistant phenotype can provide a valuable insight into the target of the drug. For example, one study identified a novel entry inhibitor of HRSV and following passage in the presence of this drug, a series of escape mutants were isolated [417]. All the resistant strains carried single point mutations within the F protein, underpinning the mode of action of this drug against F-mediated attachment and entry. The authors of this study highlighted the ease of which HRSV could adapt to, and overcome, entry inhibition, not only to the novel compound they had identified but also to other entry inhibitors in clinical development, via mutations of the F protein, some of which did not affect viral fitness [417].

Another study identified a novel HRSV replication inhibitor cyclopamine and following passage, generated escape mutants that mapped to the M2-1 protein [71]. Three resistant strains were generated, each of which harboured one common mutation that mapped to a region on M2-1 involved in binding to RNA and P, indicating an inhibition of the formation of the replication complex, consistent with the drugs ability to inhibit minigenome replication [71].

Chapter 4 aimed to decipher the mechanistic role of TMEM16A during HRSV infection. It was hoped that the generation of a T16Ainh-A01-resistant HRSV strain would provide an insight into this phenomenon, as in previous publications. After careful optimisation of the parameters of blind passaging, a method was

devised. After 10 passages over 30 days, no T16Ainh-A01 escape mutants were identified (Figure 4-6 E). However, the levels of virus had recovered in the solvent-treated and ribavirin-treated control. Whilst absence of an escape mutant precluded the identification of any viral proteins targeted by T16Ainh-A01, some clues were able to be taken from this data.

Firstly, this data provided promising evidence that TMEM16A-modulators represent a viable anti-HRSV therapeutic option, as, unlike the entry inhibitors described above, the virus could not easily overcome the effects of T16Ainh-A01. This would ensure the long-term use of these drugs were they to reach the clinic.

Secondly, in the studies described above, the novel inhibitors of HRSV were found to be having direct effects on the expression levels viral proteins. Perhaps the lack of an escape mutant is indicative of cell-mediated effects of T16Ainh-A01 on the virus. This is consistent with data in Chapter 3, which showed the treatment of the virion directly with T16Ainh-A01 had no effect on infection. The TMEM16A channel plays many roles within the cell, including movement of Cl^- across membranes [208], regulation of Ca^{2+} signalling [222], exocytosis of mucus-filled granules [225] and involvement in various cell signalling pathways [238,411]. According to the hypothesis that TMEM16A is required for HRSV genome replication and/or transcription, which necessitates the co-ordination of many viral and cellular proteins, it is feasible that TMEM16A mediates any number of these interactions either directly or indirectly and therefore T16Ainh-A01 may not exert its action on one viral protein only. A key strength of host-directed therapies is that the likelihood of resistant strains developing is much lower than drugs which target viral processes.

5.9 TMEM16A localisation studies reveal a possible role for TMEM16A within the Golgi and/or HRSV IBs

Confocal microscopy is a valuable tool for determining the subcellular localisation of proteins. It has also been used to successfully determine the roles of ion channels during viral infection. One recent study used confocal microscopy to show that the voltage-gated K^+ channel Kv1.3 localised to acidic organelles by observing co-localisation between the channel and markers for early endosomes (Rab5), late endosomes (Rab7) and lysosomes (LAMP1) in Huh7.5 cells [313]. In contrast, no localisation was observed between Kv1.3 and markers for the ER (PDI), Golgi (GM130) or mitochondria (COX VIII). The study went on to reveal Kv1.3 as a host factor in the entry of HCV, DENV and ZIKV, all viruses which utilise clathrin-mediated endocytosis for cell entry [313]. Another study used confocal microscopy to help characterise the 6K protein of CHIKV [418]. The authors showed that 6K co-localised with cellular markers for the ER (KDEL) and Golgi (GM130) in HEK293T cells, but not with markers of the mitochondria (mitotracker), nucleus (DAPI), or plasma membrane (WGA). This interaction with subcellular membranous structures was one of the features of the CHIKV 6K protein which alluded to its function as a viroporin [418].

A similar strategy was utilised in Chapter 4 to discern further clues about the role of TMEM16A during HRSV infection. Antibodies for TMEM16A (and other ion channel proteins) are often unreliable (Appendix A, Figure A-1), therefore tagged constructs are commonly used as an alternative method of detecting channel proteins. For example, in the two studies described above, plasmids encoding Kv1.3-EGFP [313] and 6K-EGFP [418] were transfected into cells, which were

stained with antibodies targeting subcellular markers for confocal microscopy analysis.

The staining pattern of TMEM16A-mycDDK in A549 cells was diffuse throughout the cytoplasm with some speckling of TMEM16A-myckDDK-positive puncta (Figure 4-7 C), consistent with previous studies in various other cell lines displaying this same pattern [419–422]. HRSV is thought to utilise the endocytic pathway for cell entry [48], however, no co-localisation was observed between TMEM16A-mycDDK and components of this pathway (early endosomes; EEA1, and lysosomes; LAMP1, Figure 4-8 and Figure 4-9, respectively). This is consistent with the previous data in Chapter 4 suggesting that HRSV does not require TMEM16A during entry, and that HRSV does not require TMEM16A to mediate pH changes within endosomes.

Line scan analysis revealed positive co-localisation between TMEM16A-mycDDK and the ER stain ConA (Figure 4-10). This is consistent with the known functions of the channel (1.7.4.2). The ER houses the intracellular Ca^{2+} stores, which are activated by IP3R, and TMEM16A regulates local Ca^{2+} signalling by tethering to the ER via interaction with IP3R, creating a compartment in which TMEM16A can control Ca^{2+} signalling (Figure 1-10) [222]. TMEM16A-mycDDK also co-localised with the Golgi marker GM130 (Figure 4-11). This contrasts with a previous study stating that the Golgi is not required for TMEM16A biosynthesis or trafficking [222]. In CFBE cells (a bronchial epithelial cell line from a CF patient), the expression and cellular localisation of TMEM16A remained unchanged following treatment with brefeldin A, a protein transport inhibitor which collapses the Golgi. However, the membrane localisation of the CFTR was completely suppressed by brefeldin A, as it could no longer traffic via the Golgi [222]. Analysis of TMEM16A

localisation in that publication focussed on changes to the membrane expression in the absence of Golgi function and did not include the use of a Golgi marker, therefore whilst TMEM16A trafficking to the plasma membrane was shown to be independent of Golgi functionality, there was no evidence to suggest that it does not localise there. No other assessments of TMEM16A localisation to the Golgi were found within the literature to date, therefore the preliminary data in this thesis may offer the first recording of the presence of TMEM16A within the Golgi. It is interesting to speculate that TMEM16A may play a role in the packaging or trafficking of cellular proteins.

Both the ER and Golgi are known to harbour HRSV proteins at various stages of the virus life cycle: the glycoproteins F and G are synthesised within the ER and F is trafficked via the Golgi (where the first of two cleavage events occurs [47]) to the apical cell membrane [423]. The finding that TMEM16A is expressed on these membranous structures is promising in terms of deciphering its role during HRSV infection as IBs, which are the sites of genome transcription and replication [83], are also formed on or near intracellular membranes [80,81] (1.5.3). In HEp-2 cells, confocal microscopy analysis identified the formation of IBs in close proximity to the Golgi markers (GM130 and BODIPY Fl C_5 ceramide) [81]. These data together may imply that TMEM16A interacts with HRSV IBs on or near the Golgi and play a role in the transcription and/or replication of the viral genome. Consistent with this, assessment of the localisation of TMEM16A in HRSV-infected cells also revealed some co-localisation between the channel and viral proteins (Figure 4-14). In these cells, structures resembling HRSV IBs were observed (white triangles) and these IBs were also positive for TMEM16A-mycDDK expression (Figure 4-14 B and C). However, due to time restrictions,

the addition of a fourth colour to observe sub-cellular markers in HRSV-infected cells was not possible. Future work should attempt to assess the co-localisation between HRSV IBs, the Golgi and TMEM16A to determine whether HRSV recruits TMEM16A into IBs. This work would complement the proposed future co-immunoprecipitation and confocal microscopy experiments described in 5.6.

5.10 TMEM16A modulation may also offer symptomatic relief from HRSV infection by inhibiting ISG expression

IP-10 is a chemokine that is secreted in response to IFN-γ and therefore is a good marker for the antiviral IFN response. IP-10 acts as a ligand for the CXCR5 receptor expressed on activated type 1 T cells and natural killer cells, therefore mediating the Th1 inflammatory response. However, IP-10 is also upregulated in respiratory diseases such as asthma and COPD, where it contributes to Th2-type airway inflammation and hyperreactivity [424].

In Chapter 3, IP-10 was validated and used as a surrogate marker to assess HRSV infection in *ex vivo* PCLS. It was revealed that treatment of PCLS with T16Ainh-A01 resulted in a concentration-dependent decrease in HRSV-induced IP-10 expression (Figure 3-11). However, it was unclear from these experiments whether T16Ainh-A01 was having a direct effect on the virus and therefore triggering less IP-10 production, or whether the inhibition of TMEM16A activity was directly affecting the secretion of IP-10 from PCLS. Therefore, experiments in Chapter 4 sought to clarify this.

Firstly, it was confirmed that infection with HRSV stimulated the expression and release of IP-10 in A549 cells (Figure 4-15 A, C). This agreed with previously published literature showing that IP-10 secretion was increased during HRSV infection *in vitro*-infected A549 cells [425]*, in vivo* animal models [426], and in

clinical studies with infants with RSV disease [427]. IP-10 was also released in response to transfection with poly(I:C), a synthetic analogue of dsRNA (Figure 4-15 A). Again, this corroborated previous literature reporting that poly(I:C) stimulated IP-10 secretion [428]. These results confirmed that IP-10 secretion was not specific to HRSV infection but more likely a response to the dsRNA intermediate formed during HRSV replication. This was supported by the findings reported in Chapter 3 in which only actively replicating HRSV induced IP-10 release in PCLS whereas UV-inactivated virus did not (Figure 3-11 A).

A range of viruses that also produce dsRNA intermediates have been reported to induce IP-10 secretion. For example, symptomatic infection with rhinovirus (RV) induced IP-10 production *in vivo* [428]. The authors found that RV-mediated IP-10 expression was independent of IFNs and was mediated by NFκB. IP-10 was also upregulated during IAV infection and correlated with disease severity and mortality of avian and human strains [429]. It was shown that IAV activated the PI3K/Akt pathway in A549 cells, which led to the activation of IRF3 and the induction of IP-10 expression by IRF3 binding to the ISRE sites within the IP-10 promoter [430].

When treated with TMEM16A-modulators, the HRSV-induced expression and release of IP-10 was completely inhibited (Figure 4-15 A, C). However, ribavirin treatment did not affect the level of IP-10 expression in HRSV infected cells. All three drugs would have elicited a reduction in HRSV replication, therefore the difference in outcome between TMEM16A-modulators and ribavirin indicated that the inhibitory effect was linked to a cellular response to the reduction of TMEM16A activity rather than the existence of less viral dsRNA. The data from poly(I:C) was consistent with this: as the synthetic dsRNA was transfected directly

into the cells (and therefore did not rely on replication and/or transcription events), the inhibition of poly(I:C)-induced IP-10 production by TMEM16A-modulation must have been downstream of dsRNA sensing. This was in agreement with the finding that ribavirin had no effect on poly(I:C)-induced IP-10 expression. Altogether, these data indicated that TMEM16A was directly involved in the antiviral response which produces IP-10, independent of its role in HRSV replication.

Additionally, both HRSV and poly(I:C) are known to stimulate IL-8 secretion in cells [380,381,431]. An increase in IL-8 release was observed in HRSV-infected and poly(I:C)-transfected cells compared to mock infected cells (Figure 4-15 B). Treatment with T16Ainh-A01, MONNA or ribavirin did not inhibit HRSV- or poly(I:C)-induced IL-8 release, indicating that inhibition of cytokine secretion by TMEM16A-modulation was specific to IP-10.

Chapter 4 investigated whether TMEM16A-inhibitors affected the direct (IRF3) or indirect (IFN-dependent) pathway (Figure 4-16). To achieve this, IFN-α or IFN-γ were used to stimulate IP-10 production via the IFN-dependent pathway (Figure 4-17 A-B). Treatment with TMEM16A-inhibitors completely abolished IFN-induced IP-10 expression and release, indicating the involvement of TMEM16A in the indirect, IFN-dependent pathway. Ruxolitinib is an FDA-approved anti-cancer drug which competitively interacts with the ATP-binding site of JAK1 and JAK2 kinases, thus preventing the phosphorylation of STAT and the continuation of the signalling cascade [385]. Treatment of cells with ruxolitinib resulted in the potent inhibition of IFN-α-, HRSV- or poly(I:C)-induced IP-10 production (Figure 4-17 C-H) suggesting that the IFN-dependent, JAK-STAT pathway was the predominant mechanism of IP-10 expression.

Previous reports have also highlighted the importance of the IFN-dependent pathway of IP-10 expression during viral infection. For example, dendritic cells infected with DENV produced IP-10, however this was blocked by treatment with anti-CD118, which targets the IFN-α/β receptor 2 (IFNAR2) [432]. This demonstrated that DENV induced IP-10 expression via an IFN-dependent manner. Furthermore, the authors found that IP-10 production was induced in the bystander cells to much higher levels than actively infected cells, supporting the indirect pathway of activation [432]. Additionally, infection of dendritic cells with WNV grown in mammalian cells induced high levels of IFN-α, and consequently IP-10, whereas WNV grown in mosquito cells did not [433]. The authors also discovered that WNV-induced IFN-α expression occurred via IRF3 activated by the sensing of viral dsRNA by RIG-I/MDA5 or TLR3 [433].

Taken together, these data implicated a role for TMEM16A in the IFN-dependent, JAK-STAT pathway of IP-10 gene expression induced by the sensing of dsRNA (Figure 4-16). Furthermore, this pathway could be inhibited by T16Ainh-A01 and MONNA. As IP-10 contributes to airway hyperactivity and inflammation in respiratory disease [424], it may be possible to ameliorate some of the symptoms of HRSV using these TMEM16A-modulators to target IP-10 production in infected cells. There is precedent for this in previous literature; a humanised monoclonal antibody targeting IP-10 (MDX-1100, or Eldelumab) was found to protect mice from acute lung injury induced by pathogenic IAV infection (H1N1, 2009 Swine-origin) [434]. MDX-1100 is well tolerated and is being tested in phase II trials for inflammatory diseases such as rheumatoid arthritis and ulcerative colitis [435,436]. Furthermore, levels of IP-10 are elevated in the plasma and CNS during HIV infection and positively correlate with disease progression [437,438].

It was revealed that IP-10 stimulated HIV replication *in vitro* and that treatment with an anti-IP10 antibody could inhibit this [439].

On the other hand, the IFN response is critical for antiviral immunity and therefore using TMEM16A-modulators to inhibit the production of IP-10 and potentially other ISGs could be counter-productive for treating HRSV infection and result in increased HRSV disease severity [440]. HRSV is known to actively modulate the IFN response through the NS1 and NS2 proteins (1.5.5.3, [104,108]), suggesting that IFNs and ISGs play an important role in anti-HRSV immunity. Care must therefore be taken when choosing to inhibit the antiviral response to dampen the associated inflammatory symptoms.

The lack of at least 3 biological repeats is a limitation of these experiments, therefore future work should aim to assess the reliability and reproducibility of this data. Elucidation of the role of TMEM16A in IP-10 production is a critical next step.

5.11 Modulation of TMEM16A by other pathogens

TMEM16A is highly expressed within the respiratory tract and upregulated during airway inflammation and asthma [220], however a role for this channel during respiratory virus infection had not previously been described until the publication of data within this thesis [326]. However, a role for TMEM16A during viral infection of the colon had been discovered [441]. During rotavirus infection, the non-structural protein NSP4 acts as an enterotoxin, causing the common rotavirus symptom of diarrhoea. NSP4 was shown to enhance the activity of TMEM16A and inhibit the absorption of Na^+ through ENaC [441]. Furthermore, various inhibitors of TMEM16A were used to prevent rotavirus-induced secretory

diarrhoea [442–444]. The mechanism of NSP4-mediated activation of TMEM16A remains to be elucidated; intracellular [Ca^{2+}] was a factor in enterotoxin-induced activation of Cl^- secretion, however direct interaction between the NSP4 and TMEM16A had not been ruled out [441]. These studies set a precedent for the modulation of TMEM16A by a viral pathogen.

Bacterial pathogens have also been reported to modulate TMEM16A. Pyocyanin is the major virulence factor of *P. aeruginosa*, an important opportunistic pathogen in CF. It was reported that pyocyanin stimulated increased expression of TMEM16A in bronchial epithelial cells and that this facilitated the upregulation of Muc5AC mucin [445]. This indicated that the overexpression of TMEM16A observed in CF patients may be caused by the build-up of bacterial contaminants in the airway, and that this facilitated the mucus hypersecretion observed in CF patients. The role of TMEM16A in mucus hypersecretion within the airway is discussed in more detail in the following section.

5.12 A potential role for TMEM16A in HRSV-induced mucus hyperproduction in the airway

As alluded to in section 1.7.4.2, TMEM16A plays an important role within the airways and its expression is highly upregulated in mucus-producing goblet cells, and in ciliated epithelial cells (to a lesser extent) during airway inflammation, CF, and asthma [220]. Inhibition of TMEM16A activity with pharmacological inhibitors such as niflumic acid prevented mucus secretion in an asthma model [446]. Additionally, TMEM16A-knockout mouse models also showed defects in mucus secretion [225]. Interestingly, mucus hyperproduction is often observed in HRSV patients and contributes to the severity of infection in infants by producing a mucus plug which obstructs the airways [447,448]. It is interesting to speculate

that there may be a link between mucus hyperproduction during HRSV infection and TMEM16A, however no such data currently exists in the literature.

Various reports have shown that HRSV infection results in the upregulation of mucins such as Muc5AC. HRSV induces a Th2 response producing inflammatory mediators such as IL-4 and IL-13, as well as the Th17-produced cytokine IL-17. IL-13 causes the upregulation of Muc5AC via the JAK-STAT6-ERK signalling pathway, or by the JAK-STAT6-IKK-NFkB pathway. Additionally, IL-17 has been reported to stimulate the JAK2-STAT3-ERK signalling pathway resulting in the expression of Muc5AB and Muc5B mucins [431].

Intriguingly, TMEM16A is also activated by the Th2 response. In goblet cells within the airway, the inflammatory mediators IL-4 and IL-13 signal through STAT6 which binds to the promoter region of the TMEM16A gene and acts as a transcriptional regulator, thereby increasing the expression of TMEM16A in these cells [411,449]. Furthermore, knocking out STAT6 not only decreases TMEM16A expression, but also the expression of Muc5AC mucin. The authors concluded that IL-13-induced Muc5AC expression occurs via STAT6-TMEM16A-NFkB and STAT6-TMEM16A-ERK1/2 pathways [450,451]. An interesting experiment would be to test whether IL-13 induced by HRSV infection is able to stimulate this pathway, and whether blocking TMEM16A (and/or other components of these signalling pathways) can help recover HRSV-mediated mucus hyperproduction. This could provide an additional benefit of TMEM16A modulation to HRSV sufferers.

Aside from the above, there are more overlaps between signalling pathways involved in the HRSV-mediated hyperproduction of mucus and the role of TMEM16A in mucus secretion [411,447]. Both TMEM16A and HRSV have

individually been reported to contribute to mucin secretion through EGF/EGFR signalling [452,453]. Furthermore, TMEM16A is reported to be co-expressed with TRPV1 and IP3R in DRG neurones wherein TRPV1 activates TMEM16A activity through both direct and indirect effects on Ca^{2+} signalling [411,454]. Studies have also implicated the TRPV1 channel in the hyperproduction of mucus in the airway during HRSV infection; TRPV1 signals through PKC to activate NFκB, which in turn mediates the transcription of Muc5AC mucin [455,456]. Based on this evidence combined with the data provided within this thesis, a deeper understanding of the role of TMEM16A in HRSV-induced mucus hyperproduction is warranted.

5.13 Ion channel drug repurposing

Drug repurposing is the discovery of new uses for approved drugs, and it offers many benefits over novel drug development: the approved drug will have already passed safety tests, therefore reducing both the cost and time frame for preclinical testing as well as reducing the risk of failure [457]. Some well-known examples of drug repurposing, which resulted in huge benefits for pharmaceutical companies as well as for patients, stem largely from serendipitous discoveries of pharmacological activity on new targets. Thalidomide, once used to treat morning sickness, was withdrawn due to a link with birth defects. It has since found success in treating erythema nodosum leprosum (an immunological complication in leprosy) and multiple myeloma (bone marrow cancer). Anti-cancer drug Zidovudine became the first drug to be approved to treat HIV infection. Sildenafil was repurposed from an anti-hypertension drug to a treatment for erectile dysfunction (Viagra) which went on to become a market-leader with sales between $1-2 billion per year. The current COVID-19 pandemic has led to a surge

in drug repurposing through more systematic approaches such as the large-scale screening of clinically approved small-molecule drugs [458].

The human ‘channelome’ consists of over 300 known proteins which play vital roles within cells and tissues. As of 2017, ion channels made up the largest proportion (19%) of human protein drug targets of all gene families and 18% of all FDA-approved small-molecule drugs targeted ion channels, second in number only to those targeting GPCRs (33%) [135]. This demonstrates that the use of ion channel modulators has proven to be both safe and efficacious in the treatment of a wide range of diseases. Many ion channels play important roles in the transmission of signals throughout the body. Reflecting this, ion channel inhibitors are currently licensed for use as anaesthetic, anti-hypertension, anti-arrhythmia, anti-epileptic and anti-depressant drugs [459]. Some well-known examples include local anaesthetics lidocaine and bupivacaine, which block voltage-gated Na^+ channels; verapamil, which blocks L-type voltage-gated Ca^{2+} channels to treat high blood pressure; and benzodiazepines, which activate $GABA_A$ receptors and are used in the treatment of anxiety and depression.

The modulation of ion channels by viruses is an emerging and rapidly developing area of research [305,306]. Ion channel inhibitors are perfectly suited for repurposing as antiviral therapeutics. Large scale screens using libraries of FDA-approved drugs against virus infection has yielded some promising results. For example, EBOV entry was inhibited by dopamine receptor drugs fluphenazine, trifluoperazine, prochlorperazine and thioridazine, which are licenced anti-psychotics, through inhibition of TPCs (Ca^{2+} channels) [319]. Anti-hypertension drugs benidipine hydrochloride and nifedipine which block Ca^{2+} channels were shown to inhibit SFTSV infection both *in vitro* and *in vivo* by

blocking virus internalisation and post-entry replication [460]. Similarly, benidipine hydrochloride, along with two other anti-hypertensive Ca^{2+} channel blockers manidipine and cilnidipine, inhibited the replication of JEV, DENV and ZIKV but not YFV, through an effect on the viral protein NS4B, an essential component of the replication complex [325].

5.13.1 Repurposing TMEM16A-modulating drugs as HRSV replication inhibitors

Whilst there are many FDA-approved drugs targeting ion channels, there are not many specifically targeting Cl^- channels. Drugs targeting Ca^{2+}, K^+ and Na^+ channels are well-documented treatments for hypertension, arrhythmia, and angina, however historically, understanding of Cl^- channel functions has lagged behind the other families. A rare example of an FDA-approved Cl^- channel drug is lubiprostone, which is used in the treatment of chronic constipation. An analysis of clinically approved drugs which modulate TMEM16A follows.

5.13.1.1 Niflumic acid, talniflumate, and benzbromarone

Some of the Cl^- modulators investigated in Chapter 3 are used clinically as anti-inflammatory agents, however these are 'off-label' indications for which there is currently no FDA-approval. For example, CaCC inhibitor niflumic acid and its prodrug talniflumate are used to treat rheumatoid arthritis in some European countries [461]. Studies into the use of talniflumate as a mucin regulator in CF and COPD progressed to phase II trials but have since been discontinued [462]. TMEM16A-modulator benzbromarone is effective in the treatment of gout. Whilst still used in many countries, some have discontinued it over concerns of hepatotoxicity, a decision which many authors disagreed with [463,464]. Therefore, the repurposing of these CaCC inhibitors as anti-HRSV therapeutics

may be possible in countries that they are already used for other indications, and if successful, may be later adopted by other countries.

5.13.1.2 Niclosamide

In 2019, utilising a library of FDA-approved drugs for repurposing to the treatment of asthma, anti-helminthics niclosamide and nitazoxanide were discovered to potently inhibit TMEM16A activity [465]. Consistent with previous reports on the role of TMEM16A in asthma [390], treatment with niclosamide resulted in bronchodilation of mouse airways [465]. Further investigations found that niclosamide also inhibited mucus secretion (likely by augmenting Ca^{2+} signalling in goblet cells), airway smooth muscle contraction and airway inflammation *in vivo* [466]. These studies highlighted the promise of repurposing niclosamide for use in inflammatory respiratory diseases such as asthma or CF.

Other drug repurposing studies have highlighted further uses for niclosamide as an anti-cancer, anti-hypertension, anti-diarrheal and anti-infective agent drug [467]. Interestingly, the mode of action of niclosamide described during cancers links to the pathways known to be involved in TMEM16A signalling, such as the NFκB or IL-6–JAK1–STAT3 pathways [238,411,465,467,468]. Therefore, the potent anti-cancer effects of niclosamide could be a result of TMEM16A inhibition, although this is not yet well described.

In 2020, through another drug repurposing study, niclosamide was identified as an antiviral against SARS-CoV-2 [469], the causative agent of the COVID-19 pandemic. Niclosamide was found to inhibit SARS-CoV-2 replication (as well as that of MERS-CoV) and was subsequently launched into clinical trials. This comes after a long line of previous reports of the antiviral activity of niclosamide (reviewed recently in [470]). For example, niclosamide inhibited the replication of

Flaviviruses (ZIKV, DENV, WNV, JEV and YFV) by blocking the interaction between the two viral protease complex proteins NS2B and NS3 [471]. Moreover, the entry and cell-to-cell transmission of CHIKV was inhibited by niclosamide, however a mechanism of action was not alluded to [472]. Other viruses with reported sensitivity to niclosamide include Epstein-Barr virus, EBOV, RV, human adenovirus, and HCV.

In 2021, the only report to date on the sensitivity of HRSV to niclosamide was published [473]. Niclosamide inhibited HRSV infection in a time- and concentration-dependent manner in HEp-2 cells *in vitro*. Like CaCC-modulators in Chapter 4 (Figure 4-2 F-I), niclosamide was active against HRSV when added up to 6 hpi [473]. The authors found that HRSV induced the phosphorylation of Akt, a pro-survival marker (also known as protein kinase B; PKB). In mammalian cells, Akt phosphorylation mediates cell survival via a direct anti-apoptotic pathway and an indirect, NFκB-dependent, pro-survival pathway [474]. Niclosamide treatment reversed the HRSV-induced phosphorylation of Akt and prevented signalling via the direct anti-apoptotic pathway, therefore inducing early apoptosis and limiting HRSV infection [473]. However, the authors did not investigate the effect of niclosamide on the NFκB-dependent pro-survival pathway induced by Akt. HRSV is known to modulate the Akt-NFκB pathway via the viral NS proteins to delay apoptosis and allow more time for viral replication [475]. Intriguingly, NFκB knockouts inhibited LPS-induced TMEM16A upregulation in IEC-6 (rat intestinal epithelial) cells [476], indicating that NFκB affects TMEM16A expression. This could be indicative of a link between the anti-HRSV activities of niclosamide and CaCC blockers such as T16Ainh-A01 through their shared ability to modulate TMEM16A (Figure 5-2).

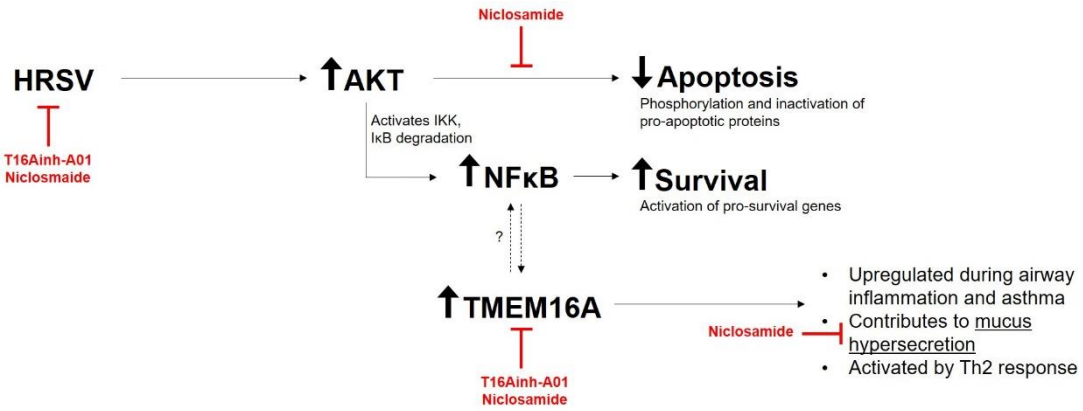

Figure 5-2 Depiction of the anti-apoptosis and pro-survival pathways stimulated by HRSV, and their inhibition by TMEM16A modulators. HRSV infection induces the upregulation of AKT and therefore the activation of the anti-apoptosis pathway (direct) and pro-survival pathway (NFκB-dependent). Treatment with TMEM16A-modulators T16Ainh-A01 or niclosamide has been shown to inhibit HRSV infection (present study [326] and [473], respectively). A possible link to TMEM16A via NFκB is shown.

Future studies should utilise the HRSV minigenome system to test whether niclosamide inhibits HRSV replication and/or transcription and should further investigate whether niclosamide inhibits HRSV via a TMEM16A-dependent mechanism, like T16Ainh-A01. The data presented over the past couple of years has strongly implicated that niclosamide could be repurposed to treat the symptoms of inflammatory respiratory diseases such as mucus hypersecretion by targeting TMEM16A [466]. Given that HRSV infection induces many of these symptoms, niclosamide could provide relief from these symptoms in HRSV sufferers. Furthermore, targeting TMEM16A using niclosamide may have the added benefits of inhibiting HRSV replication ([326] and Chapter 4), and inhibiting HRSV-induced pro-survival mechanisms, therefore inducing early apoptosis in infected cells [473]. Given the good safety profile of niclosamide, including in

paediatric patients which represent the majority of HRSV sufferers, it would make a promising candidate for drug repurposing.

5.13.2 Repurposing TMEM16A-modulating drugs for targeting interferonopathies

As previously mentioned in 5.10, treatment with TMEM16A inhibitors could offer symptomatic relief to HRSV patients by inhibiting the production of IP-10 and other ISGs and therefore dampening down the immune response. However, inhibiting this antiviral response could also provide unwanted benefits for the virus. Therefore, an alternative use for these drugs could be in the treatment of interferonopathies. These are autoinflammatory diseases characterised by dysregulation of the IFN response resulting in the upregulation of activatory mechanisms or the downregulation of inhibitory mechanisms [477]. An example of an interferonopathy is Aicardi-Goutières syndrome (AGS), a progressive encephalopathy caused by the upregulation of the type I IFN response, resulting in severe neurological dysfunctions [478]. JAK inhibitors such as ruxolitinib and baricitinib have been highlighted as promising therapeutic strategies for AGS and other interferonopathies [479–481]. As T16Ainh-A01 and MONNA showed an inhibition on the IFN-dependent pathway of IP-10 production similar to that of ruxolitinib (Figure 4-17), it may be possible that the inhibition of TMEM16A would help to correct the overproduction of ISG and therefore provide therapeutic benefits for interferonopathies.

5.14 Final summary and concluding remarks

HRSV is a global human pathogen that causes a significant number of hospitalisations and deaths each year. Infants and the elderly are at high risk of the severe respiratory symptoms of HRSV infection, which can lead to

bronchiolitis and pneumonia. Despite this, there are currently very few effective treatment options and no licenced vaccines. This thesis aimed to uncover novel antiviral targets for the potential treatment of HRSV infection. To achieve this, the role of Cl^- ion channels during infection was dissected. The reasoning for this was the wealth of emerging data implicating host ion channels as host factors for a range of viruses, combined with the rapid expansion in the understanding of Cl^- channel roles, especially within the respiratory tract; the physiological target of HRSV.

Using a selected panel of pharmacological inhibitors, a role for Cl^- channels during HRSV infection was revealed. After ruling out the other Cl^- channel families, this study discovered a role for CaCCs, and TMEM16A, during HRSV infection. TMEM16A and the CFTR play vital roles within the respiratory tract and their functions are thought to be intricately linked, with TMEM16A both regulating and relying on the function of CFTR [219,222,482]. Therefore, the discovery that HRSV required one of these channels during its life cycle, but not both, was surprising.

Further work in Chapter 3 confirmed that TMEM16A inhibitors were not virucidal and instead their inhibitory effects were mediated by blocking cellular mechanisms. The requirement for TMEM16A was conserved in both lung and neuronal cells lines, both of which represent physiological targets of HRSV infection. The use of PCLS as an infection model for HRSV was validated and utilised to confirm that the inhibition of TMEM16A had a negative impact on HRSV infection in a more physiologically relevant environment. Lastly, the requirement for TMEM16A during infection with IAV and HAZV, but not BUNV, was revealed, suggesting a conserved mechanism of action between some, but not all, NSVs.

An investigation into the mechanisms underpinning the requirement for TMEM16A during HRSV infection was undertaken in Chapter 4. Assays which isolated various steps in the virus life cycle revealed that the channel was likely required for early, post-entry stages of infection. This was confirmed with the use of a minigenome system which highlighted the role of TMEM16A during HRSV genome replication and/or transcription. Therefore, the targeted inhibition of the TMEM16A was shown to offer potential therapeutic benefit to HRSV sufferers through its ability to reduce viral gene expression when administered following HRSV infection, highlighting TMEM16A inhibitors as a novel post-exposure prophylaxis for HRSV [326]. Furthermore, HRSV was not easily able to develop resistance to TMEM16A-specific drug T16Ainh-A01, further highlighting the promise of these drugs as antiviral therapeutics.

A deeper understanding of the role of TMEM16A during HRSV infection was sought. Confocal microscopy was used to determine the subcellular localisation of TMEM16A in A549 cells. A role for TMEM16A in the entry of HRSV was ruled out when no expression of the channel was observed within the endocytic pathway, the route of virus entry, consistent with the results of the entry assays. This thesis provided the first description of TMEM16A expression within the Golgi, as well as confirming its expression in the ER. As the Golgi was previously implicated in the formation of HRSV IBs, this was consistent with a role in HRSV replication and/or transcription. In line with this, the lack of an escape mutant during the passaging of virus in T16Ainh-A01 was indicative of cell-mediated inhibition which affected more than one viral protein. Furthermore, increasing the channel activity of TMEM16A through treatment with Eact did not affect HRSV infection, indicating that the virus relies on the protein function of TMEM16A

rather than its channel activity. Lastly, preliminary confocal microscopy analysis indicated an interaction between HRSV and TMEM16A. These data further support a role for TMEM16A within IBs as many viral and host cell proteins interact here to enable viral genome replication and/or transcription to occur. Altogether, the data in this thesis fulfilled the initial aims of 1) investigating the role of Cl^- channels during HRSV infection; 2) highlighting a channel of interest; and 3) determining the stage of the viral life cycle at which TMEM16A is required.

IP-10 is a cytokine involved in the recruitment of immune cells in response to viral infection. It is upregulated in the airways in response to HRSV, and other respiratory pathogens, and can exacerbate the inflammatory symptoms of infection. In Chapter 3, IP-10 was utilised as a marker of HRSV infection in PCLS, however after discovering that TMEM16A-modulators also abolished poly(I:C)-induced IP-10 expression in Chapter 4, a role for TMEM16A in the secretion of this cytokine was explored. It was found that treatment with T16Ainh-A01 inhibited the expression of IP-10 via an IFN-dependent JAK-STAT signalling pathway. Additionally, TMEM16A channel activation by Eact also partially inhibited the production of IP-10, suggesting the alteration of the ionic balance within cells by modulating TMEM16A channel activity may affect this signalling pathway. However, this conclusion was based on preliminary data and therefore more evidence should be acquired.

Another finding of this thesis was related to the antiviral activity of tannic acid. Although this compound inhibited TMEM16A, it was not specific for this channel and presented differing results to the other CaCC inhibitors in many of the experiments in Chapter 4. For the first time, tannic acid was identified as an entry inhibitor of both HRSV and BUNV. Further investigation revealed that tannic acid

treatment prevented the binding of BUNV to cells, in agreement with reports on other viruses, highlighting its potential as a broad antiviral agent.

5.14.1 Conclusions

Firstly, this thesis has provided evidence which demonstrated a novel role for TMEM16A during HRSV replication and/or transcription. This role may be carried out by TMEM16A interacting with viral or other cellular proteins directly or indirectly within the viral IBs located at the Golgi. Based on these data, TMEM16A-modulators represent a novel class of HRSV antiviral and the development of TMEM16A drugs which are safe for human use, or the repurposing of drugs which target TMEM16A, could be invaluable to HRSV sufferers.

Secondly, use of TMEM16A-modulators may offer multiple therapeutic benefits by also alleviating inflammatory symptoms associated with respiratory infection through their inhibition of IFN-dependent IP-10 release. Whilst the mechanism behind this remained to be fully elucidated, the data in this thesis predicts two possibilities. The first is that TMEM16A-specific inhibitors such as T16Ainh-A01 and MONNA independently inhibit HRSV genome replication and IP-10 production through different mechanisms. Alternatively, HRSV recruits or sequesters TMEM16A for replication (perhaps within IBs or Golgi), therefore preventing the channel being used to generate the antiviral response, thus resulting in a decrease in ISGs such as IP-10. Further work is therefore necessary to untangle the relationship between TMEM16A, IP-10 and HRSV. Intriguingly, mucus hypersecretion, another symptom of HRSV, is mediated by TMEM16A in goblet cells of the airways and can be prevented using TMEM16A inhibitors (such

as niflumic acid or niclosamide), potentially adding a third benefit to TMEM16A modulation in HRSV sufferers.

References

1 Rima B, Collins P, Easton A, *et al.* ICTV virus taxonomy profile: Pneumoviridae. *Journal of General Virology* 2017;**98**:2912–3. doi:10.1099/jgv.0.000959

2 Morris JA, R. E. Blount Jr, Savage RE. Recovery of Cytopathogenic Agent from Chimpanzees with Goryza: *https://doi.org/103181/00379727-92-22538* 1956;**92**:544–9. doi:10.3181/00379727-92-22538

3 Chanock RM, Kim HW, Brandt C, *et al.* Respiratory Syncytial Virus. In: *Viral Infections of Humans*. Boston, MA: : Springer US 1976. 365–82. doi:10.1007/978-1-4613-3988-5_17

4 Chanock RM, Finberg L. Recovery From Infants with Respiratory Illness of a Virus Releated to Chimpanzee Coryza Agent (CCA). *American Journal of Epidemiology* 1957;**66**:291–300. doi:10.1093/oxfordjournals.aje.a119902

5 Kahn JS, Schnell MJ, Buonocore L, *et al.* Recombinant Vesicular Stomatitis Virus Expressing Respiratory Syncytial Virus (RSV) Glycoproteins: RSV Fusion Protein Can Mediate Infection and Cell Fusion. *Virology* 1999;**254**:81–91. doi:10.1006/VIRO.1998.9535

6 Cifuentes-Muñoz N, Ellis Dutch R. To assemble or not to assemble: The changing rules of pneumovirus transmission. *Virus Research* 2019;**265**:68–73. doi:10.1016/J.VIRUSRES.2019.03.002

7 Obando-Pacheco P, Justicia-Grande AJ, Rivero-Calle I, *et al.* Respiratory Syncytial Virus Seasonality: A Global Overview. *The Journal of Infectious Diseases* 2018;**217**:1356–64. doi:10.1093/INFDIS/JIY056

8 Hall CB, Douglas RG. Modes of transmission of respiratory syncytial virus. *The Journal of Pediatrics* 1981;**99**:100–3. doi:10.1016/S0022-3476(81)80969-9

9 Kutter JS, Spronken MI, Fraaij PL, *et al.* Transmission routes of respiratory viruses among humans. *Current Opinion in Virology* 2018;**28**:142–51. doi:10.1016/J.COVIRO.2018.01.001

10 Hall CB, Douglas RG, Schnabel KC, *et al.* Infectivity of respiratory syncytial virus by various routes of inoculation. *Infection and immunity* 1981;**33**:779–

83.http://www.pubmedcentral.nih.gov/articlerender.fcgi?artid=350778&tool=pmcentrez&rendertype=abstract (accessed 10 Apr 2014).

11 Yusuf S, Piedimonte G, Auais A, *et al.* The relationship of meteorological conditions to the epidemic activity of respiratory syncytial virus. *Epidemiology & Infection* 2007;**135**:1077–90. doi:10.1017/S095026880600776X

12 Suryadevara M, Domachowske JB. Epidemiology and Seasonality of Childhood Respiratory Syncytial Virus Infections in the Tropics. *Viruses* 2021;**13**. doi:10.3390/V13040696

13 Hall CB, Weinberg GA, Iwane MK, *et al.* The Burden of Respiratory Syncytial Virus Infection in Young Children. *New England Journal of Medicine* 2009;**360**:588–98. doi:10.1056/NEJMoa0804877

14 Hall CB, Powell KR, MacDonald NE, *et al.* Respiratory Syncytial Viral Infection in Children with Compromised Immune Function. *The New England Journal of Medicine* 1986;**352**:77–81.http://www.nejm.org/doi/pdf/10.1056/NEJM198607103150201 (accessed 10 Apr 2014).

15 Hall CB. Respiratory syncytial virus: its transmission in the hospital environment. *The Yale journal of biology and medicine* 1982;**55**:219–23.http://www.ncbi.nlm.nih.gov/pubmed/6758370 (accessed 12 Jun 2018).

16 Taylor S, Taylor RJ, Lustig RL, *et al.* Modelling estimates of the burden of respiratory syncytial virus infection in children in the UK. *BMJ Open* 2016;**6**:e009337. doi:10.1136/BMJOPEN-2015-009337

17 Shi T, McAllister DA, O'Brien KL, *et al.* Global, regional, and national disease burden estimates of acute lower respiratory infections due to respiratory syncytial virus in young children in 2015: a systematic review and modelling study. *The Lancet* 2017;**390**:946–58. doi:10.1016/S0140-6736(17)30938-8

18 Fleming DM, Taylor RJ, Lustig RL, *et al.* Modelling estimates of the burden of Respiratory Syncytial virus infection in adults and the elderly in the United Kingdom. *BMC Infectious Diseases* 2015;**15**. doi:10.1186/S12879-015-1218-Z

19 Falsey AR, Hennessey PA, Formica MA, *et al.* Respiratory Syncytial Virus Infection in Elderly and High-Risk Adults. *The New England Journal of*

Medicine 2005;**352**:1749–59.http://dev.im.org/AcademicAffairs/Aging/IGP/ExpandingResearchEfforts/Documents/falsey_RSVandFLU.pdf (accessed 10 Apr 2014).

20 Mattia G di, Nenna R, Mancino E, *et al.* During the COVID-19 pandemic where has respiratory syncytial virus gone? *Pediatric Pulmonology* 2021;**56**:3106–9. doi:10.1002/PPUL.25582

21 Vittucci AC, Piccioni L, Coltella L, *et al.* The Disappearance of Respiratory Viruses in Children during the COVID-19 Pandemic. *International Journal of Environmental Research and Public Health 2021, Vol 18, Page 9550* 2021;**18**:9550. doi:10.3390/IJERPH18189550

22 Baker RE, Park SW, Yang W, *et al.* The impact of COVID-19 nonpharmaceutical interventions on the future dynamics of endemic infections. *Proceedings of the National Academy of Sciences of the United States of America* 2020;**117**:30547. doi:10.1073/PNAS.2013182117

23 Palivizumab, a humanized respiratory syncytial virus monoclonal antibody, reduces hospitalization from respiratory syncytial virus infection in high-risk infants. The IMpact-RSV Study Group. *Pediatrics* 1998;**102**:295–6.https://pubmed.ncbi.nlm.nih.gov/9738173/ (accessed 30 Sep 2021).

24 Luna MS, Manzoni P, Paes B, *et al.* Expert consensus on palivizumab use for respiratory syncytial virus in developed countries. *Paediatric Respiratory Reviews* 2020;**33**:35–44. doi:10.1016/J.PRRV.2018.12.001

25 Willis RC, Carson DA, Seegmiller JE. Adenosine kinase initiates the major route of ribavirin activation in a cultured human cell line. *Proceedings of the National Academy of Sciences* 1978;**75**:3042–4. doi:10.1073/PNAS.75.7.3042

26 Graci JD, Cameron CE. Mechanisms of action of ribavirin against distinct viruses. *Reviews in Medical Virology* 2006;**16**:37–48. doi:10.1002/RMV.483

27 Streeter DG, Witkowski JT, Khare GP, *et al.* Mechanism of Action of 1-β-D-Ribofuranosyl-1,2,4-Triazole-3-Carboxamide (Virazole), A New Broad-Spectrum Antiviral Agent. *Proceedings of the National Academy of Sciences of the United States of America* 1973;**70**:1174. doi:10.1073/PNAS.70.4.1174

28 Galli A, Mens H, Gottwein JM, *et al.* Antiviral Effect of Ribavirin against HCV Associated with Increased Frequency of G-to-A and C-to-U Transitions in Infectious Cell Culture Model. *Scientific Reports 2018 8:1* 2018;**8**:1–13. doi:10.1038/s41598-018-22620-2

29 Aljabr W, Touzelet O, Pollakis G, *et al.* Investigating the Influence of Ribavirin on Human Respiratory Syncytial Virus RNA Synthesis by Using a High-Resolution Transcriptome Sequencing Approach. *Journal of Virology* 2016;**90**:4876–88. doi:10.1128/jvi.02349-15

30 Goswami BB, Borek E, Sharma OK, *et al.* The broad spectrum antiviral agent ribavirin inhibits capping of mRNA. *Biochemical and Biophysical Research Communications* 1979;**89**:830–6. doi:10.1016/0006-291X(79)91853-9

31 KIM HW, CANCHOLA JG, BRANDT CD, *et al.* RESPIRATORY SYNCYTIAL VIRUS DISEASE IN INFANTS DESPITE PRIOR ADMINISTRATION OF ANTIGENIC INACTIVATED VACCINE. *American Journal of Epidemiology* 1969;**89**:422–34. doi:10.1093/OXFORDJOURNALS.AJE.A120955

32 Acosta PL, Caballero MT, Polack FP. Brief History and Characterization of Enhanced Respiratory Syncytial Virus Disease. *Clinical and Vaccine Immunology* 2016;**23**:189–95. doi:10.1128/CVI.00609-15

33 WHO Expert Committee on Biological Standardization. Annex 2 Guidelines on the quality, safety and efficacy of respiratory syncytial virus vaccines. 2020.

34 Killikelly A, Tunis M, House A, *et al.* Respiratory syncytial virus : Overview of the respiratory syncytial virus vaccine candidate pipeline in Canada. *Canada Communicable Disease Report* 2020;**46**:56. doi:10.14745/CCDR.V46I04A01

35 Smidansky ED, Arnold JJ, Cameron CE. Nucleic Acid Polymerase Fidelity and Viral Population Fitness. *Origin and Evolution of Viruses* 2008;:135–60. doi:10.1016/B978-0-12-374153-0.00006-0

36 RSV Clinical Trial Tracker | PATH. https://www.path.org/resources/rsv-and-mab-trial-tracker/?i=2682 (accessed 1 Oct 2021).

37 Griffin MP, Yuan Y, Takas T, *et al.* Single-Dose Nirsevimab for Prevention of RSV in Preterm Infants. *New England Journal of Medicine* 2020;**383**:415–25.

doi:10.1056/NEJMOA1913556/SUPPL_FILE/NEJMOA1913556_DATA-SHARING.PDF

38 Kuo L, Grosfeld H, Cristina J, *et al.* Effects of mutations in the gene-start and gene-end sequence motifs on transcription of monocistronic and dicistronic minigenomes of respiratory syncytial virus. *Journal of virology* 1996;**70**:6892–901.http://www.ncbi.nlm.nih.gov/pubmed/8794332 (accessed 13 Jun 2018).

39 Tawar RG, Duquerroy S, Vonrhein C, *et al.* Crystal structure of a nucleocapsid-like nucleoprotein-RNA complex of respiratory syncytial virus. *Science (New York, NY)* 2009;**326**:1279–83. doi:10.1126/science.1177634

40 Bakker SE, Duquerroy S, Galloux M, *et al.* The respiratory syncytial virus nucleoprotein-RNA complex forms a left-handed helical nucleocapsid. *The Journal of general virology* 2013;**94**:1734–8. doi:10.1099/vir.0.053025-0

41 Kiss G, Holl JM, Williams GM, *et al.* Structural Analysis of Respiratory Syncytial Virus Reveals the Position of M2-1 between the Matrix Protein and the Ribonucleoprotein Complex. *Journal of Virology* 2014;**88**:7602–17. doi:10.1128/JVI.00256-14/SUPPL_FILE/ZJV999099222SO1.PDF

42 Liljeroos L, Krzyzaniak MA, Helenius A, *et al.* Architecture of respiratory syncytial virus revealed by electron cryotomography. *Proceedings of the National Academy of Sciences of the United States of America* 2013;**110**:11133–8. doi:10.1073/pnas.1309070110

43 Ke Z, Dillard RS, Chirkova T, *et al.* The Morphology and Assembly of Respiratory Syncytial Virus Revealed by Cryo-Electron Tomography. *Viruses* 2018;**10**:446. doi:10.3390/V10080446

44 Bukreyev A, Yang L, Fricke J, *et al.* The secreted form of respiratory syncytial virus G glycoprotein helps the virus evade antibody-mediated restriction of replication by acting as an antigen decoy and through effects on Fc receptor-bearing leukocytes. *Journal of virology* 2008;**82**:12191–204. doi:10.1128/JVI.01604-08

45 Zimmer G, Budz L, Herrler G. Proteolytic Activation of Respiratory Syncytial Virus Fusion Protein: CLEAVAGE AT TWO FURIN CONSENSUS SEQUENCES. *Journal of Biological Chemistry* 2001;**276**:31642–50. doi:10.1074/JBC.M102633200

46 González-Reyes L, Ruiz-Argüello MB, García-Barreno B, *et al.* Cleavage of the human respiratory syncytial virus fusion protein at two distinct sites is required for activation of membrane fusion. *Proceedings of the National Academy of Sciences of the United States of America* 2001;**98**:9859–64. doi:10.1073/pnas.151098198

47 Collins PL, Mottet G. Post-translational processing and oligomerization of the fusion glycoprotein of human respiratory syncytial virus. *Journal of General Virology* 1991;**72**:3095–101. doi:10.1099/0022-1317-72-12-3095/CITE/REFWORKS

48 Krzyzaniak MA, Zumstein MT, Gerez JA, *et al.* Host Cell Entry of Respiratory Syncytial Virus Involves Macropinocytosis Followed by Proteolytic Activation of the F Protein. *PLoS Pathogens* 2013;**9**:1003309. doi:10.1371/journal.ppat.1003309

49 Chirkova T, Lin S, Oomens AGP, *et al.* CX3CR1 is an important surface molecule for respiratory syncytial virus infection in human airway epithelial cells. *The Journal of General Virology* 2015;**96**:2543. doi:10.1099/VIR.0.000218

50 Johnson SM, McNally BA, Ioannidis I, *et al.* Respiratory Syncytial Virus Uses CX3CR1 as a Receptor on Primary Human Airway Epithelial Cultures. *PLoS pathogens* 2015;**11**:e1005318. doi:10.1371/journal.ppat.1005318

51 Anderson CS, Chu C-Y, Wang Q, *et al.* CX3CR1 as a respiratory syncytial virus receptor in pediatric human lung. *Pediatric Research 2019 87:5* 2019;**87**:862–7. doi:10.1038/s41390-019-0677-0

52 Krusat T, Streckert H-J. Heparin-dependent attachment of respiratory syncytial virus (RSV) to host cells Brief Report. *Arch Virol* 1997;**142**:1247–54.

53 Kurt-Jones EA, Popova L, Kwinn L, *et al.* Pattern recognition receptors TLR4 and CD14 mediate response to respiratory syncytial virus. *Nature Immunology* 2000;**1**:398–401. doi:10.1038/80833

54 Behera AK, Matsuse H, Kumar M, *et al.* Blocking Intercellular Adhesion Molecule-1 on Human Epithelial Cells Decreases Respiratory Syncytial Virus Infection. *Biochemical and Biophysical Research Communications* 2001;**280**:188–95. doi:10.1006/BBRC.2000.4093

55 Tayyari F, Marchant D, Moraes TJ, *et al.* Identification of nucleolin as a cellular receptor for human respiratory syncytial virus. *Nature Medicine* 2011;**17**:1132–5. doi:10.1038/nm.2444

56 Mastrangelo P, Hegele RG. RSV fusion: time for a new model. *Viruses* 2013;**5**:873–85. doi:10.3390/v5030873

57 Anderson CS, Chirkova T, Slaunwhite CG, *et al.* CX3CR1 Engagement by Respiratory Syncytial Virus Leads to Induction of Nucleolin and Dysregulation of Cilium-Related Genes. *Journal of Virology* 2021;**95**. doi:10.1128/JVI.00095-21

58 Griffiths CD, Bilawchuk LM, McDonough JE, *et al.* IGF1R is an entry receptor for respiratory syncytial virus. *Nature 2020 583:7817* 2020;**583**:615–9. doi:10.1038/s41586-020-2369-7

59 Battles MB, McLellan JS. Respiratory syncytial virus entry and how to block it. *Nature Reviews Microbiology* 2019;**17**:233. doi:10.1038/S41579-019-0149-X

60 Collins PL, Melero JA. Progress in understanding and controlling respiratory syncytial virus: Still crazy after all these years. *Virus Research* 2011;**162**:80–99. doi:10.1016/J.VIRUSRES.2011.09.020

61 Krarup A, Truan D, Furmanova-Hollenstein P, *et al.* A highly stable prefusion RSV F vaccine derived from structural analysis of the fusion mechanism. *Nature communications* 2015;**6**:8143. doi:10.1038/ncomms9143

62 Gan SW, Ng L, Lin X, *et al.* Structure and ion channel activity of the human respiratory syncytial virus (hRSV) small hydrophobic protein transmembrane domain. *Protein Science : A Publication of the Protein Society* 2008;**17**:813. doi:10.1110/PS.073366208

63 Gan S-W, Tan E, Lin X, *et al.* The Small Hydrophobic Protein of the Human Respiratory Syncytial Virus Forms Pentameric Ion Channels. *The Journal of Biological Chemistry* 2012;**287**:24671. doi:10.1074/JBC.M111.332791

64 Techaarpornkul S, Barretto N, Peeples ME. Functional analysis of recombinant respiratory syncytial virus deletion mutants lacking the small hydrophobic and/or attachment glycoprotein gene. *Journal of virology* 2001;**75**:6825–34. doi:10.1128/JVI.75.15.6825-6834.2001

65 Bukreyev A, Whitehead SS, Murphy BR, *et al.* Recombinant respiratory syncytial virus from which the entire SH gene has been deleted grows efficiently in cell culture and exhibits site-specific attenuation in the respiratory tract of the mouse. *Journal of Virology* 1997;**71**:8973./pmc/articles/PMC230197/?report=abstract (accessed 5 Oct 2021).

66 Fuentes S, Tran KC, Luthra P, *et al.* Function of the Respiratory Syncytial Virus Small Hydrophobic Protein. *Journal of Virology* 2007;**81**:8361. doi:10.1128/JVI.02717-06

67 Tran T-L, Castagné N, Bhella D, *et al.* The nine C-terminal amino acids of the respiratory syncytial virus protein P are necessary and sufficient for binding to ribonucleoprotein complexes in which six ribonucleotides are contacted per N protein protomer. *Journal of General Virology* 2007;**88**:196–206. doi:10.1099/VIR.0.82282-0

68 Selvaraj M, Yegambaram K, Todd EJAA, *et al.* The Structure of the Human Respiratory Syncytial Virus M2-1 Protein Bound to the Interaction Domain of the Phosphoprotein P Defines the Orientation of the Complex. *mBio* 2018;**9**:1–13. doi:10.1128/MBIO.01554-18

69 Richard C-A, Rincheval V, Lassoued S, *et al.* RSV hijacks cellular protein phosphatase 1 to regulate M2-1 phosphorylation and viral transcription. *PLoS Pathogens* 2018;**14**. doi:10.1371/JOURNAL.PPAT.1006920

70 Bajorek M, Galloux M, Richard C-A, *et al.* Tetramerization of Phosphoprotein Is Essential for Respiratory Syncytial Virus Budding while Its N-Terminal Region Mediates Direct Interactions with the Matrix Protein. *Journal of Virology* 2021;**95**. doi:10.1128/JVI.02217-20

71 Bailly B, Richard C-A, Sharma G, *et al.* Targeting human respiratory syncytial virus transcription anti-termination factor M2-1 to inhibit in vivo viral replication. *Scientific reports* 2016;**6**:25806. doi:10.1038/srep25806

72 Braun MR, Noton SL, Blanchard EL, *et al.* Respiratory syncytial virus M2-1 protein associates non-specifically with viral messenger RNA and with specific cellular messenger RNA transcripts. *PLOS Pathogens* 2021;**17**:e1009589. doi:10.1371/JOURNAL.PPAT.1009589

73 Tanner SJ, Ariza A, Richard CA, *et al.* Crystal structure of the essential transcription antiterminator M2-1 protein of human respiratory syncytial virus and implications of its phosphorylation. *Proceedings of the National*

Academy of Sciences of the United States of America 2014;**111**:1580–5. doi:10.1073/PNAS.1317262111/-/DCSUPPLEMENTAL

74 Fearns R, Peeples ME, Collins PL. Mapping the transcription and replication promoters of respiratory syncytial virus. *Journal of virology* 2002;**76**:1663–72. doi:10.1128/JVI.76.4.1663-1672.2002

75 Cowton VM, McGivern DR, Fearns R. Unravelling the complexities of respiratory syncytial virus RNA synthesis. *Journal of General Virology* 2006;**87**:1805–21. doi:10.1099/vir.0.81786-0

76 Tremaglio CZ, Noton SL, Deflubé LR, *et al.* Respiratory Syncytial Virus Polymerase Can Initiate Transcription from Position 3 of the Leader Promoter. *Journal of Virology* 2013;**87**:3196. doi:10.1128/JVI.02862-12

77 Noton SL, Tremaglio CZ, Fearns R. Killing two birds with one stone: How the respiratory syncytial virus polymerase initiates transcription and replication. *PLoS Pathogens* 2019;**15**. doi:10.1371/JOURNAL.PPAT.1007548

78 Cressey TN, Noton SL, Nagendra K, *et al.* Mechanism for de novo initiation at two sites in the respiratory syncytial virus promoter. *Nucleic Acids Research* 2018;**46**:6785. doi:10.1093/NAR/GKY480

79 Bermingham A, Collins PL. The M2–2 protein of human respiratory syncytial virus is a regulatory factor involved in the balance between RNA replication and transcription. *Proceedings of the National Academy of Sciences of the United States of America* 1999;**96**:11259. doi:10.1073/PNAS.96.20.11259

80 Norrby E, Marusyk H, Orvell C. Morphogenesis of respiratory syncytial virus in a green monkey kidney cell line (Vero). *Journal of virology* 1970;**6**:237–42.http://www.ncbi.nlm.nih.gov/pubmed/4100527 (accessed 13 Jun 2018).

81 McDonald TP, Pitt AR, Brown G, *et al.* Evidence that the respiratory syncytial virus polymerase complex associates with lipid rafts in virus-infected cells: a proteomic analysis. *Virology* 2004;**330**:147–57. doi:10.1016/J.VIROL.2004.09.034

82 Jobe F, Simpson J, Hawes P, *et al.* Respiratory Syncytial Virus Sequesters NF-κB Subunit p65 to Cytoplasmic Inclusion Bodies To Inhibit Innate Immune Signaling. *Journal of Virology* 2020;**94**:1380–400. doi:10.1128/jvi.01380-20

83 Rincheval V, Lelek M, Gault E, *et al.* Functional organization of cytoplasmic inclusion bodies in cells infected by respiratory syncytial virus. *Nature Communications* 2017;**8**:563. doi:10.1038/s41467-017-00655-9

84 García J, García-Barreno B, Vivo A, *et al.* Cytoplasmic Inclusions of Respiratory Syncytial Virus-Infected Cells: Formation of Inclusion Bodies in Transfected Cells That Coexpress the Nucleoprotein, the Phosphoprotein, and the 22K Protein. *Virology* 1993;**195**:243–7. doi:10.1006/viro.1993.1366

85 Santangelo P, Nitin N, LaConte L, *et al.* Live-Cell Characterization and Analysis of a Clinical Isolate of Bovine Respiratory Syncytial Virus, Using Molecular Beacons. *Journal of Virology* 2006;**80**:682. doi:10.1128/JVI.80.2.682-688.2006

86 Dolnik O, Gerresheim GK, Biedenkopf N. New Perspectives on the Biogenesis of Viral Inclusion Bodies in Negative-Sense RNA Virus Infections. *Cells* 2021;**10**. doi:10.3390/CELLS10061460

87 Lahaye X, Vidy A, Pomier C, *et al.* Functional Characterization of Negri Bodies (NBs) in Rabies Virus-Infected Cells: Evidence that NBs Are Sites of Viral Transcription and Replication. *Journal of Virology* 2009;**83**:7948–58. doi:10.1128/JVI.00554-09

88 Hoenen T, Shabman RS, Groseth A, *et al.* Inclusion Bodies Are a Site of Ebolavirus Replication. *Journal of Virology* 2012;**86**:11779–88. doi:10.1128/JVI.01525-12

89 Heinrich BS, Cureton DK, Rahmeh AA, *et al.* Protein Expression Redirects Vesicular Stomatitis Virus RNA Synthesis to Cytoplasmic Inclusions. *PLOS Pathogens* 2010;**6**:e1000958. doi:10.1371/JOURNAL.PPAT.1000958

90 Cifuentes-Muñoz N, Branttie J, Slaughter KB, *et al.* Human Metapneumovirus Induces Formation of Inclusion Bodies for Efficient Genome Replication and Transcription. *Journal of Virology* 2017;**91**. doi:10.1128/JVI.01282-17

91 Ringel M, Heiner A, Behner L, *et al.* Nipah virus induces two inclusion body populations: Identification of novel inclusions at the plasma membrane. *PLOS Pathogens* 2019;**15**:e1007733. doi:10.1371/JOURNAL.PPAT.1007733

92 el Najjar F, Schmitt AP, Dutch RE. Paramyxovirus glycoprotein incorporation, assembly and budding: a three way dance for infectious particle production. *Viruses* 2014;**6**:3019–54. doi:10.3390/v6083019

93 Förster A, Maertens GN, Farrell PJ, *et al.* Dimerization of Matrix Protein Is Required for Budding of Respiratory Syncytial Virus. *Journal of Virology* 2015;**89**:4624. doi:10.1128/JVI.03500-14

94 Money VA, McPhee HK, Mosely JA, *et al.* Surface features of a Mononegavirales matrix protein indicate sites of membrane interaction. *Proceedings of the National Academy of Sciences* 2009;**106**:4441–6. doi:10.1073/PNAS.0805740106

95 Ghildyal R, Baulch-Brown C, Mills J, *et al.* The matrix protein of Human respiratory syncytial virus localises to the nucleus of infected cells and inhibits transcription. *Archives of Virology 2003 148:7* 2003;**148**:1419–29. doi:10.1007/S00705-003-0112-Y

96 Meshram CD, Baviskar PS, Ognibene CM, *et al.* The Respiratory Syncytial Virus Phosphoprotein, Matrix Protein, and Fusion Protein Carboxy-Terminal Domain Drive Efficient Filamentous Virus-Like Particle Formation. *Journal of Virology* 2016;**90**:10612. doi:10.1128/JVI.01193-16

97 Ghildyal R, Li D, Peroulis I, *et al.* Interaction between the respiratory syncytial virus G glycoprotein cytoplasmic domain and the matrix protein. *Journal of General Virology* 2005;**86**:1879–84. doi:10.1099/VIR.0.80829-0

98 Mitra R, Baviskar P, Duncan-Decocq RR, *et al.* The Human Respiratory Syncytial Virus Matrix Protein Is Required for Maturation of Viral Filaments. *Journal of Virology* 2012;**86**:4432. doi:10.1128/JVI.06744-11

99 Li D, Jans DA, Bardin PG, *et al.* Association of Respiratory Syncytial Virus M Protein with Viral Nucleocapsids Is Mediated by the M2-1 Protein. *Journal of Virology* 2008;**82**:8863. doi:10.1128/JVI.00343-08

100 Shahriari S, Gordon J, Ghildyal R. Host cytoskeleton in respiratory syncytial virus assembly and budding. *Virology journal* 2016;**13**:161. doi:10.1186/s12985-016-0618-z

101 Santangelo PJ, Bao G. Dynamics of filamentous viral RNPs prior to egress. *Nucleic acids research* 2007;**35**:3602–11. doi:10.1093/nar/gkm246

102 Utley TJ, Ducharme NA, Varthakavi V, *et al.* Respiratory syncytial virus uses a Vps4-independent budding mechanism controlled by Rab11-FIP2.

Proceedings of the National Academy of Sciences of the United States of America 2008;**105**:10209. doi:10.1073/PNAS.0712144105

103 Tian J, Huang K, Krishnan S, *et al.* RAGE inhibits human respiratory syncytial virus syncytium formation by interfering with F-protein function. *The Journal of General Virology* 2013;**94**:1691. doi:10.1099/VIR.0.049254-0

104 Thornhill EM, Verhoeven D. Respiratory Syncytial Virus's Non-structural Proteins: Masters of Interference. *Frontiers in Cellular and Infection Microbiology* 2020;**10**:225. doi:10.3389/FCIMB.2020.00225

105 Swedan S, Andrews J, Majumdar T, *et al.* Multiple Functional Domains and Complexes of the Two Nonstructural Proteins of Human Respiratory Syncytial Virus Contribute to Interferon Suppression and Cellular Location. *Journal of Virology* 2011;**85**:10090. doi:10.1128/JVI.00413-11

106 Atreya PL, Peeples ME, Collins PL. The NS1 Protein of Human Respiratory Syncytial Virus Is a Potent Inhibitor of Minigenome Transcription and RNA Replication. *Journal of Virology* 1998;**72**:1452./pmc/articles/PMC124626/ (accessed 12 Oct 2021).

107 West AP, Shadel GS, Ghosh S. Mitochondria in innate immune responses. *Nature Reviews Immunology 2011 11:6* 2011;**11**:389–402. doi:10.1038/nri2975

108 Sedeyn K, Schepens B, Saelens X. Respiratory syncytial virus nonstructural proteins 1 and 2: Exceptional disrupters of innate immune responses. *PLoS Pathogens* 2019;**15**. doi:10.1371/JOURNAL.PPAT.1007984

109 Takeuchi O, Akira S. Innate immunity to virus infection. *Immunological Reviews* 2009;**227**:75–86. doi:10.1111/J.1600-065X.2008.00737.X

110 Lifland AW, Jung J, Alonas E, *et al.* Human respiratory syncytial virus nucleoprotein and inclusion bodies antagonize the innate immune response mediated by MDA5 and MAVS. *Journal of virology* 2012;**86**:8245–58. doi:10.1128/JVI.00215-12

111 Hall CB, Douglas RG, Simons RL, *et al.* Interferon production in children with respiratory syncytial, influenza, and parainfluenza virus infections. *The Journal of pediatrics* 1978;**93**:28–32. doi:10.1016/S0022-3476(78)80594-0

112 Goswami R, Majumdar T, Dhar J, *et al.* Viral degradasome hijacks mitochondria to suppress innate immunity. *Cell Research* 2013;**23**:1025. doi:10.1038/CR.2013.98

113 Ling Z, Tran KC, Teng MN. Human respiratory syncytial virus nonstructural protein NS2 antagonizes the activation of beta interferon transcription by interacting with RIG-I. *Journal of virology* 2009;**83**:3734–42. doi:10.1128/JVI.02434-08

114 Pei J, Wagner ND, Zou AJ, *et al.* Structural basis for IFN antagonism by human respiratory syncytial virus nonstructural protein 2. *Proceedings of the National Academy of Sciences of the United States of America* 2021;**118**. doi:10.1073/PNAS.2020587118/-/DCSUPPLEMENTAL

115 Boyapalle S, Wong T, Garay J, *et al.* Respiratory Syncytial Virus NS1 Protein Colocalizes with Mitochondrial Antiviral Signaling Protein MAVS following Infection. *PLoS ONE* 2012;**7**:29386. doi:10.1371/JOURNAL.PONE.0029386

116 Swedan S, Musiyenko A, Barik S. Respiratory Syncytial Virus Nonstructural Proteins Decrease Levels of Multiple Members of the Cellular Interferon Pathways. *Journal of Virology* 2009;**83**:9682. doi:10.1128/JVI.00715-09

117 Spann KM, Tran KC, Collins PL. Effects of Nonstructural Proteins NS1 and NS2 of Human Respiratory Syncytial Virus on Interferon Regulatory Factor 3, NF-κB, and Proinflammatory Cytokines. *Journal of Virology* 2005;**79**:5353. doi:10.1128/JVI.79.9.5353-5362.2005

118 Ren J, Liu T, Pang L, *et al.* A novel mechanism for the inhibition of interferon regulatory factor-3-dependent gene expression by human respiratory syncytial virus NS1 protein. *The Journal of General Virology* 2011;**92**:2153. doi:10.1099/VIR.0.032987-0

119 Zhang Y, Yang L, Wang H, *et al.* Respiratory syncytial virus non-structural protein 1 facilitates virus replication through miR-29a-mediated inhibition of interferon-α receptor. *Biochemical and biophysical research communications* 2016;**478**:1436–41. doi:10.1016/J.BBRC.2016.08.142

120 Ramaswamy M, Shi L, Varga SM, *et al.* Respiratory syncytial virus nonstructural protein 2 specifically inhibits type I interferon signal transduction. *Virology* 2006;**344**:328–39. doi:10.1016/J.VIROL.2005.09.009

121 Lo MS, Brazas RM, Holtzman MJ. Respiratory syncytial virus nonstructural proteins NS1 and NS2 mediate inhibition of Stat2 expression and alpha/beta interferon responsiveness. *Journal of virology* 2005;**79**:9315–9. doi:10.1128/JVI.79.14.9315-9319.2005

122 Elliott J, Lynch OT, Suessmuth Y, *et al.* Respiratory syncytial virus NS1 protein degrades STAT2 by using the Elongin-Cullin E3 ligase. *Journal of virology* 2007;**81**:3428–36. doi:10.1128/JVI.02303-06

123 Fricke J, Koo LY, Brown CR, *et al.* p38 and OGT Sequestration into Viral Inclusion Bodies in Cells Infected with Human Respiratory Syncytial Virus Suppresses MK2 Activities and Stress Granule Assembly. *Journal of Virology* 2013;**87**:1333. doi:10.1128/JVI.02263-12

124 Alberts B, Johnson A, Lewis J, *et al.* Ion Channels and the Electrical Properties of Membranes. In: *Molecular Biology of the Cell*. New York: : Garland Science 2002. https://www.ncbi.nlm.nih.gov/books/NBK26910/ (accessed 14 Dec 2021).

125 Kefauver JM, Ward AB, Patapoutian A. Discoveries in structure and physiology of mechanically activated ion channels. *Nature* 2020;**587**:567. doi:10.1038/S41586-020-2933-1

126 Vriens J, Nilius B, Voets T. Peripheral thermosensation in mammals. *Nature Reviews Neuroscience 2014 15:9* 2014;**15**:573–89. doi:10.1038/nrn3784

127 Deisseroth K, Hegemann P. The form and function of channelrhodopsin. *Science (New York, NY)* 2017;**357**. doi:10.1126/SCIENCE.AAN5544

128 Doyle DA, Cabral JM, Pfuetzner RA, *et al.* The structure of the potassium channel: Molecular basis of K+ conduction and selectivity. *Science* 1998;**280**:69–77. doi:10.1126/SCIENCE.280.5360.69/ASSET/8B1C6173-341A-4492-9124-7C65D5D3CB23/ASSETS/GRAPHIC/SE1586417008.JPEG

129 Bardou O, Trinh NTN, Brochiero E. Molecular diversity and function of K+ channels in airway and alveolar epithelial cells. *https://doi.org/101152/ajplung905252008* 2009;**296**:145–55. doi:10.1152/AJPLUNG.90525.2008

130 Roger S, Gillet L, Guennec J-Y le, *et al.* Voltage-gated sodium channels and cancer: is excitability their primary role? *Frontiers in Pharmacology* 2015;**6**:152. doi:10.3389/FPHAR.2015.00152

131 Hübner CA, Jentsch TJ. Ion channel diseases. *Human Molecular Genetics* 2002;**11**:2435–45. doi:10.1093/HMG/11.20.2435

132 Jentsch TJ, Hübner CA, Fuhrmann JC. Ion channels: Function unravelled by dysfunction. *Nature Cell Biology 2004 6:11* 2004;**6**:1039–47. doi:10.1038/ncb1104-1039

133 O'Grady SM, Lee SY. Chloride and potassium channel function in alveolar epithelial cells. *American Journal of Physiology-Lung Cellular and Molecular Physiology* 2003;**284**:L689–700. doi:10.1152/ajplung.00256.2002

134 Kim J-B. Channelopathies. *Korean Journal of Pediatrics* 2014;**57**:1. doi:10.3345/KJP.2014.57.1.1

135 Santos R, Ursu O, Gaulton A, *et al.* A comprehensive map of molecular drug targets. *Nature Publishing Group* Published Online First: 2017. doi:10.1038/nrd.2016.230

136 Zhou Y, Ä Morais-Cabral JH, Kaufman A, *et al.* Chemistry of ion coordination and hydration revealed by a K + channel±Fab complex at 2.0 A Ê resolution. *NATURE* 2001;**414**.www.nature.com43 (accessed 14 Dec 2021).

137 Feinshreiber L, Singer-Lahat D, Ashery U, *et al.* Voltage-gated Potassium Channel as a Facilitator of Exocytosis. *Annals of the New York Academy of Sciences* 2009;**1152**:87–92. doi:10.1111/J.1749-6632.2008.03997.X

138 Bachmann M, Li W, Edwards MJ, *et al.* Voltage-Gated Potassium Channels as Regulators of Cell Death. *Frontiers in Cell and Developmental Biology* 2020;**8**. doi:10.3389/FCELL.2020.611853

139 Wulff H, Castle NA, Pardo LA. Voltage-gated Potassium Channels as Therapeutic Drug Targets. *Nature reviews Drug discovery* 2009;**8**:982. doi:10.1038/NRD2983

140 Thompson-Vest N, Shimizu Y, Hunne B, *et al.* The distribution of intermediate-conductance, calcium-activated, potassium (IK) channels in epithelial cells. *Journal of Anatomy* 2006;**208**:219. doi:10.1111/J.1469-7580.2006.00515.X

141 Hibino H, Inanobe A, Furutani K, *et al.* Inwardly rectifying potassium channels: Their structure, function, and physiological roles. *Physiological Reviews* 2010;**90**:291–366.

doi:10.1152/PHYSREV.00021.2009/ASSET/IMAGES/LARGE/Z9J0011025300018.JPEG

142 Enyedi P, Czirják G. Molecular background of leak K+ currents: Two-pore domain potassium channels. *Physiological Reviews* 2010;**90**:559–605. doi:10.1152/PHYSREV.00029.2009/ASSET/IMAGES/LARGE/Z9J0021025400009.JPEG

143 O'Connell AD, Morton MJ, Hunter M. Two-pore domain K+ channels—molecular sensors. *Biochimica et Biophysica Acta (BBA) - Biomembranes* 2002;**1566**:152–61. doi:10.1016/S0005-2736(02)00597-7

144 Bagur R, Hajnóczky G. Intracellular Ca2+ sensing: role in calcium homeostasis and signaling. *Molecular cell* 2017;**66**:780. doi:10.1016/J.MOLCEL.2017.05.028

145 Berridge MJ, Lipp P, Bootman MD. The versatility and universality of calcium signalling. *Nature Reviews Molecular Cell Biology 2000 1:1* 2000;**1**:11–21. doi:10.1038/35036035

146 Ashby MC, Tepikin A v. ER calcium and the functions of intracellular organelles. *Seminars in Cell & Developmental Biology* 2001;**12**:11–7. doi:10.1006/SCDB.2000.0212

147 Tyson JR, Snutch TP. Molecular nature of voltage-gated calcium channels: structure and species comparison. *Wiley Interdisciplinary Reviews: Membrane Transport and Signaling* 2013;**2**:181–206. doi:10.1002/WMTS.91

148 Parys JB, de Smedt H. Inositol 1,4,5-Trisphosphate and Its Receptors. *Advances in Experimental Medicine and Biology* 2012;**740**:255–79. doi:10.1007/978-94-007-2888-2_11

149 Lanner JT, Georgiou DK, Joshi AD, *et al.* Ryanodine Receptors: Structure, Expression, Molecular Details, and Function in Calcium Release. *Cold Spring Harbor Perspectives in Biology* 2010;**2**:a003996. doi:10.1101/CSHPERSPECT.A003996

150 Patel S, Docampo R. Acidic calcium stores open for business: expanding the potential for intracellular Ca2+ signaling. *Trends in cell biology* 2010;**20**:277. doi:10.1016/J.TCB.2010.02.003

151 Hess P, Tsien RW. Mechanism of ion permeation through calcium channels. *Nature 1984 309:5967* 1984;**309**:453–6. doi:10.1038/309453a0

152 Tang L, Gamal El-Din TM, Payandeh J, *et al.* Structural basis for Ca2+ selectivity of a voltage-gated calcium channel. *Nature* 2014;**505**:56. doi:10.1038/NATURE12775

153 Sather WA, McCleskey EW. Permeation and Selectivity in Calcium Channels. *Annual Review of Physiology* 2003;**65**:133–59. doi:10.1146/ANNUREV.PHYSIOL.65.092101.142345

154 Motoike HK, Liu H, Glaaser IW, *et al.* The Na+ Channel Inactivation Gate Is a Molecular Complex: A Novel Role of the COOH-terminal Domain. *The Journal of General Physiology* 2004;**123**:155. doi:10.1085/JGP.200308929

155 Flood E, Boiteux C, Allen TW. Selective ion permeation involves complexation with carboxylates and lysine in a model human sodium channel. *PLoS Computational Biology* 2018;**14**. doi:10.1371/JOURNAL.PCBI.1006398

156 Roger S, Gillet L, le Guennec JY, *et al.* Voltage-gated sodium channels and cancer: is excitability their primary role? *Frontiers in Pharmacology* 2015;**6**:152. doi:10.3389/FPHAR.2015.00152

157 Black JA, Waxman SG. Noncanonical Roles of Voltage-Gated Sodium Channels. *Neuron* 2013;**80**:280–91. doi:10.1016/J.NEURON.2013.09.012

158 Duran C, Thompson CH, Xiao Q, *et al.* Chloride channels: often enigmatic, rarely predictable. *Annual review of physiology* 2010;**72**:95–121. doi:10.1146/annurev-physiol-021909-135811

159 Linsdell P. Anion conductance selectivity mechanism of the CFTR chloride channel. *Biochimica et Biophysica Acta (BBA) - Biomembranes* 2016;**1858**:740–7. doi:10.1016/J.BBAMEM.2016.01.009

160 Fahlke C. Ion permeation and selectivity in CIC-type chloride channels. *American Journal of Physiology - Renal Physiology* 2001;**280**. doi:10.1152/AJPRENAL.2001.280.5.F748/ASSET/IMAGES/LARGE/H20510295003.JPEG

161 Schroeder BC, Cheng T, Jan YN, *et al.* Expression cloning of TMEM16A as a calcium-activated chloride channel subunit. *Cell* 2008;**134**:1019–29. doi:10.1016/j.cell.2008.09.003

162 Hwang TC, Yeh JT, Zhang J, *et al.* Structural mechanisms of CFTR function and dysfunction. Journal of General Physiology. 2018;**150**:539–70. doi:10.1085/jgp.201711946

163 Zhang Z, Liu F, Chen J. Molecular structure of the ATP-bound, phosphorylated human CFTR. *Proceedings of the National Academy of Sciences of the United States of America* 2018;**115**:12757–62. doi:10.1073/pnas.1815287115

164 Ikuma M, Welsh MJ. Regulation of CFTR Cl - channel gating by ATP binding and hydrolysis. *Proceedings of the National Academy of Sciences of the United States of America* 2000;**97**:8675–80. doi:10.1073/pnas.140220597

165 Csanády L, Vergani P, Gadsby DC. Structure, Gating, and Regulation of the CFTR Anion Channel. *Physiological Reviews* 2018;**99**:707–38. doi:10.1152/PHYSREV.00007.2018

166 Verkman AS, Galietta LJ v. Chloride channels as drug targets. *Nature reviews Drug discovery* 2009;**8**:153–71. doi:10.1038/nrd2780

167 Wang K, Preisler SS, Zhang L, *et al.* Structure of the human ClC-1 chloride channel. *PLOS Biology* 2019;**17**:e3000218. doi:10.1371/JOURNAL.PBIO.3000218

168 Saint-Criq V, Gray MA. Role of CFTR in epithelial physiology. Cellular and Molecular Life Sciences. 2017;**74**:93–115. doi:10.1007/s00018-016-2391-y

169 Haq IJ, Gray MA, Garnett JP, *et al.* Airway surface liquid homeostasis in cystic fibrosis: Pathophysiology and therapeutic targets. Thorax. 2016;**71**:284–7. doi:10.1136/thoraxjnl-2015-207588

170 Poroca DR, Pelis RM, Chappe VM. ClC Channels and Transporters: Structure, Physiological Functions, and Implications in Human Chloride Channelopathies. *Frontiers in Pharmacology* 2017;**8**. doi:10.3389/FPHAR.2017.00151

171 Jentsch TJ, Pusch M. CLC Chloride Channels and Transporters: Structure, Function, Physiology, and Disease. *Physiological Reviews* 2018;**98**:1493–590. doi:10.1152/PHYSREV.00047.2017

172 Accardi A, Miller C. Secondary active transport mediated by a prokaryotic homologue of ClC Cl- channels. *Nature 2004 427:6977* 2004;**427**:803–7. doi:10.1038/nature02314

173 Dutzler R, Campbell EB, MacKinnon R. Gating the Selectivity Filter in ClC Chloride Channels. *Science* 2003;**300**:108–12. doi:10.1126/SCIENCE.1082708

174 Feng L, Campbell EB, MacKinnon R. Molecular mechanism of proton transport in CLC Cl-/H+ exchange transporters. *Proceedings of the National Academy of Sciences of the United States of America* 2012;**109**:11699. doi:10.1073/PNAS.1205764109

175 Park E, MacKinnon R. Structure of the CLC-1 chloride channel from Homo sapiens. *eLife* 2018;**7**. doi:10.7554/ELIFE.36629

176 Altamura C, Desaphy J-F, Conte D, *et al.* Skeletal muscle ClC-1 chloride channels in health and diseases. *Pflügers Archiv - European Journal of Physiology 2020 472:7* 2020;**472**:961–75. doi:10.1007/S00424-020-02376-3

177 Wang H, Xu M, Kong Q, *et al.* Research and progress on ClC-2. *Molecular Medicine Reports* 2017;**16**:11. doi:10.3892/MMR.2017.6600

178 Ishida Y, Nayak S, Mindell JA, *et al.* A model of lysosomal pH regulation. *The Journal of General Physiology* 2013;**141**:705. doi:10.1085/JGP.201210930

179 Fisher SE, van Bakel I, Lloyd SE, *et al.* Cloning and Characterization of CLCN5, the Human Kidney Chloride Channel Gene Implicated in Dent Disease (an X-Linked Hereditary Nephrolithiasis). *Genomics* 1995;**29**:598–606. doi:10.1006/GENO.1995.9960

180 Pusch M, Zifarelli G. ClC-5: Physiological role and biophysical mechanisms. *Cell Calcium* 2015;**58**:57–66. doi:10.1016/J.CECA.2014.09.007

181 Lange PF, Wartosch L, Jentsch TJ, *et al.* ClC-7 requires Ostm1 as a β-subunit to support bone resorption and lysosomal function. *Nature 2006 440:7081* 2006;**440**:220–3. doi:10.1038/nature04535

182 Kornak U, Kasper D, Bösl MR, *et al.* Loss of the ClC-7 Chloride Channel Leads to Osteopetrosis in Mice and Man. *Cell* 2001;**104**:205–15. doi:10.1016/S0092-8674(01)00206-9

183 Grudzinska J, Schemm R, Haeger S, *et al.* The β Subunit Determines the Ligand Binding Properties of Synaptic Glycine Receptors. *Neuron* 2005;**45**:727–39. doi:10.1016/J.NEURON.2005.01.028

184 Hevers W, Lüddens H. The diversity of GABAA receptors. *Molecular Neurobiology 1998 18:1* 1998;**18**:35–86. doi:10.1007/BF02741459

185 Burgos CF, Yévenes GE, Aguayo LG. Structure and Pharmacologic Modulation of Inhibitory Glycine Receptors. *Molecular Pharmacology* 2016;**90**:318. doi:10.1124/MOL.116.105726

186 Clar DT, Maani C v. Physiology, Ligand Gated Chloride Channel. *StatPearls* Published Online First: 9 August 2021.https://www.ncbi.nlm.nih.gov/books/NBK540983/ (accessed 19 Oct 2021).

187 Moghaddam HS, Zare-Shahabadi A, Rahmani F, *et al.* Neurotransmission systems in Parkinson's disease. *Reviews in the Neurosciences* 2017;**28**:509–36. doi:10.1515/REVNEURO-2016-0068

188 Govindpani K, Guzmán BC-F, Vinnakota C, *et al.* Towards a Better Understanding of GABAergic Remodeling in Alzheimer's Disease. *International Journal of Molecular Sciences* 2017;**18**. doi:10.3390/IJMS18081813

189 Hsu Y-T, Chang Y-G, Chern Y. Insights into GABAAergic system alteration in Huntington's disease. *Open Biology* 2018;**8**. doi:10.1098/RSOB.180165

190 Hernandez CC, Macdonald RL. A structural look at GABAA receptor mutations linked to epilepsy syndromes. *Brain Research* 2019;**1714**:234–47. doi:10.1016/J.BRAINRES.2019.03.004

191 Vuilleumier PH, Fritsche R, Schliessbach J, *et al.* Mutations affecting glycinergic neurotransmission in hyperekplexia increase pain sensitivity. *Brain* 2018;**141**:63–71. doi:10.1093/BRAIN/AWX289

192 Pilorge M, Fassier C, Corronc H le, *et al.* Genetic and functional analyses demonstrate a role for abnormal glycinergic signaling in autism. *Molecular Psychiatry* 2016;**21**:936. doi:10.1038/MP.2015.139

193 Qu Z, Wei RW, Mann W, *et al.* Two bestrophins cloned from Xenopus laevis oocytes express Ca(2+)-activated Cl(-) currents. *The Journal of biological chemistry* 2003;**278**:49563–72. doi:10.1074/jbc.M308414200

194 Caputo A, Caci E, Ferrera L, *et al.* TMEM16A, a membrane protein associated with calcium-dependent chloride channel activity. *Science (New York, NY)* 2008;**322**:590–4. doi:10.1126/science.1163518

195 Yang YD, Cho H, Koo JY, *et al.* TMEM16A confers receptor-activated calcium-dependent chloride conductance. *Nature* 2008;**455**:1210–5. doi:10.1038/nature07313

196 Kane Dickson V, Pedi L, Long SB. Structure and insights into the function of a Ca(2+)-activated Cl(-) channel. *Nature* 2014;**516**:213–8. doi:10.1038/nature13913

197 Petrukhin K, Koisti MJ, Bakall B, *et al.* Identification of the gene responsible for Best macular dystrophy. *Nature Genetics* 1998;**19**:241–7. doi:10.1038/915

198 Milenkovic A, Brandl C, Milenkovic VM, *et al.* Bestrophin 1 is indispensable for volume regulation in human retinal pigment epithelium cells. *Proceedings of the National Academy of Sciences of the United States of America* 2015;**112**:E2630-9. doi:10.1073/pnas.1418840112

199 Marmorstein AD, Kinnick TR, Stanton JB, *et al.* Bestrophin-1 influences transepithelial electrical properties and Ca2+ signaling in human retinal pigment epithelium. *Molecular vision* 2015;**21**:347–59.

200 Johnson AA, Guziewicz KE, Lee CJ, *et al.* Bestrophin 1 and retinal disease. *Progress in retinal and eye research* 2017;**58**:45–69. doi:10.1016/j.preteyeres.2017.01.006

201 Cui CY, Childress V, Piao Y, *et al.* Forkhead transcription factor FoxA1 regulates sweat secretion through Bestrophin 2 anion channel and Na-K-Cl cotransporter 1. *Proceedings of the National Academy of Sciences of the United States of America* 2012;**109**:1199–203. doi:10.1073/PNAS.1117213109/-/DCSUPPLEMENTAL

202 Ito G, Okamoto R, Murano T, *et al.* Lineage-Specific Expression of Bestrophin-2 and Bestrophin-4 in Human Intestinal Epithelial Cells. *PLOS ONE* 2013;**8**:e79693. doi:10.1371/JOURNAL.PONE.0079693

203 Song W, Yang Z, He B. Bestrophin 3 Ameliorates TNFα-Induced Inflammation by Inhibiting NF-κB Activation in Endothelial Cells. *PLOS ONE* 2014;**9**:e111093. doi:10.1371/JOURNAL.PONE.0111093

204 Pifferi S, Dibattista M, Menini A. TMEM16B induces chloride currents activated by calcium in mammalian cells. *Pflügers Archiv - European Journal of Physiology 2009 458:6* 2009;**458**:1023–38. doi:10.1007/S00424-009-0684-9

205 Kalienkova V, Clerico Mosina V, Paulino C. The Groovy TMEM16 Family: Molecular Mechanisms of Lipid Scrambling and Ion Conduction. *Journal of Molecular Biology* 2021;**433**:166941. doi:10.1016/J.JMB.2021.166941

206 Suzuki J, Umeda M, Sims PJ, *et al.* Calcium-dependent phospholipid scrambling by TMEM16F. *Nature* 2010;**468**:834–8. doi:10.1038/nature09583

207 Scudieri P, Caci E, Venturini A, *et al.* Ion channel and lipid scramblase activity associated with expression of TMEM16F/ANO6 isoforms. *The Journal of Physiology* 2015;**593**:3829–48. doi:10.1113/JP270691

208 Pedemonte N, Galietta LJ v. Structure and function of TMEM16 proteins (anoctamins). *Physiological reviews* 2014;**94**:419–59. doi:10.1152/physrev.00039.2011

209 Jiang T, Yu K, Hartzell HC, *et al.* Lipids and ions traverse the membrane by the same physical pathway in the nhTMEM16 scramblase. *eLife* 2017;**6**. doi:10.7554/ELIFE.28671

210 Paulino C, Kalienkova V, Lam AKM, *et al.* Activation mechanism of the calcium-activated chloride channel TMEM16A revealed by cryo-EM. *Nature* 2017;**552**:421–5. doi:10.1038/nature24652

211 Dang S, Feng S, Tien J, *et al.* Cryo-EM structures of the TMEM16A calcium-activated chloride channel. *Nature* 2017;**552**:426–9. doi:10.1038/nature25024

212 Paulino C, Neldner Y, Lam AK, *et al.* Structural basis for anion conduction in the calcium-activated chloride channel TMEM16A. *eLife* 2017;**6**. doi:10.7554/ELIFE.26232

213 Ferrera L, Caputo A, Ubby I, *et al.* Regulation of TMEM16A chloride channel properties by alternative splicing. *The Journal of biological chemistry* 2009;**284**:33360–8. doi:10.1074/jbc.M109.046607

214 Sanders KM, Zhu MH, Britton F, *et al.* Anoctamins and gastrointestinal smooth muscle excitability. *Experimental Physiology* 2012;**97**:200–6. doi:10.1113/expphysiol.2011.058248

215 Cho H, Yang YD, Lee J, *et al.* The calcium-activated chloride channel anoctamin 1 acts as a heat sensor in nociceptive neurons. *Nature Neuroscience* 2012;**15**:1015–21. doi:10.1038/nn.3111

216 Romanenko VG, Catalán MA, Brown DA, *et al.* Tmem16A encodes the Ca2+-activated Cl- channel in mouse submandibular salivary gland acinar cells. *The Journal of biological chemistry* 2010;**285**:12990–3001. doi:10.1074/jbc.M109.068544

217 Oh U, Jung J. Cellular functions of TMEM16/anoctamin. *Pflugers Archiv : European journal of physiology* 2016;**468**:443–53. doi:10.1007/s00424-016-1790-0

218 Tarran R, Loewen ME, Paradiso AM, *et al.* Regulation of murine airway surface liquid volume by CFTR and Ca2+-activated Cl- conductances. *The Journal of general physiology* 2002;**120**:407–18. doi:10.1085/JGP.20028599

219 Benedetto R, Ousingsawat J, Wanitchakool P, *et al.* Epithelial Chloride Transport by CFTR Requires TMEM16A. *Scientific Reports* 2017;**7**:12397. doi:10.1038/s41598-017-10910-0

220 Kunzelmann K, Ousingsawat J, Cabrita I, *et al.* TMEM16A in cystic fibrosis: Activating or inhibiting? Frontiers in Pharmacology. 2019;**9**. doi:10.3389/fphar.2019.00003

221 Kunzelmann K, Cabrita I, Wanitchakool P, *et al.* Modulating Ca2+ signals: a common theme for TMEM16, Ist2, and TMC. *Pflügers Archiv - European Journal of Physiology 2015 468:3* 2015;**468**:475–90. doi:10.1007/S00424-015-1767-4

222 Lérias J, Pinto M, Benedetto R, *et al.* Compartmentalized crosstalk of CFTR and TMEM16A (ANO1) through EPAC1 and ADCY1. *Cellular Signalling* 2018;**44**:10–9. doi:10.1016/J.CELLSIG.2018.01.008

223 Huang F, Zhang H, Wu M, *et al.* Calcium-activated chloride channel TMEM16A modulates mucin secretion and airway smooth muscle contraction. *Proceedings of the National Academy of Sciences of the United States of America* 2012;**109**:16354–9. doi:10.1073/pnas.1214596109

224 Scudieri P, Caci E, Bruno S, *et al.* Association of TMEM16A chloride channel overexpression with airway goblet cell metaplasia. *The Journal of Physiology* 2012;**590**:6141–55. doi:10.1113/jphysiol.2012.240838

225 Benedetto R, Cabrita I, Schreiber R, *et al.* TMEM16A is indispensable for basal mucus secretion in airways and intestine. *The FASEB Journal* 2019;**33**:4502–12. doi:10.1096/FJ.201801333RRR

226 Simões FB, Quaresma MC, Clarke LA, *et al.* TMEM16A chloride channel does not drive mucus production. *Life Science Alliance* 2019;**2**. doi:10.26508/LSA.201900462

227 Danahay H, Gosling M. TMEM16A: An Alternative Approach to Restoring Airway Anion Secretion in Cystic Fibrosis? *International Journal of Molecular Sciences* 2020;**21**. doi:10.3390/IJMS21072386

228 Forrest AS, Joyce TC, Huebner ML, *et al.* Increased TMEM16A-encoded calcium-activated chloride channel activity is associated with pulmonary hypertension. *American Journal of Physiology-Cell Physiology* 2012;**303**:C1229–43. doi:10.1152/ajpcell.00044.2012

229 Davis AJ, Shi J, Pritchard HA, *et al.* Potent vasorelaxant activity of the TMEM16A inhibitor T16Ainh-A01. *British Journal of Pharmacology* 2013;**168**:773–84. doi:10.1111/j.1476-5381.2012.02199.x

230 Ji Q, Shi S, Guo S, *et al.* Activation of TMEM16A by natural product canthaxanthin promotes gastrointestinal contraction. *The FASEB Journal* 2020;**34**:13430–44. doi:10.1096/FJ.202000443RR

231 Dubin AE, Patapoutian A. Nociceptors: the sensors of the pain pathway. *The Journal of clinical investigation* 2010;**120**:3760–72. doi:10.1172/JCI42843

232 Salzer I, Boehm S. Calcium-activated chloride channels: Potential targets for antinociceptive therapy. *The International Journal of Biochemistry & Cell Biology* 2019;**111**:37–41. doi:10.1016/J.BIOCEL.2019.04.006

233 Liu B, Linley JE, Du X, *et al.* The acute nociceptive signals induced by bradykinin in rat sensory neurons are mediated by inhibition of M-type K+ channels and activation of Ca2+-activated Cl- channels. *The Journal of clinical investigation* 2010;**120**:1240–52. doi:10.1172/JCI41084

234 García G, Martínez-Rojas VA, Rocha-González HI, *et al.* Evidence for the participation of Ca2+-activated chloride channels in formalin-induced acute and chronic nociception. *Brain Research* 2014;**1579**:35–44. doi:10.1016/J.BRAINRES.2014.07.011

235 F D, BF B. Anoctamin-1 Cl(-) channels in nociception: activation by an N-aroylaminothiazole and capsaicin and inhibition by T16A[inh]-A01. *Molecular pain* 2015;**11**. doi:10.1186/S12990-015-0061-Y

236 Hoffmann EK, Sørensen BH, Sauter DPR, *et al.* Role of volume-regulated and calcium-activated anion channels in cell volume homeostasis, cancer and drug resistance. *Channels (Austin, Tex)* 2015;**9**:380–96. doi:10.1080/19336950.2015.1089007

237 Almaça J, Tian Y, Aldehni F, *et al.* TMEM16 proteins produce volume-regulated chloride currents that are reduced in mice lacking TMEM16A. *The Journal of biological chemistry* 2009;**284**:28571–8. doi:10.1074/jbc.M109.010074

238 Wang H, Zou L, Ma K, *et al.* Cell-specific mechanisms of TMEM16A Ca(2+)-activated chloride channel in cancer. *Molecular cancer* 2017;**16**:152. doi:10.1186/s12943-017-0720-x

239 Crottès D, Jan LY. The Multifaceted Role of TMEM16A in Cancer. *Cell calcium* 2019;**82**:102050. doi:10.1016/J.CECA.2019.06.004

240 Ubby I, Bussani E, Colonna A, *et al.* TMEM16A alternative splicing coordination in breast cancer. *Molecular Cancer* 2013;**12**:75. doi:10.1186/1476-4598-12-75

241 Bill A, Gutierrez A, Kulkarni S, *et al.* ANO1/TMEM16A interacts with EGFR and correlates with sensitivity to EGFR-targeting therapy in head and neck cancer. *Oncotarget* 2015;**6**:9173–88. doi:10.18632/oncotarget.3277

242 Duvvuri U, Shiwarski DJ, Xiao D, *et al.* TMEM16A Induces MAPK and Contributes Directly to Tumorigenesis and Cancer Progression. *Cancer Research* 2012;**72**:3270–81. doi:10.1158/0008-5472.CAN-12-0475-T

243 Cao Q, Liu F, Ji K, *et al.* MicroRNA-381 inhibits the metastasis of gastric cancer by targeting TMEM16A expression. *Journal of Experimental & Clinical Cancer Research* 2017;**36**:29. doi:10.1186/s13046-017-0499-z

244 Galindo B, Vacquier V. Phylogeny of the TMEM16 protein family: Some members are overexpressed in cancer. *International Journal of Molecular Medicine* Published Online First: 1 November 2005. doi:10.3892/ijmm.16.5.919

245 Sui Y, Sun M, Wu F, *et al.* Inhibition of TMEM16A Expression Suppresses Growth and Invasion in Human Colorectal Cancer Cells. *PLoS ONE* 2014;**9**:e115443. doi:10.1371/journal.pone.0115443

246 Mokutani Y, Uemura M, Munakata K, *et al.* Down-Regulation of microRNA-132 is Associated with Poor Prognosis of Colorectal Cancer. *Annals of Surgical Oncology* 2016;**23**:599–608. doi:10.1245/s10434-016-5133-3

247 Britschgi A, Bill A, Brinkhaus H, *et al.* Calcium-activated chloride channel ANO1 promotes breast cancer progression by activating EGFR and

CAMK signaling. *Proceedings of the National Academy of Sciences* 2013;**110**:E1026–34. doi:10.1073/pnas.1217072110

248 Liu F, Cao Q-H, Lu D-J, *et al.* TMEM16A overexpression contributes to tumor invasion and poor prognosis of human gastric cancer through TGF-β signaling. *Oncotarget* 2015;**6**:11585–99. doi:10.18632/oncotarget.3412

249 Wu H, Guan S, Sun M, *et al.* Ano1/TMEM16A Overexpression Is Associated with Good Prognosis in PR-Positive or HER2-Negative Breast Cancer Patients following Tamoxifen Treatment. *PLOS ONE* 2015;**10**:e0126128. doi:10.1371/journal.pone.0126128

250 Shiwarski DJ, Shao C, Bill A, *et al.* To “Grow” or “Go”: TMEM16A Expression as a Switch between Tumor Growth and Metastasis in SCCHN. *Clinical Cancer Research* 2014;**20**:4673–88. doi:10.1158/1078-0432.CCR-14-0363

251 Shi Z-Z, Shang L, Jiang Y-Y, *et al.* Consistent and Differential Genetic Aberrations between Esophageal Dysplasia and Squamous Cell Carcinoma Detected By Array Comparative Genomic Hybridization. *Clinical Cancer Research* 2013;**19**:5867–78. doi:10.1158/1078-0432.CCR-12-3753

252 Ruiz C, Martins JR, Rudin F, *et al.* Enhanced Expression of ANO1 in Head and Neck Squamous Cell Carcinoma Causes Cell Migration and Correlates with Poor Prognosis. *PLoS ONE* 2012;**7**:e43265. doi:10.1371/journal.pone.0043265

253 Meredith SD, Levine PA, Burns JA, *et al.* Chromosome 11q13 amplification in head and neck squamous cell carcinoma. Association with poor prognosis. *Archives of otolaryngology--head & neck surgery* 1995;**121**:790–4.

254 Muller D, Millon R, Velten M, *et al.* Amplification of 11q13 DNA markers in head and neck squamous cell carcinomas: correlation with clinical outcome. *European journal of cancer (Oxford, England : 1990)* 1997;**33**:2203–10.

255 Stephan AB, Shum EY, Hirsh S, *et al.* ANO2 is the cilial calcium-activated chloride channel that may mediate olfactory amplification. *Proceedings of the National Academy of Sciences of the United States of America* 2009;**106**:11776–81. doi:10.1073/pnas.0903304106

256 Huang WC, Xiao S, Huang F, *et al.* Calcium-Activated Chloride Channels (CaCCs) Regulate Action Potential and Synaptic Response in Hippocampal Neurons. *Neuron* 2012;**74**:179. doi:10.1016/J.NEURON.2012.01.033

257 Ha GE, Lee J, Kwak H, *et al.* The Ca2+-activated chloride channel anoctamin-2 mediates spike-frequency adaptation and regulates sensory transmission in thalamocortical neurons. *Nature Communications 2016 7:1* 2016;**7**:1–13. doi:10.1038/ncomms13791

258 Zhang W, Schmelzeisen S, Parthier D, *et al.* Anoctamin Calcium-Activated Chloride Channels May Modulate Inhibitory Transmission in the Cerebellar Cortex. *PLoS ONE* 2015;**10**. doi:10.1371/JOURNAL.PONE.0142160

259 Li K-X, He M, Ye W, *et al.* TMEM16B regulates anxiety-related behavior and GABAergic neuronal signaling in the central lateral amygdala. *eLife* 2019;**8**. doi:10.7554/ELIFE.47106

260 Neureither F, Ziegler K, Pitzer C, *et al.* Impaired Motor Coordination and Learning in Mice Lacking Anoctamin 2 Calcium-Gated Chloride Channels. *Cerebellum (London, England)* 2017;**16**:929. doi:10.1007/S12311-017-0867-4

261 Wang L, Simms J, Peters CJ, *et al.* TMEM16B Calcium-Activated Chloride Channels Regulate Action Potential Firing in Lateral Septum and Aggression in Male Mice. *The Journal of Neuroscience* 2019;**39**:7102. doi:10.1523/JNEUROSCI.3137-18.2019

262 Zhang Y, Zhang Z, Xiao S, *et al.* Inferior olivary TMEM16B mediates cerebellar motor learning. *Neuron* 2017;**95**:1103. doi:10.1016/J.NEURON.2017.08.010

263 Wang Q, Curran ME, Splawski I, *et al.* Positional cloning of a novel potassium channel gene: KVLQT1 mutations cause cardiac arrhythmias. *Nature Genetics 1996 12:1* 1996;**12**:17–23. doi:10.1038/ng0196-17

264 Curran ME, Splawski I, Timothy KW, *et al.* A molecular basis for cardiac arrhythmia: HERG mutations cause long QT syndrome. *Cell* 1995;**80**:795–803. doi:10.1016/0092-8674(95)90358-5

265 Wang Q, Shen J, Splawski I, *et al.* SCN5A mutations associated with an inherited cardiac arrhythmia, long QT syndrome. *Cell* 1995;**80**:805–11. doi:10.1016/0092-8674(95)90359-3

266 Bellocq C, van Ginneken ACG, Bezzina CR, *et al.* Mutation in the KCNQ1 gene leading to the short QT-interval syndrome. *Circulation* 2004;**109**:2394–7. doi:10.1161/01.CIR.0000130409.72142.FE

267 Brugada R, Hong K, Dumaine R, *et al.* Sudden death associated with short-QT syndrome linked to mutations in HERG. *Circulation* 2004;**109**:30–5. doi:10.1161/01.CIR.0000109482.92774.3A

268 Priori SG, Pandit S v., Rivolta I, *et al.* A novel form of short QT syndrome (SQT3) is caused by a mutation in the KCNJ2 gene. *Circulation research* 2005;**96**:800–7. doi:10.1161/01.RES.0000162101.76263.8C

269 Koch MC, Steinmeyer K, Lorenz C, *et al.* The skeletal muscle chloride channel in dominant and recessive human myotonia. *Science (New York, NY)* 1992;**257**:797–800. doi:10.1126/SCIENCE.1379744

270 Lossin C, Wang DW, Rhodes TH, *et al.* Molecular Basis of an Inherited Epilepsy. *Neuron* 2002;**34**:877–84. doi:10.1016/S0896-6273(02)00714-6

271 Sugawara T, Tsurubuchi Y, Agarwala KL, *et al.* A missense mutation of the Na+ channel alpha II subunit gene Na(v)1.2 in a patient with febrile and afebrile seizures causes channel dysfunction. *Proceedings of the National Academy of Sciences of the United States of America* 2001;**98**:6384–9. doi:10.1073/PNAS.111065098

272 Baulac S, Huberfeld G, Gourfinkel-An I, *et al.* First genetic evidence of GABA(A) receptor dysfunction in epilepsy: a mutation in the gamma2-subunit gene. *Nature genetics* 2001;**28**:46–8. doi:10.1038/NG0501-46

273 Riordan JR, Rommens JM, Kerem BS, *et al.* Identification of the cystic fibrosis gene: Cloning and characterization of complementary DNA. *Science* 1989;**245**:1066–73. doi:10.1126/SCIENCE.2475911

274 Scotet V, L'Hostis C, Férec C. The Changing Epidemiology of Cystic Fibrosis: Incidence, Survival and Impact of the CFTR Gene Discovery. *Genes* 2020;**11**. doi:10.3390/GENES11060589

275 Cystic Fibrosis Genetic Analysis Consortium 1989. Cystic Fibrosis Mutation Database. http://www.genet.sickkids.on.ca/cftr/Home.html (accessed 15 Dec 2021).

276 Dalemans W, Barbry P, Champigny G, *et al.* Altered chloride ion channel kinetics associated with the delta F508 cystic fibrosis mutation. *Nature* 1991;**354**:526–8. doi:10.1038/354526A0

277 Cheng SH, Gregory RJ, Marshall J, *et al.* Defective intracellular transport and processing of CFTR is the molecular basis of most cystic fibrosis. *Cell* 1990;**63**:827–34. doi:10.1016/0092-8674(90)90148-8

278 Fraser SP, Diss JKJ, Chioni AM, *et al.* Voltage-gated sodium channel expression and potentiation of human breast cancer metastasis. *Clinical cancer research : an official journal of the American Association for Cancer Research* 2005;**11**:5381–9. doi:10.1158/1078-0432.CCR-05-0327

279 Yang M, Kozminski DJ, Wold LA, *et al.* Therapeutic potential for phenytoin: targeting Na(v)1.5 sodium channels to reduce migration and invasion in metastatic breast cancer. *Breast cancer research and treatment* 2012;**134**:603–15. doi:10.1007/S10549-012-2102-9

280 Diss JKJ, Stewart D, Pani F, *et al.* A potential novel marker for human prostate cancer: voltage-gated sodium channel expression in vivo. *Prostate cancer and prostatic diseases* 2005;**8**:266–73. doi:10.1038/SJ.PCAN.4500796

281 Royle J, Dobson S, Müller M, *et al.* Emerging Roles of Viroporins Encoded by DNA Viruses: Novel Targets for Antivirals? *Viruses* 2015;**7**:5375–87. doi:10.3390/v7102880

282 Scott C, Griffin S. Viroporins: Structure, function and potential as antiviral targets. *Journal of General Virology* 2015;**96**:2000–27. doi:10.1099/VIR.0.000201/CITE/REFWORKS

283 Wang C, Lamb RA, Pinto LH. Direct Measurement of the Influenza A Virus M2 Protein Ion Channel Activity in Mammalian Cells. *Virology* 1994;**205**:133–40. doi:10.1006/VIRO.1994.1628

284 Sempere Borau M, Stertz S. Entry of influenza A virus into host cells — recent progress and remaining challenges. *Current Opinion in Virology* 2021;**48**:23–9. doi:10.1016/J.COVIRO.2021.03.001

285 Dou D, Revol R, Östbye H, *et al.* Influenza A Virus Cell Entry, Replication, Virion Assembly and Movement. *Frontiers in Immunology* 2018;**9**:1. doi:10.3389/FIMMU.2018.01581

286 Wharton SA, Belshe RB, Skehel JJ, *et al.* Role of virion M2 protein in influenza virus uncoating: Specific reduction in the rate of membrane fusion between virus and liposomes by amantadine. *Journal of General Virology* 1994;**75**:945–8. doi:10.1099/0022-1317-75-4-945/CITE/REFWORKS

287 Bui M, Whittaker G, Helenius A. Effect of M1 protein and low pH on nuclear transport of influenza virus ribonucleoproteins. *Journal of Virology* 1996;**70**:8391–401. doi:10.1128/JVI.70.12.8391-8401.1996

288 Jalily PH, Duncan MC, Fedida D, *et al.* Put a cork in it: Plugging the M2 viral ion channel to sink influenza. *Antiviral Research* 2020;**178**:104780. doi:10.1016/J.ANTIVIRAL.2020.104780

289 Bright RA, Medina MJ, Xu X, *et al.* Incidence of adamantane resistance among influenza A (H3N2) viruses isolated worldwide from 1994 to 2005: a cause for concern. *Lancet (London, England)* 2005;**366**:1175–81. doi:10.1016/S0140-6736(05)67338-2

290 Willey RL, Maldarelli F, Martin MA, *et al.* Human immunodeficiency virus type 1 Vpu protein induces rapid degradation of CD4. *Journal of Virology* 1992;**66**:7193–200. doi:10.1128/JVI.66.12.7193-7200.1992

291 Willey RL, Maldarelli F, Martin MA, *et al.* Human immunodeficiency virus type 1 Vpu protein regulates the formation of intracellular gp160-CD4 complexes. *Journal of Virology* 1992;**66**:226–34. doi:10.1128/JVI.66.1.226-234.1992

292 Neil SJD, Zang T, Bieniasz PD. Tetherin inhibits retrovirus release and is antagonized by HIV-1 Vpu. *Nature 2008 451:7177* 2008;**451**:425–30. doi:10.1038/nature06553

293 Ewart GD, Sutherland T, Gage PW, *et al.* The Vpu protein of human immunodeficiency virus type 1 forms cation-selective ion channels. *Journal of Virology* 1996;**70**:7108–15. doi:10.1128/JVI.70.10.7108-7115.1996

294 Hsu K, Han J, Shinlapawittayatorn K, *et al.* Membrane Potential Depolarization as a Triggering Mechanism for Vpu-Mediated HIV-1 Release. *Biophysical Journal* 2010;**99**:1718–25. doi:10.1016/J.BPJ.2010.07.027

295 Strebel K. HIV-1 Vpu — an ion channel in search of a job. *Biochimica et Biophysica Acta (BBA) - Biomembranes* 2014;**1838**:1074–81. doi:10.1016/J.BBAMEM.2013.06.029

296 Agirre A, Barco A, Carrasco L, *et al.* Viroporin-mediated Membrane Permeabilization: PORE FORMATION BY NONSTRUCTURAL POLIOVIRUS 2B PROTEIN *. *Journal of Biological Chemistry* 2002;**277**:40434–41. doi:10.1074/JBC.M205393200

297 Danthi P, Tosteson M, Li Q, *et al.* Genome Delivery and Ion Channel Properties Are Altered in VP4 Mutants of Poliovirus. *Journal of Virology* 2003;**77**:5266–74. doi:10.1128/JVI.77.9.5266-5274.2003/ASSET/0923CEDA-A0F9-4066-8DF1-9E35B107ECB7/ASSETS/GRAPHIC/JV0932371008.JPEG

298 Clarke D, Griffin S, Beales L, *et al.* Evidence for the Formation of a Heptameric Ion Channel Complex by the Hepatitis C Virus P7 Protein in Vitro*. *Journal of Biological Chemistry* 2006;**281**:37057–68. doi:10.1074/JBC.M602434200

299 Premkumar A, Horan CR, Gage PW. Dengue Virus M Protein C-Terminal Peptide (DVM-C) Forms Ion Channels. doi:10.1007/s00232-005-0744-9

300 Hyser JM, Collinson-Pautz MR, Utama B, *et al.* Rotavirus disrupts calcium homeostasis by NSP4 viroporin activity. *mBio* 2010;**1**. doi:10.1128/MBIO.00265-10/ASSET/19A8D6B7-F933-44F7-BF8A-721C37FC9BB3/ASSETS/GRAPHIC/MBO0051010610008.JPEG

301 Wilson L, Mckinlay C, Gage P, *et al.* SARS coronavirus E protein forms cation-selective ion channels. *Virology* 2004;**330**:322–31. doi:10.1016/J.VIROL.2004.09.033

302 Nieto-Torres JL, Verdiá-Báguena C, Jimenez-Guardeño JM, *et al.* Severe acute respiratory syndrome coronavirus E protein transports calcium ions and activates the NLRP3 inflammasome. *Virology* 2015;**485**:330–9. doi:10.1016/J.VIROL.2015.08.010

303 Schoeman D, Fielding BC. Coronavirus envelope protein: current knowledge. *Virology Journal* 2019;**16**. doi:10.1186/S12985-019-1182-0

304 Wetherill LF, Holmes KK, Verow M, *et al.* High-Risk Human Papillomavirus E5 Oncoprotein Displays Channel-Forming Activity Sensitive to Small-Molecule Inhibitors. *Journal of Virology* 2012;**86**:5341–51. doi:10.1128/JVI.06243-11/ASSET/99E43BC9-CF29-4F89-9F72-90E0CF46C90F/ASSETS/GRAPHIC/ZJV9990959440009.JPEG

305 Hover S, Foster B, Barr JN, *et al.* Viral dependence on cellular ion channels – an emerging anti- viral target? *Journal of General Virology* 2017;:345–51. doi:10.1099/jgv.0.000712

306 Charlton FW, Pearson HM, Hover S, *et al.* Ion Channels as Therapeutic Targets for Viral Infections: Further Discoveries and Future Perspectives. *Viruses* 2020;**12**:844. doi:10.3390/v12080844

307 Scott CC, Gruenberg J. Ion flux and the function of endosomes and lysosomes: PH is just the start. *BioEssays* 2011;**33**:103–10. doi:10.1002/BIES.201000108

308 Hover S, Foster B, Fontana J, *et al.* Bunyavirus requirement for endosomal K+ reveals new roles of cellular ion channels during infection. *PLOS Pathogens* 2018;**14**:e1006845. doi:10.1371/journal.ppat.1006845

309 Punch EK, Hover S, Blest HTW, *et al.* Potassium is a trigger for conformational change in the fusion spike of an enveloped RNA virus. *The Journal of Biological Chemistry* 2018;**293**:9937. doi:10.1074/JBC.RA118.002494

310 Hover S, King B, Hall B, *et al.* Modulation of Potassium Channels Inhibits Bunyavirus Infection. *The Journal of biological chemistry* 2016;**291**:3411–22. doi:10.1074/jbc.M115.692673

311 Charlton FW, Hover S, Fuller J, *et al.* Cellular cholesterol abundance regulates potassium accumulation within endosomes and is an important determinant in bunyavirus entry. *Journal of Biological Chemistry* 2019;**294**:7335–47. doi:10.1074/jbc.RA119.007618

312 Sandler ZJ, Firpo MR, Omoba OS, *et al.* Novel Ionophores Active against La Crosse Virus Identified through Rapid Antiviral Screening. *Antimicrobial Agents and Chemotherapy* 2020;**64**. doi:10.1128/AAC.00086-20

313 Lang Y, Li F, Liu Q, *et al.* The Kv1.3 ion channel acts as a host factor restricting viral entry. *FASEB Journal* 2021;**35**:e20995. doi:10.1096/fj.202000879RR

314 Fujioka Y, Nishide S, Ose T, *et al.* A Sialylated Voltage-Dependent Ca2+ Channel Binds Hemagglutinin and Mediates Influenza A Virus Entry into Mammalian Cells. *Cell Host & Microbe* 2018;**23**:809-818.e5. doi:10.1016/J.CHOM.2018.04.015

315 Stauffer S, Feng Y, Nebioglu F, *et al.* Stepwise Priming by Acidic pH and a High K+ Concentration Is Required for Efficient Uncoating of Influenza A Virus Cores after Penetration. *Journal of Virology* 2014;**88**:13029–46. doi:10.1128/JVI.01430-14

316 Sakurai Y, Kolokoltsov AA, Chen C-C, *et al.* Two pore channels control Ebolavirus host cell entry and are drug targets for disease treatment. *Science (New York, NY)* 2015;**347**:995. doi:10.1126/SCIENCE.1258758

317 Das DK, Bulow U, Diehl WE, *et al.* Conformational changes in the Ebola virus membrane fusion machine induced by pH, Ca2+, and receptor binding. *PLoS Biology* 2020;**18**. doi:10.1371/JOURNAL.PBIO.3000626

318 Sakurai Y, Kolokoltsov AA, Chen CC, *et al.* Two-pore channels control Ebola virus host cell entry and are drug targets for disease treatment. *Science* 2015;**347**:995–8. doi:10.1126/science.1258758

319 Penny CJ, Vassileva K, Jha A, *et al.* Mining of Ebola virus entry inhibitors identifies approved drugs as two-pore channel pore blockers. *Biochimica et Biophysica Acta Molecular Cell Research* 2019;**1866**:1151. doi:10.1016/J.BBAMCR.2018.10.022

320 Panou M-M, Antoni M, Morgan EL, *et al.* Glibenclamide inhibits BK polyomavirus infection in kidney cells through CFTR blockade. *Antiviral Research* 2020;**178**:104778. doi:10.1016/j.antiviral.2020.104778

321 Tao YJ, Ye Q. RNA virus replication complexes. *PLoS Pathogens* 2010;**6**:1–3. doi:10.1371/journal.ppat.1000943

322 Han C, Zeng X, Yao S, *et al.* Voltage-Dependent Anion Channel 1 Interacts with Ribonucleoprotein Complexes To Enhance Infectious Bursal Disease Virus Polymerase Activity. *Journal of virology* 2017;**91**:e00584-17. doi:10.1128/JVI.00584-17

323 Müller M, Slivinski N, Todd EJAA, *et al.* Chikungunya virus requires cellular chloride channels for efficient genome replication. *PLoS Neglected Tropical Diseases* 2019;**13**. doi:10.1371/journal.pntd.0007703

324 Igloi Z, Mohl B-P, Lippiat JD, *et al.* Requirement for Chloride Channel Function during the Hepatitis C Virus Life Cycle. *Journal of Virology* 2015;**89**:4023–9. doi:10.1128/jvi.02946-14

325 Wang S, Liu Y, Guo J, *et al.* Screening of FDA-Approved Drugs for Inhibitors of Japanese Encephalitis Virus Infection. *Journal of Virology* 2017;**91**. doi:10.1128/JVI.01055-17

326 Pearson H, Todd EJAA, Ahrends M, *et al.* TMEM16A/ANO1 calcium-activated chloride channel as a novel target for the treatment of human respiratory syncytial virus infection. *Thorax* 2021;**76**:64–72. doi:10.1136/thoraxjnl-2020-215171

327 Neumann G, Watanabe T, Ito H, *et al.* Generation of influenza A viruses entirely from cloned cDNAs. *Proceedings of the National Academy of*

Sciences of the United States of America 1999;**96**:9345–50. doi:10.1073/pnas.96.16.9345

328 Gias E, Nielsen SU, Morgan LAF, *et al.* Purification of human respiratory syncytial virus by ultracentrifugation in iodixanol density gradient. *Journal of Virological Methods* 2008;**147**:328. doi:10.1016/J.JVIROMET.2007.09.013

329 Sun Y, López CB. Preparation of Respiratory Syncytial Virus with High or Low Content of Defective Viral Particles and Their Purification from Viral Stocks Materials and Reagents. doi:10.21769/BioProtoc.1820

330 Yu Q, Hardy RW, Wertz GW. Functional cDNA clones of the human respiratory syncytial (RS) virus N, P, and L proteins support replication of RS virus genomic RNA analogs and define minimal trans-acting requirements for RNA replication. *Journal of Virology* 1995;**69**:2412. doi:10.1128/jvi.69.4.2412-2419.1995

331 Hardy RW, Wertz GW. The Product of the Respiratory Syncytial Virus M2 Gene ORF1 Enhances Readthrough of Intergenic Junctions during Viral Transcription. *Journal of Virology* 1998;**72**:520. doi:10.1128/jvi.72.1.520-526.1998

332 Tran T-L, Castagné N, Dubosclard V, *et al.* The Respiratory Syncytial Virus M2-1 Protein Forms Tetramers and Interacts with RNA and P in a Competitive Manner. *Journal of Virology* 2009;**83**:6363. doi:10.1128/JVI.00335-09

333 Blondot ML, Dubosclard V, Fix J, *et al.* Structure and Functional Analysis of the RNA- and Viral Phosphoprotein-Binding Domain of Respiratory Syncytial Virus M2-1 Protein. *PLoS Pathogens* 2012;**8**. doi:10.1371/JOURNAL.PPAT.1002734

334 Neuhaus V, Danov O, Konzok S, *et al.* Assessment of the cytotoxic and immunomodulatory effects of substances in human precision-cut lung slices. *Journal of Visualized Experiments* 2018;**2018**. doi:10.3791/57042

335 Vasou A. Development of a novel cell-based screening platform to identify inhibitors of viral interferon antagonists from clinically important viruses. Published Online First: 2016.https://research-repository.st-andrews.ac.uk/handle/10023/8266 (accessed 13 Sep 2021).

336 Perini AP, Barbosa ML, Botosso VF, *et al.* Comparison of HeLa-I, HEp-2 and NCI-H292 cell lines for the isolation of human respiratory syncytial

virus (HRSV). *Journal of Virological Methods* 2007;**146**:368–71. doi:10.1016/J.JVIROMET.2007.07.004

337 Gagliardi TB, Criado MF, Proença-Módena JL, *et al.* Syncytia Induction by Clinical Isolates of Human Respiratory Syncytial Virus A. *Intervirology* 2017;**60**:56–60. doi:10.1159/000480014

338 Bohmwald K, Gálvez NMS, Canedo-Marroquín G, *et al.* Contribution of Cytokines to Tissue Damage During Human Respiratory Syncytial Virus Infection. *Frontiers in Immunology* 2019;**0**:452. doi:10.3389/FIMMU.2019.00452

339 Hillyer P, Shepard R, Uehling M, *et al.* Differential Responses by Human Respiratory Epithelial Cell Lines to Respiratory Syncytial Virus Reflect Distinct Patterns of Infection Control. *Journal of Virology* 2018;**92**. doi:10.1128/jvi.02202-17

340 Hruska JF, Bernstein JM, Douglas RG, *et al.* Effects of ribavirin on respiratory syncytial virus in vitro. *Antimicrobial Agents and Chemotherapy* 1980;**17**:770. doi:10.1128/AAC.17.5.770

341 Benítez-Rangel E, López-Méndez M, García L, *et al.* DIDS (4,4'-Diisothiocyanatostilbene-2,2'-disulfonate) directly inhibits caspase activity in HeLa cell lysates. *Cell Death Discovery 2015 1:1* 2015;**1**:1–9. doi:10.1038/cddiscovery.2015.37

342 Begenisich T, Melvin JE. Regulation of Chloride Channels in Secretory Epithelia. *The Journal of Membrane Biology 1998 163:2* 1998;**163**:77–85. doi:10.1007/S002329900372

343 Zhao B, Quan H, Ma T, *et al.* 4,4'-Diisothiocyanostilbene-2,2'-disulfonic Acid (DIDS) Ameliorates Ischemia-Hypoxia-Induced White Matter Damage in Neonatal Rats through Inhibition of the Voltage-Gated Chloride Channel ClC-2. *International journal of molecular sciences* 2015;**16**:10457–67. doi:10.3390/IJMS160510457

344 Zhang ZR, Zeltwanger S, McCarty NA. Direct Comparison of NPPB and DPC as Probes of CFTR Expressed in Xenopus Oocytes. *The Journal of Membrane Biology 2000 175:1* 2000;**175**:35–52. doi:10.1007/S002320001053

345 Valenzuela SM, Mazzanti M, Tonini R, *et al.* The nuclear chloride ion channel NCC27 is involved in regulation of the cell cycle. *The Journal of Physiology* 2000;**529**:541. doi:10.1111/J.1469-7793.2000.00541.X

346 Khamici H al, Brown LJ, Hossain KR, *et al.* Members of the Chloride Intracellular Ion Channel Protein Family Demonstrate Glutaredoxin-Like Enzymatic Activity. *PLOS ONE* 2015;**10**:e115699. doi:10.1371/JOURNAL.PONE.0115699

347 Landry DW, Akabas MH, Redhead C, *et al.* Purification and reconstitution of chloride channels from kidney and trachea. *Science* 1989;**244**:1469–72. doi:10.1126/SCIENCE.2472007

348 Caci E, Caputo A, Hinzpeter A, *et al.* Evidence for direct CFTR inhibition by CFTRinh-172 based on Arg347 mutagenesis. *Biochemical Journal* 2008;**413**:135–42. doi:10.1042/BJ20080029

349 Melis N, Tauc M, Cougnon M, *et al.* Revisiting CFTR inhibition: A comparative study of CFTRinh-172 and GlyH-101 inhibitors. *British Journal of Pharmacology* 2014;**171**:3716–27. doi:10.1111/bph.12726

350 Bachmann A, Quast U, Russ U. Chromanol 293b, a blocker of the slow delayed rectifier K+ current (IKs), inhibits the CFTR Cl- current. *Naunyn-Schmiedeberg's Archives of Pharmacology* 2001;**363**:590–6. doi:10.1007/s002100100410

351 Gupta J, Linsdell P. Point mutations in the pore region directly or indirectly affect glibenclamide block of the CFTR chloride channel. *Pflugers Archiv European Journal of Physiology* 2002;**443**:739–47. doi:10.1007/s00424-001-0762-0

352 Seibert FS, Linsdell P, Loo TW, *et al.* Cytoplasmic Loop Three of Cystic Fibrosis Transmembrane Conductance Regulator Contributes to Regulation of Chloride Channel Activity *. *Journal of Biological Chemistry* 1996;**271**:27493–9. doi:10.1074/JBC.271.44.27493

353 Melin P, Hosy E, Vivaudou M, *et al.* CFTR inhibition by glibenclamide requires a positive charge in cytoplasmic loop three. *Biochimica et Biophysica Acta - Biomembranes* 2007;**1768**:2438–46. doi:10.1016/j.bbamem.2007.05.013

354 Syeda R, Qiu Z, Dubin AE, *et al.* LRRC8 proteins form volume-regulated anion channels that sense ionic strength. *Cell* 2016;**164**:499. doi:10.1016/J.CELL.2015.12.031

355 Decher N, Lang HJ, Nilius B, *et al.* DCPIB is a novel selective blocker of ICl,swell and prevents swelling-induced shortening of guinea-pig atrial

action potential duration. *British Journal of Pharmacology* 2001;**134**:1467. doi:10.1038/SJ.BJP.0704413

356 Kern DM, Oh S, Hite RK, *et al.* Cryo-EM structures of the DCPIB-inhibited volume-regulated anion channel LRRC8A in lipid nanodiscs. *eLife* 2019;**8**. doi:10.7554/ELIFE.42636

357 Dang S, Feng S, Tien J, *et al.* Cryo-EM structures of the TMEM16A calcium-activated chloride channel. *Nature* 2017;**552**:426–9. doi:10.1038/nature25024

358 Shi S, Guo S, Chen Y, *et al.* Molecular mechanism of CaCCinh-A01 inhibiting TMEM16A channel. *Archives of Biochemistry and Biophysics* 2020;**695**. doi:10.1016/J.ABB.2020.108650

359 Bill A, Hall ML, Borawski J, *et al.* Small molecule-facilitated degradation of ANO1 protein: a new targeting approach for anticancer therapeutics. *The Journal of biological chemistry* 2014;**289**:11029–41. doi:10.1074/jbc.M114.549188

360 Bradley E, Fedigan S, Webb T, *et al.* Pharmacological characterization of TMEM16A currents. *Channels* 2014;**8**:308. doi:10.4161/CHAN.28065

361 Namkung W, Thiagarajah JR, Phuan P-W, *et al.* Inhibition of Ca2+-activated Cl- channels by gallotannins as a possible molecular basis for health benefits of red wine and green tea. *FASEB journal : official publication of the Federation of American Societies for Experimental Biology* 2010;**24**:4178–86. doi:10.1096/fj.10-160648

362 Namkung W, Phuan P-W, Verkman AS. TMEM16A inhibitors reveal TMEM16A as a minor component of calcium-activated chloride channel conductance in airway and intestinal epithelial cells. *The Journal of biological chemistry* 2011;**286**:2365–74. doi:10.1074/jbc.M110.175109

363 Oh S-J, Hwang SJ, Jung J, *et al.* MONNA, a potent and selective blocker for transmembrane protein with unknown function 16/anoctamin-1. *Molecular pharmacology* 2013;**84**:726–35. doi:10.1124/mol.113.087502

364 Li X -q., Fu ZF, Alvarez R, *et al.* Respiratory Syncytial Virus (RSV) Infects Neuronal Cells and Processes That Innervate the Lung by a Process Involving RSV G Protein. *Journal of Virology* 2006;**80**:537–40. doi:10.1128/jvi.80.1.537-540.2006

365 Yuan X, Hu T, He H, *et al.* Respiratory syncytial virus prolifically infects N2a neuronal cells, leading to TLR4 and nucleolin protein modulations

and RSV F protein co-localization with TLR4 and nucleolin. doi:10.1186/s12929-018-0416-6

366 Alves MP, Schögler A, Muster R, *et al.* IP-10 is selectively produced in the airways upon respiratory virus infection. *European Respiratory Journal* 2013;**42**.

367 McGeoch D, Fellner P, Newton C. Influenza virus genome consists of eight distinct RNA species. *Proceedings of the National Academy of Sciences of the United States of America* 1976;**73**:3045–9. doi:10.1073/PNAS.73.9.3045

368 Worobey M, Han GZ, Rambaut A. Genesis and pathogenesis of the 1918 pandemic H1N1 influenza a virus. *Proceedings of the National Academy of Sciences of the United States of America* 2014;**111**:8107–12. doi:10.1073/PNAS.1324197111/-/DCSUPPLEMENTAL

369 Influenza (Seasonal). World Health Organisation. 2018.https://www.who.int/news-room/fact-sheets/detail/influenza-(seasonal) (accessed 25 Nov 2021).

370 Elliott RM. Molecular biology of the Bunyaviridae. *Journal of General Virology* 1990;**71**:501–22. doi:10.1099/0022-1317-71-3-501/CITE/REFWORKS

371 Dowall SD, Findlay-Wilson S, Rayner E, *et al.* Hazara virus infection is lethal for adult type I interferon receptor-knockout mice and may act as a surrogate for infection with the human-pathogenic Crimean-Congo hemorrhagic fever virus. *Journal of General Virology* 2012;**93**:560–4. doi:10.1099/VIR.0.038455-0/CITE/REFWORKS

372 World Health Organisation. WHO: Crimean-Congo haemorrhagic fever. 2013.https://www.who.int/news-room/fact-sheets/detail/crimean-congo-haemorrhagic-fever (accessed 25 Nov 2021).

373 Surtees R, Ariza A, Punch EK, *et al.* The crystal structure of the Hazara virus nucleocapsid protein. *BMC Structural Biology* 2015;**15**:1–13. doi:10.1186/S12900-015-0051-3/TABLES/1

374 Zheng LL, Li CM, Zhen SJ, *et al.* A dynamic cell entry pathway of respiratory syncytial virus revealed by tracking the quantum dot-labeled single virus. *Nanoscale* 2017;**9**:7880–7. doi:10.1039/c7nr02162c

375 Lingemann M, McCarty T, Liu X, *et al.* The alpha-1 subunit of the Na+,K+-ATPase (ATP1A1) is required for macropinocytic entry of respiratory

syncytial virus (RSV) in human respiratory epithelial cells. *PLoS pathogens* 2019;**15**:e1007963. doi:10.1371/journal.ppat.1007963

376 Marchant DJ, Griffiths C, Bilawchuk L, *et al.* Respiratory Syncytial Virus (RSV) Recruitment of Its Receptor, Nucleolin, to the Cell Surface is the Rate Limiting Step in RSV Fusion and Entry in Bronchial Epithelial Cells. *American Journal of Respiratory and Critical Care Medicine* 2015;**191**.

377 Liu S, Chen R, Hagedorn CH. Tannic acid inhibits hepatitis C virus entry into Huh7.5 cells. *PLoS ONE* 2015;**10**. doi:10.1371/journal.pone.0131358

378 Zhang XF, Dai YC, Zhong W, *et al.* Tannic acid inhibited norovirus binding to HBGA receptors, a study of 50 Chinese medicinal herbs. *Bioorganic and Medicinal Chemistry* 2012;**20**:1616–23. doi:10.1016/j.bmc.2011.11.040

379 Kedersha N, Chen S, Gilks N, *et al.* Evidence that ternary complex (eIF2-GTP-tRNA(i)(Met))-deficient preinitiation complexes are core constituents of mammalian stress granules. *Molecular biology of the cell* 2002;**13**:195–210. doi:10.1091/MBC.01-05-0221

380 Gern JE, French DA, Grindle KA, *et al.* Double-Stranded RNA Induces the Synthesis of Specific Chemokines by Bronchial Epithelial Cells. *https://doi.org/101165/rcmb2002-0055OC* 2012;**28**:731–7. doi:10.1165/RCMB.2002-0055OC

381 Bermejo-Martin JF, Garcia-Arevalo MC, de Lejarazu RO, *et al.* Predominance of Th2 cytokines, CXC chemokines and innate immunity mediators at the mucosal level during severe respiratory syncytial virus infection in children. *European cytokine network* 2007;**18**:162–7. doi:10.1684/ECN.2007.0096

382 Qi XF, Kim DH, Yoon YS, *et al.* Essential involvement of cross-talk between IFN-γ and TNF-α in CXCL10 production in human THP-1 monocytes. *Journal of Cellular Physiology* 2009;**220**:690–7. doi:10.1002/JCP.21815

383 Motani K, Ito S, Nagata S. DNA-Mediated Cyclic GMP–AMP Synthase–Dependent and –Independent Regulation of Innate Immune Responses. *The Journal of Immunology* 2015;**194**:4914–23. doi:10.4049/JIMMUNOL.1402705/-/DCSUPPLEMENTAL

384 Müller M, Carter S, Hofer MJ, *et al.* Review: The chemokine receptor CXCR3 and its ligands CXCL9, CXCL10 and CXCL11 in neuroimmunity –

a tale of conflict and conundrum. *Neuropathology and Applied Neurobiology* 2010;**36**:368–87. doi:10.1111/J.1365-2990.2010.01089.X

385 Mascarenhas J, Hoffman R. Ruxolitinib: The First FDA Approved Therapy for the Treatment of Myelofibrosis. *Clinical Cancer Research* 2012;**18**:3008–14. doi:10.1158/1078-0432.CCR-11-3145

386 Namkung W, Yao Z, Finkbeiner WE, *et al.* Small-molecule activators of TMEM16A, a calcium-activated chloride channel, stimulate epithelial chloride secretion and intestinal contraction. *The FASEB Journal* 2011;**25**:4048. doi:10.1096/FJ.11-191627

387 Cabrita I, Kraus A, Scholz JK, *et al.* Cyst growth in ADPKD is prevented by pharmacological and genetic inhibition of TMEM16A in vivo. *Nature Communications* 2020;**11**. doi:10.1038/S41467-020-18104-5

388 Boedtkjer DMB, Kim S, Jensen AB, *et al.* New selective inhibitors of calcium-activated chloride channels - T16A(inh) -A01, CaCC(inh) -A01 and MONNA - what do they inhibit? *British journal of pharmacology* 2015;**172**:4158–72. doi:10.1111/bph.13201

389 Liu Y, Liu Z, Wang KW. The Ca2+-activated chloride channel ANO1/TMEM16A: An emerging therapeutic target for epithelium-originated diseases? *Acta Pharmaceutica Sinica B* 2021;**11**:1412–33. doi:10.1016/J.APSB.2020.12.003

390 Zhang CH, Li Y, Zhao W, *et al.* The Transmembrane Protein 16A Ca2+-activated Cl− Channel in Airway Smooth Muscle Contributes to Airway Hyperresponsiveness. *American Journal of Respiratory and Critical Care Medicine* 2013;**187**:374. doi:10.1164/RCCM.201207-1303OC

391 Cell line - ANO2. The Human Protein Atlas. https://www.proteinatlas.org/ENSG00000047617-ANO2/cell+line (accessed 2 Dec 2021).

392 Uhlén M, Fagerberg L, Hallström BM, *et al.* Tissue-based map of the human proteome. *Science* 2015;**347**. doi:10.1126/SCIENCE.1260419

393 Liu G, Betts C, Cunoosamy DM, *et al.* Use of precision cut lung slices as a translational model for the study of lung biology. *Respiratory Research 2019 20:1* 2019;**20**:1–14. doi:10.1186/S12931-019-1131-X

394 Hess A, Wang-Lauenstein L, Braun A, *et al.* Prevalidation of the ex-vivo model PCLS for prediction of respiratory toxicity. *Toxicology in vitro : an*

international journal published in association with BIBRA 2016;**32**:347–61. doi:10.1016/J.TIV.2016.01.006

395 Danov O, Delgado SMJ, Obernolte H, *et al.* Human lung tissue provides highly relevant data about efficacy of new anti-asthmatic drugs. *PloS one* 2018;**13**. doi:10.1371/JOURNAL.PONE.0207767

396 Wu W, Booth JL, Duggan ES, *et al.* Innate Immune Response to H3N2 and H1N1 Influenza Virus Infection in a Human Lung Organ Culture Model. *Virology* 2010;**396**:178. doi:10.1016/J.VIROL.2009.10.016

397 Donovan C, Seow HJ, Bourke JE, *et al.* Influenza A virus infection and cigarette smoke impair bronchodilator responsiveness to β-adrenoceptor agonists in mouse lung. *Clinical Science (London, England : 1979)* 2016;**130**:829. doi:10.1042/CS20160093

398 Medicine: War Wounds. TIME. 1939.https://web.archive.org/web/20080530022321/http://www.time.com/time/magazine/article/0,9171,762600-2,00.html (accessed 30 Nov 2021).

399 Hupkens P, Boxma H, Dokter J. Tannic acid as a topical agent in burns: historical considerations and implications for new developments. *Burns* 1995;**21**:57–61. doi:10.1016/0305-4179(95)90784-W

400 Theisen LL, Erdelmeier CAJ, Spoden GA, *et al.* Tannins from Hamamelis virginiana Bark Extract: Characterization and Improvement of the Antiviral Efficacy against Influenza A Virus and Human Papillomavirus. *PLoS ONE* 2014;**9**. doi:10.1371/JOURNAL.PONE.0088062

401 Wang S-C, Chen Y, Wang Y-C, *et al.* Tannic acid suppresses SARS-CoV-2 as a dual inhibitor of the viral main protease and the cellular TMPRSS2 protease. *American Journal of Cancer Research* 2020;**10**:4538./pmc/articles/PMC7783773/ (accessed 30 Nov 2021).

402 Uchiumi F, Sato T, Tanuma SI. Identification and characterization of a tannic acid-responsive negative regulatory element in the mouse mammary tumor virus promoter. *The Journal of biological chemistry* 1998;**273**:12499–508. doi:10.1074/JBC.273.20.12499

403 Uchiumi F, Maruta H, Inoue JI, *et al.* Inhibitory effect of tannic acid on human immunodeficiency virus promoter activity induced by 12-O-tetra decanoylphorbol-13-acetate Jurkat T-cells. *Biochemical and Biophysical Research Communications* Published Online First: 1996. doi:10.1006/bbrc.1996.0419

404 Su J, Dou Y, You Y, *et al.* Application of minigenome technology in virology research of the Paramyxoviridae family. *Journal of Microbiology, Immunology and Infection* 2015;**48**:123–9. doi:10.1016/j.jmii.2014.02.008

405 Jasenosky LD, Neumann G, Kawaoka Y. Minigenome-based reporter system suitable for high-throughput screening of compounds able to inhibit Ebolavirus replication and/or transcription. *Antimicrobial Agents and Chemotherapy* 2010;**54**:3007–10. doi:10.1128/AAC.00138-10/ASSET/5B03FDEF-806C-43F5-81D6-981A93F5B89E/ASSETS/GRAPHIC/ZAC9991090810002.JPEG

406 Peeples ME, Collins PL. Mutations in the 5′ Trailer Region of a Respiratory Syncytial Virus Minigenome Which Limit RNA Replication to One Step. *Journal of Virology* 2000;**74**:146. doi:10.1128/JVI.74.1.146-155.2000

407 Fontana J, López-Montero N, Elliott RM, *et al.* The unique architecture of Bunyamwera virus factories around the Golgi complex. *Cellular Microbiology* 2008;**10**:2012–28. doi:10.1111/j.1462-5822.2008.01184.x

408 Liu Y, Zhang H, Huang D, *et al.* Characterization of the effects of Cl− channel modulators on TMEM16A and bestrophin-1 Ca2+ activated Cl− channels. *Pflügers Archiv - European Journal of Physiology* 2015;**467**:1417–30. doi:10.1007/s00424-014-1572-5

409 Cell line - BEST1. The Human Protein Atlas. https://www.proteinatlas.org/ENSG00000167995-BEST1/cell+line (accessed 2 Dec 2021).

410 Herz C, Stavnezer E, Krug RM, *et al.* Influenza virus, an RNA virus, synthesizes its messenger RNA in the nucleus of infected cells. *Cell* 1981;**26**:391–400. doi:10.1016/0092-8674(81)90208-7

411 Bai W, Liu M, Xiao Q. The diverse roles of TMEM16A Ca2+-activated Cl− channels in inflammation. *Journal of Advanced Research* 2021;**33**:53. doi:10.1016/J.JARE.2021.01.013

412 Carter SD, Dent KC, Atkins E, *et al.* Direct visualization of the small hydrophobic protein of human respiratory syncytial virus reveals the structural basis for membrane permeability. *Febs Letters* 2010;**584**:2786. doi:10.1016/J.FEBSLET.2010.05.006

413 Cui R, Wang Y, Wang L, *et al.* Cyclopiazonic acid, an inhibitor of calcium-dependent ATPases with antiviral activity against human respiratory

syncytial virus. *Antiviral Research* 2016;**132**:38–45. doi:10.1016/J.ANTIVIRAL.2016.05.010

414 Norris MJ, Malhi M, Duan W, *et al.* Targeting Intracellular Ion Homeostasis for the Control of Respiratory Syncytial Virus. Published Online First: 2018. doi:10.1165/rcmb.2017-0345OC

415 Lingemann M, McCarty T, Liu X, *et al.* The alpha-1 subunit of the Na+,K+-ATPase (ATP1A1) is required for macropinocytic entry of respiratory syncytial virus (RSV) in human respiratory epithelial cells. *PLoS Pathogens* 2019;**15**. doi:10.1371/JOURNAL.PPAT.1007963

416 Yan Y, Shapiro JI. The physiological and clinical importance of sodium potassium ATPase in cardiovascular diseases. *Current Opinion in Pharmacology* 2016;**27**:43–9. doi:10.1016/J.COPH.2016.01.009

417 Yan D, Lee S, Thakkar VD, *et al.* Cross-resistance mechanism of respiratory syncytial virus against structurally diverse entry inhibitors. *Proceedings of the National Academy of Sciences of the United States of America* 2014;**111**:E3441–9. doi:10.1073/PNAS.1405198111/-/DCSUPPLEMENTAL

418 Dey D, Siddiqui SI, Mamidi P, *et al.* The effect of amantadine on an ion channel protein from Chikungunya virus. *PLoS neglected tropical diseases* 2019;**13**. doi:10.1371/JOURNAL.PNTD.0007548

419 Sala-Rabanal M, Yurtsever Z, Nichols CG, *et al.* Secreted CLCA1 modulates TMEM16A to activate Ca2+-dependent chloride currents in human cells. *eLife* 2015;**2015**. doi:10.7554/ELIFE.05875

420 Li H, Yan X, Li R, *et al.* Increased TMEM16A Involved in Alveolar Fluid Clearance After Lipopolysaccharide Stimulation. *Inflammation* 2016;**39**:881–90. doi:10.1007/S10753-016-0320-8/FIGURES/6

421 Zhang M, Gao CX, Wang YP, *et al.* The association between the expression of PAR2 and TMEM16A and neuropathic pain. *Molecular Medicine Reports* 2018;**17**:3744–50. doi:10.3892/MMR.2017.8295/HTML

422 Skofic Maurer D, Zabini D, Nagaraj C, *et al.* Endothelial Dysfunction Following Enhanced TMEM16A Activity in Human Pulmonary Arteries. *Cells* 2020;**9**. doi:10.3390/CELLS9091984

423 Brock SC, Heck JM, McGraw PA, *et al.* The Transmembrane Domain of the Respiratory Syncytial Virus F Protein Is an Orientation-Independent

Apical Plasma Membrane Sorting Sequence. *Journal of Virology* 2005;**79**:12528. doi:10.1128/JVI.79.19.12528-12535.2005

424 Medoff BD, Sauty A, Tager AM, *et al.* IFN-γ-Inducible Protein 10 (CXCL10) Contributes to Airway Hyperreactivity and Airway Inflammation in a Mouse Model of Asthma. *The Journal of Immunology* 2002;**168**:5278–86. doi:10.4049/JIMMUNOL.168.10.5278

425 Zhang Y, Luxon BA, Casola A, *et al.* Expression of Respiratory Syncytial Virus-Induced Chemokine Gene Networks in Lower Airway Epithelial Cells Revealed by cDNA Microarrays. *Journal of Virology* 2001;**75**:9044. doi:10.1128/JVI.75.19.9044-9058.2001

426 Power UF, Huss T, Michaud V, *et al.* Differential Histopathology and Chemokine Gene Expression in Lung Tissues following Respiratory Syncytial Virus (RSV) Challenge of Formalin-Inactivated RSV- or BBG2Na-Immunized Mice. *Journal of Virology* 2001;**75**:12421. doi:10.1128/JVI.75.24.12421-12430.2001

427 McNamara PS, Flanagan BF, Hart CA, *et al.* Production of chemokines in the lungs of infants with severe respiratory syncytial virus bronchiolitis. *Journal of Infectious Diseases* 2005;**191**:1225–32. doi:10.1086/428855/2/191-8-1225-TAB002.GIF

428 Spurrell JCL, Wiehler S, Zaheer RS, *et al.* Human airway epithelial cells produce IP-10 (CXCL10) in vitro and in vivo upon rhinovirus infection. *American Journal of Physiology - Lung Cellular and Molecular Physiology* 2005;**289**:85–95. doi:10.1152/AJPLUNG.00397.2004/ASSET/IMAGES/LARGE/ZH50070522560010.JPEG

429 Betakova T, Kostrabova A, Lachova V, *et al.* Cytokines Induced During Influenza Virus Infection. *Current Pharmaceutical Design* 2017;**23**. doi:10.2174/1381612823666170316123736

430 Lu X, Masic A, Liu Q, *et al.* Regulation of influenza A virus induced CXCL-10 gene expression requires PI3K/Akt pathway and IRF3 transcription factor. *Molecular Immunology* 2011;**48**:1417–23. doi:10.1016/J.MOLIMM.2011.03.017

431 Russell CD, Unger SA, Walton M, *et al.* The Human Immune Response to Respiratory Syncytial Virus Infection. *Clinical Microbiology Reviews* 2017;**30**:481. doi:10.1128/CMR.00090-16

432 Nightingale ZD, Patkar C, Rothman AL. Viral replication and paracrine effects result in distinct, functional responses of dendritic cells following infection with dengue 2 virus. *Journal of Leukocyte Biology* 2008;**84**:1028. doi:10.1189/JLB.0208105

433 Silva MC, Guerrero-Plata A, Gilfoy FD, *et al.* Differential Activation of Human Monocyte-Derived and Plasmacytoid Dendritic Cells by West Nile Virus Generated in Different Host Cells. *Journal of Virology* 2007;**81**:13640. doi:10.1128/JVI.00857-07

434 Wang W, Yang P, Zhong Y, *et al.* Monoclonal antibody against CXCL-10/IP-10 ameliorates influenza A (H1N1) virus induced acute lung injury. *Cell Research* 2013;**23**:577. doi:10.1038/CR.2013.25

435 Mayer L, Sandborn WJ, Stepanov Y, *et al.* Anti-IP-10 antibody (BMS-936557) for ulcerative colitis: A phase II randomised study. *Gut* 2014;**63**:442–50. doi:10.1136/GUTJNL-2012-303424

436 Yellin M, Paliienko I, Balanescu A, *et al.* A phase II, randomized, double-blind, placebo-controlled study evaluating the efficacy and safety of MDX-1100, a fully human anti-CXCL10 monoclonal antibody, in combination with methotrexate in patients with rheumatoid arthritis. *Arthritis and rheumatism* 2012;**64**:1730–9. doi:10.1002/ART.34330

437 Lei J, Yin X, Shang H, *et al.* IP-10 is highly involved in HIV infection. *Cytokine* 2019;**115**:97–103. doi:10.1016/J.CYTO.2018.11.018

438 Asensio VC, Maier J, Milner R, *et al.* Interferon-Independent, Human Immunodeficiency Virus Type 1 gp120-Mediated Induction of CXCL10/IP-10 Gene Expression by Astrocytes In Vivo and In Vitro. *Journal of Virology* 2001;**75**:7067. doi:10.1128/JVI.75.15.7067-7077.2001

439 Lane BR, King SR, Bock PJ, *et al.* The C-X-C chemokine IP-10 stimulates HIV-1 replication. *Virology* 2003;**307**:122–34. doi:10.1016/S0042-6822(02)00045-4

440 Stephens LM, Varga SM. Function and Modulation of Type I Interferons during Respiratory Syncytial Virus Infection. *Vaccines* 2020;**8**. doi:10.3390/VACCINES8020177

441 Ousingsawat J, Mirza M, Tian Y, *et al.* Rotavirus toxin NSP4 induces diarrhea by activation of TMEM16A and inhibition of Na+ absorption. *Pflugers Archiv European Journal of Physiology* 2011;**461**:579–89. doi:10.1007/S00424-011-0947-0/FIGURES/6

442 Yu B, Zhu X, Yang X, *et al.* Plumbagin Prevents Secretory Diarrhea by Inhibiting CaCC and CFTR Channel Activities. *Frontiers in Pharmacology* 2019;**10**:1181. doi:10.3389/FPHAR.2019.01181

443 Yu B, Xie R, Jin L, *et al.* trans-δ-Viniferin inhibits Ca2+-activated Cl− channels and improves diarrhea symptoms. *Fitoterapia* 2019;**139**:104367. doi:10.1016/J.FITOTE.2019.104367

444 Jiang Y, Yu B, Yang H, *et al.* Shikonin Inhibits Intestinal Calcium-Activated Chloride Channels and Prevents Rotaviral Diarrhea. *Frontiers in Pharmacology* 2016;**7**:270. doi:10.3389/FPHAR.2016.00270

445 Caci E, Scudieri P, Carlo E di, *et al.* Upregulation of TMEM16A Protein in Bronchial Epithelial Cells by Bacterial Pyocyanin. *PLoS ONE* 2015;**10**. doi:10.1371/JOURNAL.PONE.0131775

446 Kondo M, Nakata J, Arai N, *et al.* Niflumic Acid Inhibits Goblet Cell Degranulation in a Guinea Pig Asthma Model. *Allergology International* 2012;**61**:133–42. doi:10.2332/ALLERGOLINT.11-OA-0307

447 Li Y, Tang XX. Abnormal Airway Mucus Secretion Induced by Virus Infection. *Frontiers in Immunology* 2021;**12**:3897. doi:10.3389/FIMMU.2021.701443/BIBTEX

448 Stier MT, Peebles RS. Host and viral determinants of respiratory syncytial virus-induced airway mucus. *Annals of the American Thoracic Society* 2018;**15**:S205–9. doi:10.1513/ANNALSATS.201806-380AW/SUPPL_FILE/DISCLOSURES.PDF

449 Mazzone A, Gibbons SJ, Bernard CE, *et al.* Identification and characterization of a novel promoter for the human ANO1 gene regulated by the transcription factor signal transducer and activator of transcription 6 (STAT6). *The FASEB Journal* 2015;**29**:152. doi:10.1096/FJ.14-258541

450 Lin J, Jiang Y, Li L, *et al.* TMEM16A mediates the hypersecretion of mucus induced by Interleukin-13. *Experimental Cell Research* 2015;**334**:260–9. doi:10.1016/J.YEXCR.2015.02.026

451 Qin Y, Jiang Y, Sheikh AS, *et al.* Interleukin-13 stimulates MUC5AC expression via a STAT6-TMEM16A-ERK1/2 pathway in human airway epithelial cells. *International Immunopharmacology* 2016;**40**:106–14. doi:10.1016/J.INTIMP.2016.08.033

452 Jiao J, Zhang T, Zhang Y, *et al.* Epidermal growth factor upregulates expression of MUC5AC via TMEM16A, in chronic rhinosinusitis with nasal

polyps. *Allergy, Asthma, and Clinical Immunology : Official Journal of the Canadian Society of Allergy and Clinical Immunology* 2020;**16**:40. doi:10.1186/S13223-020-00440-2

453 Currier MG, Lee S, Stobart CC, *et al.* EGFR Interacts with the Fusion Protein of Respiratory Syncytial Virus Strain 2-20 and Mediates Infection and Mucin Expression. *PLoS Pathogens* 2016;**12**. doi:10.1371/JOURNAL.PPAT.1005622

454 Shah S, Carver CM, Mullen P, *et al.* Local Ca2+ signals couple activation of TRPV1 and ANO1 sensory ion channels. *Science signaling* 2020;**13**. doi:10.1126/SCISIGNAL.AAW7963

455 Joseph J, Qu L, Wang S, *et al.* Phosphorylation of TRPV1 S801 Contributes to Modality-Specific Hyperalgesia in Mice. *The Journal of neuroscience : the official journal of the Society for Neuroscience* 2019;**39**:9954–66. doi:10.1523/JNEUROSCI.1064-19.2019

456 Jing X, Yan W, Zeng H, *et al.* Qingfei oral liquid alleviates airway hyperresponsiveness and mucus hypersecretion via TRPV1 signaling in RSV-infected asthmatic mice. *Biomedicine & Pharmacotherapy* 2020;**128**:110340. doi:10.1016/J.BIOPHA.2020.110340

457 Pushpakom S, Iorio F, Eyers PA, *et al.* Drug repurposing: progress, challenges and recommendations. *Nature Reviews Drug Discovery 2018 18:1* 2018;**18**:41–58. doi:10.1038/nrd.2018.168

458 Sultana J, Crisafulli S, Gabbay F, *et al.* Challenges for Drug Repurposing in the COVID-19 Pandemic Era. *Frontiers in Pharmacology* 2020;**11**:1657. doi:10.3389/FPHAR.2020.588654/BIBTEX

459 Bagal SK, Brown AD, Cox PJ, *et al.* Ion channels as therapeutic targets: a drug discovery perspective. *Journal of medicinal chemistry* 2013;**56**:593–624. doi:10.1021/JM3011433

460 Li H, Zhang L-K, Li S-F, *et al.* Calcium channel blockers reduce severe fever with thrombocytopenia syndrome virus (SFTSV) related fatality. *Cell Research* 2019;**29**:739. doi:10.1038/S41422-019-0214-Z

461 Tilve GH, Lengade JK, Bavadekar A v., *et al.* Niflumic acid in the management of rheumatoid and osteoarthritis. *Journal of Postgraduate Medicine* 1976;**22**:124.https://www.jpgmonline.com/article.asp?issn=0022-

3859;year=1976;volume=22;issue=3;spage=124;epage=129;aulast=Tilve (accessed 6 Dec 2021).

462 Walker NM, Simpson JE, Levitt RC, *et al.* Talniflumate increases survival in a cystic fibrosis mouse model of distal intestinal obstructive syndrome. *Journal of Pharmacology and Experimental Therapeutics* 2006;**317**:275–83. doi:10.1124/jpet.105.094847

463 Lee MHH, Graham GG, Williams KM, *et al.* A benefit-risk assessment of benzbromarone in the treatment of gout: Was its withdrawal from the market in the best interest of patients? *Drug Safety* 2008;**31**:643–65. doi:10.2165/00002018-200831080-00002/FIGURES/TAB3

464 Azevedo VF, Kos IA, Vargas-Santos AB, *et al.* Benzbromarone in the treatment of gout. *Advances in rheumatology (London, England)* 2019;**59**:37. doi:10.1186/S42358-019-0080-X/METRICS

465 Miner K, Labitzke K, Liu B, *et al.* Drug repurposing: The anthelmintics niclosamide and nitazoxanide are potent TMEM16A antagonists that fully bronchodilate airways. *Frontiers in Pharmacology* 2019;**10**. doi:10.3389/FPHAR.2019.00051/FULL

466 Cabrita I, Benedetto R, Schreiber R, *et al.* Niclosamide repurposed for the treatment of inflammatory airway disease. *JCI Insight* 2019;**4**. doi:10.1172/JCI.INSIGHT.128414

467 Chen W, Mook RA, Premont RT, *et al.* Niclosamide: Beyond an antihelminthic drug. *Cellular Signalling* 2018;**41**:89. doi:10.1016/J.CELLSIG.2017.04.001

468 Kunzelmann K, Ousingsawat J, Benedetto R, *et al.* Contribution of Anoctamins to Cell Survival and Cell Death. *Cancers* 2019;**11**. doi:10.3390/CANCERS11030382

469 Mostafa A, Kandeil A, Elshaier YAMM, *et al.* FDA-Approved Drugs with Potent In Vitro Antiviral Activity against Severe Acute Respiratory Syndrome Coronavirus 2. *Pharmaceuticals* 2020;**13**:1–24. doi:10.3390/PH13120443

470 Xu J, Shi PY, Li H, *et al.* Broad Spectrum Antiviral Agent Niclosamide and Its Therapeutic Potential. *ACS Infectious Diseases* 2020;**6**:909–15. doi:10.1021/ACSINFECDIS.0C00052

471 Li Z, Brecher M, Deng YQ, *et al.* Existing drugs as broad-spectrum and potent inhibitors for Zika virus by targeting NS2B-NS3 interaction. *Cell Research* 2017;**27**:1046. doi:10.1038/CR.2017.88

472 Wang YM, Lu JW, Lin CC, *et al.* Antiviral activities of niclosamide and nitazoxanide against chikungunya virus entry and transmission. *Antiviral Research* 2016;**135**:81. doi:10.1016/J.ANTIVIRAL.2016.10.003

473 Niyomdecha N, Suptawiwat O, Boonarkart C, *et al.* Repurposing of antiparasitic niclosamide to inhibit respiratory syncytial virus (RSV) replication. *Virus Research* 2021;**295**:198277. doi:10.1016/J.VIRUSRES.2020.198277

474 Downward J. PI 3-kinase, Akt and cell survival. *Seminars in Cell & Developmental Biology* 2004;**15**:177–82. doi:10.1016/J.SEMCDB.2004.01.002

475 Bitko V, Shulyayeva O, Mazumder B, *et al.* Nonstructural Proteins of Respiratory Syncytial Virus Suppress Premature Apoptosis by an NF-B-Dependent, Interferon-Independent Mechanism and Facilitate Virus Growth. *JOURNAL OF VIROLOGY* 2007;**81**:1786–95. doi:10.1128/JVI.01420-06

476 Sui J, Zhang C, Fang X, *et al.* Dual role of Ca 2+-activated Cl − channel transmembrane member 16A in lipopolysaccharide-induced intestinal epithelial barrier dysfunction in vitro. doi:10.1038/s41419-020-2614-x

477 d'Angelo DM, di Filippo P, Breda L, *et al.* Type I Interferonopathies in Children: An Overview. *Frontiers in Pediatrics* 2021;**9**:11. doi:10.3389/FPED.2021.631329/BIBTEX

478 Crow YJ, Black DN, Ali M, *et al.* Cree encephalitis is allelic with Aicardi-Goutières syndrome: implications for the pathogenesis of disorders of interferon alpha metabolism. *J Med Genet* 2003;**40**:183–7. doi:10.1136/jmg.40.3.183

479 Frémond ML, Rodero MP, Jeremiah N, *et al.* Efficacy of the Janus kinase 1/2 inhibitor ruxolitinib in the treatment of vasculopathy associated with TMEM173-activating mutations in 3 children. *Journal of Allergy and Clinical Immunology* 2016;**138**:1752–5. doi:10.1016/J.JACI.2016.07.015/ATTACHMENT/B74F3F6D-57C3-4A2D-A9F7-C753B443FA67/MMC14.PDF

480 Liu Y, Jesus AA, Marrero B, *et al.* Activated STING in a Vascular and Pulmonary Syndrome. *New England Journal of Medicine* 2014;**371**:507–18. doi:10.1056/NEJMOA1312625/SUPPL_FILE/NEJMOA1312625_DISCLOSURES.PDF

481 Meesilpavikkai K, Dik WA, Schrijver B, *et al.* Efficacy of Baricitinib in the Treatment of Chilblains Associated With Aicardi-Goutières Syndrome, a Type I Interferonopathy. *Arthritis & Rheumatology (Hoboken, N.j)* 2019;**71**:829. doi:10.1002/ART.40805

482 Benedetto R, Ousingsawat J, Cabrita I, *et al.* Plasma membrane-localized TMEM16 proteins are indispensable for expression of CFTR. *Journal of Molecular Medicine* 2019;**97**:711–22. doi:10.1007/s00109-019-01770-4

Appendix A

A.1 Evaluation of TMEM16A antibodies

Endogenous TMEM16A expression was assessed using lysates from infected A549 cells via western blot. As shown in Figure A-1 A, bands were observed at the expected size of 114 kDa (shown by an arrow), however several other non-specific bands were observed, most of which were denser than the band of interest. Confocal analysis of endogenous TMEM16A expression in HRSV infected A549 cells was performed using the same anti-TMEM16A antibody (Figure A-1 B). Large distinct puncta of TMEM16A staining were observed within the nucleus of each cell, whereas cytoplasmic expression of TMEM16A was not observed. The same observation was made using SH-SH5Y cells. As TMEM16A is a well-documented ion channel with plasma membrane and cytoplasmic expression, the staining observed here was assumed to be non-specific, likely related to the dense bands observed on the western blot. Therefore, to look for cytoplasmic expression of TMEM16A, lysis buffers of differing strengths were used to isolate cytoplasmic and nuclear fractions (Figure A-1 C). When analysed via western blot using the same anti-TMEM16A antibody, dense bands at the expected size of TMEM16A were observed in the nuclear fraction, but not in the cytoplasmic fraction. However, bands of a smaller size were observed within the cytoplasmic fraction. The loss of GAPDH from the nuclear fractions confirmed the successful separation of the two populations of protein. This was consistent with the confocal microscopy data; however, this was not convincing of accurate TMEM16A binding. Another anti-TMEM16A antibody from a different company was used to stain the cytoplasmic and nuclear fractions (Figure A-1 D). This antibody also revealed a band at the expected size for TMEM16A, and this time it was observed in the nuclear fraction. However, non-specific bands were also

observed, this time both larger and smaller than the band of interest. These figures represent two examples of unreliable antibodies against TMEM16A. Based on these data, for the experiments outlined in this thesis, TMEM16A expression was probed using an expression plasmid encoding TMEM16A with both myc and FLAG tags.

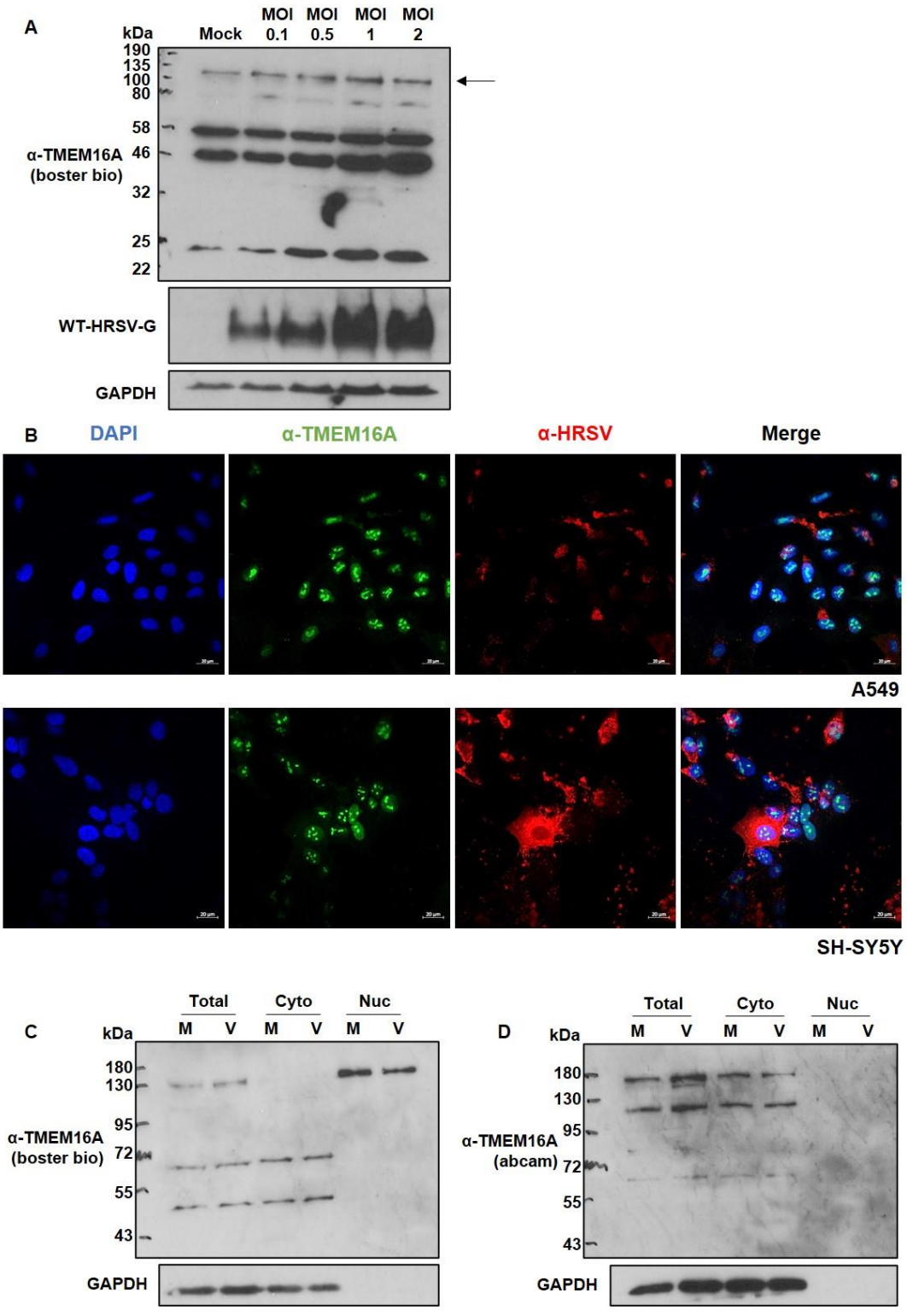

Figure A-1 Evaluation of antibodies targeting TMEM16A. A) Western blot probing the endogenous expression of TMEM16A in A549 cells infected with HRSV at a range of multiplicity of infections (MOIs), or mock infected. Predicted size of TMEM16A is 114 kDa (arrow). Several non-specific bands can be observed using the Boster Bio antibody. **B)** Confocal microscopy images of A549 (top) and SH-SY5Y (bottom) cells stained with antibodies targeting TMEM16A (green), and co-stained for HRSV (red). Nucleus is stained using DAPI (blue). Nuclear puncta can be observed using the TMEM16A antibody from Boster Bio. **C-D)** Western blots probing endogenous expression of TMEM16A in A549 cells infected (V) (or mock infected; M) with HRSV. The lysates have been fractionated and the total cell extract, alongside the cytoplasmic (cyto) and nuclear (nuc) extracts are shown. Using the TMEM16A antibody from Boster Bio (C), nuclear expression of TMEM16A is observed, and non-specific bands remain in the cytoplasm. However, the Abcam antibody (D) shows TMEM16A expression in the cytoplasm, along with non-specific bands. GAPDH is shown as a loading control and a cytoplasmic protein.